

Climate Change Assessment in the Arctic Basin Part 1: Trends and Projections - A Contribution to the Aquatic Climate Change Adaptation Services Program

N. Steiner, K. Azetsu-Scott, P. Galbraith, J. Hamilton,
K. Hedges, X. Hu, M. Y. Janjua, N. Lambert, P. Larouche,
D. Lavoie, J. Loder, H. Melling, A. Merzouk, P. G. Myers,
W. Perrie, I. Peterson, R. Pettipas, M. Scarratt, T. Sou,
M. Starr, R. F. Tallmann and A. van der Baaren

Fisheries and Oceans Canada
Science Branch,
Pacific Region
Institute of Ocean Sciences
P.O. Box 6000
Sidney, B.C. V8L 4B2

2013

Canadian Technical Report of
Fisheries and Aquatic Sciences 3042



Canadian Technical Report of Fisheries and Aquatic Sciences

Technical reports contain scientific and technical information that contributes to existing knowledge but which is not normally appropriate for primary literature. Technical reports are directed primarily toward a worldwide audience and have an international distribution. No restriction is placed on subject matter and the series reflects the broad interests and policies of Fisheries and Oceans Canada, namely, fisheries and aquatic sciences.

Technical reports may be cited as full publications. The correct citation appears above the abstract of each report. Each report is abstracted in the data base *Aquatic Sciences and Fisheries Abstracts*.

Technical reports are produced regionally but are numbered nationally. Requests for individual reports will be filled by the issuing establishment listed on the front cover and title page.

Numbers 1-456 in this series were issued as Technical Reports of the Fisheries Research Board of Canada. Numbers 457-714 were issued as Department of the Environment, Fisheries and Marine Service, Research and Development Directorate Technical Reports. Numbers 715-924 were issued as Department of Fisheries and Environment, Fisheries and Marine Service Technical Reports. The current series name was changed with report number 925.

Rapport technique canadien des sciences halieutiques et aquatiques

Les rapports techniques contiennent des renseignements scientifiques et techniques qui constituent une contribution aux connaissances actuelles, mais qui ne sont pas normalement appropriés pour la publication dans un journal scientifique. Les rapports techniques sont destinés essentiellement à un public international et ils sont distribués à cet échelon. Il n'y a aucune restriction quant au sujet; de fait, la série reflète la vaste gamme des intérêts et des politiques de Pêches et Océans Canada, c'est-à-dire les sciences halieutiques et aquatiques.

Les rapports techniques peuvent être cités comme des publications à part entière. Le titre exact figure au-dessus du résumé de chaque rapport. Les rapports techniques sont résumés dans la base de données *Résumés des sciences aquatiques et halieutiques*.

Les rapports techniques sont produits à l'échelon régional, mais numérotés à l'échelon national. Les demandes de rapports seront satisfaites par l'établissement auteur dont le nom figure sur la couverture et la page du titre.

Les numéros 1 à 456 de cette série ont été publiés à titre de Rapports techniques de l'Office des recherches sur les pêcheries du Canada. Les numéros 457 à 714 sont parus à titre de Rapports techniques de la Direction générale de la recherche et du développement, Service des pêches et de la mer, ministère de l'Environnement. Les numéros 715 à 924 ont été publiés à titre de Rapports techniques du Service des pêches et de la mer, ministère des Pêches et de l'Environnement. Le nom actuel de la série a été établi lors de la parution du numéro 925.

Canadian Technical Report of
Fisheries and Aquatic Sciences 3042

2013

CLIMATE CHANGE ASSESSMENT IN THE ARCTIC BASIN PART 1: TRENDS AND
PROJECTIONS - A CONTRIBUTION TO THE AQUATIC CLIMATE CHANGE
ADAPTATION SERVICES PROGRAM

by

N. Steiner¹, K. Azetsu-Scott³, P. Galbraith², J. Hamilton³, K. Hedges⁴, X. Hu⁵, M. Y.
Janjua⁴, N. Lambert², P. Larouche⁴, D. Lavoie², J. Loder³, H. Melling¹, A. Merzouk², P. G.
Myers⁵, W. Perrie³, I. Peterson³, R. Pettipas³, M. Scarratt², T. Sou¹, M. Starr², R. F.
Tallmann⁵ and A. van der Baaren³

¹ Fisheries and Oceans Canada, Institute of Ocean Sciences Sidney, BC

² Fisheries and Oceans Canada, Institut Maurice-Lamontagne, Mont Joli, QC

³ Fisheries and Oceans Canada, Bedford Institute of Oceanography, Dartmouth, NS

⁴ Fisheries and Oceans Canada, Freshwater Institute, Winnipeg, MB

⁵ Department of Earth and Atmospheric Sciences, University of Alberta, Edmonton, Alberta

© Her Majesty the Queen in Right of Canada, 2013
Cat. No. Fs 97-6/3042E ISSN 0706-6457 (print version)
Cat. No. Fs 97-6/3042E-PDF ISSN 1488-5379 (online version)

Correct citation for this publication:

Steiner, N., Azetsu-Scott, K., Galbraith, P., Hamilton, J., Hedges, K., Hu, X., Janjua, M.Y., Lambert, N., Larouche, P., Lavoie, D., Loder, J., Melling, H., Merzouk, A., Myers, P., Perrie, W., Peterson, I., Pettipas, R., Scarratt, M., Sou, T., Starr, M., Tallmann, R.F. and van der Baaren, A. 2013. Climate change assessment in the Arctic Basin Part 1: Trends and projections - A contribution to the Aquatic Climate Change Adaptation Services Program. Can. Tech. Rep. Fish. Aquat. Sci. 3042: xv + 163 pp.

TABLE OF CONTENTS

TABLE OF CONTENTS.....	iii
LIST OF TABLES.....	v
LIST OF FIGURES.....	vi
ABSTRACT.....	xii
RESUMÉ.....	xiv
1: INTRODUCTORY MATERIALS.....	1
1.1 GENERAL INTRODUCTION.....	1
1.2 GENERAL OCEANOGRAPHY.....	3
1.1.1 Beaufort Sea.....	3
1.1.2 Canadian Polar Shelf.....	4
1.1.3 Baffin Bay/Davis Strait.....	5
1.1.4 Hudson Bay.....	6
2: STATUS AND TRENDS.....	7
2.1 ATMOSPHERIC FORCING.....	7
2.1.1 Air temperature.....	7
2.1.2 Precipitation.....	11
2.1.3 Circulation and wind.....	13
2.1.4 Storm waves and surges.....	19
2.2 PHYSICAL OCEANOGRAPHY.....	19
2.2.1 Introduction.....	19
2.2.2 Sea Ice (Thickness, extent, and freeze/break-up).....	20
2.2.3 Water Properties and Stratification.....	32
2.2.4 Ocean Currents.....	37
2.2.5 Freshwater input.....	39
2.2.6 Relative Sea Level.....	43
2.3 CHEMICAL OCEANOGRAPHY.....	46
2.3.1. Nutrients, Carbon, Acidification.....	46
2.4 PHYTOPLANKTON AND PRIMARY PRODUCTION.....	51
2.5 ZOOPLANKTON AND HIGHER TROPHIC LEVELS.....	54
2.6 TRENDS IN THE MACKENZIE RIVER BASIN.....	56
2.6.1 Introduction.....	56
2.6.2 Air temperature.....	59
2.6.3 Precipitation.....	60
2.6.4 Hydrology.....	61
2.6.5 Cryosphere.....	63
2.6.6 Permafrost.....	64
3: PROJECTIONS OF THE FUTURE CLIMATE STATE.....	64
3.1 SOURCES FOR PROJECTIONS AND MODEL DESCRIPTIONS.....	64
3.1.1 Introduction.....	64
3.1.2 Global.....	66
3.1.3 Regional.....	70
3.2 ATMOSPHERIC FORCING.....	72
3.2.1 Air temperature.....	72
3.2.2 Precipitation.....	78
3.2.3 Circulation and wind.....	81
3.2.4 Wind, storm patterns and waves.....	83
3.2.5 Climate Extremes.....	83

3.3 PHYSICAL OCEANOGRAPHY	85
3.3.1. Freshwater input.....	86
3.3.2 Water properties and Stratification	87
3.3.3 Sea Level Change	99
3.3.4 Sea Ice Extent, Thickness and freeze/break up.....	100
3.4 CHEMICAL OCEANOGRAPHY.....	103
3.4.1 Carbon system and acidification.....	103
3.5 NUTRIENTS AND PRIMARY PRODUCTION.....	110
3.6 MACKENZIE RIVER BASIN	112
3.6.1 Air temperature	112
3.6.2 Precipitation	116
3.6.3 Wind.....	117
3.6.4 Hydrology	118
3.6.5 Lakes.....	119
3.6.6 Flooding and ice jams	120
3.6.7 Cryosphere.....	121
3.6.8 Permafrost.....	121
3.6.9 Primary Production	122
4: CONCLUSIONS AND RECOMMENDATIONS	122
5: ACKNOWLEDGEMENTS.....	127
6: REFERENCES	127
7: APPENDICES	155
7.1 APPENDIX 1	155
7.1.1 AR5-ESM Multi-Model Means and Standard Deviations.....	155
7.2 APPENDIX 2.....	157
7.2.1 Summary of Climate Change Trends and Projection for the Arctic Large Aquatic Basin - Beaufort Sea and Canadian Polar Shelf.....	157
7.2.2 Summary of Climate Change Trends and Projection for the Arctic Large Aquatic Basin - Baffin Bay and Davis Strait.....	159
7.2.3 Summary of Climate Change Trends and Projection for the Arctic Large Aquatic Basin - Hudson Bay	161
7.2.4 Summary of Climate Change Trends and Projection for the Arctic Large Aquatic Basin - Mackenzie River Basin.....	162

LIST OF TABLES

Table 1. Annual budget (August 2003 to August 2004) for the freshwater (FW) and volume (Vol.) of Hudson and James bays, in $\text{km}^3 \text{y}^{-1}$ relative to $S_0 = 33$ ppt. The upper portion lists the sources and sinks of freshwater, and the lower portion details the fluxes through the four channels (see St-Laurent et al. 2011, their Figure 1) making up the mouth of Hudson Bay (positive fluxes are outward). Note that the river runoff for this period is slightly lower than the long-term mean ($635 \text{ km}^3 \text{y}^{-1}$, Lammers et al. 2001). P – E stands for precipitation minus evaporation rate. (Table adapted from St-Laurent et al. 2011).....	42
Table 2: List of AR5 - Earth System Models	67
Table 3: NAA_NEMO change in T_s , S_s , SIC and SIT for BS, CPS and BB subbasins.	93
Table 4: AR5-ESM multimodel mean sea ice concentration (SIC) for 1996 – 2005 and 2046 – 2065 and simulated differences (2046 – 2065 minus 1986 – 2005) for RCP8.5 and RCP4.5 emission scenarios.	101
Table 5: AR5-ESM individual model and multimodel means of surface saturation state (Ω) from 1966-2085 (bidecadal averages) for the BS and CPS regions.....	106
Table 6: Multimodel ensemble mean (3AR5-ESMs, IPSL-CM5A-LR, CanESM2, MPI-ESM-LR) of the projected (2012 - 2062) DIC concentration for Hudson and Baffin Bays	110
Table 7. Trends and projections summary table for the Arctic LAB (CSAS 2013).....	122
Table 8. AR5-ESM multimodel means and standard deviations for the BS, CPS, BB, HB subbasins for T_s , S_s , Z_m , SIC, NO_3 , pH, PP, and CaCO_3 at 100 m for bidecades 1986 - 2005, 1966 - 1985, 2005 - 2025 and 2045 – 2065. Also included are the differences between the most recent past (1986 – 2005) and the past (1966 – 1985) and the recent past and the future (20 years and 60 years.	155
Table 9. AR5-ESM March (above) and September (below) SIC individual and multimodel means for RCP8.5 (green=model with least ice cover, red= model with most ice cover).	156

LIST OF FIGURES

Figure 1: Map of the Arctic Large Aquatic Basin (LAB) as defined by the Aquatic Climate Change Adaptation Services Program (ACCASP). The Arctic LAB is divided into five sub basins: Beaufort Sea, Canadian Arctic Archipelago, Baffin Bay/ Davis Strait, Hudson Bay Complex, and Mackenzie River Basin.....	2
Figure 2: Anomaly (re 1948 - 2000) in annual mean temperature at Tuktoyaktuk on the Beaufort coast. Data come from different locations in the village at different times (http://climate.weatheroffice.gc.ca/).....	7
Figure 3: Change in mean annual temperature, 1950 - 2007 (Figure 1 from Zhang et al. 2011)...	8
Figure 4: Air temperature at stations along the eastern coastline of the CAA, showing mean (black), minimum (blue) and maximum (red) annual values. Annual values (dots), long term means (dashed lines) and trends (solid lines) with slope m ($^{\circ}/y$) are shown. Stations were located in the communities of Alert (upper panel), Pond Inlet (middle panel) and Clyde River (lower panel). (Figure 18 from Hamilton and Wu 2013).....	10
Figure 5: June-July-August air temperature anomaly averages (1971 - 2000 climatology) and SST averages in Hudson Strait (top) and Hudson Bay (bottom). Air temperature is the NCEP 20 th century version 2 reanalysis surface temperature averaged at all grid points of each region and grey areas show the mean plus and minus one standard deviations of the 56 model runs (from Galbraith, unpublished data).....	11
Figure 6: Change in mean annual precipitation, 1950 - 2007, as a percentage of the 1961 - 1990 norm. (Figure 3 from Zhang et al. 2011).....	12
Figure 7: Time series of annual mean total precipitation at Alert (upper) and Clyde River (lower). Dots, dashed lines and solid lines indicate raw data, means of raw data and trend lines. The trend at Alert is statistically significant but that at Clyde River is not.	13
Figure 8: Anomaly in annual mean sea-level pressure north of 70°N, relative to the 1950 - 94 mean (Walsh et al. 1996).....	14
Figure 9: Average sea level pressure (mb) for June during 2007 – 2012 (from the NCEP-NCAR Reanalysis, NOAA/Earth Systems Research Laboratory).....	15
Figure 10: Variation in the June-mean sea-level pressure anomalies related to the AO and AD anomaly patterns. Series are normalized by the standard deviation during 1948 – 2012 (Overland et al. 2012).....	16
Figure 11: Time series of annual mean wind speed at Alert (upper) and Clyde River (lower). Dots, dash lines and solid lines indicate raw data, means of raw data and trend lines. There is strong statistical certainty that there are positive trends at both stations.....	18
Figure 12: Percentage frequency of wind occurrence by direction in January (A) and July (B) (Stewart and Lockhart 2005 and Maxwell 1986).....	18
Figure 13: Annual curves of northern sea ice extent from satellite observations using passive microwave sensors. Observations began late in 1978.	20
Figure 14: Distribution of ice at minimum annual ice extent in 2012, on 16 September. Median in orange (source: http://nsidc.org/arcticseaicenews/).....	21
Figure 15: Summertime anomaly in total accumulated concentration of sea ice on the Canadian Beaufort shelf. It is clear how variability masks trend (Melling et al. 2012).....	22

Figure 16: Formation of fast ice across the deep waters of eastern Amundsen Gulf. Data from Canadian Ice Service charts.....	22
Figure 17: Dates of ice break-up and freeze-up over four decades in the Canadian Beaufort Sea. Data from Canadian Ice Service charts.....	23
Figure 18: Thickness of coastal ice (red) and snow (blue) in mid May at Cape Parry. The snow axis is inverted to illustrate the correlation of thinner ice with deeper snow. The shaded zone represents 95% bounds of confidence. Data from the Canadian Ice Service (http://www.ec.gc.ca/glaces-ice/default.asp?lang=En&n=E1B3129D-1).....	24
Figure 19: Monthly anomalies in the draft of moving pack ice near 70.33°N 133.75°W on the middle shelf of the Canadian Beaufort Sea (Melling et al. 2005, 2012).	25
Figure 20: Mean pack-ice thickness in regions of the central Arctic during three periods of the last half century. Values are adjusted to the time of minimum, September 15 (Tucker et al. 2001).	26
Figure 21: Thickness (red) and snow depth (blue) for coastal ice at three latitudes on the Canadian Polar Shelf. Data from the Canadian Ice Service (CIS) dataset.	26
Figure 22: Summer sea ice area and trends (1968 - 2012) derived from the Canadian Ice Service (CIS) dataset.....	28
Figure 23: Annual mean sea ice area and trends (1900 - 2011) for Baffin Bay and Davis Strait derived from the HadISST1 and CIS datasets.	28
Figure 24: Mean sea ice area and trends (1900 - 2011) for Baffin Bay and Davis Strait, derived from the HadISST1 and CIS datasets for winter, spring, summer and autumn.....	29
Figure 25: Temperature at mid-shelf of the Beaufort Sea from early 1985. The 50-m depth of measurement is 5 m above the seabed at this location. Values plotted (top) are 3-month means. The same data are displayed as seasonal anomalies (bottom). A weak cooling trend is not significant (Melling 2013, unpublished data).	32
Figure 26: Temperature near the seabed in western Lancaster Sound (southern side). The likelihood of a real change in conditions here is about 85% (Hamilton and Wu 2013).	33
Figure 27: Salinity at 40 m depth in western Lancaster Sound (southern side). The likelihood of a real change in conditions here is about 85% (Hamilton and Wu 2013).....	34
Figure 28: Freshening trend on the Baffin Island Shelf (50 – 200 m) in Aug - Oct; -0.15 ppt/decade between 1977 – 2002 (Hamilton and Wu 2013).....	34
Figure 29: Warming of Baffin Bay intermediate waters in Aug - Oct; +0.13 °C/decade over the last half century (Hamilton and Wu 2013).	35
Figure 30: Time rate of change of temperature and salinity as a function of depth over the Baffin Island shelf break (defined by bottom depth 2000 m > H > 600 m). The warming is significant from 600 to 2000 m with a maximum value of about 0.13 °C/decade. The freshening is limited to the near-surface (Zweng and Münchow 2006).	36
Figure 31: Sea surface temperature climatologies for the warmest week of the year (late August) for the two alternating cold and warm states observed (Galbraith and Larouche 2011).	37
Figure 32: Average velocity of ice movement during October through December based on continuous measurements by sonar at mid shelf. (Melling 2013, unpublished data).	38

Figure 33: Varying flows of seawater through Lancaster Sound and Nares Strait since 1998 (Melling et al. 2012).	39
Figure 34: Storage of freshwater in the Canada Basin in late summer, re. 34.8 salinity. (Updated from Proshutinsky et al. 2009).....	40
Figure 35: Annual mean freshwater transport through Barrow Strait with trend line of slope m (mSv/y) and 95% confidence limits shown.	41
Figure 36: Temporal evolution of the total annual streamflow into Hudson Bay, 1964 - 2008. The thick line represents the 5-year running mean. The dashed line represents the linear trend for the overall 45-year period (Déry et al. 2011).	43
Figure 37: Present rate of post-glacial rebound (mm/y) from calculations using a glacial systems model (Tarasov and Peltier 2004).	43
Figure 38: Preliminary results from continuous GPS logging since the early 2000s (Herron et al. 2008).	44
Figure 39: Spatial pattern of the change in absolute sea level caused by melting of Greenland's ice cap. Red shading denotes areas of rising sea level and blue dropping sea level (Kopp et al. 2010).	45
Figure 40: Relative water level measured at the tide gauge at Tuktoyaktuk (Manson and Solomon 2007).	45
Figure 41: Monthly Relative Sea Level (RSL) Time Series for Alert and Ulukhaktok (Craymer et al. 2006).	46
Figure 42: Measurement programs in the Canada Basin and Canadian Arctic Archipelago.	46
Figure 43: Saturation state of seawater with respect to aragonite (Ω_A) and pH in the total scale (pH_{total}) in surface waters during the periods 1990 - 1999 and 2000 - 2011.	48
Figure 44: a) Temporal variability of saturation state in different water masses along Davis Strait from 2004 - 2010 and b) cross section of density (σ_θ) and aragonite saturation state (Ω_A).	49
Figure 45: Spatial distribution of (A) water temperature, (B) salinity, (C) $\text{NO}_3^- + \text{NO}_2^-$, and (D) in vivo chlorophyll a fluorescence in northern Hudson Bay, Hudson Strait and Foxe Basin on 1 - 13 September, 2005. Thin gray lines and dashed lines: surface mixed layer depth (Z_m); thick white lines and dotted lines: euphotic zone depth (Z_{eu}). Station locations are shown at the top of the figure (from Ferland et al. 2011).....	50
Figure 46: Variation in mean fork length of male charr caught on the Hornaday River over 18 years during the August fishery (Harwood 2009).....	54
Figure 47: Date of ice clearance in Amundsen Gulf and condition factor of Charr caught in the under-ice fishery at Tatik Lake (Harwood et al. 2013).....	54
Figure 48: Average body condition index of adult ringed seals sampled at Masoyak in June and July, 1992-2010 (Harwood et al. 2012).	55
Figure 49: Map of Mackenzie River Basin showing major rivers, 6 subbasins and important communities. Adapted from Mackenzie River Basin State of the Ecosystem report 2003 (MRBB 2004).	57
Figure 50: Monthly mean precipitation (a) and monthly mean air temperature (b) based on the NCEP data from 1988 to 2007 in the different basins (Tong et al. 2010).	59

Figure 51: Trends in (a) Maximum daily temperatures (°C) in winter and (b) increase in precipitation (mm/y) in the Mackenzie River Basin. Units refer to change in the 49 years between 1950 and 1998. Adapted from Mackenzie River Basin State of the Ecosystem Report 2003 (MRBB2004).	60
Figure 52: a) Representative Concentration Pathways as used for the IPCC AR5 (Moss et al. 2010). b) Comparison of projected warming in SRES and RCP scenarios (Roeglj et al. 2012).	68
Figure 53: Locations of the ACCASP subregions on each of the AR5-ESM models. Note that the models have different land masks. Color index: Beaufort Sea - light-blue, Canadian Polar Shelf - green, Baffin Bay - cyan, Hudson Bay - red.	69
Figure 54: Number of models available per grid point (left panel); ACCASP subbasins with multimodel areas (right panel).	69
Figure 55: Location of the ACCASP subbasins on the ARC grid (left panel, green = Sea, orange = Canadian Polar Shelf, brown = Baffin Bay) and on the NAM grid north of 35°N (right panel, Mackenzie River Delta region, green = Hudson Bay).	70
Figure 56: NAA-NEMO domain.	72
Figure 57: AR5-ESM multimodel mean sixty year change (difference between 1986 - 2005 and 2046 - 2065) of near surface air temperature for RCP8.5.	74
Figure 58: AR5-ESM multimodel mean annual cycles for 1986 - 2005, and 2046 - 2065 (RCP4.5 and 8.5).	74
Figure 59: AR5-ESM individual model, sixty year change (difference between 1986 - 2005 and 2046 - 2065), in TAS annual cycles at specific site locations (see text).	75
Figure 60: CanRCM4-ARC annual mean air temperature with bidecadal trends as well as a historical (1961 - 2005), a future fifty year (2012 - 2061), and a long term (1961 - 2100) trend for scenarios RCP4.5 and RCP8.5, averaged over the Arctic ACCASP subbasins. All trends are °C/decade. If marked with an asterisk, the trend is significant (on a 5% level).	75
Figure 61: Annual mean and bidecadal changes of surface air temperature in the Canadian Arctic as modelled by CanRCM4 for RCP8.5.	76
Figure 62: CanRCM-NAM annual mean air temperature with bidecadal trends as well as a historical (1961 - 2005), a future fifty year (2012 - 2061), and a long term (1961 - 2100) trend for scenarios RCP4.5 and RCP8.5, averaged over the ACCASP Hudson Bay subbasin. All trends are °C/decade. If marked with an asterisk, the trend is significant (on a 5% level).	77
Figure 63: Annual mean and bidecadal changes of air temperature (TAS, °C) over North America, as modelled by CanRCM-NAM for RCP8.5.	78
Figure 64: CanRCM4-ARC annual mean precipitation with bidecadal trends as well as a historical (1961 - 2005), a future fifty year (2012 - 2061), and a long term (1961 - 2100) trend for scenarios RCP4.5 and RCP8.5, averaged over the ACCASP subbasins. All trends are mm/day/decade. If marked with an asterisk, the trend is significant (on a 5% level).	79
Figure 65: Annual mean and bidecadal changes of precipitation (mm/day) over the Canadian Arctic as modelled by CanRCM4-ARC for scenario RCP8.5.	80
Figure 66: CanRCM4-NAM annual mean precipitation with bidecadal trends as well as a historical (1961 - 2005), a future fifty year (2012 - 2061), and a long term (1961 - 2100) trend for scenarios RCP4.5 and RCP8.5, averaged over the ACCASP Hudson Bay subbasins as shown in	

Figure 55. All trends are mm/day/decade. If marked with an asterisk, the trend is significant (on a 5% level).	80
Figure 67: Annual mean and bidecadal changes of precipitation (mm/day) over North America as modelled by CanRCM4-NAM for scenario RCP8.5.	81
Figure 68: Annual mean and bidecadal changes of windspeed squared (m^2/s^2) in the Canadian Arctic as modelled by CanRCM4-ARC for scenario RCP8.5.	81
Figure 69: CanRCM-NAM annual mean windspeed squared (m^2/s^2) with bidecadal trends as well as a historical (1961 - 2005), a future fifty year (2012 - 2061), and a long term (1961 - 2100) trend for scenarios RCP4.5 and RCP8.5, averaged over the ACCASP Hudson Bay subbasin as shown in Figure 55. All trends are $^{\circ}C/decade$. If marked with an asterisk, the trend is significant (on a 5% level).	82
Figure 70: Annual mean and bidecadal changes of windspeed squared (WSS) (m^2/s^2) over North America as modelled by CanRCM for scenario RCP8.5.	82
Figure 71: Bidecadally, annually and spatially averaged, AR5-ESM multimodel mean values for RCP4.5 (thin line) and RCP8.5 (thick line) for the Canadian Arctic subbasins: Beaufort Sea, Canadian Polar Shelf, Baffin Bay and Hudson Bay. Variables shown are: sea surface temperature (T_s) and salinity (S_s), maximum mixed layer depth (Z_m), sea ice concentration, (SIC) surface nitrate (NO_3), pH, and primary production (PP).	87
Figure 72: Bidecadally averaged, individual model results and multimodel means for RCP8.5: spatially averaged values for the Beaufort Sea (upper panel) and Canadian Polar Shelf (lower panel). Variables include: sea surface temperature (T_s) and salinity (S_s), maximum mixed layer depth (Z_m) and sea ice concentration (SIC). Averages are for annual means (ann, circles), March (mar, downward pointing triangles) or September (sep, upward pointing triangles). Solid lines are multimodel means, error bars are overplotted.	88
Figure 73: AR5-ESM multimodel differences (left panel) and standard deviation (right panel) for T_s , S_s , Z_m , SIC, NO_3 , pH, PP under RCP8.5 scenario forcing for 2045 - 2065 minus 1986 - 2005.	91
Figure 74: Simulated and observed ocean temperature (T), salinity (S), Ω_C , Ω_A , DIC, and TA_35 profiles from AR5-ESMs at $140^{\circ}W$, $75^{\circ}N$ for 1986 - 2005 (left panel), simulated profiles for 2046 - 2065 for all models (middle panel), and multimodel mean change as indicated in the legend (right panel).	92
Figure 75: Simulations with the NAA-NEMO model for surface temperature T_s , salinity S_s , sea ice concentration SIC, and thickness SIT. Shown are the historical mean (1971 - 2000) and a projected mean (2041 - 2070) as well as the difference between both time periods on the right hand side.	95
Figure 76: Time series of NAA-NEMO modeled variables averaged over the BS (a), CPS (b) and BB (c) subbasins. Each subfigure shows upper left and right panels: T_s and S_s . Lower left and right panels: SIC and SIT. Bidecadal means are included.	96
Figure 77: AR5-ESM multimodel averaged plots for September SIC under RCP4.5 scenario forcing. From left to right: difference (2045 - 2065 minus 1986 - 2005), standard deviation, 1986 - 2005 mean, 2045 - 2065 mean.	102
Figure 78: NAA-NEMO annual ice transport through Davis Strait (mSv).	103

Figure 79: Bidecadally, annually averaged, individual mean and multimodel mean time series for scenario RCP8.5 for the BS (a) and CPS (b) regions for surface nitrate, sea water pH, and primary production and Ω_A	105
Figure 80: Mean simulated pH at the surface for the historical period (1986 - 2005) and future period (2066 - 2085) with the emission scenario RCP8.5 with three ESMs (IPSL-CM5A-LR, CanESM2, MPI-ESM-LR).	108
Figure 81: Mean simulated dissolved inorganic carbon (DIC) concentration (mol m^{-3}) at the surface for the historical period (1986 - 2005) and future period (2066 - 2085) for RCP8.5 with three ESMs (IPSL-CM5A-LR, CanESM2, MPI-ESM-LR).	109
Figure 82: Projected change in annual mean air temperature from (1961 - 1990) to (2041 - 2070) (a) CCCSN (2009) mean ensemble analysis from the IPCC AR4 (2007) modelling assessment for Canada contributed by 24 international modelling centres. (b) Mean model results from two recent versions of the OURANOS Canadian Regional Climate Model (CRCM).	113
Figure 83: Projected change in mean winter air temperature from (1961 - 1990) to (2041 - 2070) (a) CCCSN (2009) mean ensemble analysis from the IPCC AR4 (2007) modelling assessment for Canada contributed by 24 international modelling centres. (b) Mean model results from two recent versions of the OURANOS Canadian Regional Climate Model (CRCM).	114
Figure 84: Projected change in mean summer air temperature from (1961 - 1990) to (2041 - 2070). (a) CCCSN (2009) mean ensemble analysis from the IPCC AR4 (2007) modelling assessment for Canada contributed by 24 international modelling centres. (b) Mean model results from two recent versions of the Canadian Regional Climate Model (CRCM).	115
Figure 85: CanRCM-NAM annual mean air temperature with bidecadal trends as well as a historical (1961 - 2005), a future fifty year (2012 - 2061), and a long term (1961 - 2100) trend for scenarios RCP4.5 and RCP8.5, averaged over the Mackenzie River Basin as shown in Figure 55. All trends are $^{\circ}\text{C}/\text{decade}$. If marked with an asterisk, the trend is significant (on a 5% level). 115	
Figure 86: Projected percentage change in annual precipitation from (1961 - 1990) to (2041 - 2070). (a) CCCSN (2009) mean ensemble analysis from the IPCC AR4 (2007) modelling assessment for Canada contributed by 24 international modelling centres. (b) Mean model results from two recent versions of the Canadian Regional Climate Model (CRCM).	116
Figure 87: Same as Figure 85 but for annual mean precipitation (mm/day).	117
Figure 88: Same as Figure 85 but for annual mean windspeed squared (m^2/s^2).....	118
Figure 89: (a) Current lake surface-water temperatures in Canada based on multiple-regression Model 1. (b - d) Predicted future lake surface-water temperatures in Canada based on multiple-regression Model 2 and climate-change scenarios CGCM2-IS92a, A2 and B2 in July 2100 (Sharma et al. 2007).	120

ABSTRACT

Steiner, N., Azetsu-Scott, K., Galbraith, P., Hamilton, J., Hedges, K., Hu, X., Janjua, M.Y., Lambert, N., Larouche, P., Lavoie, D., Loder, J., Melling, H., Merzouk, A., Myers, P., Perrie, W., Peterson, I., Pettipas, R., Scarratt, M., Sou, T., Starr, M., Tallmann, R.F. and van de Baaren, A. 2013. Climate change assessment in the Arctic Basin Part 1: Trends and projections - A contribution to the Aquatic Climate Change Adaptation Services Program. Can. Tech. Rep. Fish. Aquat. Sci. 3042: xv + 163 pp.

Within the Aquatic Climate Change Adaptation Services Program (ACCASP), past trends and future projections of key climatic variables such as air and water temperature, precipitation, winds and storms, sea ice and biogeochemical variables are assessed. The assessment forms the basis for the impact, vulnerabilities, and opportunities analysis needed to increase our understanding of the impacts of climate change on the marine ecosystem and departmental operations and enable adaptation in support of DFO's strategic outcomes. This report summarizes observed trends and projections on a 50-year timescale for the Arctic region, including the four marine basins of the Beaufort Sea, Canadian Polar Shelf, Baffin Bay/Davis Strait and Hudson Bay as well as the predominately terrestrial Mackenzie Basin. To evaluate past trends, national and international data archives (which include land-based station data and cruise data) as well as publications, reports, and earlier assessments have been used. Limited observations in the Arctic, especially for ecosystem variables, lead to significant gaps and limitations in the assessment. Future projections are mostly derived from global models, which give a general tendency and range of expected future changes, but lack local details. Most regional modelling efforts are limited to the atmosphere. Those have been included for higher resolution projections of air temperature, precipitation and wind. Only a few models are available on the aquatic basin scale that simulate ocean properties and sea ice. The main outcomes of the assessment show significant increases in air temperature (0 - 3°C in summer and 3 - 7°C in winter over the next 50 years), a slight increase in precipitation and snow depth as well as an intensification in extreme events (hot spells, extreme precipitation). With respect to atmospheric circulation patterns, appreciable changes have been observed. Projections suggest an increase in storm strength and size (storm surges and coastal erosion) as well as a slight increase in wave heights with only small changes in windspeed. An Arctic-wide decrease in the extent of multi-year ice has been observed, together with an increase in ice-free waters in summer (longer time periods and larger areas). These observed sea ice trends are projected to continue into the future. It can be anticipated that the longer open water period will allow wind and storms to have a greater impact on the coast, i.e. erosion. Limited observations of ocean properties show local freshening (e.g. Beaufort Sea) and summer warming (e.g. Baffin Bay). These trends are projected to continue along with localized strengthening in stratification. Increased ocean acidification has been observed and is projected to continue throughout the Canadian Arctic, leading to decreased saturation states of calcium carbonate (aragonite and calcite). Within the Mackenzie Basin, increased lake temperatures and stratification, as well as later freeze/earlier break-up dates have been observed and are projected for lakes. A widespread warming of terrestrial permafrost and thickening of the permafrost active layer has been observed, as well as a slow warming of sub-sea permafrost. Again, this pattern is likely to continue in the future. Changes expected for the next 10 years may in some cases be proportional to the 50-year projections. However, in most instances, natural intra-decadal variability is expected to be at least as important as the overall trends during the next decade. A continuation of the past decade's trends is expected in the case of ocean acidity, surface air temperature, multi-year ice extent, first-year ice characteristics, storm waves, and permafrost. The assessment concludes

that to improve our capability to assess and project climate change adaptation in aquatic ecosystems, more consistent data sets are needed, especially over marine areas and for biogeochemical variables. Higher resolution basin-scale ocean ecosystem models are also required to provide locally applicable projections relevant for Arctic communities and DFO management.

RESUMÉ

Steiner, N., Azetsu-Scott, K., Galbraith, P., Hamilton, J., Hedges, K., Hu, X., Janjua, M.Y., Lambert, N., Larouche, P., Lavoie, D., Loder, J., Melling, H., Merzouk, A., Myers, P., Perrie, W., Peterson, I., Pettipas, R., Scarratt, M., Sou, T., Starr, M., Tallmann, R.F. and van de Baaren, A. 2013. Climate change assessment in the Arctic Basin Part 1: Trends and projections - A contribution to the Aquatic Climate Change Adaptation Services Program. Can. Tech. Rep. Fish. Aquat. Sci. 3042: xv + 163 pp.

Dans le cadre du Programme des services d'adaptation aux changements climatiques en milieu aquatique (PSACCMA), les tendances passées et les projections pour l'avenir des paramètres clés tels que la température de l'air et de l'eau, précipitation, vents et tempêtes, glace de mer et variables biogéochimiques sont évalués. Cette évaluation constitue la base de l'analyse nécessaire des effets, des vulnérabilités et des possibilités pour améliorer notre compréhension des impacts du changement climatique sur l'écosystème marin et permettre l'adaptation en vue d'appuyer les résultats stratégiques du MPO. Ce rapport donne un aperçu des tendances observées et des projections sur une échelle de temps de 50 ans pour la région de l'Arctique, y inclut les quatre bassins marins, c'est-à-dire la mer de Beaufort, le plateau continental polaire canadien, la baie de Baffin/détroit de Davis et la baie d'Hudson ainsi que le bassin surtout sec du Mackenzie. Afin d'évaluer les tendances passées, des archives de données informatiques nationales et internationales (y compris des données provenant de stations terrestres et de croisières) ainsi que des publications, rapports et évaluations antérieures ont été utilisés. Le nombre limité d'observations dans l'Arctique surtout pour les variables écosystémiques entraîne des limites et lacunes importantes dans l'évaluation. Les projections pour l'avenir proviennent pour la plupart de modèles globaux, qui signalent les tendances et la portée à grande échelle des changements attendus à l'avenir mais sont insuffisants par rapport à l'information locale. La modélisation régionale s'articule surtout sur l'atmosphère. Ceux-ci ont été inclus pour les projections à plus haute résolution de la température de l'air, de la précipitation et du vent. Il existe seulement quelques modèles qui se concentrent sur la simulation des caractéristiques océaniques et de glace de mer à l'échelle de bassin aquatique. Les résultats principaux de l'évaluation font apparaître une hausse marquée de la température de l'air observée et prévue (0 - 3°C en été et 3 - 7°C en hiver sur les 50 prochaines années) ainsi qu'une légère augmentation de la précipitation et de la profondeur de neige. Quant aux modes de circulation atmosphérique, des changements notables ont été observés. Une augmentation de l'étendue et de l'intensité des tempêtes (ondes de tempêtes et érosion côtière) de même qu'une légère augmentation des hauteurs de vagues avec seulement de moindres changements de la vitesse du vent est prévue. Une réduction de l'étendue de la glace pluriannuelle dans l'ensemble de l'Arctique a été observée ainsi qu'une augmentation des eaux libres de glace en été (plus grandes périodes de temps et étendues). Ces tendances de glace de mer observées se poursuivront à l'avenir. Des observations restreintes des propriétés de l'océan indiquent la dessalure des eaux locales (p. ex. la mer de Beaufort) et le réchauffement d'été (p. ex. la baie de Baffin). Ces tendances se poursuivront ainsi que l'intensification localisée de la stratification. L'augmentation de l'acidification de l'océan a été observée et se poursuivra dans l'ensemble de l'Arctique canadien, ce qui provoquera une chute de l'état de saturation d'aragonite et de calcite. Dans le bassin du Mackenzie, une hausse des températures, de la stratification, des débâcles plus tôt et englacement plus tard ont été observés et sont prévus pour les lacs. Un réchauffement répandu du pergélisol terrestre et l'épaississement de la couche active du pergélisol ont été observés ainsi qu'un lent réchauffement du pergélisol sous marin. Encore une fois, cette tendance est susceptible de

persister dans l'avenir. Les changements prévus pour les dix prochaines années peuvent, dans certains cas, être proportionnels à la projection de 50 ans. Toutefois, dans la plupart des cas, on s'attend à ce que la variabilité naturelle intra-décennale soit au moins aussi importante que les tendances générales au cours de la prochaine décennie. Les tendances de la dernière décennie devraient se poursuivre dans le cas de l'acidité des océans, température de l'air à la surface, étendue de la glace pluriannuelle, caractéristiques de la glace de première année, ondes de tempête et le pergélisol. Cette évaluation conclut que des ensembles de données plus cohérentes sont nécessaires pour améliorer notre capacité d'évaluer et de prévoir l'adaptation au changement climatique des écosystèmes aquatiques en particulier pour les zones marines et les variables biogéochimiques. Également des modèles écosystème-océan à plus haute résolution sur l'échelle bassin sont nécessaire pour fournir des projections locales qui s'appliquent aux communautés de l'Arctique et à la gestion du MPO.

1: INTRODUCTORY MATERIALS

1.1 GENERAL INTRODUCTION

As part of a broader federal strategy, Fisheries and Oceans Canada (DFO) received funding from the Aquatic Climate Change Adaptation Services Program (ACCASP; 2011 - 2016) in order to integrate climate change considerations into the mainstream of decision-making for the delivery of DFO Departmental programs and policies. The ACCASP will assess regional threats and risks and foster the development of applied science-based tools and research projects to increase our understanding of the impacts of climate change and enable adaptation in support of DFO's strategic outcomes. One of the primary objectives of the program is to assess the risks that climate change poses to the delivery of DFO's mandate within four defined Large Aquatic Basins (LABs), namely the Arctic, Pacific, Freshwater and Atlantic. The current report focuses on likely the most diverse of those basins: the Arctic. To facilitate the assessment, the Arctic LAB has been further divided into five subbasins: Beaufort Sea, the Canadian Polar Shelf (or Canadian Arctic Archipelago for terrestrial purposes), Baffin Bay/Davis Strait, Hudson Bay and the Mackenzie Basin. The regional coverage of each subbasin is indicated in Figure 1.

The objectives of this report, which were prepared at the beginning of the ACCASP, are to examine key climatic variables such as air and water temperature, precipitation, wind and storm patterns, sea ice conditions, freshwater input and stratification as well as biogeochemical variables (e.g. primary production, pH, nutrients); to assess available observations with respect to recent (~10 y) and longer term (30 – 50 y) trends, and to evaluate available model projections on 10 and 50 y time scales. Four of the Arctic subbasins are marine basins, while one (the Mackenzie basin) is a terrestrial basin. The latter is hence treated separately and includes analysis of changes in freshwater systems such as rivers and lakes. Results of this report provide input and support for an ongoing impacts, vulnerabilities, and opportunities (IVO) analysis. The latter includes risks for ecosystems and fisheries, potential endangered species listings, effects on infrastructure, search and rescue (SAR), and safe shipping.

A variety of sources and types of trends information have been used in the assessment; namely DFO internal and other national or international data archives including station data, land based data and cruise data. The data sets are generally very limited in space and time. It has been agreed that a minimum of 10 years of data should be available to allow any kind of trend assessment. Given the extreme sparsity of data in the Arctic, especially in ocean areas, a time period of 10 years is in fact still too short. In addition to observations, results from earlier reports on variability and trends, e.g. Natural Resources Canada (NRCan) or Environment Canada (EC), DFO Zonal Monitoring Programs (ZMPs), Ecosystem Status and Trends Report (ESTR), and State of the Ocean Reporting (SOTO) have been used as sources of information as well as international publications, reports and assessments, e.g. Intergovernmental Panel on Climate Change 4th and 5th Assessment Reports (IPCC AR4,5), Arctic Council Arctic Monitoring and Assessment Program (AMAP) Assessments, and US Climate Change Science Program Reports (US CCSP).

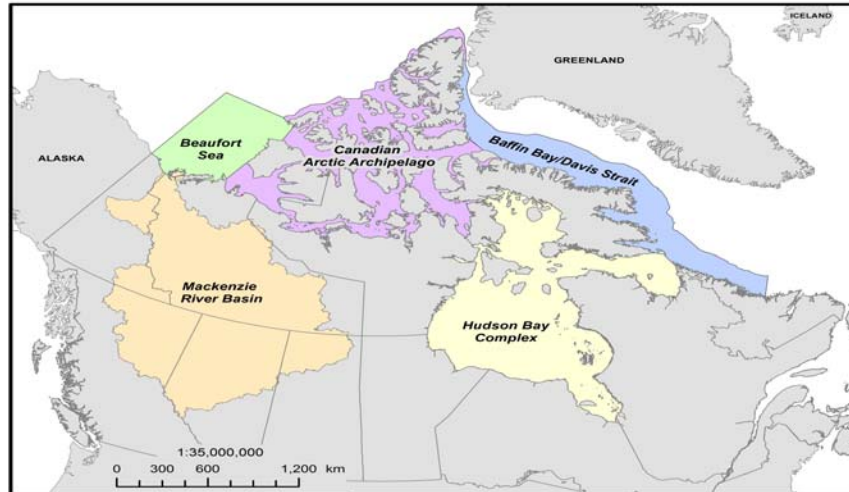


Figure 1: Map of the Arctic Large Aquatic Basin (LAB) as defined by the Aquatic Climate Change Adaptation Services Program (ACCASP). The Arctic LAB is divided into five sub-basins: Beaufort Sea, Canadian Arctic Archipelago, Baffin Bay/ Davis Strait, Hudson Bay Complex, and Mackenzie River Basin.

Sources and types of projection information are described in more detail in Section 3.1. To summarize briefly, they include:

- Global Climate Models (GCMs) or Earth System Models (ESMs), which generally have limited resolution and complexity.
- Regional Climate Models (RCMs) that downscale GCM or ESM simulations to continental and subcontinental scales. At this point in time those models are mostly limited to the atmosphere. Main sources used are data provided via the North American Regional Climate Change Assessment Program (NARCCAP), which provides output from multiple models but has only an incomplete coverage of the Arctic; as well as via the more recent Coordinated Regional Downscaling Experiment (CORDEX) which includes a domain that fully covers the Arctic but at the time of the analysis contained limited data.
- Regional model output from the OURANOS Consortium on Regional Climatology and Adaptation to Climate Change, again with limited coverage of the Arctic and limited to one model.
- Aquatic basin and subbasin scale models. The latter are still at an early stage of development and output was only available for physical ocean properties and sea ice (e.g. from the University of Alberta and the Bedford Institute of Oceanography (BIO)).

However, both international publications, reports and assessments have been reviewed to extract additional projection information. The assessment includes projections on 10 and 50 year timescales. However, both projection time periods have limitations and require somewhat different approaches. On short term (10 y) timescales, natural variability may be as important as anthropogenic change, i.e. some tendencies for changes might be similar to the 50-year ones, but natural multi-year to multidecadal variability can be expected to be as or more important for some variables in some regions during the next decade. In this case, we need to rely on recent observed variability and trends with consideration of larger-scale projections. On the longer term (50 y) anthropogenic change will generally become more dominant. Here we need to rely

on a combination of observed trends and variability, understanding of processes involved, and available models of various form (e.g. GCM and RCM projections, which do not resolve natural variability on scales of years to a decade).

Based on the information summarized in this report a set of trends and projections summary tables has been created in support of an initial risk assessment. The results thereof are published in the Arctic LAB Canadian Science and Advisory Secretariat (CSAS) Science Response Report (SRR, DFO2013).

1.2 GENERAL OCEANOGRAPHY

1.1.1 Beaufort Sea

The Beaufort Sea occupies the southern to eastern segment of the Canada Basin and adjacent areas of continental shelf. Its boundaries are a chord joining Point Barrow to Prince Patrick Island, a line across the mouth of M'Clure Strait, Banks Island, a line across the mouth of Amundsen Gulf, and the mainland coast of North America. Continental shelves less than 100-m deep exist along about 100 - 200 km of most of its southern-to-eastern margin. The shelf break is at about 400-m depth seaward of Amundsen Gulf and M'Clure Strait. The remainder is the Canada Basin, reaching a depth of 3600 m on the north-western margin.

The general circulation in the deep part of the Beaufort is a clockwise gyre which carries sea ice and surface water down from the north-east and out to the west at an average speed of 5 - 15 cm/s. Over the continental slope, there is an under-current in the opposite direction below 50 - 100 m depth that reaches similar speed; the upper part of this current carries water of Pacific origin eastward from Point Barrow, while the lower part is a continuation of the Arctic boundary current that carries water of Atlantic origin counter-clockwise around the Arctic from the Barents Sea. The circulation on the shallow continental shelves is strongly influenced by wind and varies seasonally; persistent easterly wind in spring and autumn drive shelf waters rapidly westward, whereas weaker and more variable wind in winter and summer have less net impact and may in some years cause flow to the east. Run-off from the North American mainland, primarily via the Mackenzie River creates a stable cap over shelf waters of the Beaufort in summer, which has an important impact on primary production and the ecosystem.

These interleaved flows establish a distinctive vertical variation of temperature, salinity and dissolved nutrients in the Beaufort. Centred near 400 m depth is a thick layer of warm saline (0.5°C, 35 ppt) water from the Atlantic. Above this layer, salinity decreases steadily to values near 31 ppt at about 40 m depth. However, temperature decreases much more quickly with depth to create a zone of approximately constant low temperature (-1.5°C) within the halocline; this layer is maintained by inflow from the Pacific reaching the Beaufort in winter. With nutrients acquired via regeneration from the seabed of the Chukchi Sea, this flow maintains nutrient maxima at about 125 m depth in the Beaufort. Between about 100 and 40 m depths, there is a warmer (0°C) layer that is maintained by inflow from the Pacific that reaches the Beaufort in summer. Properties of the topmost 40 m vary greatly with season, location, ice cover and weather events in the Beaufort. In general terms, the surface layer is appreciably thinner in the summer (5 - 15 m) than in the winter (25 - 50 m), warmer (0 - 10°C versus -1.6°C) and of lower salinity. Salinity is low both near the Mackenzie Delta and within the Beaufort gyre in summer, whereas in winter, shelf salinity can become quite high though ice growth and upwelling.

1.1.2 Canadian Polar Shelf

The Canadian Polar Shelf is a vast shallow area with many islands. From the terrestrial perspective, it is often referred to as the Canadian Arctic Archipelago (CAA). The area of the shelf is about 2.8 million square kilometres. Since islands cover 48% of this area, there are 1.5 million square kilometres of ocean, 50% more than in the Hudson and James Bays. The Canadian Polar Shelf has been depressed by the weight of ice during the Quaternary and scoured by glaciers; with the resulting marine topography being a pattern of basins separated by sills. There is a line of sills at about 350 m along the edge of the Canada Basin and a cluster at about 80 - 150 m depth near the centre of the archipelago. The intervening basins reach about 600 m depth. The deepest pathway across the shelf is via Nares Strait, where the limiting sill is 220 m deep.

The Canadian Polar Shelf provides an oceanic connection between the Arctic Ocean and the Atlantic. The pattern of circulation is complicated with flows entering from and leaving both bounding reservoirs. This pattern is a consequence of three factors: 1. the density of water increases appreciably from surface to sill depth, so that the currents are quite narrow (10 - 20 km, controlled by the internal Rossby scale); 2. the channels between islands are at least several times wider (30 km and up), so that opposing currents can flow on the two sides of a channel; and 3. external pressure forces water from the Arctic to Baffin Bay, while internal pressure gradients created via tidal mixing near the central sills drive flow from the opposite direction. Water from Baffin Bay has been identified via hydrographic measurements well over halfway to the Arctic Ocean.

Tides are much stronger over the eastern and central parts of the Canadian Polar Shelf than in the Arctic Ocean. The Canadian Polar Shelf is the place where a strong tidal wave incoming from the Atlantic meets an Arctic tidal wave, originally also from the Atlantic, but seriously weakened by friction during its journey to the Beaufort. The contrast creates large sea-level differences at tidal frequency across the polar shelf, and these create a strong tidal current.

The net effect of flows and counter-flows through the CAA is a net movement of seawater from the Arctic to Baffin Bay at about 1.5 Sv ($10^6 \text{ m}^3 \text{ s}^{-1}$) per year. Consequently, the waters of the Canadian Polar Shelf on first glance look like those of the Canada Basin. It is clear on closer examination that the deep water is cooler and less saline than that at the same depth to the west, because the basins are filled with water capable of passing over the shallow intervening sills; the halocline is warmer, because tidal mixing on the shelf diffuses heat upwards from warmer deep waters and the surface salinity is higher because the archipelago is a desert (very low run-off) and mixing diffuses salt upwards from more saline deep waters. The latter effect, in combination with the lower salinity of bottom water entering from Baffin Bay (34.5 versus 34.85 ppt), reduces the density stability of waters over the Canadian Polar Shelf.

Enhanced mixing by tides maintains polynyas (areas of much reduced ice cover in winter) and contributes to biological hotspots at special locations on the polar shelf. These occur on scales from kilometres (in Penny Strait, for example), to tens of kilometres (in Cardigan Strait and Fram Sound, for example). Polynyas on hundred-kilometre scales also exist on the Canadian Polar Shelf (in Amundsen Gulf, Lancaster Sound and northern Baffin Bay, for example) but these are attributable to energy from wind, rather than tide.

The ice cover over most of the Canadian Polar Shelf is distinctive in being fast (locked in position) for 6 - 9 months per year. The ice edges, when mobile pack separates from fast ice, are the discontinuities that enable prevailing wind to create polynyas and the important ecological consequences that arise from them. The northern part of the Canadian Polar Shelf is also distinctive in a high year-round presence of multi-year ice. It is possible that this area may be the final Arctic reservoir for multi-year ice in a warming climate.

1.1.3 Baffin Bay/Davis Strait

Baffin Bay and Davis Strait comprise the large basin between Nunavut's Baffin Island and Greenland. The basin is part of the marine connection between the Arctic and Atlantic Oceans. Baffin Bay is a large semi enclosed basin with a maximum depth of approximately 2,500 m that extends southward into Davis Strait. The area of Baffin Bay is about 1,400 by 550 km with a large abyssal plain in the central region having depths in excess of 2,300 m. The bathymetry of Baffin Bay is unique among Arctic Seas; the Bay has a relatively isolated body of deep polar water, with shallow shelves both on the North and South. The continental shelf off Baffin Island is relatively narrow compared to the Greenland side. Both shelves are deeply cut by canyons running across the shelf (Tang et al. 2004). The Baffin Bay-Davis Strait sub-region spans more than 1.1 million square kilometres.

Baffin Bay is distinguished by cyclonic circulation and its isolated deep water (Tang et al. 2004). Both Pacific and Atlantic origin water mass properties are evident in northern Baffin Bay (Jones et al. 2003). Water circulation in Baffin Bay is strongly affected by counter-clockwise flowing currents. Northward flow on the eastern side of Baffin Bay-Davis Strait consists of the fresh West Greenland Current (WGC), which is of Arctic origin, on the shelf and the warm, salty West Greenland Slope Current (WGSC), which is of North Atlantic origin, on the slope. The WGC is a mixture of deeper Arctic Ocean outflows combined with warmer water from the North Atlantic and the Irminger Sea commonly referred to as Irminger Water (Tang et al. 2004; Myers et al. 2009). The WGC follows the continental slope off West Greenland and travels through Davis Strait into the Baffin Bay.

Arctic Ocean water enters Baffin Bay through three passages with shelf depths less than 250 m. Canadian Arctic Archipelago (CAA) flow enters Northern Baffin Bay through Nares Strait, Jones Sound and Lancaster Sound. Arctic Ocean waters flow southward along Baffin Island through Davis Strait (on its western side) as the broad, surface-intensified cold Baffin Island Current (BIC) (Tang et al. 2004; Stein 2004; Cuny et al. 2005). A weak nutrient maximum in the region indicates the presence of Pacific-origin water in the upper 50 to 60 m. The temperature maximum is much warmer and occurs at a much lower salinity than the equivalent maximum that is observed in the Canada Basin, indicating the presence of Atlantic-origin waters that have followed a different pathway (Carmack and MacLaughlin 2011). Nutrient regeneration is evident in waters below 500 m in the Baffin Bay subbasin (Jones et al. 1984; Carmack and MacLaughlin 2011). The net Baffin Bay outflow combines CAA flows, river runoff, sea ice, and inputs from Greenland and the North Atlantic. Flow through Davis Strait forms a complicated circulation pattern. Topographically-steered bifurcations in the southward flowing BIC and the northward flowing WGC in Davis Strait result in a pronounced thermohaline front. This front is also evident in oxygen saturation, separating the weakly-ventilated Baffin Basin from the highly-ventilated Labrador Basin. Upon reaching the sill the inner portion of the BIC continues

southward, joining the outer portion of the WGC that turns back on the southeastern side of the sill at Davis Strait; together, they form the south-flowing Labrador Current. The outer portion of the BIC turns eastward and then northward, joining the inner portion of the WGC that crosses the sill at Davis Strait (Carmack and MacLaughlin 2011). Recent interest in Baffin Bay arises from its role in Arctic Ocean-North Atlantic interaction. The pan-arctic system is tightly connected to the subarctic by through-flowing Atlantic and Pacific water masses (Carmack and MacLaughlin 2011). Changes in Arctic ice-cover and marine ecosystems are also linked to the global system, especially the bordering subarctic Pacific and Atlantic areas. Therefore, changes within Baffin Bay cannot be understood in regional isolation.

Baffin Bay is dominated by first-year ice with a strong seasonal cycle, with ice extent covering approximately $1.4 \times 10^6 \text{ km}^2$ during its maximum in February or March, but decreasing to near zero during August and September (Meier et al. 2006). Ice extent is correlated with winter air temperature, with cold winters having high ice extent, and vice versa (Tang et al. 2004). In the north Baffin region, sea ice begins to form in autumn, with complete freeze-up by early winter. The ocean remains frozen throughout the winter, until leads begin to form, approximately in April, and in July ice begins to break up (Gearheard et al. 2006). During the ice season, there is always more ice in the western than the eastern half of Baffin Bay due to the inflow of the relatively warm WGC. From April to August, the ice area decreases, starting along the Greenland coast and in the North Water (Tang et al. 2004). Freeze-up in north western Baffin Bay has developed as early as the last week of August and been delayed until the middle of October. Ice thickness is variable in the region; ice formed in newly opened leads can acquire a thickness of half a meter during the winter and older ice can attain a thickness of 1.2 m. The ice in Baffin Bay is a combination of first year medium (0.7 - 1.2 m), first year thin (0.3 - 0.7 m), young ice (0.1 - 0.3 m) and new ice (0 - 0.1 m), with first year ice being dominant (Tang et al. 2004). Thick first year (>1.2m) and old ice are also found in Baffin Bay, particularly late in the season. The CIS Sea Ice Climatic Atlas (at <http://www.ec.gc.ca/glaces-ice/>) shows old ice is often the predominant ice type in the summer. About 95% of icebergs in the northern latitudes originate on Greenland (mostly western Greenland) where they flow directly into Baffin Bay (Tang et al. 2004) or remain trapped in the fjords where they originated (Diemand 2001). Icebergs originating from eastern Greenland are also carried into the WGC and move towards northern Baffin Bay. Some icebergs remain in Baffin Bay for years, circulating north along the Greenland coast and then south along Baffin Island. However, many of them escape southward through Davis Strait and drift down the Labrador coast in the cold Labrador Current.

1.1.4 Hudson Bay

Hudson Bay is connected to the Labrador Sea and the Atlantic through Hudson Strait (HS) which has a mean depth of 300 m and a maximum depth of 900 m (Saucier et al. 2004; Straneo and Saucier 2008) and is an area of intense mixing driven by three major surface currents: a flow of Labrador Sea (Atlantic) water entering northwestward toward the Arctic Archipelago and Foxe Basin, a more intense current from Hudson Bay outflowing southeastward, and a strong cross-channel flow in the eastern half of the Strait. Strong tidal currents enhance the mixing, affecting vertical stratification of the water column, surface nutrient concentrations, and biological production processes in the area (Ferland et al. 2011). A more extensive description of the oceanographic features of Hudson Bay can be found in Chapter 5 of Stewart and Lockhart (2005).

2: STATUS AND TRENDS

2.1 ATMOSPHERIC FORCING

2.1.1 Air temperature

Beaufort Sea: Long series of weather observations in the Beaufort region all come from stations on land; there are no prolonged observations from the marine area. It is the stations at the coast that have the greatest relevance to conditions offshore. There are four coastal stations in the Beaufort area with records spanning the last 50 years: Tuktoyaktuk starting in 1948, Sachs Harbour in 1955, Cape Parry in 1956 and Holman Island in 1953.

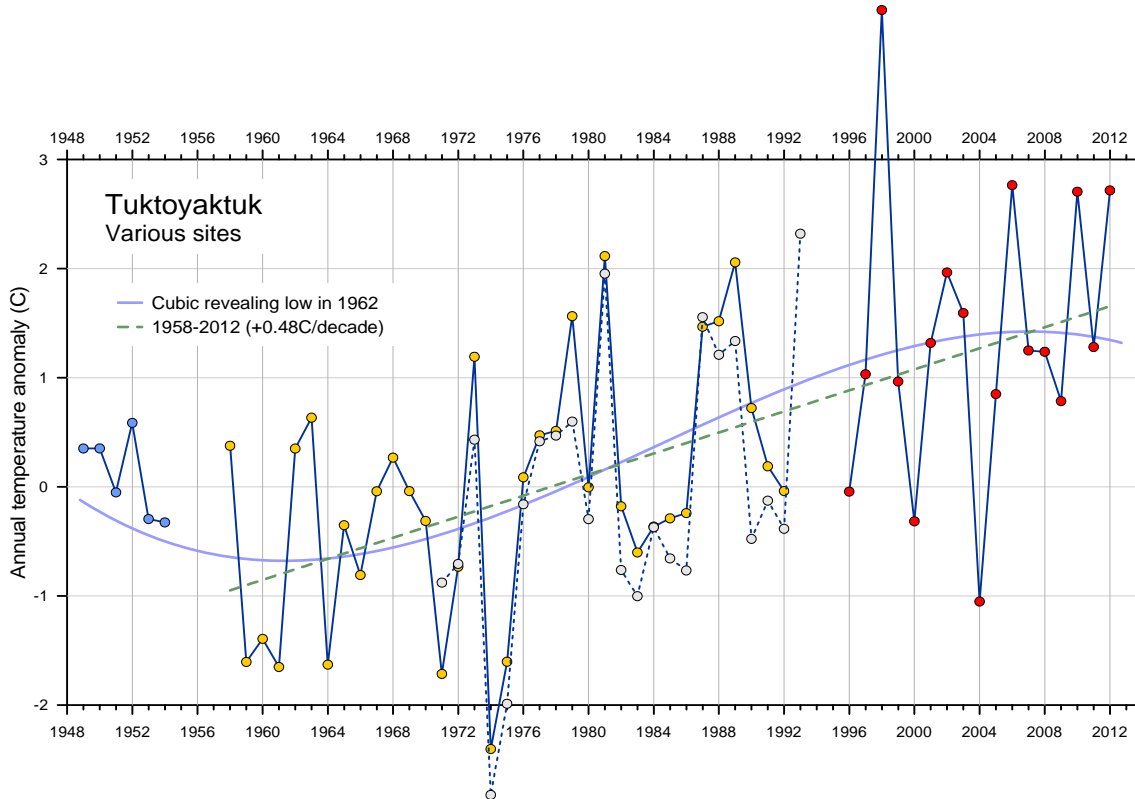


Figure 2: Anomaly (re 1948 - 2000) in annual mean temperature at Tuktoyaktuk on the Beaufort coast. Data come from different locations in the village at different times (<http://climate.weatheroffice.gc.ca/>).

Figure 2 displays the 64-year record from Tuktoyaktuk. This record starts early enough to capture the end of the 1930s warm period in the Arctic, which is best documented in records from the Atlantic sector (Wood et al. 2010). According to Wood et al. (2010), the warming in the 1920s and 1930s occurred in the Atlantic sector, and in contrast, the largest surface air temperature (SAT) anomalies in Alaska and western Canada occurred in the early 1940s and were associated with a severe El Nino event. The temperature reached a minimum at Tuktoyaktuk in the early 1960s. Since the mid 1960s Tuktoyaktuk has been warming at 0.5°C per decade, for a total change of about 2.5°C . However, the net change since the 1940s has been only about 1.5°C . The data from Tuktoyaktuk possibly indicates a decline in the rate of warming since 2000.

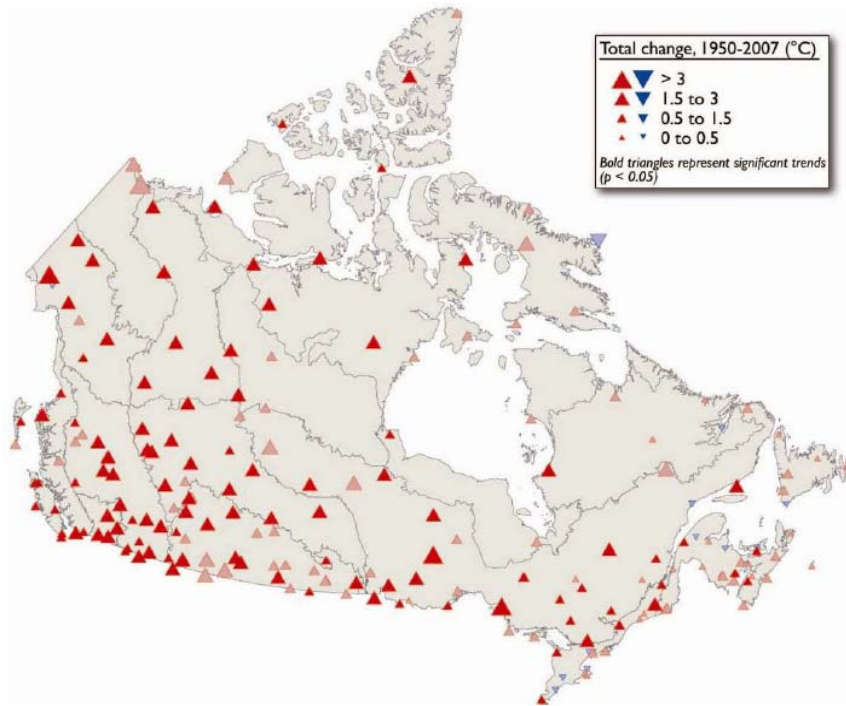


Figure 3: Change in mean annual temperature, 1950 - 2007 (Figure 1 from Zhang et al. 2011).

Figure 3 summarizes temperature changes across Canada calculated during the 1950 - 2007 interval (Zhang et al. 2011). Symbols plotted for stations in the Beaufort Hinterland (Komakuk, Aklavik, Inuvik, Cape Parry, Sachs Harbour) indicate 57-year temperature increases comparable to those at Tuktoyaktuk. However, only those trends at Inuvik and Cape Parry are significant at a 5% significance level. Although annual trends in the Beaufort Sea area are about 1.5 – 3 °C/decade and not significant; in winter, trends are >3 °C/decade and significant (Zhang et al. 2011).

Extrapolating this result over the adjacent ocean is not straightforward. The terrestrial and marine environments differ greatly in terms of substrate (land, vegetation, snow, ice and water), sky conditions and seasonality. Because an ice cap on the ocean inhibits transfers of heat and moisture to the overlying atmosphere, winter is the season when the Arctic Ocean most resembles land in the Arctic. Air temperature trends at Tuktoyaktuk calculated separately for the winter (ONDJFMA) and summer (JJAS) months are quite different, at 0.6 and 0.3°C per decade respectively. Because the strongest warming has occurred in those months when the offshore microclimate is most similar to that onshore, it is reasonable to presume that the 5-decade change in SAT offshore has been similar to that at the coast.

Figure 2 clearly illustrates the broad span of interannual variation in SAT at Tuktoyaktuk – about 7°C. Moreover, the annual anomalies come in clusters, alternating warmer and cooler intervals of several years duration. Because this interdecadal variability exceeds by several times the 5 decades' change, it must influence DFO's strategy for managing climate-change impact in the Arctic.

Canadian Polar Shelf: All long series of weather observations for the Canadian Polar Shelf come from coastal land stations. There are no prolonged observations from the marine area. There are seven stations scattered across the Canadian Archipelago with records spanning the last 50 years: Alert, Eureka, Isachsen, Mould Bay, Resolute, Arctic Bay and Cambridge Bay all starting in 1953. Two other records of interest are from Rae Point, starting in 1969 (43 years) and from Dundas Harbour (1930 -1950), which extends the record furthest back in time.

The calculated changes in temperature during 1950 - 2007 are depicted in Figure 3, which include Alert, Eureka, Mould Bay, Resolute Bay and Cambridge Bay, all within the Canadian Archipelago. Stations to the south-east are deemed indicative of conditions in the Baffin and Hudson basins. The stations in the Canadian Archipelago fall into two groups, some having warmed by more than 1.5°C and some having warmed less. The net warming of marine areas of the Canadian Polar Shelf since 1950 has probably been about 1.5°C, a little more than half that in the Beaufort. However, the scarcity of useful observations in this vast area is very obvious. Zhang et al. (2011) report significant annual trends for 1950 - 2007 of about 0.1-0.5 °C/decade. Seasonal trends are generally highest and most significant in spring and autumn.

Baffin Bay: Sixty year records of air temperature from 2 stations along the eastern coastline of the Canadian Archipelago (Vincent et al. 2002) are shown in Figure 4 (Hamilton and Wu 2013).

From north to south the stations are Pond Inlet (72.70°N, 77.97°W) in central Baffin Bay and Clyde River (70.48°N, 68.52°W) in southern Baffin Bay (1600 km south of Alert). The air temperature records reflect 2 distinct periods. Over the period 1950 - 1999, there is a suggestion of some slight warming but the signal is not statistically significant above the observed interannual variability (Hamilton and Wu 2013). While not reliable statistically, trends in mean temperature of +0.1, +0.5 and +0.1 °C/decade were computed over this earlier period. In recent years, the data reveal a sharp increase in temperature at all three stations. From 1999 - 2011 trends of +2.9, +2.2 and +1.6 °C/decade were computed for Alert, Pond Inlet and Clyde River respectively. Note that the warming is greatest at the northern station and weakest at the southern station, but dramatic and significant at all 3 stations. Zhang et al. (2011) state that annual trends for 1950 - 2007 are variable and not significant. They report trends to be generally highest and most significant in spring and autumn with winter trends at Iqaluit and Clyde River of 1.5-3°C/decade (significant).

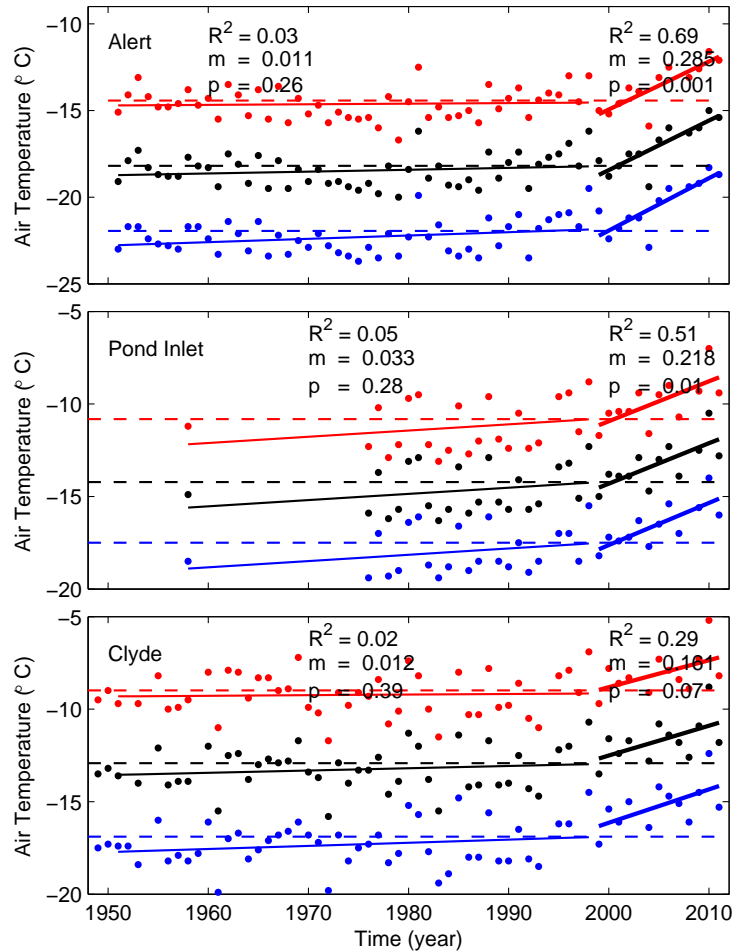


Figure 4: Air temperature at stations along the eastern coastline of the CAA, showing mean (black), minimum (blue) and maximum (red) annual values. Annual values (dots), long term means (dashed lines) and trends (solid lines) with slope m ($^{\circ}/y$) are shown. Stations were located in the communities of Alert (upper panel), Pond Inlet (middle panel) and Clyde River (lower panel). (Figure 18 from Hamilton and Wu 2013).

Hudson Bay: Offshore weather data are extremely scarce in Hudson Bay, and essentially absent in winter. Stewart and Lockhart (2005) provide a comprehensive summary of historical weather data from coastal stations around the bay, including air temperatures, winds, and precipitation, drawn principally from Maxwell (1986).

Galbraith and Larouche (2011), updated recently by Galbraith (unpublished data), reported averaged air temperatures in June to August for Hudson Bay and Hudson Strait from the 1930s to 2011. Air temperature data were obtained from Environment Canada (Adjusted and Homogenized Canadian Climate Data; AHCCD) and from the NCEP reanalysis (NOAA/OAR/ESRL Physical Sciences Division, Boulder, Colorado, USA; <http://www.esrl.noaa.gov/psd/>). The two datasets show good agreement and record a warm period between 1940 and 1964, and a significant warming trend between 1992 and 2011. The climate data (AHCCD) showed an overall warming trend since the 1930s and 1940s, ranging from +0.1 to +0.3 $^{\circ}C$ per decade depending on the location of stations within Hudson Bay and

Hudson Strait. The warmest years on record have all been recent, with 12 of the 19 warmest summers in Hudson Bay and Hudson Strait occurring between 1991 and 2009. NCEP reanalysis updated and extended by Galbraith (unpublished data) showed that air temperature cooled between 1873 and 1918, and warmed thereafter (Figure 5). Summer air temperature showed no trend from 1946 to 1992 except for a cool period in the early 1970s, followed by a marked warming trend since 1992. <http://www.esrl.noaa.gov/psd/>

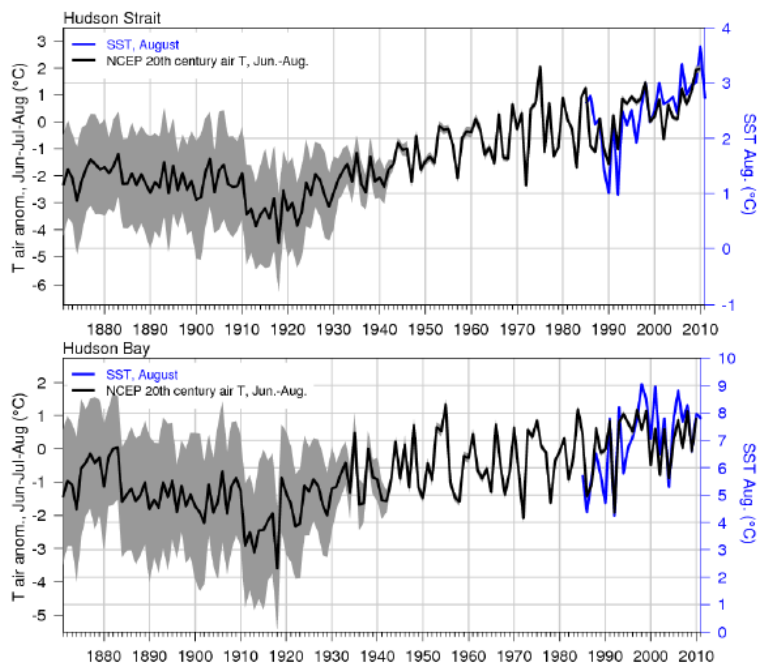


Figure 5: June-July-August air temperature anomaly averages (1971 - 2000 climatology) and SST averages in Hudson Strait (top) and Hudson Bay (bottom). Air temperature is the NCEP 20th century version 2 reanalysis surface temperature averaged at all grid points of each region and grey areas show the mean plus and minus one standard deviations of the 56 model runs (from Galbraith, unpublished data).

Using similar climate datasets of air temperature in spring and fall between 1951 and 2005, warming trends range from +0.2 to +1.8°C per decade in fall (Hochheim and Barber 2010) and +0.22 ± 0.1°C per decade in spring (Hochheim et al. 2011). Again in fall and spring, accelerated warming is reported since the early 1990s. On average, fall was the season with the most pronounced warming (0.3 - 0.5 °C/decade, Zhang et al. 2011).

2.1.2 Precipitation

Beaufort Sea: Normal precipitation at coastal stations in the Beaufort region ranges between 14 cm/y in the west (at Tuktoyaktuk) and 16 cm/y at Ulukhaktok in the east. At most, half of this falls as rain (8 cm at Ulukhaktok, 5 cm at Sachs Harbour). The nominal precipitation threshold for a desert is 25 cm/y.

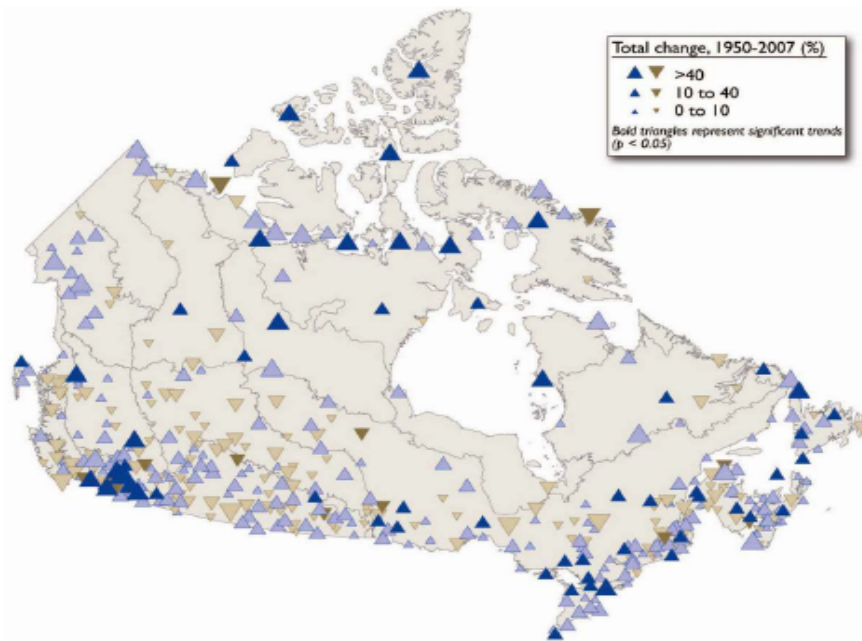


Figure 6: Change in mean annual precipitation, 1950 - 2007, as a percentage of the 1961 - 1990 norm. (Figure 3 from Zhang et al. 2011).

A recent analysis of Canadian trends in precipitation (Figure 6) suggests that very large fractional changes, more than 40%, have occurred at some stations in the Beaufort region since 1950, while comparably large decreases have occurred at others. The changes are only significant at Sachs Harbour (10 - 40% increase) and at nearby Cape Parry (more than 40% decrease). The lack of a consistent regional picture likely reflects the large year-to-year variation in precipitation at these stations, and precludes an educated guess concerning even the sign of change in precipitation over the adjacent ocean. It must also be noted that even a 40% change in precipitation does not amount to much water in a zone as arid as the Beaufort – only 5 - 6 cm/y. However if half this amount affects the snow pack, the resulting change in the depth of wind-packed snow, about 10 cm, has greater relevance.

Canadian Polar Shelf: Normal precipitation at stations in the Canadian Archipelago is about 15 cm/y at Alert, 7.6 at Eureka, 11 at Mould Bay, 15 at Resolute Bay and 14 at Cambridge Bay. Rainfall amounts increase north to south, from 1.6 cm/y at Alert to 7 cm/y at Cambridge Bay. These amounts are well below the nominal 25 cm/y threshold considered indicative of desert. The time series at Alert shows a statistically significant trend of about +10 mm/decade over the 60 year record (Figure 6 and Figure 7), and suggests that very large fractional increases, more than 40%, have occurred at most stations in the Canadian Archipelago. Zhang et al (2011) judge the increases at many of these stations to be significant.

As for the Beaufort, it must be noted that even a 40% change in precipitation does not amount to much water in a zone as arid as the Canadian Archipelago – only 3 - 6 cm/y. However, if half this amount affects the snow pack, the resulting change in the depth of wind-packed snow (about 5 - 10 cm) could have a sizeable effect on the thickness of winter sea ice, depending on when it falls.

The rugged terrain of the Canadian Archipelago makes orographic influence on precipitation amounts a certainty. Precipitation measured at Arctic stations will depend not only on local terrain, but on the location of the station and on wind direction during events. It is therefore difficult to estimate the current amount of precipitation over the marine areas of the Canadian Polar Shelf, more so any recent change. However, the waters of the Canadian Polar Shelf are the ultimate destination of precipitation falling on land, so the few centimetres of apparent increase there during the last half century will have contributed to the ocean's freshwater inventory transport over this time.

Baffin Bay: Time series of annual mean precipitation at Alert and Clyde River (Mekis and Vincent 2011) are plotted in Figure 7. Strong interannual variability can be found at both stations.

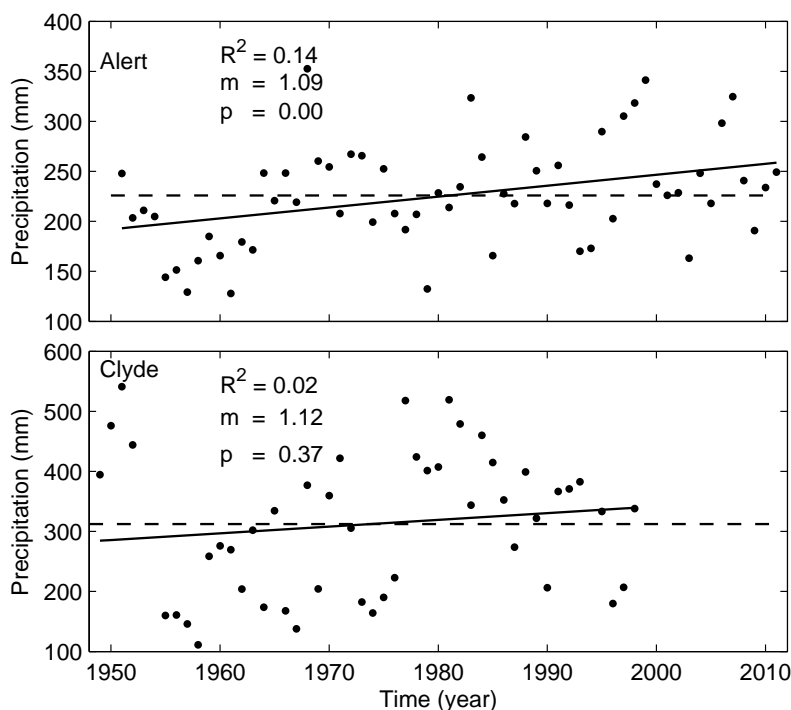


Figure 7: Time series of annual mean total precipitation at Alert (upper) and Clyde River (lower). Dots, dashed lines and solid lines indicate raw data, means of raw data and trend lines. The trend at Alert is statistically significant but that at Clyde River is not.

Hudson Bay: Precipitation data for Hudson Bay are available for only a few coastal stations. Stewart and Lockhart (2005) provide a brief summary, but no trend analysis. Precipitation is generally higher in the winter than in summer, and higher in the south than in the north.

2.1.3 Circulation and wind

Beaufort Sea: Two aspects of climate change have significance for wind in the Arctic, the general circulation of the atmosphere, and storminess. Although the two are not independent, the latter is more closely linked to extreme conditions, whereas the former reflects an average over seasons to decades.

Although surface and upper-air stations were distributed at useful density over land areas of the Arctic by the mid 1950s, there were only sporadic observations from over the Arctic Ocean until the start of the International Arctic Buoy Program (IABP) in the late 1970s. This project exploited recently developed satellite tracked radio beacons drifting on the ice to report sea-level pressure many times daily.

By the mid 1990s there were enough data from IABP to reveal interdecadal changes in the atmosphere over the Arctic Ocean. The annual mean sea-level pressure north of 70°N was 2 – 3 mb lower during 1987 - 94 than during the preceding 8-year interval (Figure 8, Walsh et al. 1996). Interdecadal differences tapered in a bull's eye pattern from a maximum near the North Pole. The change, which occurred abruptly in 1987 - 88, was larger (6 – 7 mb) in autumn-winter than in spring-summer.

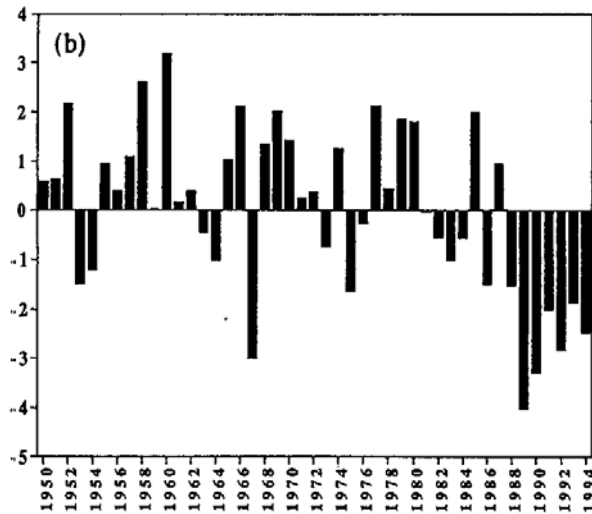


Figure 8: Anomaly in annual mean sea-level pressure north of 70°N, relative to the 1950 - 94 mean (Walsh et al. 1996).

The observed pattern of change strongly resembled that of the Arctic Oscillation (AO: Thompson and Wallace 1998), the dominant natural pattern of SLP anomalies in the Arctic atmosphere during winter (November-April). Thompson and Wallace (1998) documented a persistent bias to large positive values of the AO-index in the 1990s. The AO is the surface manifestation of fluctuations in the strength of the stratospheric polar vortex.

The effects on atmospheric circulation of the 1990s AO anomaly that occurred in winter were: enhanced penetration of a lobe of low pressure from the North Atlantic into the Eurasian Basin; decrease in the extent and strength of the Beaufort high and eastward rotation of the band of wind responding to the pressure gradient between these centres. The well-studied consequences of the 1990s AO anomaly on ice and ocean circulation are: increased and warmer Atlantic water inflow to Arctic; eastward rotation and broadening of the trans-polar drift carrying sea ice and upper ocean waters towards the exit in Fram Strait (Proshutinsky and Johnson 1997; Rigor et al. 2002); increased export of Arctic sea ice through Fram Strait (Kwok et al. 2004); eastward rotation of the ocean front separating waters of Pacific and Atlantic provenance in the Arctic (McLaughlin et al. 1996); reduction in the size of the old-ice reservoir in the Canada Basin and

in the average age (and average thickness) of ice within it (Rigor et al. 2002; Rigor and Wallace 2004).

The 1990s AO anomaly had its strongest impact in the Eurasian sector of the Arctic Ocean. Its impact in the Canadian Beaufort Sea was relatively weak.

The AO-index returned to a normal pattern of interannual variation in the late 1990s – fluctuating positive and negative anomalies of modest magnitude (Overland and Wang 2005). However, the second most common natural pattern of SLP anomalies, the Arctic Dipole (AD), rose to prominence in the mid 2000s (Wang et al. 2009; Overland et al. 2012). Whereas the AO involves the shifting of air between temperate and polar latitudes, the AD involves the shifting of air between the Siberian and North American sides of the Arctic. The 2000s AD anomaly was most evident in summer. Its pattern of high pressure over the Canadian Beaufort and low pressure over eastern Siberia (Figure 9) created a band of south wind near the date line. This wind pattern has brought anomalously warm air into the Arctic from the Pacific (Overland et al. 2012).

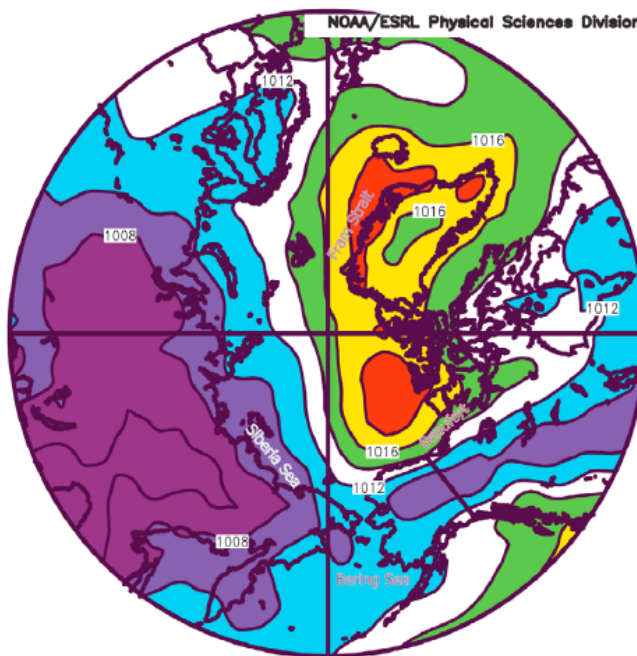


Figure 9: Average sea level pressure (mb) for June during 2007 – 2012 (from the NCEP-NCAR Reanalysis, NOAA/Earth Systems Research Laboratory).

Variation in the sign and magnitude of the AD anomaly in June over the last 60 years is shown in Figure 10. The unusual, prolonged negative phase initiated in 2006 is clear. Moreover, the AO anomaly (depicted by shaded bars in Figure 10) has been predominately negative in June over the same interval, indicating higher than normal SLP over the Arctic.

Whereas it is clear that there have been noticeable changes in Arctic atmospheric circulation, particularly during the last quarter century, it is not clear that these can be considered indicative of a trend. Moreover, a demonstrated causal link between observed changes in Arctic atmospheric circulation and climate warming is proving elusive.

The AO and AD anomalies have conspired to build higher than normal pressure over the Canada Basin which is driving stronger east winds across the southern Beaufort Sea (Moore 2012). These have kept this area unusually clear of sea ice during late spring, summer and early autumn since 2007. Moreover, as the wind pattern has veered to southerly near the date line (Figure 9), it has provided a strong push for the ice to drift from the East Siberian, Chukchi and Alaskan Beaufort Seas across the North Pole and out through Fram Strait. In earlier times this ice would have swept far westward past Wrangel Island before joining the trans-polar drift, and consequently had a residence time in the Arctic.

The Beaufort high drives a closed cell of wind at the surface in the long-term mean. In winter, however, the surface wind responds to a ridge of high pressure that stretches eastward across the Chukchi Sea from the Siberian high. A strong Beaufort high is associated with positive temperature anomalies in the lower atmosphere over much of the Arctic Ocean, except in autumn (Serreze and Barrett 2011).

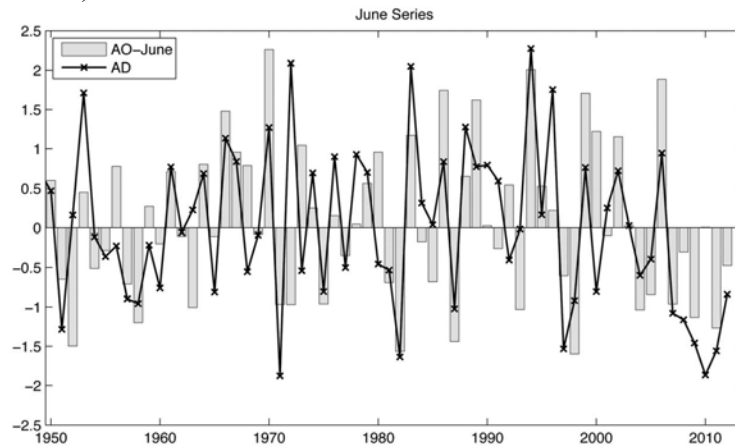


Figure 10: Variation in the June-mean sea-level pressure anomalies related to the AO and AD anomaly patterns. Series are normalized by the standard deviation during 1948 – 2012 (Overland et al. 2012).

Variation in the sign and magnitude of the AD anomaly in June over the last 60 years is shown in Figure 10. Examining atmospheric re-analyses for the mid 1950s to the late 1990s, McCabe et al. (2001) concluded that Arctic storms were most common in the summer. In this and most other studies, the area under discussion is that north of 70°N, which includes the storm-prone Greenland, Barents and Kara Seas. However, no trends were evident in summer, although there were increases in storm frequency and intensity in all other seasons. Increases are linked to the prominent AO anomaly that peaked in the 1990s. A similar analysis has been completed for a longer period of re-analysis, 1948 - 2002 (Zhang et al. 2004). Based on a metric that incorporates the intensity, frequency and duration of storms, they conclude that Arctic storm activity increased over the period analyzed; this reflects in part a northward shift of storm tracks. They note that Arctic storm activity has appreciable low-frequency variability, with a negative phase in the 1960s and a positive phase in the 1990s; oscillations of 8 and 4 years are superimposed.

Simmonds et al. (2008) analyze Arctic storminess during 1958 - 2006 and include strong storms without closed isobars which were neglected in other studies. Storms by this expanded

definition are actually more common in winter than in summer, in contrast to earlier results. For the interval 1958 - 2006, these authors find significant increases in the frequency of summer storms and in their average intensity. However, in the period with better observations, after 1979, there were no significant trends in any storm parameters. Interannual variations in the number of Arctic storms have been correlated with the AO index, even after the 1990s peak and as autumnal ice cover has diminished.

All these studies have considered storminess within the whole area north of 70°N. There has been very little work focussed on sub-areas of this vast region. A study by Hudak and Young (2002) focussing on the Canadian Beaufort Sea is one exception. These authors studied the “storm season” (June through November) during 1970 - 1995. There were 14 (sample deviation ± 5) storms per year with no discernable trend in storm frequency. 58% of the storms were Arctic in origin, 27% from the Pacific and 15% unclassified. Another study is that of Atkinson (2005), who counted storms passing through the Arctic’s shelf seas on the basis of wind observed at coastal stations; his interest was the storm season (June through October) during 1950 - 2000. Although storms were separately counted in 7 sub-areas around the Arctic Ocean, events were too rare for detection of significant trends within them. Averaged over all areas, storms were more frequent in the 1970s and 1980s than before or after. Wan et al. (2010), analyzing wind records spanning 1953-2006 for two stations near the Beaufort coast (Cape Parry, Inuvik), found a significant but small decreasing trend in wind speed, about 0.2 km/h per decade.

Canadian Polar Shelf: There is no published work on change in atmospheric circulation and storminess specific to the Canadian Polar Shelf. The general overview for the entire Arctic, summarized under the Beaufort heading, is our only guide here. Since the AO pattern affects conditions around Greenland and the AD patterns along the western side and the Canadian Archipelago and across northern Greenland, the prolonged anomalies in patterns in the 1990s (AO) and the late 2000s (AD) likely had detectable effects on circulation and storminess in the Canadian high Arctic. Wan et al. (2010), analyzing wind records spanning 1953 - 2006 for three stations on the Canadian Polar Shelf (Eureka, Resolute, Cambridge Bay), found a significant but small increasing trend in wind speed, about 0.1 km/h per decade.

Baffin Bay: Fifty-eight year records of annual mean wind speed at the coastal stations of Alert and Clyde River (Wan et al. 2010) are plotted in Figure 11. A positive trend in wind speed at both stations over the 1954 - 2011 period is shown, although there is strong interannual variability particularly at Alert. At Alert this trend is $+0.33 \text{ m}\cdot\text{s}^{-1}/\text{decade}$ while at Clyde River the trend in annual mean wind speed over the last 58 years is $+0.58 \text{ m}\cdot\text{s}^{-1}/\text{decade}$. Both of these positive trends are statistically significant at the 5% level.

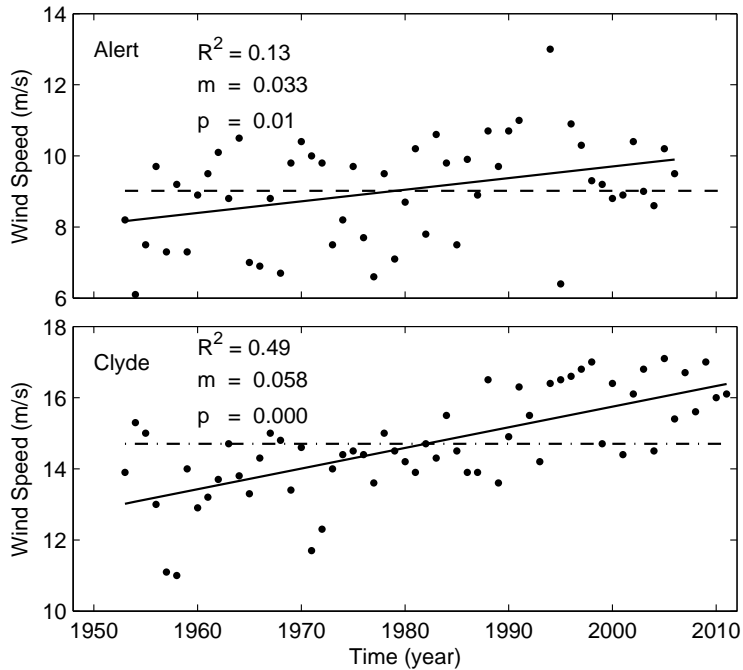


Figure 11: Time series of annual mean wind speed at Alert (upper) and Clyde River (lower). Dots, dash lines and solid lines indicate raw data, means of raw data and trend lines. There is strong statistical certainty that there are positive trends at both stations.

Hudson Bay: Stewart and Lockhart (2005) summarize wind patterns in Hudson Bay based primarily on the compilation of Maxwell (1986). Figure 12 shows the percentage of wind occurrence by direction in two representative months. No comprehensive assessment of trends in wind patterns in the region is available.

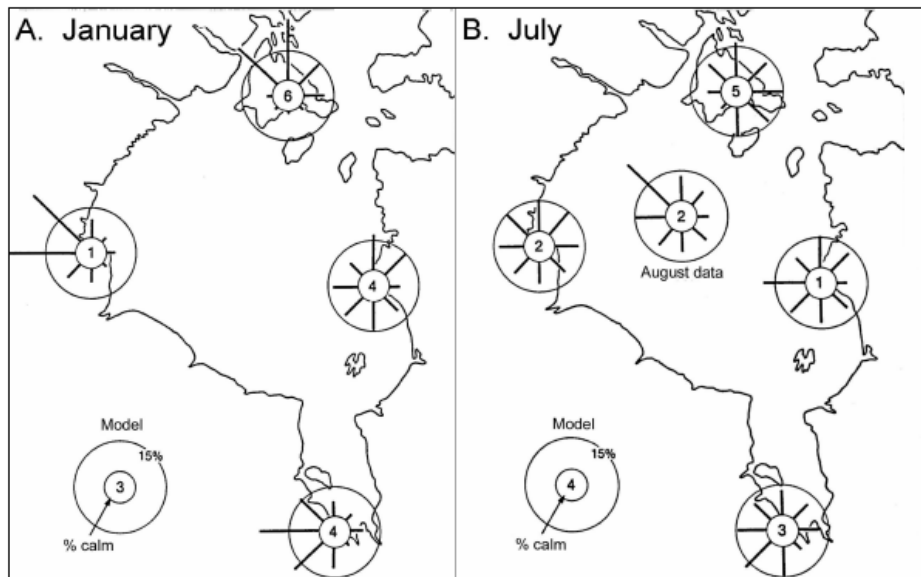


Figure 12: Percentage frequency of wind occurrence by direction in January (A) and July (B) (Stewart and Lockhart 2005 and Maxwell 1986).

2.1.4 Storm waves and surges

Beaufort Sea: Storm waves have been measured sporadically over the continental shelf of the Beaufort Sea. However, the lack of a systematic observational program prevents a reliable description of the wave climate, and precludes an empirical analysis of trend over the last half century. There is one paper, by Francis et al. (2011), that presents the results of wave-height estimates from satellite scatterometer (ERS1, Envisat) during 1993 - 2010. These authors report a trend of increasing mean significant wave height over this period, at a rate of 1 - 2 cm per decade (a few percent). Data on trends in the height, frequency and persistence of extreme waves are not yet forthcoming. A discussion on the physical processes generating storm waves in the southern Beaufort Sea is given in Xu et al. (2013).

Knowledge of storm surges is better, at least along the southern shore of the Beaufort Sea. Manson and Solomon (2007) have compiled records of positive storm surges at Tuktoyaktuk since 1959 (plus one large event in 1944), and a mass of related information on wind, mean sea level, and wind fetch. They report that relative sea level here has been rising at an average rate of 0.35 m per century. Unfortunately, with fewer than 2 events per year, it is not possible to determine whether the frequency of surges or their magnitude has changed over time.

Canadian Polar Shelf and Baffin Bay: There have been no systematic observations of storm waves and surges over the Canadian Polar Shelf or in Baffin Bay. We have no knowledge of the wave climate in these areas, and how it may have changed over the last half century.

Hudson Bay: Very little information is available on the wave climate of Hudson Bay. Stewart and Lockhart (2005) provide a very brief summary, but no trend analysis.

2.2 PHYSICAL OCEANOGRAPHY

2.2.1 Introduction

Internally consistent, un-aliased and sustained observational records are necessary prerequisites for reliable estimation of change. Unfortunately there are few long records of ocean data in Canadian Arctic waters that have these important attributes. The use of available data in documenting Arctic environmental change is critically compromised by changes in observing technology, the infrequency and brevity of observational campaigns, and seasonal bias linked to logistical factors.

Whereas the Arctic atmosphere has been relatively well observed via surface and upper-air stations for a half century now, there has not been a parallel commitment to ocean observation. Sensors on Earth satellites did introduce some capability for routine ocean surveillance in the 1970s, however, the ocean's opacity to electromagnetic waves has concealed all but its surface, which is frequently hidden by clouds and polar darkness. At depths greater than about 350 m, where weather-driven and seasonal changes are minimal, useful time series can be built from occasional surveys. However, autonomous and continuously operating instruments, either free-drifting or secured on submerged moorings, are essential in the upper ocean to avoid aliasing. Useful instruments of this type date back only to about 1980 (30 years), and their widespread use in the Arctic spans only 10 - 15 years.

The small scale of spatial variability in the ocean is a further challenge: the ocean’s analogue of a 1000 km atmospheric feature is only about 10 km across. Whereas the 2000 km span of the Canadian Arctic is only twice the atmospheric scale, it is 200 times that of the ocean. Acquiring a meaningful view of the ocean on this scale is clearly very difficult, even in modern times.

2.2.2 Sea Ice (Thickness, extent, and freeze/break-up)

Beaufort Sea: The recent decline in the extent of Arctic sea ice is well known. Figure 13 displays change in the annual variation of ice extent for 1979 - 2001, 2007 and 2012 (<http://nsidc.org/arcticseaicenews/>). The first group of 23 years represents normal conditions during the late 20th century. Decrease has been more rapid in this century; two additional curves show ice extent during the two years of extreme minimum ice in late summer; extent in mid September 2012 was only half the average of the late 20th century.

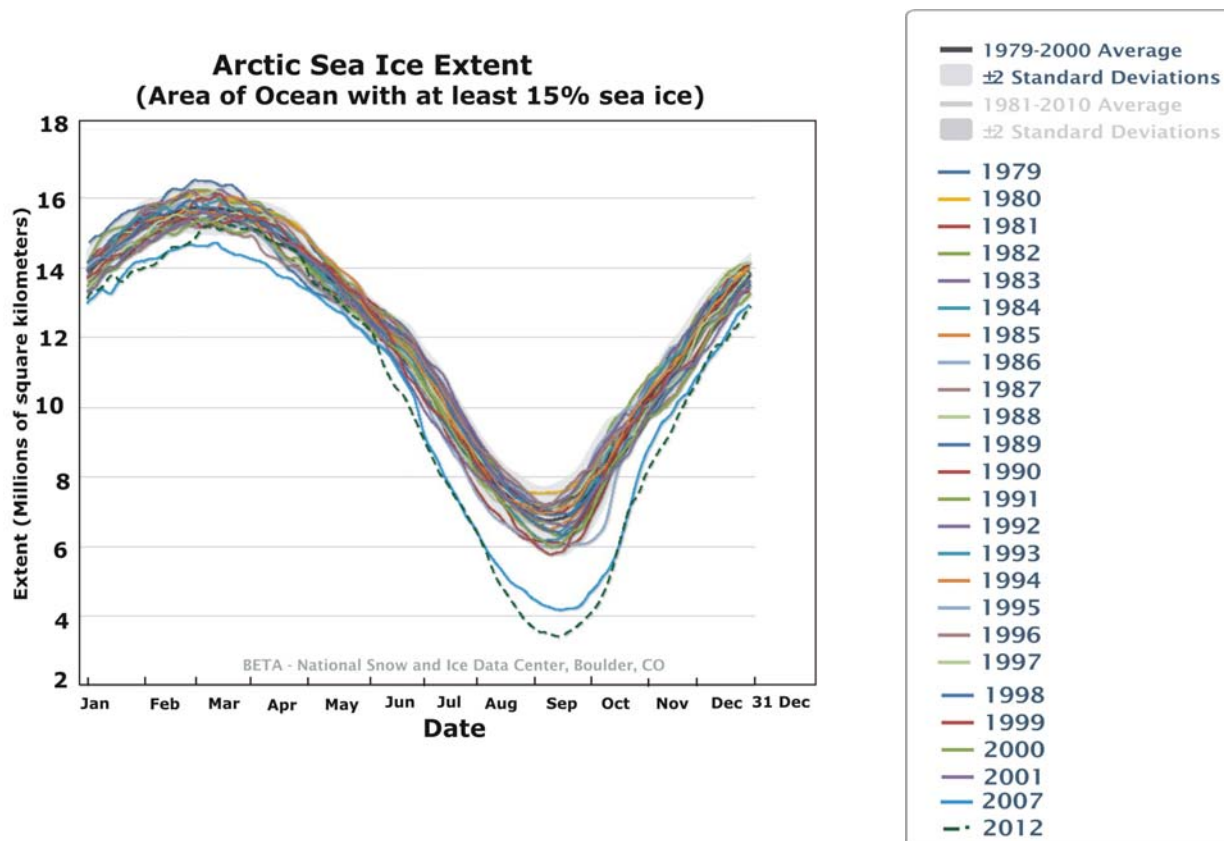


Figure 13: Annual curves of northern sea ice extent from satellite observations using passive microwave sensors. Observations began late in 1978.

The observations reveal a decrease in sea ice extent in the winter as well as in the summer. However, decreases in wintertime are not so much an Arctic issue because they occur mostly at mid latitude ice margins. For this reason it is preferable to talk of decline in northern sea ice in reference to Figure 13, not decline in Arctic sea ice.

Even in summer, some areas of the Arctic Ocean have been more susceptible than others to ice loss. Continental shelves around the southern perimeter of the Arctic Ocean have normally harboured little ice in late summer and therefore have had little ice to lose. Within the traditional

perennial ice zone of the central Arctic Ocean, ice loss has been greatest in the sector spanning the western Beaufort, the Chukchi and the East Siberian Seas, and least in that spanning the eastern Beaufort, the Canadian Polar Shelf and Greenland. Figure 14 displays this pattern in ice distribution at the time of minimum extent in 2012.

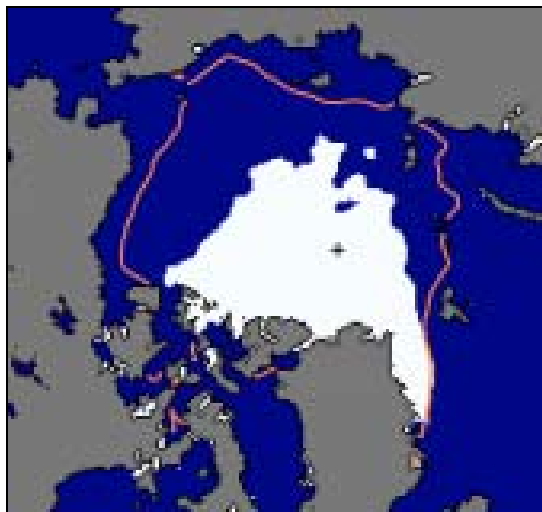


Figure 14: Distribution of ice at minimum annual ice extent in 2012, on 16 September. Median in orange (source: <http://nsidc.org/arcticseaicenews/>).

Ice remaining in the Arctic Ocean at the time of minimum ice extent in September is de facto either that part of this year's annual ice that is not destined to melt, the same from last year, now second-year ice, or old ice. For this reason, decrease in ice coverage at the end of summer is synonymous with loss of old ice.

Tivy et al. (2011a, b) have used the collection of ice charts prepared by the Canadian Ice Services during 1968 - 2008 to calculate trends in ice coverage in Canadian Arctic waters. They use a metric that is the concentration of all ice (or only of multi-year ice) averaged over defined polygons and over the number of charts available between 25 June and 15 October each year. They compile results separately for 6 polygons in the Beaufort region. The trend for the total Beaufort Sea sub-region is -5.2% per decade, and is significant at the 5% level.

From east to west, south of 72°N, are the Amundsen, Amundsen Mouth, Mackenzie and Alaska polygons. The trends in all-ice concentration here have been negative (-8.6, -3.6, -5.4 and -10.9% per decade), with only the last value, for the Alaskan sector, significant at the 5% level. The decline in the Alaskan sector is attributable to a reduced prevalence of multi-year ice (while the total ice declined by $-10.9 \pm 2.8\%$ per decade, the multi-year declined by $-16.4 \pm 4.7\%$ per decade); the ice loss here, based on a full summer's average, is likely faster than the pan-Arctic decline, which has been -11.7% per decade over the period 1979 - 2008 for the month of least ice (September): http://nsidc.org/news/press/20081002_seaice_pressrelease.html.

Figure 15 illustrates the difficulty of detecting a trend in short (30-year) sequences of observations of a parameter with high variability, in this case the summertime concentration of sea ice on the continental shelf. The total accumulated carbon (TAC) variable is the sum of ice concentration times mapping interval during the 5-month period of seasonally reduced ice

presence. Statistically acceptable trend lines can fall anywhere within the shaded band. Clearly the null result (no trend) is an acceptable interpretation of these data.

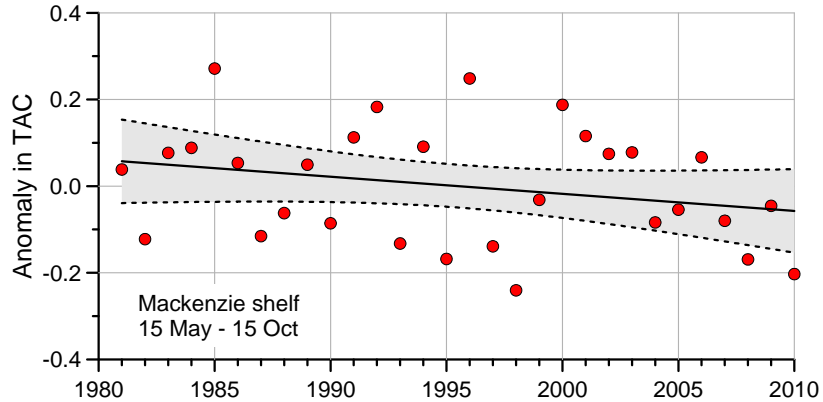


Figure 15: Summertime anomaly in total accumulated concentration of sea ice on the Canadian Beaufort shelf. It is clear how variability masks trend (Melling et al. 2012).

From east to west further north, between 72° and 75°N are the Banks, Prince Alfred and Canada Basin regions. The trends here range from +4.4% per decade (not significant) near the coast to -3.6% per decade (significant) offshore (Tivy et al. 2011a, b). The trend close to the coast is linked to more multi-year-ice, and that offshore to less. As in the Alaskan sector, it is the offshore area of formerly very concentrated multi-year ice that has changed the most. The quoted trends are for 25 June to 15 October. In late winter (March) the extent of ice in the Beaufort Sea has not changed. Very cold weather keeps the ocean almost completely ice covered. There is no trend to reduced ice extent at this time of year.

The term break-up in relation to marine ice has been borrowed from its application to ice on river, lakes and bays. In these environments it refers to the onset of ice movement in spring following months of immobility. The same definition of break-up can be applied to the extensive areas of fast ice in the Beaufort Sea. However, a range of dates is required because ice in different areas disintegrates at different times in the spring and summer.

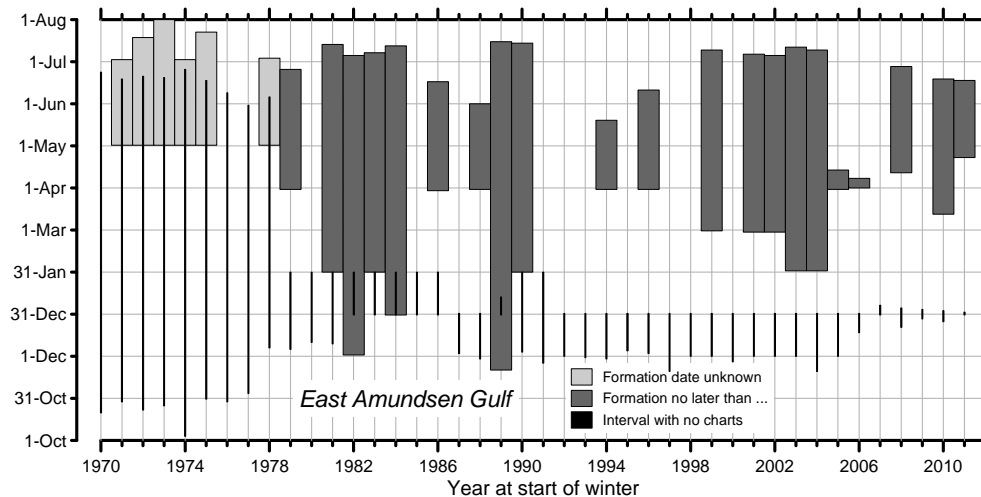


Figure 16: Formation of fast ice across the deep waters of eastern Amundsen Gulf. Data from Canadian Ice Service charts.

Figure 16 shows the record of fast-ice formation and break-up over the deep waters of eastern Amundsen Gulf. The date of break-up, uncertain by as much as the weekly charting interval, has been quite variable and fast ice has not formed at all in some winters. Although the date of formation is not known for the early years, because ice charts were not prepared between September and June (thin vertical bars), there are hints of less reliable consolidation since 1980. However, these data, in common with other fast-ice metrics in the Beaufort, do not support a confident statement on trends in timing.

In pack ice, which moves throughout the winter, the onset of mobility cannot be used to define break-up. The term has nonetheless been used in relation to pack ice in the literature without definition. Our ad hoc definition is based on the following modified concept: Leads open in pack ice as it moves. Most noticeable is the flaw lead that forms just seaward of the fast-ice edge. These leads refreeze quickly in cold wintertime conditions, but the rate of freezing slows with the return of spring sunshine and warmer weather. Usually by June in the Beaufort, if not earlier, sunshine and air temperature together prevent the freezing of a newly opened flaw lead. However, even when such conditions persist, break-up will not occur in the Beaufort until persistent east wind opens up the lead. We judge the pack ice to have “broken up” at this time. There are years with adverse behaviour (1974 and 2001, for example) when the break-up is very late and precipitated by the slow melting of pack ice rather than by speedy exit to the west. We propose an analogous definition of freeze-up which requires a 9 tenths cover of ice, (pre-existing and new) over the entire Beaufort Sea; this is close to the 10 tenths criterion used for freeze-up in sheltered waters.

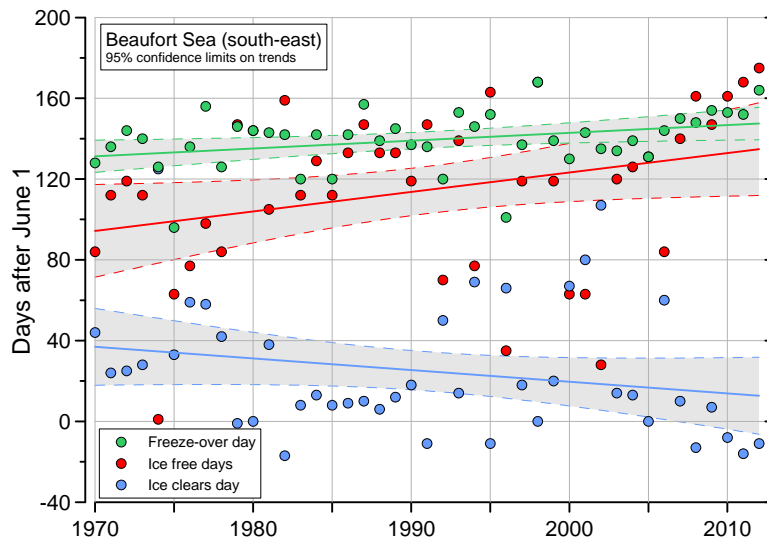


Figure 17: Dates of ice break-up and freeze-up over four decades in the Canadian Beaufort Sea. Data from Canadian Ice Service charts.

Figure 17 displays variability in the date of break-up and freeze-up in the Canadian Beaufort Sea by these definitions. Least-squares trend lines and associated bands of shading are shown. The latter represent the range of trend values (slopes) that cannot be distinguished from zero with 95% confidence. We see that break-up is tending to be earlier since 1970 and freeze-up later, both by about 20 days over 40 years. The “open season” has been lengthening at about 10 days

per decade. However, the magnitude of interannual variability does not allow 95% confidence in the reality of these trends.

Note that trends in both metrics are strongly influenced by change since 2001; since this time, (Section 2.1.3) there has been a strong dipole anomaly in atmospheric circulation which has created anomalously strong and persistent east winds in the southern Beaufort Sea. Such winds will clearly contribute to an early exit of ice from the area in spring and a late consolidation of complete ice cover in the autumn.

Sea ice initially forms in vast featureless sheets. In sheltered waters it thickens and strengthens without disturbance and remains featureless throughout the winter. Its thickness is determined by the passage of time and the net effect of heat gains and losses. Gains come via radiation from the sun and from the atmosphere, via phase change from ice growth, and via conduction from the ocean and atmosphere; losses occur via radiation to space and via conduction to the atmosphere. The thickness and high reflectivity of snow cover are important influences on radiative and conductive heat fluxes. In exposed waters, the nascent featureless ice sheets are quickly deformed into a rough and geometrically complex 'landscape' both above and below the sea surface. While typical first-year ice in the southern Beaufort Sea ranges in thickness from zero to about 2 metres in late winter, ridges accumulate to 15 - 20 times this thickness. Whereas level ice requires many months of slow growth to reach 2 metres, ridges can be built to full thickness in a few days from ice only a few days old. The mechanical process of sea ice thickening is an important contributor to the average thickness of Arctic pack ice.

Another issue of importance is the thermal weathering of sea ice during warm months. The winter's ice growth melts completely in summer around the perimeter of the Arctic where climate is relatively benign. In the harsher climate of the central Arctic and the Canadian Archipelago, level floes do not necessarily vanish during summer; they build to successively greater thickness during subsequent winters. Ice ridges and rubble, being much thicker, are even more likely to survive (Amundrud et al. 2006). The survivors constitute the multi-year ice of the Arctic. In assessing change in the thickness of Arctic sea ice, it is important to consider changes in the distribution of various ice types.

Level ice thickness has been measured by the Meteorological Service of Canada at some Arctic coastal locations since the late 1940s. The three records in the Beaufort region are not so long: 1956 - 86 at Sachs Harbour, 1959 - 1992 at Cape Parry and 1971 - 1977 at Tuktoyaktuk.

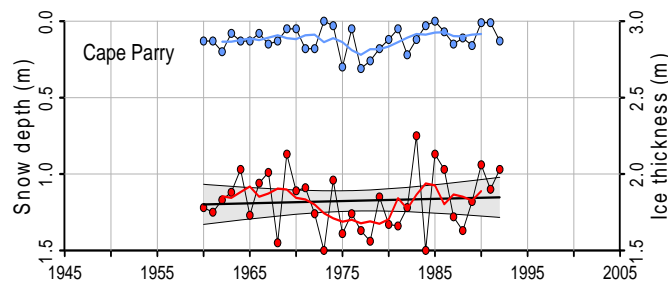


Figure 18: Thickness of coastal ice (red) and snow (blue) in mid May at Cape Parry. The snow axis is inverted to illustrate the correlation of thinner ice with deeper snow. The shaded zone represents 95% bounds of confidence. Data from the Canadian Ice Service (<http://www.ec.gc.ca/glaces-ice/default.asp?lang=En&n=E1B3129D-1>).

Figure 18 displays the 33-year record of end-of-season ice and snow thickness (blue dots) at Cape Parry. There was a weak trend to thicker ice (1.4 cm per decade) which is not significant. Reduced thickness in the 1970s was caused by more snow (Brown and Côté 1992).

The draft of first-year pack ice has been measured at the mid shelf of the Canadian Beaufort Sea since 1991 (Melling et al. 2005, 2012). The record up to 2008 of monthly ice-draft anomalies is shown in Figure 19. The data reflect a large domain of variations in the pack-ice environment, for example, the annual cycle of ice growth and decay, air temperature, ocean temperature, cloud cover, snow thickness, ridge and lead formation, ice advection, ice concentration, etc. The computed thinning trend of only 10 cm per decade is not significant even at the 50% level.

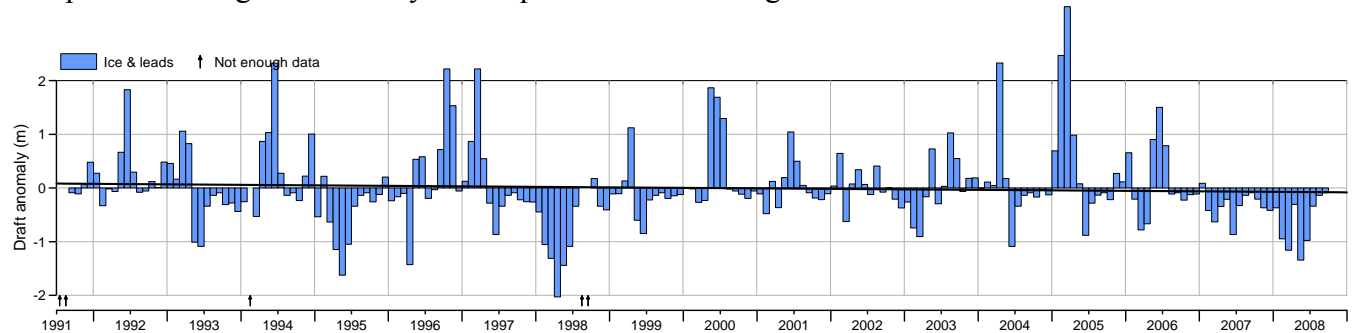


Figure 19: Monthly anomalies in the draft of moving pack ice near 70.33°N 133.75°W on the middle shelf of the Canadian Beaufort Sea (Melling et al. 2005, 2012).

Multi-year pack ice in the Arctic Ocean is found primarily in the central Arctic Ocean. The only long records of ice thickness here have been acquired by sonar on nuclear submarines; those in the central “Gore box” beyond national EEZs were declassified only recently and do not cover the Canadian Beaufort sector. Kwok and Rothrock (2009) use data acquired during 1958 - 76, 1993 - 97 and 2003 - 07 and report large reductions in the average thickness of pack ice in every part of the “Gore box”. In the region west of 141°W which is closest to the Canadian sector, average thickness (adjusted to 15 September) decreased by 0.97 m over the three decades of the first interval, but only 0.01 m over the decade of the second. A closer examination by Tucker et al. (2001) revealed that much of the change in the Beaufort region occurred abruptly in the late 1980s. The results for other sub-regions (Figure 20) show similar variation over time – a drop between the 1970s and the 1990s and not much change since.

One contributor to the reduced average ice thickness in the central Arctic is certainly the documented reduced presence of multi-year ice. Because the first-year ice that has replaced it is on average thinner than multi-year ice, and mostly disappears by mid September, it follows that the average ice thickness in autumn is proportionately reduced. However, it is also known that reduced pack-ice albedo resulting from lower ice concentration has increased the absorption of insolation in the upper ocean. Bottom-side ablation of remaining multi-year ice floes has increased and many of the remaining multi-year ice floes are thinner (Perovich et al. 2011).

The concurrence of great change in the thickness of multi-year pack ice and little change in first-year ice argues in favour of wind as a dominant driver of recent Arctic change. Changed patterns of atmospheric and ice circulation have reduced the residence time of multi-year ice in the Arctic, and thereby its average age, average thickness, and area coverage.

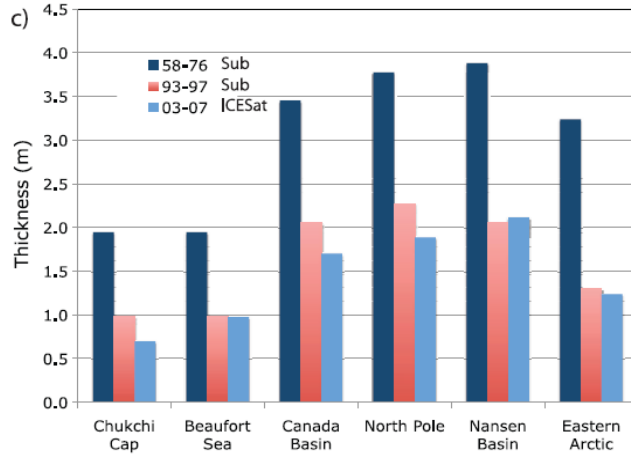


Figure 20: Mean pack-ice thickness in regions of the central Arctic during three periods of the last half century. Values are adjusted to the time of minimum, September 15 (Tucker et al. 2001).

Canadian Polar Shelf: The analysis of changing ice conditions in Canadian Arctic waters by Tivy et al. (2011a, b) included the Canadian Polar Shelf. The complex geography of this region presents a wide range of choice for regional subdivision. Trends for TAC (25 June to 15 October) in six subareas (Western High Arctic, Eastern High Arctic, Parry Channel west of Resolute Bay, Eastern Parry Channel, Peel and Larsen Sounds, Queen Maud and Coronation Gulfs) are all negative and in the range of -2 to -7% per decade, but only the trend for Parry Channel West (-2%) is significant.

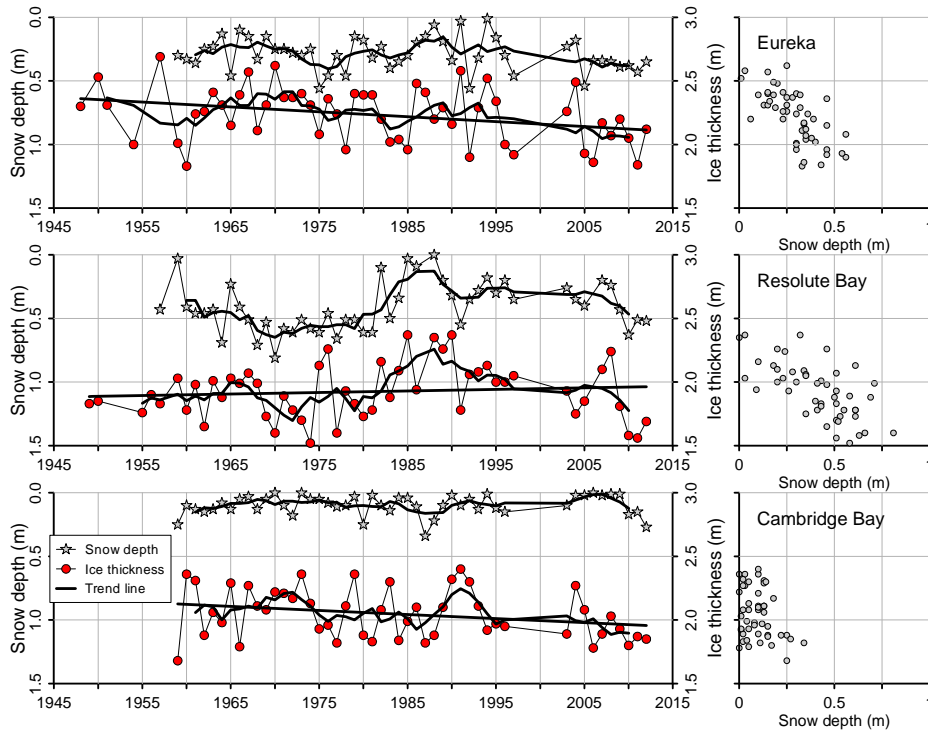


Figure 21: Thickness (red) and snow depth (blue) for coastal ice at three latitudes on the Canadian Polar Shelf. Data from the Canadian Ice Service (CIS) dataset.

The message to take from these results is that there certainly have been reductions in summertime sea ice over the Canadian Polar Shelf. However, in most instances these reductions do not fall beyond the range expected as a result of naturally occurring variability; therefore the resulting trend estimate can not be extrapolated with confidence into the future.

In late winter (March) the extent of ice on the Canadian Polar Shelf has not changed. Very cold weather keeps the ocean almost completely ice covered. There is no trend to reduced ice extent at this time of year.

Ice is land-fast for at least six months over most of the Canadian Polar Shelf. The exceptions are Lancaster Sound (in most years), Prince Regent and Fox Basin. Therefore, ice break-up over the Canadian Polar Shelf occurs principally via onset of mobility that, by allowing ice to move into the Beaufort Sea or Baffin Bay, causes decreases in ice concentration. This attribute of ice break-up over the Canadian Polar Shelf causes long-term change in break-up dates to mimic change in total accumulated concentration (TAC: 25 June to 15 October), summarized earlier. So the modest and generally not significant decreases in TAC over the Canadian Polar Shelf likely reflect, in part, modestly earlier break-up and later freeze-up. Results might be expected to resemble those for Amundsen Gulf shown in Figure 16. Unfortunately, there is no published analysis of such change.

Sea ice over the Canadian Polar Shelf is much less well studied than in the Beaufort Sea. Regional surveys across the north-western region (Sverdrup Basin) provide a picture of offshore ice conditions in the 1970s (Melling 2002), but new surveys are less comprehensive and have started only recently. Data are insufficient for assessment of change in offshore ice thickness over this vast and diverse area.

There are, however, long records for coastal ice that began before those in the Beaufort and continue – apart from an interruption in the late 1990s – to the present day. The end-of-season ice thickness and snow depth from three stations on a north-south transect of the Canadian Polar Shelf, from 80°N to south of 70°N, are shown in Figure 21. The trends over 50 - 60 years are small and spatially variable: -3.8, +1.2 and -3.2 cm per decade at Eureka, Resolute, and Cambridge Bay respectively. The scatter plots at the right reveal that ice thickness and snow depth are clearly correlated – more snow, less ice. This lack of change in first-year ice thickness is consistent with the more comprehensive data from the Beaufort Sea.

Baffin Bay/Davis Strait: Trends of annual- and seasonal–mean sea ice extent and area in various regions of the northern hemisphere were reported by Cavalieri and Parkinson (2012) for the period 1979 - 2010, based on passive microwave data. The trends for Baffin Bay/Labrador Sea are -8, -7, -7, -17 and -12 %/decade for annual-mean, winter, spring, summer, and autumn sea ice extent respectively. The trends are all statistically significant at the 1% level.

Trends of summer sea ice area in various regions of the Arctic and Hudson Bay, and Approaches domains were reported by Tivy et al. (2011a, b) for the period 1968 - 2008, based on digital ice charts produced by the Canadian Ice Service (CIS). The trends were recently updated for the period 1968 - 2010 (Henry 2011), and are -10 %/decade for the Baffin Bay region (25 June - 15

October), and -14 %/decade for the Davis Strait region (18 June - 19 November). The trends are statistically significant at the 5% level or above.

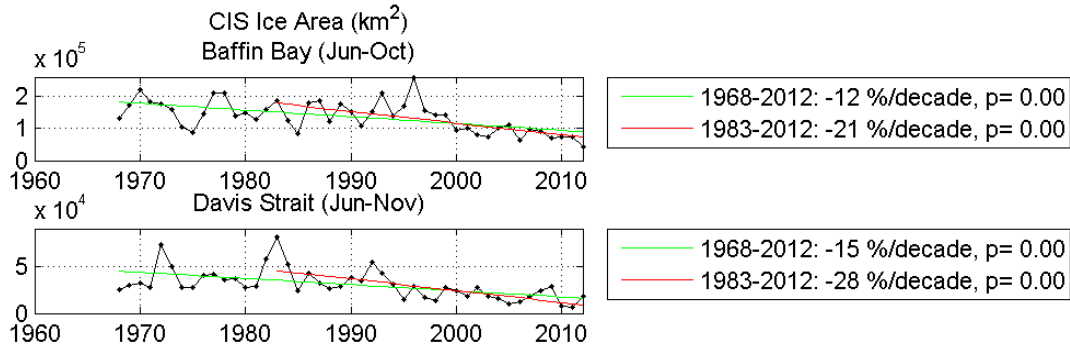


Figure 22: Summer sea ice area and trends (1968 - 2012) derived from the Canadian Ice Service (CIS) dataset.

The time series for summer sea ice area in Baffin Bay and Davis Strait for 1968 - 2012 based on the CIS dataset are shown in Figure 22. The trends for 1983 - 2012 are almost twice as high as those for 1968 - 2012. There is a steady decline in ice area since the mid-1990s in Baffin Bay, and since the early 1990s in Davis Strait. Tivy et al. (2011a, b) showed that the ice coverage has decreased by 9.5 to 11.1% per decade in Baffin Bay (depending on the regions within the Bay).

Longer time series of annual mean ice area (January – December) compiled from the HadISST1 and CIS datasets are shown in Figure 23. The HadISST1 dataset (Rayner et al. 2003) is mainly based on the Walsh (1978) dataset that was derived from ice charts for the period 1901 - 1978, and on passive microwave data for the period after 1978; missing data were filled with long-term means. Because of problems with the passive microwave data (Rayner et al. 2003), data for later years were replaced with data from the CIS for July - September after 1968, and for October - June after 1980 (see Peterson and Pettipas (2013) for further description of the analyses). There is high uncertainty associated with the data prior to 1953. Trends of annual mean ice area are not significant ($p > 0.10$) for the 1953 - 2011 period, but are -4 %/decade for Baffin Bay and -10 %/decade for Davis Strait for the 1980 - 2011 period ($p < 0.01$).

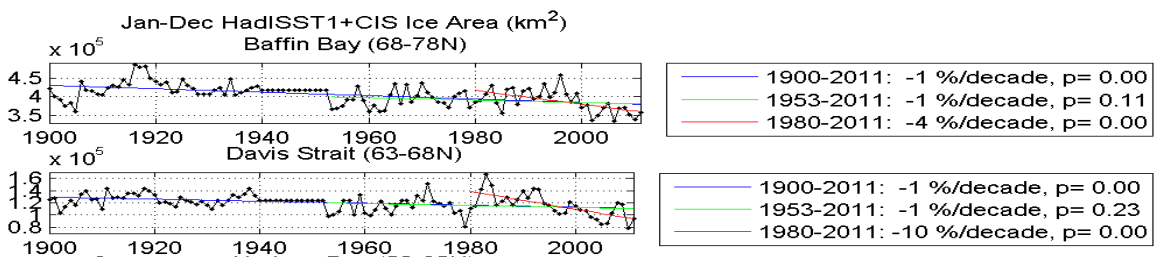


Figure 23: Annual mean sea ice area and trends (1900 - 2011) for Baffin Bay and Davis Strait derived from the HadISST1 and CIS datasets.

Crane (1978) examined sea ice retreat and advance in the Davis Strait-Labrador Sea area for the years 1964 - 1974, and concluded that early retreat is associated with an increased frequency of southerly airflow, and early advance is associated with an increased frequency of northerly and westerly flow. However, years of early ice advance corresponded to years of late retreat in 3 out

of the 5 heaviest ice years, and years of late ice advance corresponded to years of early retreat in 4 out of the 6 lightest ice years.

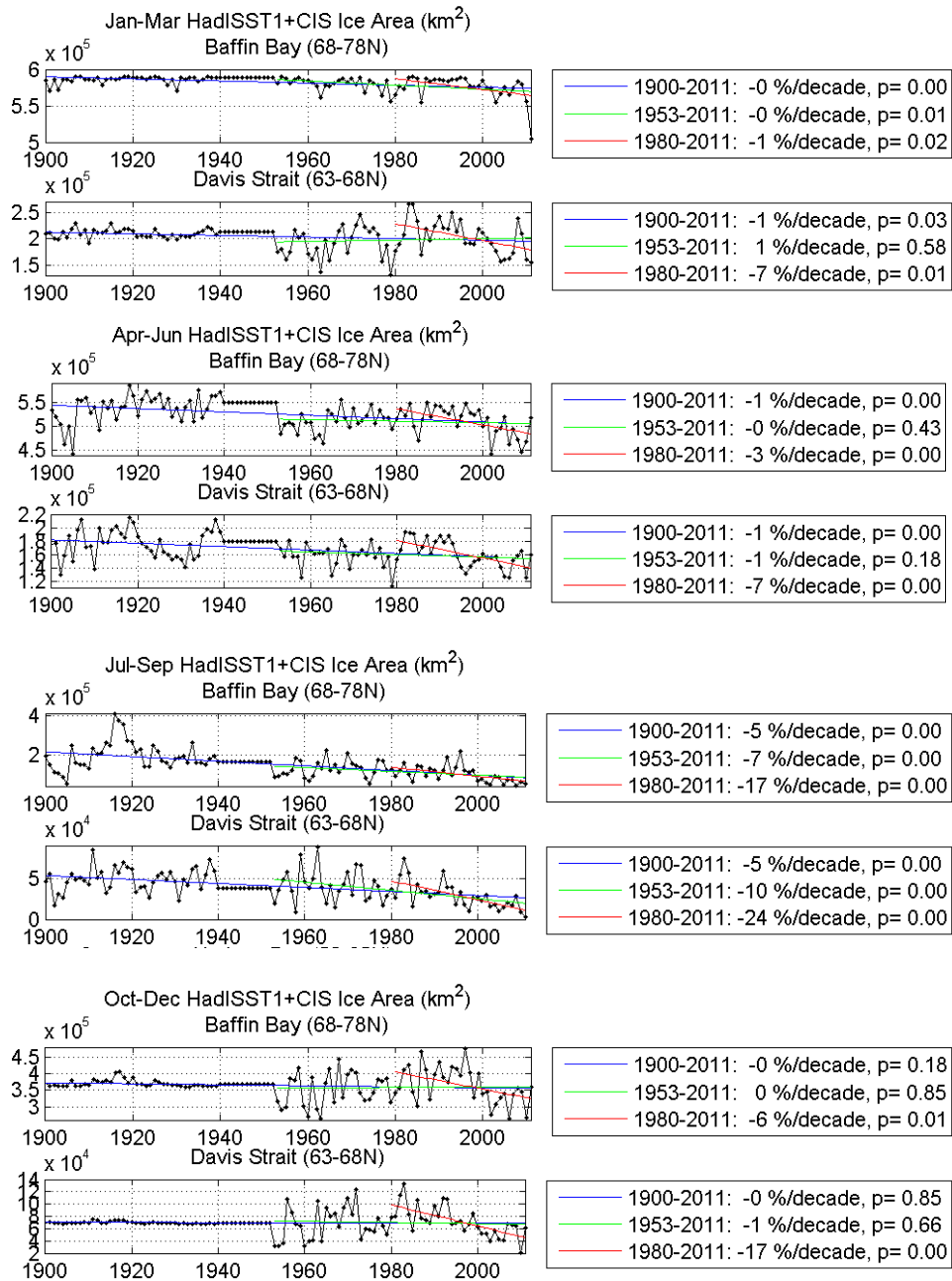


Figure 24: Mean sea ice area and trends (1900 - 2011) for Baffin Bay and Davis Strait, derived from the HadISST1 and CIS datasets for winter, spring, summer and autumn.

Markus et al. (2009) reported trends in melt and freeze onset days and melt season length for the Baffin Bay/ Labrador Sea region for the period 1979 - 2006 that were derived from passive microwave data. The trends are -3 days/decade for the first day of continuous melt, 3 days/decade for the first day of continuous freeze, and 6 days/decade for melt season length. These trends were all significant at the 5% level or above.

Trends of break-up and freeze-up in Baffin Bay and Davis Strait are not shown here. However, because sea ice area generally reaches a minimum in September, trends in sea ice area for the periods July-September (summer) and October-December (autumn) should provide good indications of trends of break-up and freeze-up respectively (Figure 24). For summer, there is a significant negative trend in ice area for both the 1953 - 2011 and 1980 - 2011 periods in both Baffin Bay and Davis Strait. For autumn, there is a significant negative trend for 1980 - 2011 but not 1953 - 2011. For winter, there is a significant negative trend for both periods in Baffin Bay, but only for the recent period in Davis Strait. Similarly, in spring, there is a significant negative trend for 1980 - 2011, but not 1953 - 2011 in both areas. To summarize, there appears to be a more monotonic decrease in ice area in the summer than in other months. This is consistent with a study of sea ice variability for the Arctic as a whole for 1958 - 1997 (Deser et al. 2000), which showed that winter sea ice variability is dominated by decadal variations associated with the North Atlantic Oscillation (NAO), but that summer sea ice variability has exhibited a nearly monotonic decline.

Sea ice thickness data in the Baffin Bay/Davis Strait area are very sparse and not adequate for identifying trends. Wadhams et al. (1985) measured a mean draft of 1.05 m in central Davis Strait from submarine sonar profiles in February 1967. In comparison, Wu et al. (2013) give mean values of 1.0 and 2.1 m in January-March 2007 and 2008 at C2, also in central Davis Strait. Respective air temperatures in the winter of 2007 - 2008 were unusually low, and lower than in the winter of 2006 - 2007 (Våge et al. 2009).

Hudson Bay: By mid-September when ice concentrations are at the annual minimum, Hudson Bay and Hudson Strait are completely ice free (Galbraith and Larouche 2011; Tivy et al. 2011a, b). Freeze-up occurs from late October to late November as a result of the cold winds originating over the landmasses of northern Manitoba and Nunavut. Sea ice begins to form in northwestern Hudson Bay and spreads rapidly southward along the western coast of Hudson and James bays and then, more slowly, eastward (Gough and Wolfe 2001; Gagnon and Gough 2005; Stewart and Lockhart 2005). Moreover, ice formed in the northwest generally moves southeastward in early winter under the action of winds where it ridges to a thickness of 1.5 to 2.0 m (Stewart and Lockhart 2005). By January, Hudson Bay and Hudson Strait are completely ice covered (Tivy et al. 2011a, b).

In winter, the strong northwest winds and tidal mixing encourage the presence of recurring leads and polynyas along the western shore of Hudson Bay (Stewart and Lockhart 2005; Kuzyk et al. 2008a). Small recurring polynyas are also present in the Belcher Islands and near other islands along the coast of southeastern Hudson Bay. These polynyas and flaw leads are among the most southerly in Canadian seas. These openings in the sea ice are often areas of increased biological productivity, and are vitally important to overwintering species and to early spring migrants.

The growth and melting of sea ice has important implications for water column mixing in winter and stratification in spring and summer. During ice growth, most of the original seawater is rejected from the ice (brine rejection). The rejected salt increases the salinity and density of the surface water, which then enhances the deepening of the surface mixed layer (Foster 1972; Kozo 1983). The surface layer deepens to 100 m in places, thus distributing the rejected salt to most of the water column. Currents and wind subsequently concentrate ice in southeastern Hudson Bay,

which results in a stronger freshwater pulse in these areas during the melt season (Stewart and Lockhart 2005; Granskog et al. 2007). The melting of the ice cover in spring constitutes a freshwater flux to the ocean surface layer, increasing the vertical stability of the water column and decreasing the vertical nutrient flux (Prinsenberg 1986), with important implications for the biological productivity in the bay during summer. The sea ice also determines the ecology of the ice biota and influences pelagic systems under the ice and at ice edges during winter.

Parkinson and Cavalieri (2008) report a decrease in sea ice extent of 19.5% per decade in Hudson Bay between 1971 and 2006. Since the mid-1990's, the Hudson Bay area has undergone a climate regime shift which has resulted in a significant reduction in sea ice during the fall freeze-up (Hochheim and Barber 2010). Also, since the Hudson Bay region is ice-free during late summer, the time series of sea ice extent does not exhibit the extreme minima observed in Arctic regions in 1998, 2007 and 2012, but the last decade is marked by consistent light ice conditions and an apparent reduction in interannual variability (Parkinson and Cavalieri 2008). These reductions in sea ice cover are associated with increasing summer air temperature. Tivy et al. (2011a, b) showed that the ice coverage has decreased by 7.5% to 17.8% per decade for Hudson Bay, (depending on the regions within the Bay).

Dates of ice break-up in spring (June) have varied by up to 6 weeks in Hudson Bay between 1971 and 2011, with a weak trend of -0.30 days/y (Gagnon and Gough 2005) or -3.7 days per decade (Galbraith and Larouche 2011; Galbraith, unpublished data), and all early break-up years have occurred more recently (since the mid-90s). Similar trends are also reported in spring by Hochheim et al. (2011). This trend toward longer ice-free conditions is even more pronounced for Hudson Strait, where break-up dates occurred earlier at a rate of 6.3 days per decade since 1971, and this trend increases to 14.1 days per decade, if only the period since 1990 is considered (Galbraith and Larouche 2011; Galbraith, unpublished data).

Sea ice thickness recorded at Coral Harbour between 1980 and 2009 also decreased by 19 cm in November and 40 cm in December (Hochheim and Barber 2010).

Summary: When smaller sub-regions are considered, trends are often not significant because (a) reductions tend to occur along the ice edge, and (b) interannual variability in winds results in ice being forced into one sub-region or another. Therefore it is important to also consider trends in the total region. With respect to ice area, Tivy et al. (2011a, b) computed the following trends: For the Beaufort Sea, Canadian Arctic Archipelago, Baffin Bay and Hudson Bay regions (1968 - 2008), trends in summer ice area are -5.2, -2.9, -8.9, and -11.3% per decade, all significant at the 5% level. Henry (2011) updated the trends to 2010 and found trends in summer ice area are -6, -4, -10 and -11% per decade, all significant at the 5% level.

Cavalieri and Parkinson (2012) looked more specifically at the ice extent and found that for the Arctic Ocean, Canadian Archipelago, Baffin Bay/Labrador Sea, and Hudson Bay (1979 - 2010), the annual trends are -2.9, -2.3, -8.7 and -5.6% per decade, winter trends are +0.4, +1.0, -6.2, -0.6 % per decade, spring trends are -1.0, -1.4, -8.1 and -5.0% per decade, summer trends are -9.1, -8.6, -19.5 and -19.4% per decade, and autumn trends are -3.3, -2.8, -12.2 and -14.3% per decade, all significant at the 5% level.

With respect to sea ice freeze-up/break-up, Markus et al. (2009) state: For Chukchi/Beaufort Sea, Canadian Archipelago, Baffin Bay, and Hudson Bay (1979 - 2007) trends in melt onset are -3.5, -2.3, -3.4 and -5.3 days, all significant at the 5% level. Trends in freeze onset are 6.9, 2.3, 3.1 and 5.4 days, all significant at the 5% level except the CAA. Trends in melt season length are 12, 4.7, 7.9 and 12.9 days, all significant at the 5% level. (Onset of continuous melt/freeze-up has been used for the analyses).

2.2.3 Water Properties and Stratification

Beaufort Sea: There have been many seawater surveys during expeditions in the Beaufort Sea since the 1950s (Fissel and Melling 1990). However, these have been brief initiatives which cannot circumvent aliasing in long time series in the rapidly fluctuating waters of the continental shelf. Therefore these surveys have little value in detecting change, although they are sufficiently numerous to illustrate the range of variation in ocean conditions. Conditions are more stable within the deep anti-cyclonic gyre of the Canada Basin, where prevailing winds establish and maintain a vast and only slowly varying reservoir of low salinity water. This area, inaccessible to ships in earlier decades, has been surveyed annually in late summer during much of the last decade. The time series here is unfortunately still shorter than a decade.

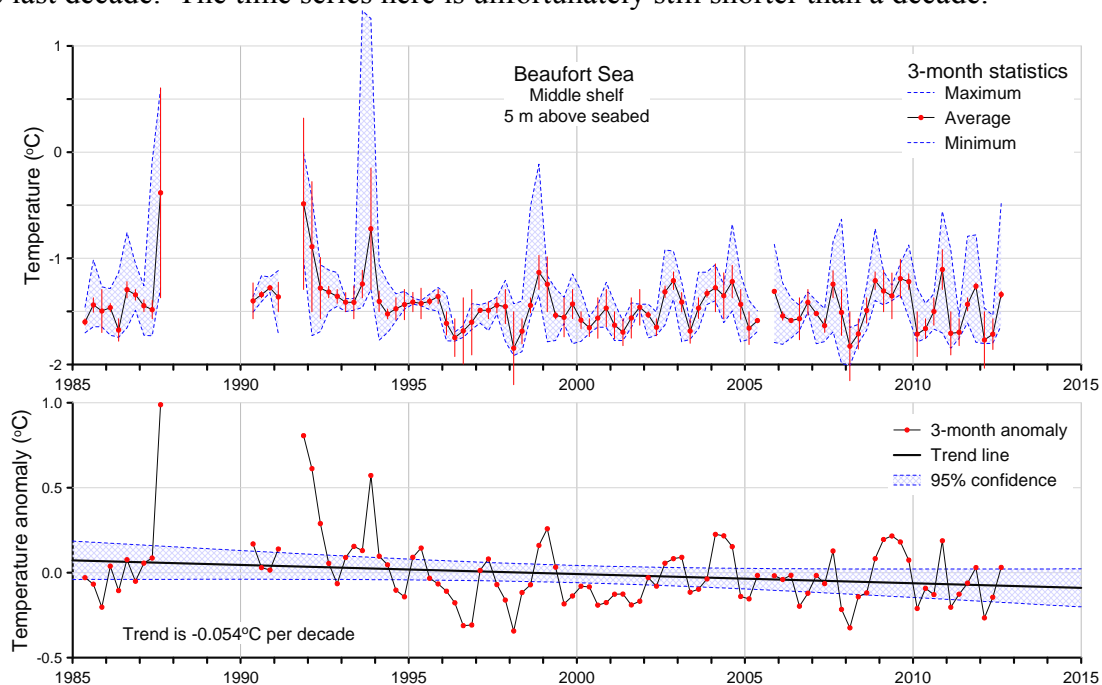


Figure 25: Temperature at mid-shelf of the Beaufort Sea from early 1985. The 50-m depth of measurement is 5 m above the seabed at this location. Values plotted (top) are 3-month means. The same data are displayed as seasonal anomalies (bottom). A weak cooling trend is not significant (Melling 2013, unpublished data).

Submerged instruments, on the other hand, deliver continuous records suitable for time series analysis, but cannot reliably measure ocean properties within the most changeable upper 30 m of the water column, as the risk from moving ice here is extreme. Therefore, we have long time series of seawater properties only at deeper levels in the ocean.

The top panel of Figure 25 displays a time series of temperature (seasonal means) at 50 m depth on the mid-shelf of the Beaufort Sea. These observations start in 1985 and provide the longest record of upper-ocean temperature in the Beaufort. The lower panel displays the seasonal temperature anomalies relative to the long-term seasonal mean. It indicates that there is substantial (and occasionally strong) interannual variability and there has not been a significant trend over the past 25+ years.

Salinity has been measured at the same mid shelf site in the Beaufort Sea, but only since 1999. There is an indication of trend in salinity here, but this is largely spurious. For temperature (Figure 25), the trend arises from a few large anomalies which cause the distribution of anomalies to be highly non-Gaussian. This characteristic invalidates the statistical attribution of significance to non-zero calculated trends.

The density stratification of seawater at Arctic temperature is almost completely dominated by the effect of salinity. However, there are very few systematic observations of salinity and those that do exist are short and at depths below 30 m. In contrast, interest in density stratification is greatest at depths less than 30 m, where biological activity that is sensitive to stratification is concentrated. We do not have data to assess how upper-ocean stratification in the Beaufort Sea may have changed in the past 10 - 50 years.

Canadian Polar Shelf: The single place of long-term observation of current on the Canadian Polar Shelf is also the sole source of data on ocean temperature. Figure 26 displays the variation in annual mean temperature near the seabed at 145 m depth in the western Lancaster Sound. The site is in the Arctic outflow on the southern side of the strait near 91°W. Temperature near the seafloor here has increased by about 0.2°C over the last decade; there is 85% certainty that the true trend is non-zero and within the shaded domain (Hamilton and Wu 2013). Since temperature increases with depth and salinity at this level, the observed rise in temperature at fixed depth could reflect two mechanisms of change: a warming of water of specified salinity without change in the depth of isohalines or a shoaling of isohalines bringing warmer water to specified depth without change in temperature-salinity correlation. Concurrent observations reveal an increase in salinity at this depth and a decrease in geostrophic flow above it. Therefore the second mechanism is most likely to have been in play.

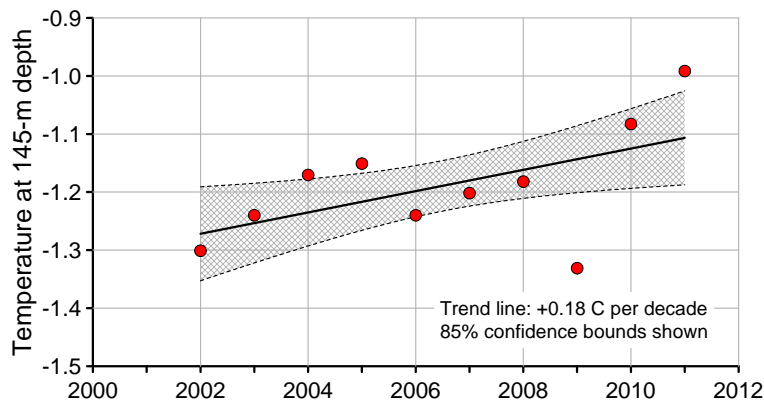


Figure 26: Temperature near the seabed in western Lancaster Sound (southern side). The likelihood of a real change in conditions here is about 85% (Hamilton and Wu 2013).

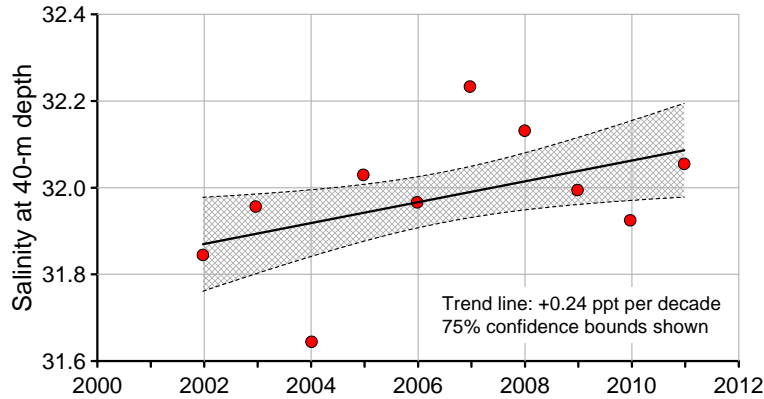


Figure 27: Salinity at 40 m depth in western Lancaster Sound (southern side). The likelihood of a real change in conditions here is about 85% (Hamilton and Wu 2013).

For salinity we also have only a single place of long-term observation on the Canadian Polar Shelf. Figure 27 displays the variation in annual mean salinity at 40 m depth in western Lancaster Sound. Salinity at that depth has increased by about 0.24 over the last decade; there is 75% certainty that the true trend is non-zero and within the shaded domain. In view of concurrent warming and weakening of current over this time period (previously discussed), the most likely explanation of the trend is baroclinic adjustment of density structure to changing geostrophic flow.

As for the Beaufort Sea, we do not have data to assess how upper-ocean stratification on the Canadian Polar Shelf may have changed in the past 10 - 50 years. Hence, we lack information where interest in density stratification is greatest due to the influence on biological activity.

Baffin Bay/Davis Strait: Long time series ocean temperature and salinity data are sparse in the Baffin Bay/Davis Strait region, making it difficult to identify trends. This is particularly true for the upper layer which is characterized by high interannual variability. However, there are some trends of note that can be extracted from a gridded climatology dataset built from field observations taken between 1910 and 2009 using an optimized interpolation algorithm (Hamilton and Wu 2013).

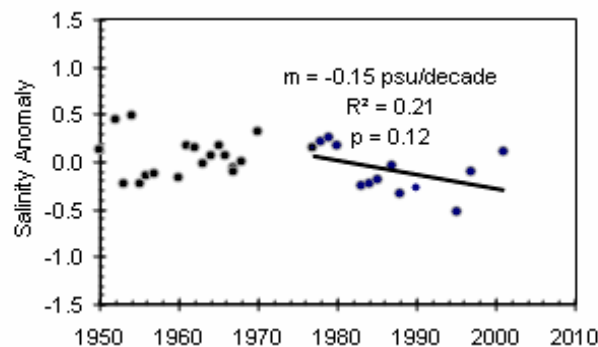


Figure 28: Freshening trend on the Baffin Island Shelf (50 – 200 m) in Aug - Oct; -0.15 ppt/decade between 1977 – 2002 (Hamilton and Wu 2013).

For the Baffin Island Shelf, from 1950 to 2005, no trend in either T or S can be identified in the 0 – 50 m layer, or the 0 – 200 m layer. However when considering a 50 – 200 m layer that excludes the highly variable top 50 m (Figure 28), there is a slight cooling trend (92% confidence) of 0.05 °C/decade for the analyzed August to October period. Over the second half of the period (1976 - 2002) there is freshening of -0.15 ppt/decade (88% confidence the trend is non-zero).

In central Baffin Bay, analysis of data from 1952 to 2005 indicates cooling in the 0 – 50 m layer of -0.16 °C/decade (94% confidence). However, in the 600 - 800 m depth interval, there is a clear warming trend of +0.13 °C/decade from 1950 - 2002 (Figure, Hamilton and Wu 2013). Zweng and Munchow (2006) saw a similar warming trend in Baffin Bay intermediate waters of 0.1 to 0.2 °C/decade over the 300 - 1000 m depth range from 1913 to 2003.

Baffin Bay's deepest waters have been warming for the last 100 years, likely as a result of Atlantic waters moving north into the eastern part of the Bay. During the last few decades, climatic conditions in regional air temperatures and offshore waters were characterized by large variation. After the warmer decades from the 1950s to the 1970s, a series of irregular cold years occurred in the 1980s and early 1990s (Drinkwater 2004; Stein 2005). However, the early years of the 21st century were warmer than normal.

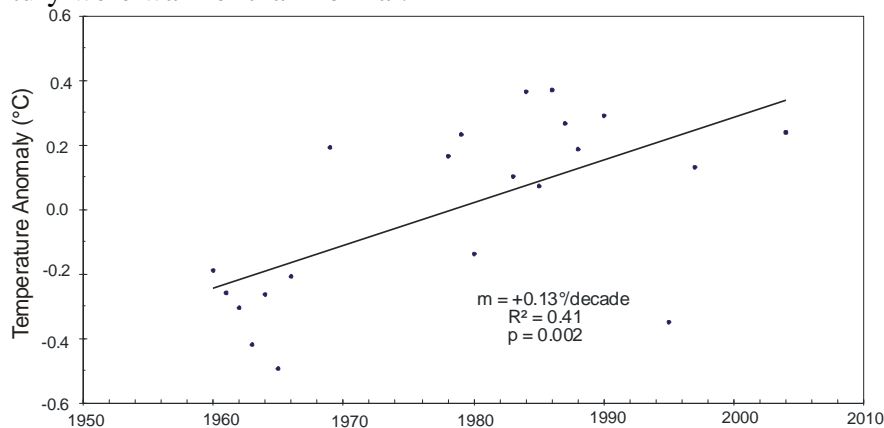


Figure 29: Warming of Baffin Bay intermediate waters in Aug - Oct; +0.13 °C/decade over the last half century (Hamilton and Wu 2013).

Zweng and Münchow (2006) used historical summertime hydrographic data from 1916 to 2003 and regression analysis to determine changes in temperature and salinity in Baffin Bay and Davis Strait. Warming trends on the Baffin and Iceland shelves are shown in Figure 30. They found two distinct sets of changes in the Baffin Bay region. First, the areas affected by the Atlantic inflow to Baffin Bay show substantial and statistically significant warming trends. The heat appears to be advected from the shelf and slope regions of the eastern Labrador Sea via Davis Strait along the west Greenland shelf break and diffuses vertically and horizontally into the deep central basin. Second, the Arctic inflow to Baffin Bay shows a marginally significant upper-layer freshening. This freshening extends along the eastern margin of Baffin Island to Davis Strait and into the Labrador Sea. Observed data from Davis Strait indicate a significant warming at 400 – 600 m depth of about 0.10 ± 0.09 °C/decade. There are no statistically significant warming trends detectable over the western portion of Davis Strait. However, the narrow shelf and slope region off Greenland south of 63°N latitude and inshore of the 1000 m isobath warmed

substantially by about 0.16 ± 0.10 °C/decade from 1925 through 1999 (Zweng and Münchow 2006).

Since 2000, persistent warm temperature anomalies have occurred in Baffin Bay, in contrast to temperatures observed during the latter part of the 20th century. This is the result of a northward displacement and strengthening of the Aleutian Low, and a weakening of the Icelandic Low; the latter being reflective of a trend toward more negative North Atlantic Oscillation and Arctic Oscillation values since the turn of the century (Overland and Wang 2005). Arctic winter, spring and autumn surface air temperature anomalies and associated sea level pressure fields have decidedly different spatial patterns at the beginning of the 21st century compared to most of the 20th century and may be considered an Arctic warm period (Overland et al. 2008). Most of the oceanographic data available for Baffin Bay, Davis Strait and West Greenland have been collected during summer and fall when the area is ice free (Ribergaard et al. 2008; Myers et al. 2009). However, Laidre et al. (2010) collected data in the West Greenland Current (WGC) in Baffin Bay during winter using narwhals as an oceanographic sampling platform. Results suggest that the twentieth century warming of the WGC documented by Zweng and Münchow (2006) has continued through the past decade. They found that this warming is associated with a warmer WGC. Laidre et al. (2010) also suggested a possible warming of central Baffin Bay subsurface waters.

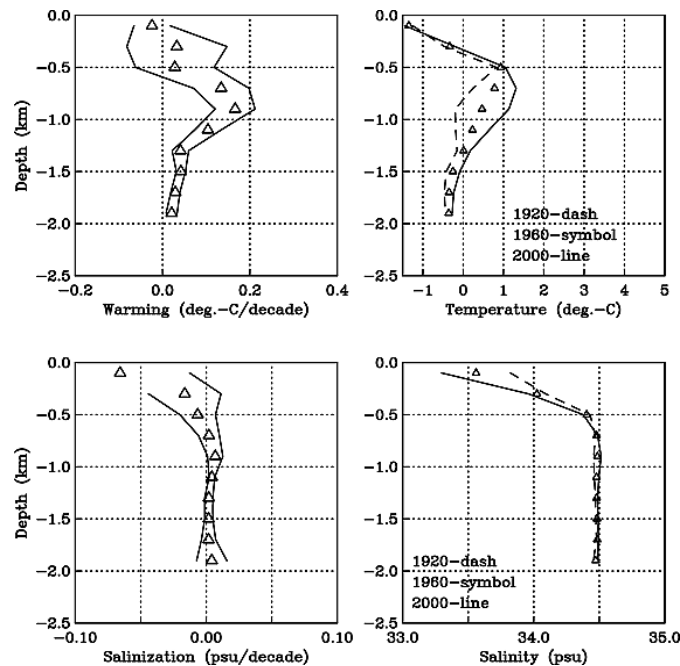


Figure 30: Time rate of change of temperature and salinity as a function of depth over the Baffin Island shelf break (defined by bottom depth $2000 \text{ m} > H > 600 \text{ m}$). The warming is significant from 600 to 2000 m with a maximum value of about 0.13 °C/decade. The freshening is limited to the near-surface (Zweng and Münchow 2006).

Hudson Bay: The distributions of salinity and water temperature in Hudson Bay and James Bay vary seasonally with freshwater runoff, ice cover, and surface heat flux. Galbraith and Larouche (2011), updated by Galbraith (unpublished data), analyzed trends in sea surface temperature (SST) for the past 35 years (1985 - 2011) in relation to ice break-up dates and air

temperatures using satellite data. Variable SST is observed in the south of the bay, where cold and warm modes might be the result of differing wind patterns. For example, years of simultaneous negative ENSO and strong NAO were found to coincide with colder summer air temperatures and late ice break-up (Wang et al. 1994).

From 1985 - 2011, the maximum summer SST increased by 0.7 - 1.3°C, depending on the region within the bay, or 2.7 °C per century using SST derived from air temperature and extended to 1918 (Galbraith, unpublished data). The coldest years occurred before 1992 while the warmest all occurred in the last decade, with a record high in 2010. SST during the warmest week of the summer (Figure 31) was fairly well predicted by the average air temperature between June and August and the date of ice retreat that precedes it (Galbraith and Larouche 2011). During the open water period the Belcher Islands area in the Southeast was consistently the coldest region, likely resulting from tidal mixing (Harvey et al. 1997).

Trends and changes in salinity, which provides the dominant control of density in Hudson Bay (Granskog et al. 2011) are strongly dependent on trends and changes in runoff, sea ice formation and melt (Section 2.2.5), however no quantitative salinity trend analysis is available. Changes in water masses and their vertical structure over the annual cycle are summarized by Granskog et al. (2011).

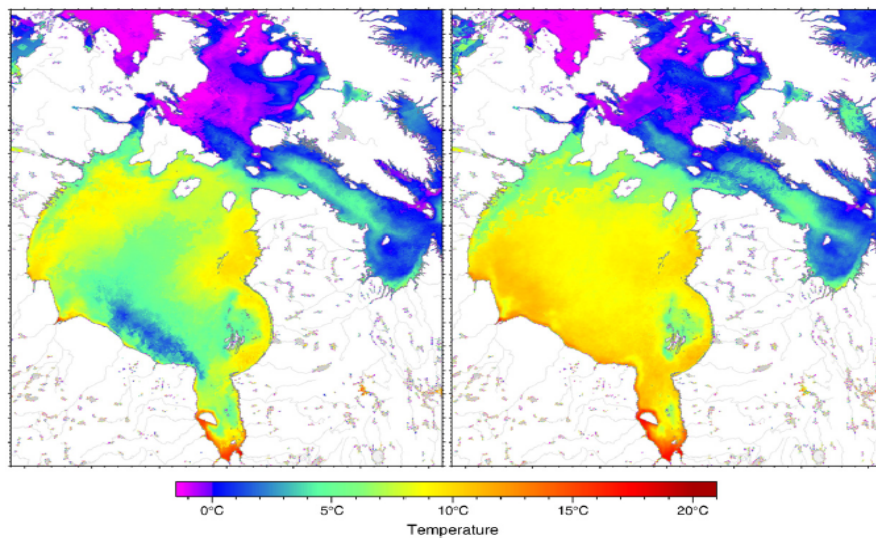


Figure 31: Sea surface temperature climatologies for the warmest week of the year (late August) for the two alternating cold and warm states observed (Galbraith and Larouche 2011).

2.2.4 Ocean Currents

Beaufort Sea: There is only one observational record from the Beaufort Sea providing comprehensive information on change in Beaufort waters over 1 - 2 decades; there are no records that come close to ACCASP's half-century target. The sites of value are at the middle and outer edge of the Mackenzie shelf north of Kugmallit Bay (depths of 55 and 110 m). These time series began in 1990.

Current measured at a single site is a poor representation of conditions across the Beaufort as its domain of relevance is only about 10 km (see above). Ice movement, however, is regionally coherent because the rigidity of the pack smooths out small-scale variations.

Ice velocity (surface current) is pertinent to the net movement of surface water over averaging times of interest and to the strength of upwelling at the coast and the shelf edge. The average velocity of ice directed west-north-west across the southern Beaufort has increased during the last two decades. Trends for overlapping trimesters Oct - Dec, Dec - Feb, Feb - Apr and Apr - Jun have been 3.7, 1.0, 1.0 and 2.4 cm/s per decade. The largest values are in autumn and spring, times of weak and strong ice respectively, while strong east wind dominates the Beaufort in both seasons. These factors suggest that faster ice movement (surface flow) is a response to stronger east wind in recent years. The time series for the period of largest trend, Oct - Dec, is shown in Figure 32. The trend in this season is statistically significant on the 10% level, whereas those in other seasons are less significant.

Ice speed (surface current) is a measure of energy in the ocean circulation and is pertinent to ocean mixing and stratification. The average speed of ice drift across the southern Beaufort has also increased during the last two decades although not as rapidly as velocity. Trends for months with annually recurrent complete ice cover (Nov, Dec, Jan, Feb, Mar, Apr) have been 2.7, 3.3, 1.6, 0.8, 0.06 and 1.6 cm/s per decade. Again the trends have been largest during autumn and spring. The weaker trends in ice speed imply that surface current has become more persistent as well as stronger; in simple terms, an earlier wiggly pattern of movement has been “stretched out” to yield greater net movement.

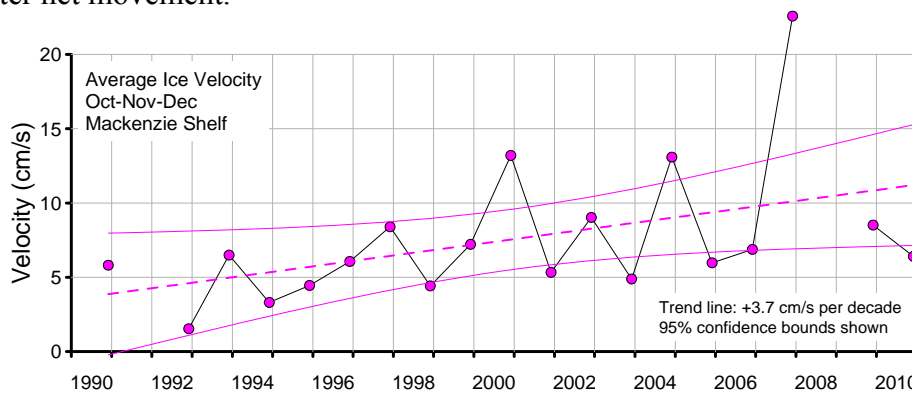


Figure 32: Average velocity of ice movement during October through December based on continuous measurements by sonar at mid shelf. (Melling 2013, unpublished data).

Canadian Polar Shelf: Records of ocean current (or ice drift) are scarcer and shorter on the Canadian Polar Shelf than in the Beaufort Sea. There is only one point of observation, in western Lancaster Sound, that meets ACCASP’s modest ten-year target. Conditions of change are unknown over the remaining 1.5M square kilometres of the shelf.

Figure 33 displays the estimated eastward flow of seawater through Lancaster Sound based on observations between 1998 and 2009. This outflow from the Arctic Ocean is generally colder than 0°C and about 7% (1/15th) fresh water. The flow varies strongly with season, being three times faster in late summer than in early winter. It also varies interannually: flow was weak during 1998 - 99 and 2007 - 08. The flow has decreased at an average rate of -0.011 Sv per

decade, [1 Sverdrup (Sv) is 1 million cubic metres per second] statistically significant on the 25% level. The expanded section of synchronous measurements in Lancaster Sound and Nares Strait illustrates how a single site cannot represent conditions throughout the polar shelf.

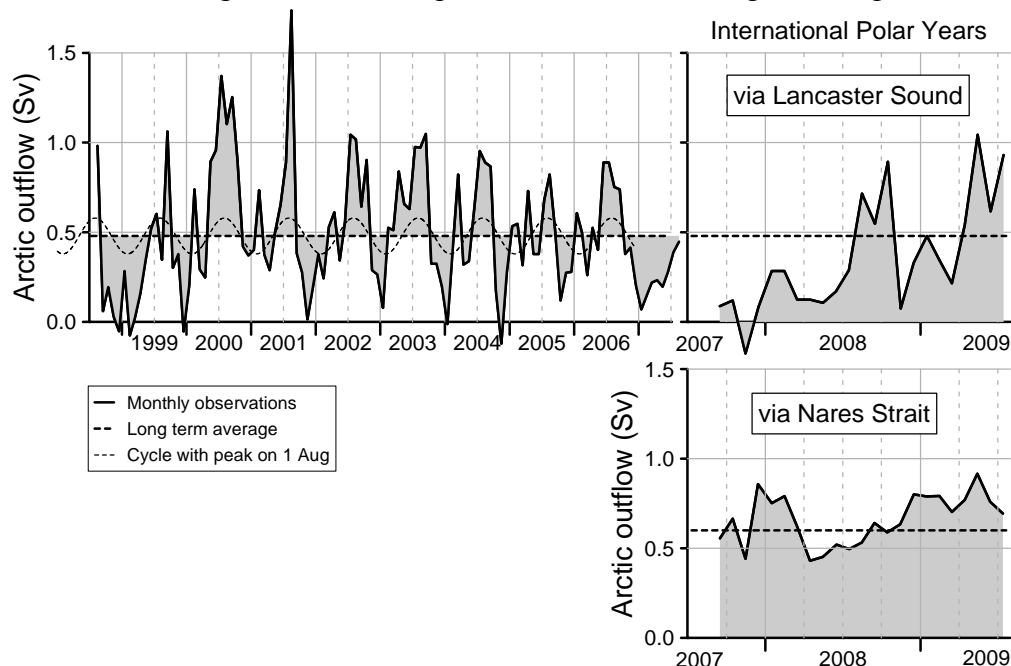


Figure 33: Varying flows of seawater through Lancaster Sound and Nares Strait since 1998 (Melling et al. 2012).

Baffin Bay/Davis Strait: Observational current data in Baffin Bay/Davis Strait provide some information about circulation patterns, transports and seasonal variability, but they are far too sparse to establish the presence of any trends. Circulation is generally cyclonic, with the main features being the southward flowing Baffin Island Current along the western side, and the northward flowing WGC on the Greenland shelf and slope. Tang et al. (2004) found that currents are generally stronger at all depths in summer and fall. They estimate a mean freshwater transport through Davis Strait of ~ 120 mSv from their observations. A comprehensive instrument array has been maintained across Davis Strait since 2004, but only data from the first year of that program are published (Curry et al. 2011), providing an estimate of 116 mSv for the southward fresh water flux. Results from the following years are soon to be published, and will be useful in looking at short term trends, but there are insufficient historical data to analyze trends over decadal or longer time scales.

2.2.5 Freshwater input

Beaufort Sea: Figure 34 displays estimates of the volume of fresh water mixed with seawater (nominal 34.8 salinity) in the Beaufort Gyre of the southern Canada Basin; the estimates are based on annual late summer surveys similar to that shown (Proshutinsky et al. 2009; R Krishfield, pers. comm. 2012). The inventory of fresh water builds up during the first pentade and is constant during the second. This time series is clearly too short to provide a meaningful estimate of trend.

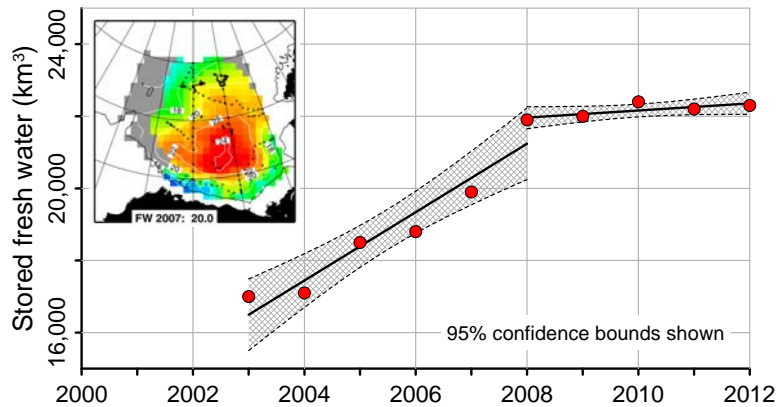


Figure 34: Storage of freshwater in the Canada Basin in late summer, re. 34.8 salinity. (Updated from Proshutinsky et al. 2009).

Long et al. (2012) investigate the interannual variations of fresh water content (FWC) and sea surface height (SSH) in the Beaufort Sea, particularly their increases during 2004 - 2009, using a coupled ice-ocean model (CIOM), adapted for the Arctic Ocean to simulate the interannual variations. The CIOM simulation shows a (relative) salinity minimum in the Beaufort Sea and a warm Atlantic water layer in the Arctic Ocean, similar to the Polar Hydrographic Climatology (PHC). The simulation also captures the observed FWC maximum in the central Beaufort Sea, and the observed variation and rapid decline of total ice concentration over the last thirty years. The model simulations of SSH and FWC suggest a significant increase in the central Beaufort Sea during 2004 - 2009. The simulated SSH increase is about 8 cm, while the FWC increase is about 2.5 m, with most of these increases occurring in the center of Beaufort Gyre. Long et al. (2012) show that these increases are due to an increased surface wind stress curl during 2004 - 2009, which increased the FWC in the Beaufort Sea by about 0.63 m/y through Ekman pumping. Moreover, the increased surface wind is related to the interannual variation of the Arctic polar vortex at 500 hPa. During 2004 - 2009, the polar vortex had significant weakness, which enhanced the Beaufort Sea High by affecting the frequency of synoptic weather systems in the region (see section 2.1.3 for a more detailed discussion on trends in the atmospheric pressure pattern). In addition to the impacts of the polar vortex, enhanced melting of sea ice also contributed to the FWC increase by about 0.3 m/y during 2004 - 2009.

Baffin Bay/Davis Strait: Water enters Baffin Bay/Davis Strait by three pathways; the Canadian Arctic Archipelago (CAA) Passages, the WGC and glacial melt water from Greenland, Ellesmere and Baffin Islands (the latter 2 being minor contributors compared to Greenland). Of the 3 passages through the CAA, analysis of sufficient data has only been conducted at Barrow Strait/Lancaster Sound (Peterson et al. 2013) to allow for a trend analysis of transports into Baffin Bay. At Barrow Strait, since 1999 there has been a trend towards lower volume and freshwater transports of -207 mSv/decade and -14 mSv/decade respectively, with a 13% statistical significance (Hamilton and Wu 2013). However, with so few data points though, the magnitude of these trends is not well defined, e.g. if the 1999 data point in Figure 35 is omitted, the computed trend is -23 mSv/decade, which is 64% larger than what is computed when all 12 points are used.

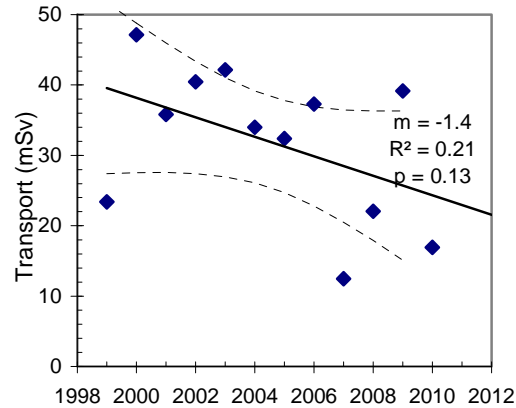


Figure 35: Annual mean freshwater transport through Barrow Strait with trend line of slope m (mSv/y) and 95% confidence limits shown.

Freshwater also enters Baffin Bay/Davis Strait from the south along the West Greenland shelf and slope via the WGC. This water is of Arctic Ocean and glacial origin, having been carried from Fram Strait by the East Greenland and East Greenland Coastal Currents southward along the east coast of Greenland to the southern tip of Greenland. About 96 mSv rounds Cape Farewell to enter the western North Atlantic. There are rather limited data to quantify the portion of this inflow that remains in the northward coastal flow to enter Davis Strait and then Baffin Bay, but these data lead to a rough estimate of 37 mSv (Hamilton and Wu 2013).

A third freshwater source is liquid and solid discharge from the Greenland ice sheet. Based on the mass loss estimate for 2010 provided by Rignot et al. (2011), and the pattern of this freshwater discharge around the Greenland coast defined by Bamber et al. (2012), the current meteoric input into Baffin Bay is about 8 mSv. Using an 18 year record of ice sheet loss rate (1992 - 2010), Rignot et al. (2011) compute an acceleration in the Greenland ice sheet loss rate of 22 Gt/y (0.76 mSv/y).

Hudson Bay: The surface waters of Hudson Bay receive unusually large volumes of freshwater in the form of river runoff and from melting sea ice. The Hudson Bay drainage basin covers more than a third of Canada's land mass (Déry et al. 2011) and is larger than those of the St. Lawrence and Mackenzie rivers combined, with double the combined average annual discharge rate (i.e. $20,700 \text{ m}^3 \text{ s}^{-1}$; Prinsenberg 1988). The river discharge fluctuates seasonally by a factor of three (low during winter, peak in spring, low but constant over the summer, and slow decrease during autumn), with a mean value of $635 \text{ km}^3 \text{ y}^{-1}$ (Déry et al. 2011). This value represents 12% of the pan-Arctic annual river runoff and would mean the annual addition of 80 cm of freshwater over the whole area of the basin (St-Laurent et al. 2011).

In a recent modeling study recreating the annual budget (2003 - 2004) of freshwater sources and sinks for Hudson and James bays, St-Laurent et al. (2011) reported that while precipitation and evaporation rates are still not well quantified based on limited observations, estimates of $P - E$ rates whether positive (Gill 1982) or negative (Prinsenberg 1980), remain smaller than the annual runoff or sea ice melt by a factor of two or more (Table 1). Ice formation in winter and melt in spring mostly offset each other on an annual basis, leaving river runoff as the main net source of freshwater to the system (St-Laurent et al. 2011).

Table 1. Annual budget (August 2003 to August 2004) for the freshwater (FW) and volume (Vol.) of Hudson and James bays, in $\text{km}^3 \text{y}^{-1}$ relative to $S_0 = 33$ ppt. The upper portion lists the sources and sinks of freshwater, and the lower portion details the fluxes through the four channels (see St-Laurent et al. 2011, their Figure 1) making up the mouth of Hudson Bay (positive fluxes are outward). Note that the river runoff for this period is slightly lower than the long-term mean ($635 \text{ km}^3 \text{y}^{-1}$, Lammers et al. 2001). P – E stands for precipitation minus evaporation rate. (Table adapted from St-Laurent et al. 2011).

	Riv	+	P-E	-	Growth	+	Melt	=	Net Flux	+	Residual
	607	+	222	-	729	+	649	=	743	+	6
	Net Flux	=	Ch. 1	+	Ch.2	+	Ch. 3	+	Ch.4	+	Residual
FW	743	=	-16	+	-5	+	14	+	802	+	-
Vol.	607	=	-556	+	-2026	+	-3474	+	6615	+	48

Spatially, sources of freshwater to the system differ (Granskog et al. 2011). The effect of sea ice on freshwater distributions in Hudson and James Bay differs from runoff in two very important ways. First, the ice melt is introduced widely across the bay's surface, but with a stronger input towards the south due to prevailing winds in spring, whereas runoff is introduced around the boundary and is then predominantly contained in a cyclonic coastal transport corridor (Granskog et al. 2009). Second, a similar amount of fresh water is withdrawn in winter, when sea ice is formed, and this withdrawal tends to occur more strongly in the northwestern part of Hudson Bay and in the flaw leads that recur at the seaward edge of the landfast ice (Kuzyk et al. 2008a; Barber and Massom 2007; Stewart and Barber 2010).

Discharge data for 42 rivers with outlets into Hudson, James, and Ungava Bays for the period of 1964 to 2000 have been compiled by Déry et al. (2005) (Figure 36). These records showed an overall 13% decline in annual streamflow, compared to a 11 to 14% increase for Eurasian rivers with outlets into the Arctic Ocean for the same period (McClelland et al. 2006), revealing a contrasting trend for the Hudson Bay region. In a more recent study of streamflows for 23 rivers discharging into Hudson and James Bays for the period of 1964 - 2008 (Déry et al. 2011), no detectable change in total discharge was observed overall, but a 5-year running mean revealed decadal trends: a downward trend from the mid-1960s to the mid-1980s, followed by relatively high flows in the mid-1980s, and then an upward trend starting in the early 1990s, marked by a record annual discharge in 2005. As with air temperature, river discharge into Hudson Bay showed a clear change in the early 1990s.

The recent trend of increasing streamflow into Hudson Bay may be a manifestation of this intensification of the hydrological cycle, consistent with other regions of the Arctic (Déry et al. 2009). Some studies argue that observed increases in Arctic river discharge in the late 20th century follow the global rise in surface air temperatures (McClelland et al. 2006; Peterson et al. 2006). Rising air temperatures allow more moisture loading in the atmosphere that in turn leads to higher net precipitation fluxes in the Arctic. Thus, warming in the Arctic is expected to drive an intensification of its hydrological cycle including increasing river discharge, as seen since the 1990s in Hudson Bay. These annual fluctuations in river discharge could also be related to

changing precipitation patterns driven by the Arctic Oscillation (Déry and Wood 2004). Continued monitoring of Hudson Bay streamflow in the coming years and decades will reveal if the recent 20-year upward trend will persist as projected by most GCM simulations, or whether it is part of an interdecadal oscillation tied to large-scale climate variability.

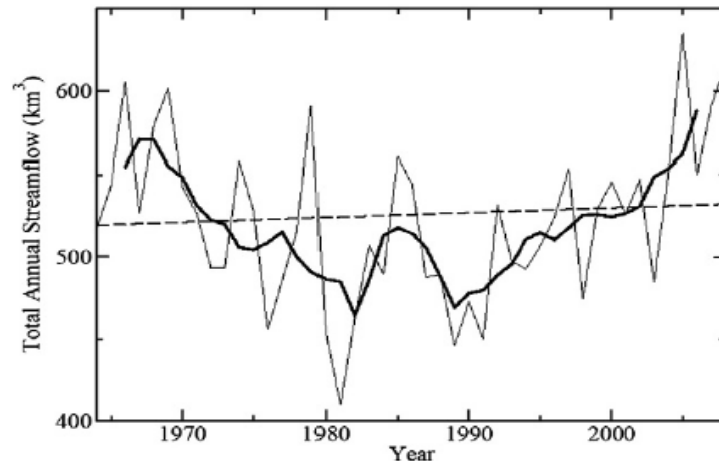


Figure 36: Temporal evolution of the total annual streamflow into Hudson Bay, 1964 - 2008. The thick line represents the 5-year running mean. The dashed line represents the linear trend for the overall 45-year period (Déry et al. 2011).

2.2.6 Relative Sea Level

Beaufort Sea and Canadian Polar Shelf: Relative sea level is the height of the sea surface relative to land at the coast. Change in relative sea level involves a number of different processes in the Canadian Arctic.

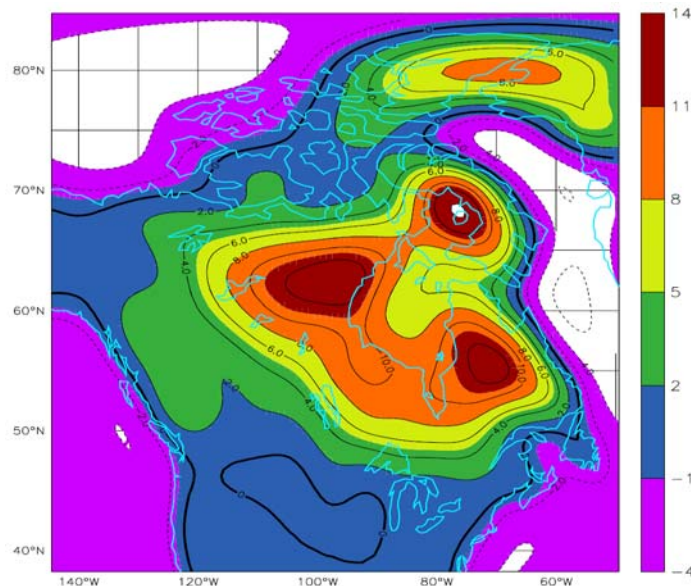


Figure 37: Present rate of post-glacial rebound (mm/y) from calculations using a glacial systems model (Tarasov and Peltier 2004).

The first is change in absolute sea level, which represents change in the volume of seawater in the ocean. Absolute sea level has been rising steadily for over a century, in response to warming

and expansion of ocean waters, and the addition of water from shrinking glaciers and small ice caps. Information compiled by the IPCC reveals that the rate of rise has averaged about 2 mm/y during the last 50 years and has been close to 3 mm/y since 2000. (http://www.ipcc.ch/publications_and_data/ar4/wg1/en/ch5s5-5-2.html).

In the Canadian Arctic, glacial effects on relative sea level modify the impact of rising absolute sea level. One aspect is the uplift of Arctic land surfaces via isostatic adjustment to the loss of continental ice sheets at the end of the Ice Age. Models suggest that the rate of post-glacial crustal rebound is more than 10 mm/y around Hudson Bay and in the High Arctic, while subsidence is predicted over the Beaufort and the western part of the Arctic Archipelago (Figure 37).

There are few corroborative data. Time series of vertical land motion are short and geographically sparse in the Arctic (Craymer et al. 2006). The pattern revealed by data from GPS receivers at a few locations since 2003 (Figure 38) shows uplift at 4 - 10 mm/y throughout the Canadian Arctic, except at Inuvik where the land surface is sinking at about 4 mm/y. The expected broad adjacent region of subsidence is presumably further to the west beneath the Beaufort Sea.

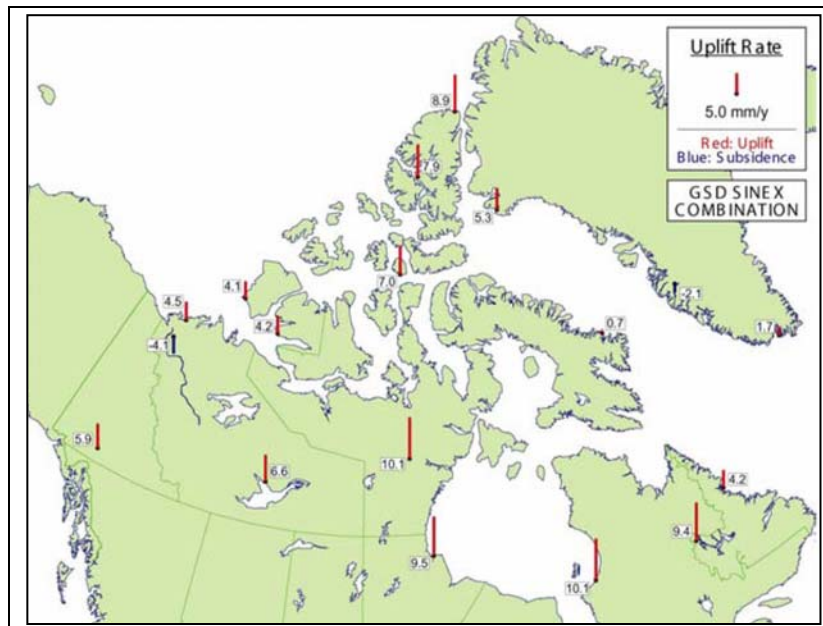


Figure 38: Preliminary results from continuous GPS logging since the early 2000s (Herron et al. 2008).

A second consequence of change in the volume of terrestrial ice caps is decrease in their gravitational pull. Although the ice lost from the ice cap is delivered as water to the ocean, thereby raising sea level, this water is spread across the globe, whereas the consequent change in gravitational attraction is concentrated locally. This disparity in effects causes sea level to drop within about 1500 km of Greenland despite rising sea level at distant locations (Kopp et al. 2010). Figure 39 depicts the spatial pattern of this effect. Roughly speaking, if Greenland ice melt is contributing 1 mm/y to global sea-level rise, sea level at Iqualuit will actually fall by 1.2

mm/y. That is, the effect of reduced gravity pull is 2.2 mm/y at Iqualuit (http://www.enr.gov.nt.ca/live/pages/wpPages/soe_big_picture.aspx#7).

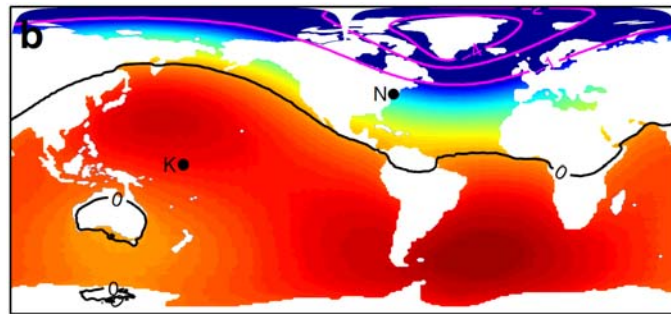


Figure 39: Spatial pattern of the change in absolute sea level caused by melting of Greenland's ice cap. Red shading denotes areas of rising sea level and blue dropping sea level (Kopp et al. 2010).

In the Mackenzie delta, there are two other effects on vertical motion of the land surface: One is the isostatic adjustment (subsidence) to the weight of sediment deposited on the shelf by the Mackenzie River over thousands of years, and the other is the compaction of that sediment as water is forced out of it. The melting of permafrost, the decomposition of gas hydrates and possibly the extraction of oil and gas from Beaufort sediments may also contribute to local subsidence.

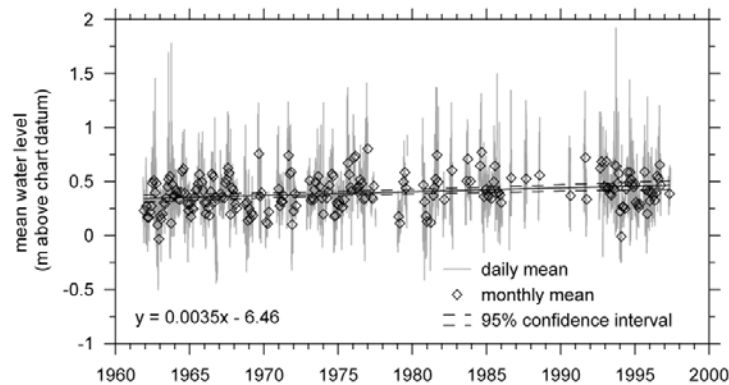


Figure 40: Relative water level measured at the tide gauge at Tuktoyaktuk (Manson and Solomon 2007).

This discussion provides little quantitative insight into recent change in relative sea level across the Canadian Arctic. The observational record at most stations is very short and the net effect of competing influences varies across the region. An analysis of 35 years of measurements at Tuktoyaktuk by Manson and Solomon (2007) suggests a relatively rapid 3.5 ± 1 mm/y rise in relative sea level at the edge of the Mackenzie Delta (Figure 40). Time series from recently established geodetically referenced gauges at other locations are not long enough. Results from Alert in the High Arctic and Ulukhaktok (formerly Holman Island) in the west are displayed in Figure 41. The plots reveal a decline in relative sea level over 3.5 years at both sites, but the rates are poorly constrained: -5 ± 11 mm/y at Alert and -20 ± 14 mm/y at Ulukhaktok. The fairest conclusion is that relative sea level has been dropping over much of the Canadian Arctic, rising in the Mackenzie Delta, and changing sign somewhere in between.

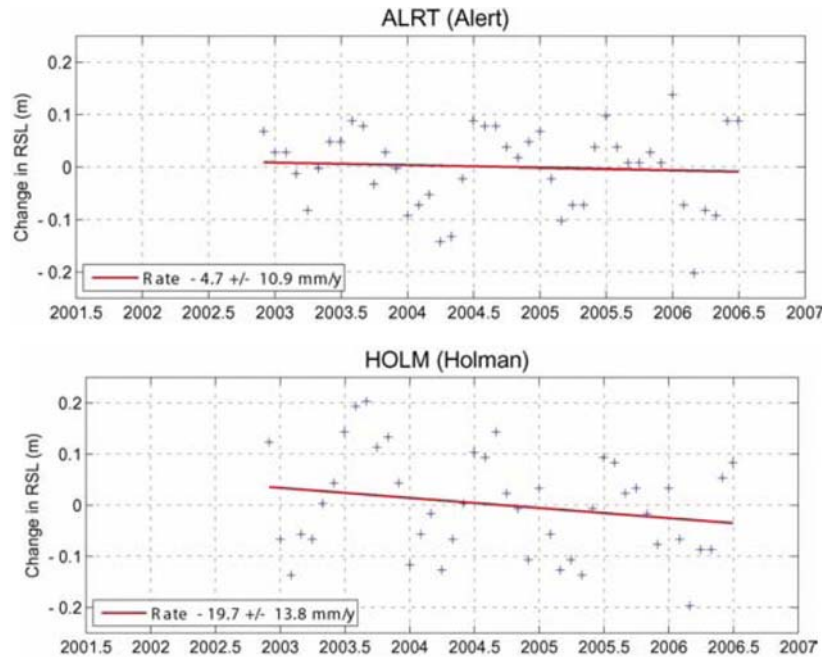


Figure 41: Monthly Relative Sea Level (RSL) Time Series for Alert and Ulukhaktok (Craymer et al. 2006).

2.3 CHEMICAL OCEANOGRAPHY

2.3.1. Nutrients, Carbon, Acidification

There are on-going and terminated time series studies for chemical oceanography in the Arctic that are mainly sustained/conducted by DFO, including the JOIS program in the Canada Basin, and Barrow Strait, Nares Strait, and Davis Strait monitoring lines (Figure 42).

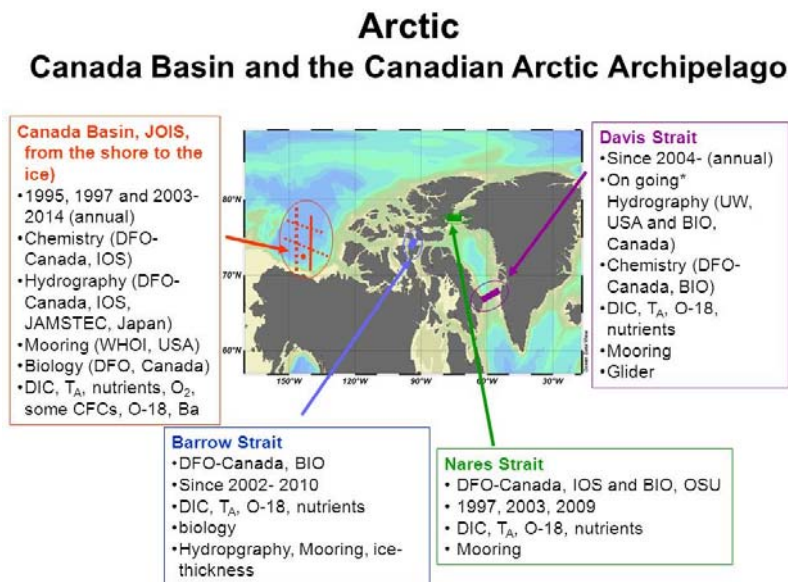


Figure 42: Measurement programs in the Canada Basin and Canadian Arctic Archipelago.

Approximately one third of the anthropogenic carbon dioxide to date has been absorbed by the ocean worldwide. The uptake has increased the acidity of seawater and reduced its carbonate concentration. Ocean acidification can significantly affect growth, metabolism, and life cycles of marine organisms (Gattuso and Hanson 2011, and references therein), and hence has received increased attention both within the scientific community and from stakeholders (AMAP 2013). Ocean acidification is intensified by increased atmospheric CO₂ and consequent ocean uptake as well as by increased freshwater inflow from river runoff, ice melt, and low pH Pacific water. Changes in sea ice (Section 3.3.3) affect the CO₂ exchange between atmosphere and ocean either directly (via changes in open water areas) or indirectly (e.g. via changes in biological uptake or changes in sea ice). Localized upwelling of acidic waters can further increase acidification in and surface and near surface waters (e.g. Chierici and Fransson 2009; Carmack and McLaughlin 2011). While enhanced primary production can seasonally increase the saturation state, subsequent remineralisation of sinking material releases CO₂ and further reduces the saturation state in the subsurface. These combined effects make Arctic waters especially vulnerable to a declining saturation state of calcium carbonate (CaCO₃) minerals such as aragonite and calcite (e.g. Bates and Mathis 2009; Yamamoto-Kawai et al. 2009; 2011; Denman et al. 2011). Aragonite and calcite are the two forms of CaCO₃ commonly produced by marine organisms; aragonite is a less stable form of CaCO₃ and consequently more vulnerable to increasing ocean acidification. The saturation state of seawater with respect to CaCO₃ (Ω) is a measure of its potential to corrode the CaCO₃ shells and skeletons of marine organisms and is defined as a product of the carbonate and calcium concentrations divided by the solubility product. CaCO₃ shells start to dissolve when the waters become undersaturated with respect to CaCO₃, i.e. the saturation state falls below 1.0 ($\Omega < 1.0$).

Beaufort Sea: The chemistry of near-surface waters is of great relevance to ocean ecosystems. Despite numerous seawater surveys in the Beaufort since the 1950s (Fissel and Melling 1990), the resulting long-term series provide only limited information. The brief and sporadic surveys cannot resolve natural variation over the wide range of time scales on which it occurs. Consequently these surveys have only limited value in detecting progressive change, and we know virtually nothing of geochemical change in the Beaufort over the last half century.

The most useful insight into recent change has emerged from annual systematic surveys of the Beaufort gyre since 2003 (McLaughlin et al. 2011). Observations during the first five years revealed increasing dilution of the gyre by fresh water. By 2008, waters at 100 - 200 m depth had become under-saturated with respect to aragonite (Yamamoto-Kawai et al. 2009; Yamamoto-Kawai et al. 2011). The water at this depth in the Canada Basin forms on Arctic shelves in winter, predominately in the Chukchi Sea where cold water allows high uptake of carbon dioxide by re-mineralization of organic material and absorption from the atmosphere (Bates et al. 2011).

Miller et al. (2013, unpublished data) evaluate changes in the marine carbonate system of the western Arctic from a recently “rescued” data set and find substantial changes since the 1970s. Averaging observations from the Beaufort Sea and Canada Basin, they find the mean at the surface still supersaturated (i.e. > 1), but upper halocline waters and deep waters now show regularly occurring aragonite undersaturation. Yamamoto-Kawai et al. (2011) calculate

decreases in aragonite saturation state of 0.2 in 1997 and 0.6 in 2008, relative to preindustrial values.

Canadian Polar Shelf/Baffin Bay/Davis Strait: There was a time series study at Barrow Strait from 2003 to 2010 showing steady decline of pH and Ω with waters at 100 - 200 m depth undersaturated with respect to aragonite (Azetsu-Scott et al. 2010), as in the Beaufort Sea, we have little notion of how the situation has changed over the last decade. All available carbon data from the Canadian Polar Shelf, Baffin Bay, Davis Strait, Hudson Bay systems and the NW Atlantic were compiled from the Carbon Dioxide Information Analysis Center (CDIAC, <http://cdiac.ornl.gov/oceans/datmet.html>) and a Canadian database (BioChem, <http://www.medsdmm.dfo-mpo.gc.ca/BioChem/biochem-eng.html>). Despite the scarcity of data, a lower saturation state and pH were evident in surface waters during the period of 2000 - 2011 compared to a decade earlier (Figure 43). The progress of ocean acidification is especially apparent at Parry Channel and along the Baffin Inland coast, where Arctic water flows out. No data are available for the Hudson Bay system in 1990 - 1999, however, the aragonite saturation state (Ω_A) and pH are low during 2000 - 2011 and the saturation horizon in the region was less than 50 m. Due to the large freshwater input from rivers and projected changes in ice cover, the Hudson Bay system is one of the most vulnerable regions for ocean acidification.

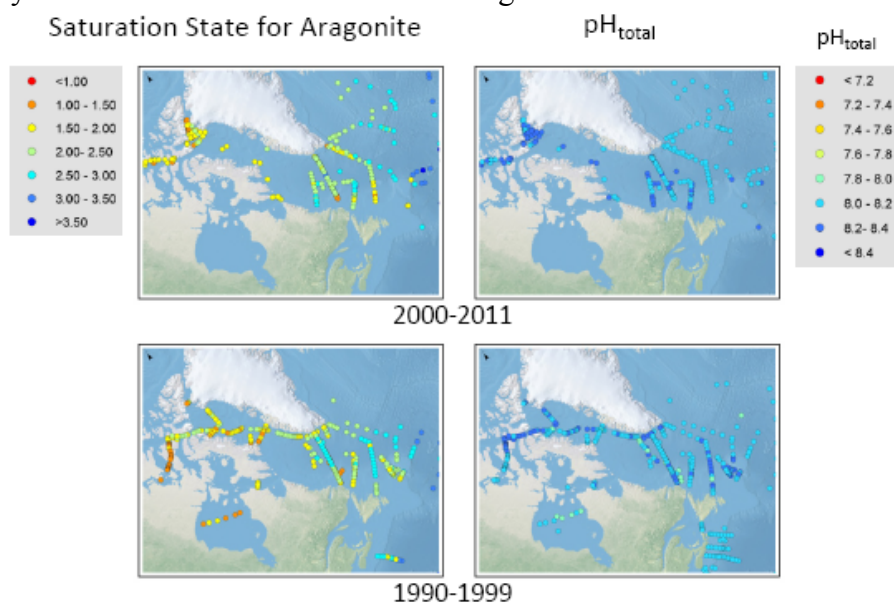


Figure 43: Saturation state of seawater with respect to aragonite (Ω_A) and pH in the total scale (pH_{total}) in surface waters during the periods 1990 - 1999 and 2000 – 2011.

In Davis Strait, low saturation states (Ω) were associated with Arctic outflows in the upper 300 m on the western side, extending to > 50 km offshore (Figure 44). The highest Ω and pH values were observed over the wide West Greenland Shelf. However, the decreasing rate of Ω and pH during a study period from 2004 to 2010 were also highest in this water mass (Azetsu-Scott et al. 2010). Total alkalinity and salinity decreased with no significant increase in dissolved inorganic carbon concentrations in West Greenland Shelf Water. The dominant freshwater source on the West Greenland Shelf is glacial meltwater which has low Ω and pH. Observed changes in West Greenland Shelf Water are due to increased input of glacial meltwater on the shelf. Although the duration of the time series is too short to show a strong trend, decreases in Ω_A (-0.058/y) and pH

(-0.016/y) on the Western Greenland Shelf were observed. This rate of pH decrease is substantially lower than reported values of 0.0017 in the subtropical North Atlantic (González-Dávila et al. 2007), 0.0024 in the Iceland Sea (Olafsson and Olafsdottir 2009), and 0.0028 in the Labrador Sea (Greenan et al. 2010). Since the Davis Strait region is strongly influenced by local and seasonal variability due to ice formation/melting and glacial meltwater and iceberg discharge, continuous observations are necessary to understand the progress of ocean acidification

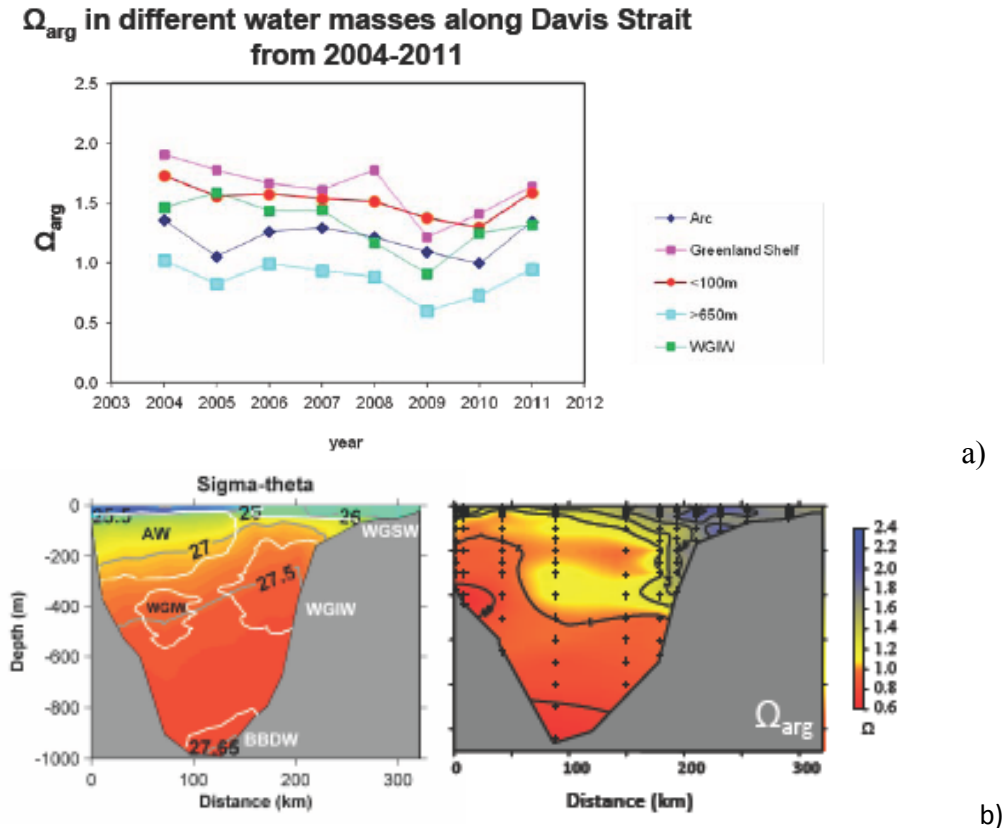


Figure 44: a) Temporal variability of saturation state in different water masses along Davis Strait from 2004 - 2010 and b) cross section of density (σ_θ) and aragonite saturation state (Ω_A).

Hudson Bay: According to the World Ocean Atlas (WOA2009), average annual nitrate concentrations at the surface vary from 1 mmol/m³ in the southern area to 7 mmol/m³ in the northern area. Ferland et al. (2011) measured surface nitrate concentrations in summer of the order of 1 mmol/m³ or less. In Baffin Bay, the average annual nitrate concentrations at the surface are less than 1 mmol/m³ in the northern area and 4 mmol/m³ in the south of the bay (WOA2009). Vertical profiles of physical variables, nutrients and biological productivity were conducted along transects across Hudson Bay and Hudson Strait between 2003 and 2006 (MERICA-Nord Program: Monitoring and Research in the Hudson Bay Complex; Figure 45) and across the Bay in 2005 - 2007 and 2010 (ArcticNet program). Temporal, spatial, and vertical patterns in nutrient concentrations and primary productivity are reported in Ferland et al. (2011), and zooplankton biomass and diversity in Estrada et al. (2012).

Mean integrated $\text{NO}_3^- + \text{NO}_2^-$ concentrations in the euphotic zone (Z_{eu}) ranged from 0.1 to 12.3 mmol m^{-3} in the Hudson Bay System (Figure 45c). Mean integrated PO_4^{3-} concentrations in Z_{eu} varied between 0.35 and 2.25 mmol m^{-3} while $\text{Si}(\text{OH})_4$ was the most abundant nutrient during the study periods, with mean integrated concentrations in Z_{eu} ranging from 0.1 to 24.4 mmol m^{-3} . There was no consistent regional pattern, except for higher $\text{Si}(\text{OH})_4$ concentrations in Hudson Bay relative to Hudson Strait and Foxe basin. Ratios of $(\text{NO}_3^- + \text{NO}_2^-) : \text{Si}(\text{OH})_4$ and $(\text{NO}_3^- + \text{NO}_2^-) : \text{PO}_4^{3-}$ in the euphotic zone were lower than the Redfield ratios of 1:1 and 16:1, suggesting that dissolved inorganic nitrogen was the macronutrient in lowest supply for phytoplankton growth. Surface waters were almost depleted in nutrients at all stations in Hudson Bay above the deep Chl-*a* maximum, while deep waters (below 100 m) represented a large nutrient reservoir, with mean concentrations of 12 mmol m^{-3} for NO_3^- , 30 mmol m^{-3} for $\text{Si}(\text{OH})_4$ and 1.7 mmol m^{-3} for PO_4^{3-} . In most parts of Hudson Bay, surface waters are replenished in nutrients during winter mixing, which appears to be a critical process to bring nutrient-rich deep water to the surface (Ferland et al. 2011).

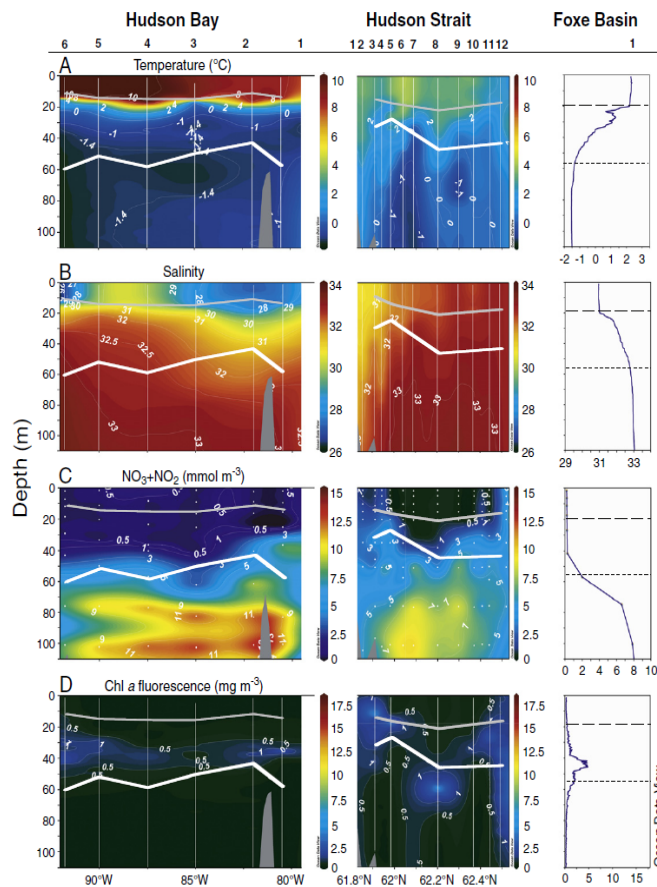


Figure 45: Spatial distribution of (A) water temperature, (B) salinity, (C) $\text{NO}_3^- + \text{NO}_2^-$, and (D) in vivo chlorophyll *a* fluorescence in northern Hudson Bay, Hudson Strait and Foxe Basin on 1 - 13 September, 2005. Thin gray lines and dashed lines: surface mixed layer depth (Z_m); thick white lines and dotted lines: euphotic zone depth (Z_{eu}). Station locations are shown at the top of the figure (from Ferland et al. 2011).

All available field observations of nutrient concentrations collected in Hudson Bay since the 1960s were compiled and analyzed by M. Starr and J.-Y. Couture (unpublished data). The

analysis of the overall dataset proved inconclusive, but trends were revealed when data from the center of the Bay only were analyzed. Between 1961 and 2006, nitrate (NO_3^-) concentration in the surface mixed layer (0 - 30 m) decreased at a rate of $0.81 \text{ mmol m}^{-3}/\text{decade}$. No trends could be revealed for phosphate (PO_4^{3-}) or silicate ($\text{Si}(\text{OH})_4$) over the study period, but silicate during the MERICA period (2003 - 2006) showed a rapid decline of $0.68 \text{ mmol m}^{-3}/\text{y}$. At depths of 100 m and more, all three nutrients exhibited significant increases at rates of $1.7 \text{ mmol m}^{-3}/\text{decade}$ for nitrate, $0.26 \text{ mmol m}^{-3}/\text{decade}$ for phosphate and $7.2 \text{ mmol m}^{-3}/\text{decade}$ for silicate. Decreasing nitrate (and silicate) in surface waters and nutrient increase at depth is likely a result of less winter mixing, and/or stronger stratification during summer.

Ship-based observations of sea-surface fugacity of CO_2 ($f\text{CO}_{2\text{sw}}$) were found to range from 259 μatm in Hudson Strait to 425 μatm at the entrance to James Bay (Else et al. 2008a, b). Spatially, strong relationships between $f\text{CO}_{2\text{sw}}$ and river discharge were identified, with coastal waters being supersaturated with respect to the atmosphere, while offshore waters were undersaturated. High correlations of $f\text{CO}_{2\text{sw}}$ with salinity, sea surface temperature, and coloured dissolved organic matter suggest that thermodynamic effects and the oxidation of riverine carbon are driving supersaturation in the coastal zone. The results of this study indicate that the offshore continental shelf regions of Hudson Bay act as a sink of CO_2 , while the nearshore outer-estuary systems act as a source (Else et al. 2008a, b).

Particles reaching the sediments in Hudson Bay are a mixture of marine and terrigenous organic matter (Kuzyk et al. 2008b; Kuzyk et al. 2009). Results from a long-term sediment trap located in southeastern Hudson Bay also revealed C:N ratios of the particles were a mixture of marine and terrigenous organic matter. Vertical fluxes at 100 m were generally highest during the ice melt period (Lalande and Fortier 2011), but important interannual variability was also observed. Elevated particulate organic carbon (POC) and total fluxes were recorded during fall 2005 and 2006 as a result of wind-induced resuspension of settled POC. A significant increase in POC fluxes in summer 2007 was recorded and the sinking particles contained a higher proportion of fresh, marine organic matter. This increase did not happen in 2006, suggesting there were variations in the processes regulating carbon export.

Historically, the saturation horizon for aragonite is shallow on the western side of the MERICA section in HB, (around 100 m deep, Azetsu-Scott 2008). In southern Hudson Strait (region of Hudson Bay water outflow), aragonite is saturated until 200 meters while calcite is saturated down to the bottom of the strait (350 meters, Azetsu-Scott et al. 2010). In Baffin Bay, the aragonite and the calcite saturation horizon vary between 200 – 500 and 1000 – 1500 m respectively, with shallower depths on the western side of the bay (Azetsu-Scott et al. 2010).

2.4 PHYTOPLANKTON AND PRIMARY PRODUCTION

There are no internally consistent, un-aliased, and sustained observational records of phytoplankton and primary production in Canadian Arctic waters.

Beaufort Sea: The most useful insight into very recent change has emerged from annual (since 2003) systematic surveys of planktonic assemblages in the Beaufort gyre (Li et al. 2009). Observations during the first pentade revealed that the smallest phytoplankton cells are thriving in the changing Canada basin and that larger cells are not. Summer-time cruise-average data

have revealed a warming, freshening upper ocean and increasing density stratification; deep water nutrients have not changed, while upper ocean nutrients have. Picoplankton, having a larger surface-area-to-volume ratio and slower sinking rate, do better under these conditions than larger nanoplankton. Meanwhile, total phytoplankton biomass has not changed.

Canadian Polar Shelf: A summary of knowledge of ecological variability on the Canadian Polar Shelf has been published by Michel et al. (2006). Results from new research during the International Polar Year are summarized in Tremblay et al. (2012). There has been no systematic programme of plankton observations over the Canadian Polar Shelf comparable to that in the Beaufort gyre since 2003 and data is insufficient for a trend analysis.

Baffin Bay/Davis Strait: Jensen et al. (1999) studied phytoplankton biomass distribution and productivity in the Davis Strait region. They determined that overall primary phytoplankton production was in the range of 67 - 3,207 mgC m⁻² d⁻¹, which is within the range of the few published results for the eastern Canadian Arctic and West Greenland waters. Martin et al. (2010) investigated the Canadian Arctic during late summer and early fall and found widespread occurrence of long-lived subsurface chlorophyll maxima in seasonally ice-free waters. They found that the vertical position of the subsurface chlorophyll maxima corresponded with the depth of the subsurface biomass maximum in Baffin Bay and suggested that the subsurface chlorophyll maxima could be an important source of carbon for the food web. Ardyna et al. (2011) assessed phytoplankton dynamics and its environmental control across the Canadian High Arctic. They measured environmental parameters including hydrographic, atmospheric and sea ice conditions, and phytoplankton production including biomass and composition along 3,500 km transects across the Beaufort Sea, the Canadian Arctic Archipelago, and Baffin Bay during late summer 2005, early fall 2006 and fall 2007. They found a eutrophic diatom-based system located in Baffin Bay and Lancaster Sound that was characterized by high production and biomass of large cells and relatively high abundance of centric diatoms, mainly *Chaetoceros* spp. They found that the phytoplankton biomass integrated over the euphotic zone was significantly higher in Baffin Bay than in the other Polar Regions. Motard-Côté et al. (2011) determined the distribution and bacterial metabolism of dimethylsulfoniopropionate (DMSP) and dimethylsulfide (DMS) in the two dominant surface water masses in northern Baffin Bay/Lancaster Sound during September 2008; the data suggested the presence of DMSP-rich phytoplankton taxa. Surface water measurements from the Baffin Bay North Water (NOW) polynya showed that photosynthetic picoeukaryotes and total prokaryotes were tenfold and threefold more abundant, respectively, than in other Arctic surface water. However, the observations are insufficient for a trend analysis.

Hudson Bay: Stewart and Lockhart (2005) provide a thorough review of the phytoplankton community and the general characteristics of primary production in Hudson Bay. The information available is largely confined to the ice-free season, and no long-term monitoring exists.

A recent three-year study by Ferland et al. (2011) shows that mean values of phytoplankton production and Chl-*a* biomass in the euphotic layer (Z_{eu}) were significantly lower in Hudson Bay (0.32 ± 0.14 g C m⁻² d⁻¹ and 30 ± 10 mg Chl-*a* m⁻²) than in Hudson Strait (1.15 ± 0.03 g C m⁻² d⁻¹ and 60 ± 30 mg Chl-*a* m⁻²), with a pattern of higher surface Chl-*a* concentrations and

phytoplankton production inshore compared to offshore (see Figure 45d, above). This enhanced primary productivity corresponded with high abundances of diatoms relative to other phytoplankton groups and could be linked to areas of strong tidal mixing, where nutrient concentrations at the surface are periodically replenished. A deep chlorophyll maximum was observed between 25 and 60 m, usually below the surface mixed layer, near the nutricline, driven mainly by a shortage of inorganic nitrogen in the upper euphotic zone. Ferland et al. (2011) conclude that primary production in Hudson Bay is typically nutrient-limited, with the physiological state and size structure of the phytoplankton determined by stratification and nitrate concentration in mid- and late summer. Year-to-year differences in the phytoplankton composition, size structure and physiology were attributed to variations in stratification, mixed layer depth and nutrient availability. However, overall productivity was less variable than community composition. Total particulate annual phytoplankton production based on the summers of 2004, 2005, and 2006 was estimated at 39 g C m^{-2} in Hudson Bay, assuming an algal growth season of 120 days. For more details on production rates and sinking fluxes, see Ferland et al. (2011) and Lapoussière et al. (2009). A trend is not discernable from this data.

Satellite-derived phytoplankton biomass and primary production data were compiled for Hudson Bay for years with available satellite coverage (1998 - 2010) (Larouche 2013, unpublished data). Monthly means were computed for the summer ice-free periods around stations sampled during the MERICA missions (2003 - 2006), and *in situ* and satellite data show reasonably good agreement. The satellite results show that both Chl-*a* biomass and primary production increased over the study period, at rates of $0.024 - 0.120 \text{ mg m}^{-3}/\text{decade}$ and $0.287 - 0.537 \text{ mg C m}^{-2} \text{ d}^{-1}/\text{decade}$ respectively. These trends may seem low, however under the oligotrophic conditions of Hudson Bay, where Chl-*a* and primary production are generally low, these rates represent a 20 - 25% increase per decade for Chl-*a* and a 15 - 20% increase per decade for primary production. These trends are consistent with increases recorded in the Beaufort Sea over a similar period and for similar oligotrophic conditions (Arrigo et al. 2011). A better resolution both at spatial (zones smaller than 725 km^2) and temporal scales (weekly rather than monthly means) may strengthen these trends, especially for the week(s) of the spring bloom period (Galbraith and Larouche 2011; Galbraith, unpublished data). These trends also do not account for changes that may have occurred at the deep chlorophyll maximum (Martin et al. 2010), which cannot be observed with remote sensing, and thus may underestimate the actual increase in phytoplankton biomass and production in Hudson Bay (Larouche, unpublished data).

Paleoceanographic studies of dinocyst assemblages found in sediments in Hudson Bay suggest an opposite trend in primary productivity in the past decades (Ladouceur 2007). Assemblages in sediment samples taken in the late 1980s were compared with samples collected during the MERICA oceanographic missions (2003 - 2006). The results suggest that primary productivity was higher in the 1980s than in the 2000s and that a shift in the algal community occurred, changing from heterotrophic dinoflagellates, associated with a diatom-dominated community, to autotrophic dinoflagellates. This may reflect changes in the plankton community that occurred at the subsurface chlorophyll maximum which is generally dominated by diatoms (Martin et al. 2010).

Field observations are too scarce to confirm either the higher primary productivity in the 1980s or the increasing trends in phytoplankton biomass and primary production over the more recent

satellite era, but studies clearly show that primary production responds to changes in the physical environment.

2.5 ZOOPLANKTON AND HIGHER TROPHIC LEVELS

There are only very few sustained observational records at higher trophic levels in Canadian Arctic waters.

Beaufort Sea: The best records for the present purpose in this area have emerged from annual subsistence catches. Harwood (2009) summarizes data related to the charr fishery on the Hornaday River that flows into the southwestern Amundsen Gulf. The data on mean fork length (Figure 46) reveal interdecadal variability and a weak (statistically insignificant) trend to increased fish size during 1990 - 2007. The catch data reveal a tendency for better body condition in fish during years of early ice clearance than those of late clearance.

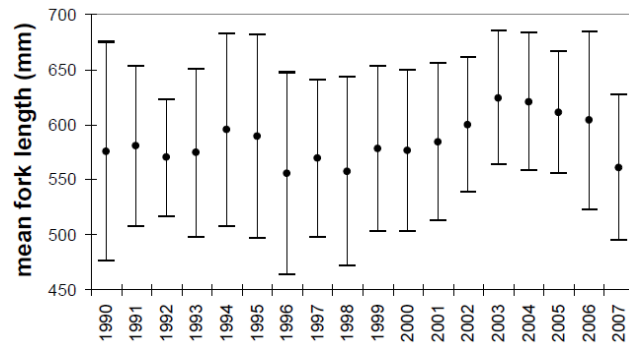


Figure 46: Variation in mean fork length of male charr caught on the Hornaday River over 18 years during the August fishery (Harwood 2009).

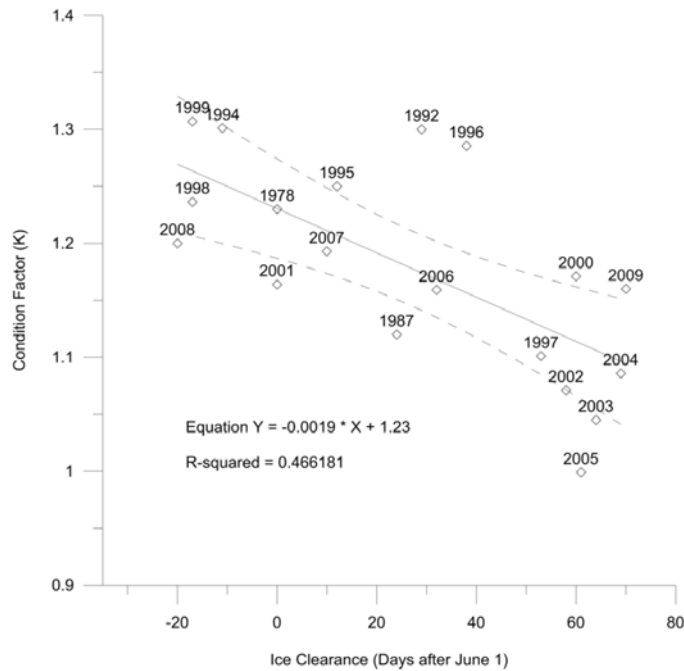


Figure 47: Date of ice clearance in Amundsen Gulf and condition factor of Charr caught in the under-ice fishery at Tatik Lake (Harwood et al. 2013).

A comparable study of charr caught in an autumn (October) fishery on the Kuujjua River that flows into Minto Inlet on north-eastern Amundsen Gulf provides similar results (Harwood et al. 2013). The body growth coefficient shows interdecadal variability (high in the early 2000's) and a weak improving trend during 1994 - 2009. Nineteen years of catch data reveal a statistically significant correlation between the fishes' condition factor and date of ice clearance from eastern Amundsen Gulf (where these fish feed in summer); fish condition has been better in years of earlier clearance (Figure 47).

Ringed seals in eastern Amundsen Gulf have also been the subject of sustained study over the past few decades. Harwood et al. (2000, 2012) present data from a harvest-based monitoring programme in Prince Albert sound, near Ulukhaktok. In contrast to the trend for charr, the body condition of this species in the Beaufort region has declined over the 20-year record (Figure 48). This study has also revealed that the annual recruitment of ringed seals in this area is strongly influenced by variation in the seasonal cycle of ice cover; early clearance ice from the eastern Amundsen Gulf in spring favors the pups' survival, except that extremely early clearance has an adverse effect. The latter circumstance may disrupt pupping habitat on fast ice before pups' viability in open warming has been established.

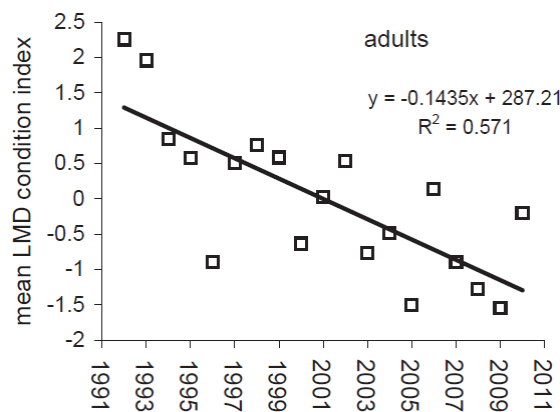


Figure 48: Average body condition index of adult ringed seals sampled at Masoyak in June and July, 1992-2010 (Harwood et al. 2012).

Canadian Polar Shelf: A summary of knowledge of ecological variability on the Canadian Polar Shelf has been published by Michel et al. (2006). Results from new research during the International Polar Year are summarized in Darnis et al. (2012) and Ferguson et al. (2012). There are presently no long-term data from systematic higher trophic observations that reveal trend in species health or abundance over the Canadian Polar Shelf.

Baffin Bay/Davis Strait: The zooplankton species that are found in north-eastern Baffin Bay and Davis Strait are common to Arctic regions in eastern Canada. Copepods are the most important zooplankton, both in abundance and biomass. Species of *Calanus*, *C. finmarchicus*, *C. hyperboreus* and *C. glacialis* are the most common (LGL 1983; Dunbar and Moore 1980; Ringuette et al. 2002). Their distribution patterns of zooplankton varied and were often directly linked to hydrographic features, such as temperature, salinity, and duration of ice cover. In the Davis Strait region, the marine planktonic ecosystem is characterized by a brief summer period of intense productivity following the spring phytoplankton bloom. The Northern Shrimp

(*Pandalus borealis*) is the most important commercial invertebrate species within the area. They are found in deep waters and are captured using trawl nets (LaPierre et al. 2011). There are presently no long-term data sets from systematic higher trophic observations that reveal trend in species health or abundance over the Canadian Polar Shelf.

Hudson Bay: Estrada et al. (2012) identified three different regions in the Hudson Bay System, each with distinct zones (i.e., west, centre, east in Hudson Bay; inflow and outflow in Hudson Strait) that were characterized by environmental variables (i.e. stratification, temperature, salinity) and zooplankton communities. During all sampling years, the total zooplankton abundance and biomass were lower in Hudson Bay than in Hudson Strait, a spatial pattern also seen in phytoplankton abundances and biomasses (Ferland et al. 2011).

There was no definite spatial pattern in total zooplankton biomass over the HB transect in 2003 and 2004, whereas it showed a slight decrease from east to west in 2005 and 2006 (41.2 – 5.7, and 23.5 – 11.0 g WM m⁻², respectively). The total abundance of macrozooplankton did not show large variations among the three regions and among the study years. The mesozooplankton community was numerically dominated by copepods in the three regions during the 4 years. Total mesozooplankton abundances were generally higher in Hudson Bay due to the presence of small copepods, which are likely well adapted to the late-summer oligotrophic and stratified water conditions. These small copepods are numerically dominant and contribute little to the overall biomass, but they may play important roles in secondary pelagic production via the microbial food web. Environmental properties, mainly water column stratification, best explain the observed spatial variability in zooplankton abundance and species composition between and within the different regions of the Hudson Bay system (Estrada et al. 2012).

Regional differences in the hatching season of Arctic cod *Boreogadus saida* were studied in contrasting oceanographic regions of the Arctic Ocean characterized by different freshwater input (Bouchard and Fortier 2011). Hatching season started as early as January and extended to July in areas receiving high river discharge such as Hudson Bay. By contrast, hatching was restricted to April-July in regions with little freshwater input (e.g. Canadian Archipelago, North Baffin Bay, and Northeast Water). Hudson Bay had the highest growth rate and pre-winter size of cod in the Arctic sites visited. Growth was dictated by the surface temperature conditions prevailing during the hatching season and the early life of polar cod in the plankton. Hudson Bay, where winter hatching combines with relatively warm surface temperatures during plankton drift, thus produced the largest pre-winter sizes. No trend analysis is available.

Summary: While observations of zooplankton and higher trophic levels are insufficient to allow a trend analysis, the studies clearly show that zooplankton distributions as well as hatching success and growth of Arctic fish species respond to changes in environmental properties. Effects can be both positive and negative.

2.6 TRENDS IN THE MACKENZIE RIVER BASIN

2.6.1 Introduction

Of the 5 regions which are part of the ACCASP Arctic assessment, the Mackenzie Basin is an outlier in the respect that it contains a terrestrially influenced freshwater ecosystem rather than a

marine ecosystem. However climate-related changes to the hydrologic and nutrient cycles in the Mackenzie River system may have implications for areas far beyond the basin in the Beaufort Sea and Arctic Ocean with impacts on global circulation patterns (Peterson et al. 2002, 2006). The changes in river inflow will affect the physical and chemical properties of coastal shelf ecosystems, which produce more than 80% of the total primary production in Arctic seas (Hill and Cota 2005). Changes in sediments, nutrients and biota entering from rivers will affect phytoplankton dynamics in Arctic coastal waters (Trefry et al. 2005; Waleron et al. 2007), as well as the organic carbon dynamics of the Arctic Ocean.

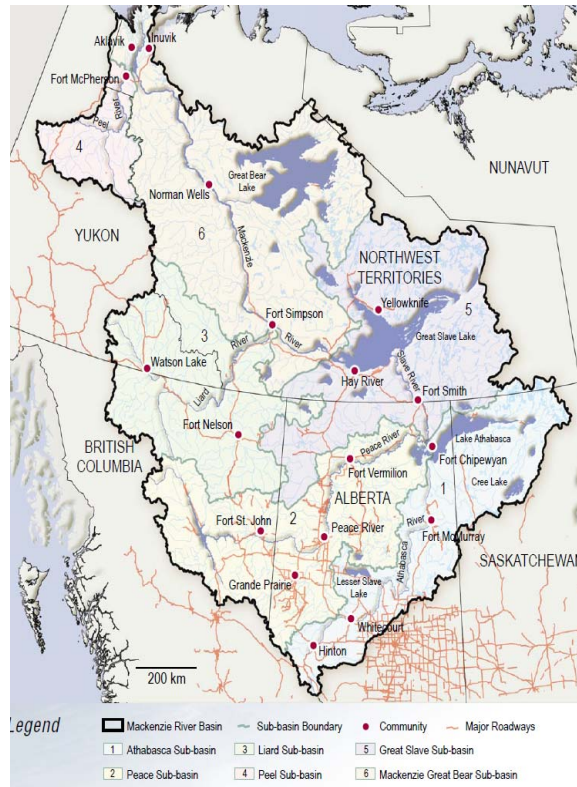


Figure 49: Map of Mackenzie River Basin showing major rivers, 6 subbasins and important communities. Adapted from Mackenzie River Basin State of the Ecosystem report 2003 (MRBB 2004).

The Mackenzie River Basin extends from central Alberta to the Beaufort Sea coast over 15° of latitude and 37° of longitude. It is the tenth largest river basin in the world draining an area of 1.8 million km², which is about one-fifth of the total land area of Canada. The main stem of the basin, the Mackenzie River, flows approximately 4,240 km from the Columbia Ice-field in Jasper National Park, Alberta, and the snowfields of the upper Peace in British Columbia up to the Beaufort Sea (Louie et al. 2002). The Mackenzie River basin includes seven major rivers, (Peace, Athabasca, Slave, Liard, Great Bear, Peel, and Mackenzie), three large lakes (Great Bear, Great Slave and Athabasca), one large estuarine delta, many freshwater deltas and 6 sub basins (Athabasca, Peace, Great Slave, Liard, Mackenzie-Great Bear and Peel subbasin, Figure 49). It has an annual discharge of ~10,000 m² s⁻¹ (Rosenberg and Barton 1986) which can reach up to 22,000 m³ s⁻¹. Within the Mackenzie Basin, there is a northward decrease in runoff that reflects the spatial trend in precipitation. Despite having the same area, mountainous subbasins in the

west (Liard, Peace, and northern mountains) contribute about 60% of the Mackenzie flow, while the interior plains and eastern Canadian Shield contribute only about 25% of the total flow (Woo and Thorne 2003). About one third of the catchment is drained by the Athabasca and Peace Rivers and one sixth by the Liard River.

The head waters of all these main tributaries are in the Rocky Mountains. Mean annual precipitation in subarctic and arctic parts of the basin is less than 500 mm. Northern segments of the Mackenzie River proper are in the Arctic and drain tundra (Cushing et al. 2006).

The basin includes many climatic regions, including the cold temperate, mountain, subarctic, and arctic zones. There are four different seasons in the Mackenzie River Basin: autumn, characterized by snow build up; winter, with light snow and constant below-freezing temperatures; spring, with enhanced runoff because of warming and rains; and summer, when convective activity dominates (MRBB 2004). The flow of the Mackenzie River reflects the contributions from its major subbasins at different times of the year. Rivers of the Mackenzie Basin exhibit several seasonal flow patterns that include the subarctic nival (snowmelt dominated), proglacial (influenced by glacier melt), wetland, pro-lacustrine (below large lakes), and regulated flow regimes (Woo and Thorne 2003). In the pro-glacial system summer high flows sustained by glacier melting and in the wetland system; summer runoff is reduced through storage and enhanced evaporation. The Mackenzie River delivers different flows including spring peak flows, declining summer discharge, and low winter flows, to the Arctic Ocean. The spring ice melt and ice jam floods are the major hydrological events in the annual hydrological cycle of the Mackenzie River Basin and help to shape the physical, chemical and biotic attributes of the basin's aquatic ecosystems (Prowse and Conly 1996). The Mackenzie is the largest North American river that brings freshwater to the Arctic Ocean (Woo and Throne 2003). The Mackenzie River accounts for 60% of the freshwater that flows into the Arctic Ocean from Canada (MRBB 2004).

Several environmental initiatives have been focusing on the Mackenzie River Basin:

1. The Mackenzie Basin Impact Study (MBIS) assessed the potential impacts of climate change scenarios on the Mackenzie River Basin. Cohen (1997) summarized the main impacts determined from the various research activities under MBIS and outlines some lessons learned.
2. The Mackenzie Global Energy and Water Cycle Experiment Study (GEWEX-MAGS) examined the climate of the Mackenzie River Basin as part of the Global Energy and Water Cycle Experiment (GEWEX). The key objectives of the project were to understand and to model the hydroclimatic behaviour and the factors that control the climate in the Mackenzie River Basin. (Stewart et al. 1998; MRBB 2004).
3. The Northern River Basins Study (NRBS) with the primary objective of advancing the understanding of how anthropogenic developments (industrial, agricultural, municipal) and other development have impacted the ecology of the Peace, Athabasca and Slave Rivers in Canada.
4. The Northern Rivers Ecosystem Initiative (NREI) was established to answer questions and address recommendations from the Northern River Basins Study (NRBS). NREI was a science-based effort to understand the impacts of human activities on aquatic

ecosystems in the region and help protect aquatic ecosystems (Culp et al. 2000; Prowse et al. 2006a).

2.6.2 Air temperature

Monthly temperature averages in the Mackenzie River basin range from about -25°C in winter to 15°C in summer (Figure 50), and are characterized by dramatic seasonal changes in air temperatures (Stewart et al. 1998). In the upper Mackenzie River basin, the mean daily temperature ranges from 16 to 21°C in summer and -20 to -25°C during the winters (January). In the lower basin, the daily mean temperature ranges from 10 - 16°C (July) and -23 to -29°C (January). Mean air temperature in the Peel subbasin is -9.5°C . The Liard River basin has a cold and dry continental climate and the mean annual temperature ranges from -1°C in southwest to -3°C near Fort Simpson. At Fort Simpson, the monthly mean range is from -27°C in January to 15°C in July (Culp et al. 2005). In the Athabasca River basin, temperature decreases from southwest to northeast. In the Rocky Mountains, the annual mean temperature is 3°C (monthly means -11 to 15°C); while at Fort McMurray the annual mean temperature is 0.2°C (monthly means -20 to 16°C). Climate in the Peace River subbasin is relatively dry and the mean annual temperature is approximately -0.9°C ranging from -27°C to 17°C . The Great Slave subbasin also has a harsh continental climate. The mean annual temperature at Fort Smith is -3°C with a monthly mean range from -25°C in January to 16°C in July. In the Peel River basin, the mean annual temperature is -9.5°C .

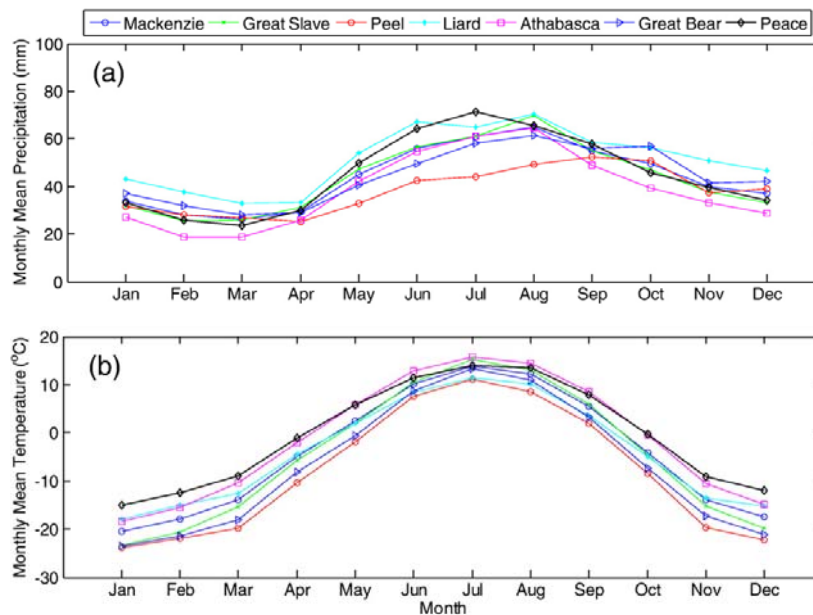


Figure 50: Monthly mean precipitation (a) and monthly mean air temperature (b) based on the NCEP data from 1988 to 2007 in the different basins (Tong et al. 2010).

The Mackenzie River Basin is currently experiencing some of the greatest rise in temperature increase anywhere in the world, especially during the winter (Stewart et al. 1998; Nijssen et al. 2001). Most of the prairie areas have already undergone a 2 - 3°C increase in temperature, mostly since 1970, and there has been a large decrease in snow packs at most locations on the prairies (Schindler and Donahue 2006). Over the past 60 years, air temperatures in the Northwest Territories part of the Mackenzie River Basin have increased more than in any other

climate region in Canada. In the Mackenzie River Basin, the temperature data exhibit an increasing trend in winter, spring and on an annual basis, and a weak increasing trend in some of the fall months (Aziz and Burn 2006). The annual maximum temperature has significantly increased by 1.5 to 2.0°C over the 49-y period in the Mackenzie basin (Figure 51). Average winter temperatures have increased between 2 - 3°C in the Mackenzie River Basin during the last few decades of the last century. Increase in winter maximum temperature is also statistically significant in parts of the Mackenzie basin. However, increase in summer temperature is not as pronounced (Zhang et al. 2000). In 1998, the Mackenzie District experienced their warmest summer on the record, 3.0°C above the 1951 - 80 normal (Atkinson et al. 2006). Maxwell (1997) identified that the Mackenzie Basin had a warming trend of 1.5°C in the past century.

Yip et al. (2012) examined changes in the hydrologic cycle in the Mackenzie River Basin in northern Canada focusing on temperature, precipitation, runoff, evapotranspiration and freshwater storage. They used WATFLOOD (Kouwen 1996), a distributed hydrological model with two different climate input data sets: Environment Canada gridded observed data and the European Centre for Medium-range Weather Forecasting (ECMWF) reanalysis data (ERA-40). The results reveal a general pattern of warming temperatures, and increasing precipitation and evapotranspiration. For both data sets, there is a warming trend on an annual and monthly basis, except for October.

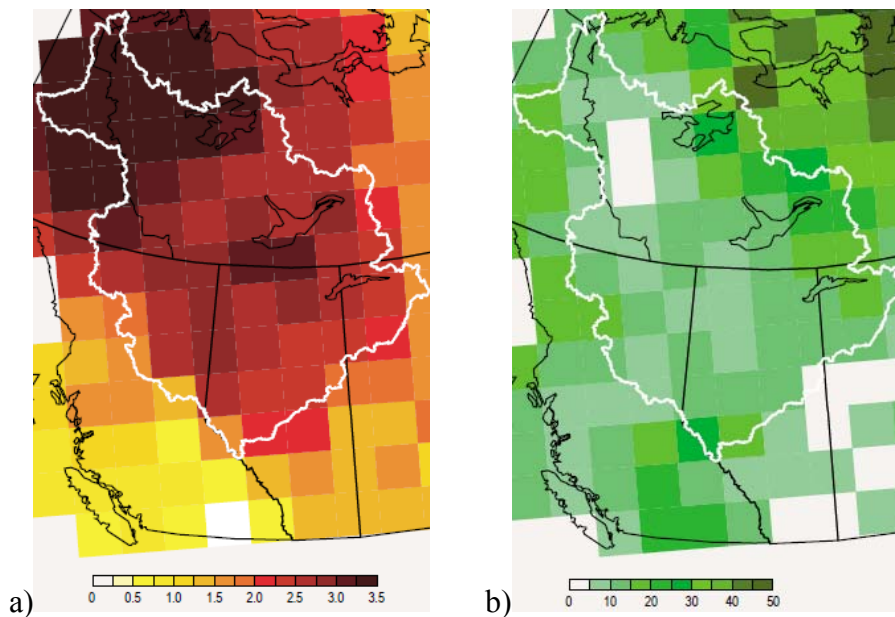


Figure 51: Trends in (a) Maximum daily temperatures (°C) in winter and (b) increase in precipitation (mm/y) in the Mackenzie River Basin. Units refer to change in the 49 years between 1950 and 1998. Adapted from Mackenzie River Basin State of the Ecosystem Report 2003 (MRBB2004).

2.6.3 Precipitation

Average precipitation over the Mackenzie basin is estimated to be 410 mm/y while snow and ice total about 230 mm/y. Minimum precipitation occurs during the winter months of February to April, and the maximum occurs during the summer months of June to August (Figure 50, Stewart et al. 2002). Mean annual precipitation in the Peel subbasin is 258 mm/y and in the

Liard subbasin approximately 450 mm/y, of which 60% falls between the months of March to October. Precipitation in the Athabasca River basin ranges from 394 mm/y to 465 mm/y with almost 70% in the form of rain (Hudson 1997; Culp et al. 2005). In the Peace River basin average annual precipitation varies from 468 mm in the upper Peace River to 381 mm/y of which 30% is in the form of snow (Culp et al. 2005). Precipitation in the Great Slave subbasin is 353 mm/y with 60 mm precipitation falling between May and October (Culp et al. 2005).

There have been changes in total annual precipitation over much of the basin. Winter precipitation has increased in the northern part of the basin but has decreased in the southwestern part of the basin. Summer precipitation has increased in the south but has decreased somewhat in the far north (Zhang et al. 2000). The Yip et al. (2012) model also detected a general decrease in winter precipitation and an increase in summer precipitation. The precipitation data in the Mackenzie River Basin exhibit a notable decrease in total precipitation in fall and winter, an increase in the spring (increase in spring rain, and a decrease in spring snow) likely related to the increasing temperature in spring (Aziz and Burn 2006).

2.6.4 Hydrology

Several hydrological variables in the Mackenzie River Basin show a number of significant trends including strong increasing trends during the winter months (December to April), increasing trends in the annual minimum flow, weak decreasing trends in the early summer and late fall flows, and decreasing trends in the annual mean flow (Aziz and Burn 2006). However, trends are variable for sub-regions.

Estimated from the Mackenzie River discharge into the Arctic Ocean, runoff is about 180 mm/y. Evapotranspiration mainly occurs from May to October and is approximately 250 mm to 277 mm (Louie et al. 2002). Mean annual water temperature is 5.3°C in the Mackenzie River, 6.1°C in the Liard River, 8.2°C in the Athabasca River and 6.4°C in the Slave River (Culp et al. 2005).

The Mackenzie River's hydrology undergoes considerable intra- and interannual variability with components of seasonal changes reflecting the strength of flow within the Mackenzie's various subdrainage basins (Woo and Thorne 2003). Strong seasonal variation in flow ranges from 3,000 – 5,000 m³ s⁻¹ during winter to as much as 40,000 m³ s⁻¹ during freshet in early June (Figure 12, Macdonald and Yanling 2006). Average monthly discharge in the Mackenzie River near the delta is 9,020 m³ s⁻¹, with a minimum of 3,373 m³ s⁻¹ in March and a maximum in June (20,626 m³ s⁻¹) (Culp et al. 2005). Outflows from the Great Slave Lake provide almost 60% of the annual flow, while 20% is provided by the Liard River. Spring break-up of ice occurs in late April to May and is triggered by the flow from Liard River. During the winter, the Great Bear River contributes to almost 12% of the flow at the mouth of the Mackenzie River. Some Aboriginal residents of the Mackenzie Delta have noticed low water levels and associated effects. However, there are no significant trends in mean annual flows in rivers of the Mackenzie-Great Bear subbasin in the late 20th century (Zhang et al. 2011). The large amount of water stored in the Great Slave and Great Bear Lakes helps to maintain flows on the Mackenzie River in dry years (MRBB 2004).

Mean monthly discharge in the Liard River is 2,500 m³ s⁻¹ with a minimum in March (~400 m³ s⁻¹) and a maximum in June (7,300 m³ s⁻¹, Culp et al. 2005). Flow in the Liard River has declined

over the past few decades, possibly as a result of decrease in precipitation in the Liard subbasin. These changes in stream flows include comparatively higher flow in wetter and warm winters and lower spring freshets due to a reduction in snow accumulations (MRBB 2004). Burn et al. (2004b) investigated the relationships between trends in hydrological variables and both meteorological variables and large-scale oceanic and atmospheric processes in the Liard River basin. They found an increasing trend in the annual minimum flow, a decreasing trend in the date of occurrence of the spring freshet and the spring maximum flood event, and also a decreasing trend in the date of occurrence of the annual maximum flood event. There was a weak indication of a decreasing trend in the summer flow and also a weaker indication of a decreasing trend in the annual flow. The identified trends in the timing of the onset of the spring freshet were found to be related to the observed increasing trends in spring temperatures for the area.

The mean annual flow in the Peel River is $670 \text{ m}^3 \text{ s}^{-1}$. There are large variations in flows throughout the year from $7,000 \text{ m}^3 \text{ s}^{-1}$ at spring peak to $500 \text{ m}^3 \text{ s}^{-1}$ at winter low (EDI 2006). It creates highly dynamic aquatic environments (Van Gerwen-Toyne et al. 2008). 90% of the flow occurs during the summer from May to September, with peak flow from mid-May to mid-June accounting for 50% of annual flows. Annual peak flows on the Peel River have decreased in the last few decades. Much of the Peel subbasin has been warmer than usual in recent years, resulting in less accumulation of ice. Summers have also been warmer and drier than usual, leaving less water to enter runoff. However, the impact of climate change on reduced peak flows in the Peel River is still unknown (MRBB 2004).

The mean monthly discharge of the Athabasca River increases from $88 \text{ m}^3 \text{ s}^{-1}$ to $783 \text{ m}^3 \text{ s}^{-1}$ near the river mouth. Maximum discharge at the river mouth occurs in July ($>1,500 \text{ m}^3 \text{ s}^{-1}$) and the minimum ($\sim 200 \text{ m}^3 \text{ s}^{-1}$) during February - March (Culp et al. 2005). Summer (May – Aug.) flows in the Athabasca River at Fort McMurray had declined by 29% between 1970 and 2005 despite increased flows from glacial sources in its headwaters caused by increased air temperatures (Schindler and Donahue 2006). Flows in the Athabasca River are affected by precipitation and evaporation and reflect the prevailing climatic conditions.

Natural variability in the hydrological regime within the lower Athabasca River is very important, particularly in the context of projected climate change and the increased water demands arising from upstream development of the Alberta oil sands. Burn et al. (2004a) found some relationship between the Pacific Decadal Oscillation and winter flows, the annual minimum flow, the timing of the spring freshet, and the timing of the spring maximum flow events. They compared trend results for the Athabasca River subbasin and the Liard River subbasin to investigate the relationships between trends in hydrological variables and meteorological variables. In general, both basins exhibit an increase in winter flows and some increase in spring runoff with an offset due to decreases in summertime flow. There was some increasing trend in the annual minimum flows. Both watersheds demonstrated that hydrological trends did not agree with the IPCC (2001) projection for increased runoff, nor with the decreasing tendency in the annual flows. These studies are very important because anthropogenic effects, such as the construction of large reservoirs or changes in land use, can hamper the ability to understand the climate change impacts on water resource systems. However, the Liard and Athabasca River Basins have very little natural or manmade storage.

Therefore, the observed trends in hydrological variables are likely due to climate change (Burn et al. 2004a).

Mean monthly discharge of the Peace River near its mouth is $2,188 \text{ m}^3 \text{ s}^{-1}$. Maximum discharge ($\sim 4,300 \text{ m}^3 \text{ s}^{-1}$) occurs in late May to early June, and minimum ($200 \text{ m}^3 \text{ s}^{-1}$) discharge during late winters (Culp et al. 2005). The spring flood in the tributaries and main stem of the Peace River plays an important role in river ice break-up in the lower Peace River. Regulation of the Peace River has shifted the pattern of seasonal flows and damped flow extremes, creating a less variable annual regime (Prowse et al. 2002). The hydrological dataset from 1974 to 2009 shows that there are decreasing trends in several key drivers of the Peace-Athabasca deltaic system hydrology, including short-term and long-term maximum and minimum runoff (Monk et al. 2012). In the Peace River, summer flow has declined 40 – 60% below historical values (Schindler and Donahue 2006). The mean annual discharge of the Slave River is $3,400 \text{ m}^3 \text{ s}^{-1}$ near Fitzgerald with a minimum discharge in February ($2,000 \text{ m}^3 \text{ s}^{-1}$) and a maximum in June ($5,600 \text{ m}^3 \text{ s}^{-1}$). During June and July about 25% of the annual discharge is observed. The normal freeze-up occurs in mid November and break-up starts in mid May. Flows in the Slave River have declined during the 20th century because of changes to the Peace and Athabasca rivers. At present, climate warming and reductions in peak flows on the Peace River caused by the operation of Bennett Dam are the primary reasons for the flow decline in the Slave River delta (Prowse et al. 2006a). Spring freshet and annual peak flow on certain rivers in the Great Slave subbasin are occurring a few days earlier than in the past because of climate warming (MRBB 2004).

Summer water supplies have already declined by 20% in the tributaries of the Mackenzie River, including the Slave, Peace, and Athabasca Rivers (Schindler and Donahue 2006). The Athabasca River is without dams or large water withdrawals; however, summer flows in its lower reaches have declined by 30% since 1970 (Schindler and Donahue 2006). Most large glaciers in the headwaters of the Athabasca Rivers have shrunk by 25% in the last century (Watson and Luckman 2004). Climate data during the last few decades have revealed that winter precipitation has also decreased in the upper portion of the Athabasca (Zhang et al. 2000). In the Slave River subbasin, lakes and rivers have lower water levels, while a few smaller bodies of water have disappeared entirely. Local communities have noticed decreases in water levels at certain locations, changes to water fluctuations, and flooding at certain locations in the subbasin (Bill et al. 1996; WKSS 2001). There are many factors contributing to this phenomenon including construction of dams and recent climate change. Many of the regulation-related effects on the Great Slave Lake water levels, including changes in the timing and magnitude of peak levels, have also been affected by climate variability. However, climatic and regulation impacts have generally counter-balanced changes in amplitude of water level fluctuations and magnitude of peak levels, but have cumulatively contributed towards earlier peak water levels in the lake (Gibson et al. 2006; Prowse et al. 2006a). Primarily because of the low slope of the water surface in the Slave River Delta, such lake-level changes have the potential of modifying other important natural processes that control delta development and flooding (Prowse et al. 2006a).

2.6.5 Cryosphere

The cryosphere includes sea ice, seasonal snow cover, glaciers and ice caps, permafrost, as well as river and lake ice (Goodison et al. 1999). The consistent high latitude warming in the

northern hemisphere during the last few decades has resulted in reductions of the cryosphere (Rouse et al. 2003). Almost over half the year, the Mackenzie River basin area is covered with snow in many parts of the basin (Woo and Thorne 2003). During the period 1946 to 1995, the largest decreases in snow depth in northern Canada were observed in the Mackenzie River basin (Brown and Braaten 1998). Decreases in snow depth have been accompanied by reductions in spring and summer snow-cover duration and reductions in spring snow-covered area (Brown et al. 2004). Warmer temperatures do not necessarily generate a predictable response because other processes are involved, such as the effect of snow cover on ground temperatures (Atkinson et al. 2006). Rivers in the Northern Hemisphere, including the Mackenzie River, show an average delay of 5.8 days per century in freeze-up dates and an average advance of 6.3 days per century in break-up dates (Magnuson et al. 2000).

Trends for the 20 year historical satellite records of lake ice phenology events in the northern Canadian Lakes including the Great Bear Lake (GBL), Great Slave Lake (GSL), and Lake Athabasca in the Mackenzie River Basin showed earlier break-up (average 0.99 days per year) and later freeze-up (average 0.76 days per year, Latifovic and Pouliot 2007). However, there is a difference in timing for the individual lakes. During the freeze-up period, both freeze-onset and ice-on dates occur about one week earlier, and freeze duration lasts approximately one week longer on the GBL compared to the GSL. During the ice break-up period, melt-onset and ice-off dates happen one week and approximately four weeks later, respectively on the GBL. Therefore, ice duration is usually four to five weeks longer on the GBL compared to the GSL (Howell et al. 2009; Kang et al. 2012).

2.6.6 Permafrost

Recent warming of permafrost has occurred in many regions of the Canadian permafrost zone during the last two to three decades, and summer thaw penetration has increased in the 1990s (Smith et al. 2003, 2005). Permafrost underlies about 75% of the Mackenzie River basin. Over the past few decades, permafrost temperatures have generally been increasing in the Mackenzie River basin. Permafrost temperature observations in the Arctic have documented changes ranging from 0.3°C to 0.8°C in the Mackenzie Delta at depths of 20 m to 30 m between 1990 and 2002. Climatic warming is probably the dominant factor leading to permafrost degradation. There is an increase in thickness of the active layer, the soil above permafrost that undergoes the freeze-thaw cycle (IPCC 2007). The impact of climate change on permafrost is evident in the thickness of the active layer, which has increased on average by 8 cm at 12 sites on northern Richards Island during 1983 - 2008 (Burn and Kokelj 2009).

3: PROJECTIONS OF THE FUTURE CLIMATE STATE

3.1 SOURCES FOR PROJECTIONS AND MODEL DESCRIPTIONS

3.1.1 Introduction

In order to assess potential impacts, vulnerabilities and opportunities, and thus support decision making for DFO management, potential future scenarios need to be evaluated with respect to environmental variables influencing marine ecosystems. While limited projections may be derived by extrapolation of recent trends, the main information, especially on longer timescales,

comes from general circulation models (GCMs). Based on different emission scenarios (usually defined in context of IPCC assessments) which represent a variety of management choices from intense mitigation to no mitigation (business as usual), GCMs compute the planet's radiative and circulation responses. These affect variables like air/ocean temperature, precipitation, evaporation, atmospheric and oceanic circulation patterns, sea ice conditions, and air-sea exchanges of momentum, heat and gases. In the last decade, the atmosphere-ocean-land components represented in GCMs have been expanded to include global biogeochemical cycles (i.e. ocean biochemistry, land vegetation, soil chemistry and expanded atmospheric chemistry). These models are more commonly called Earth System Models (ESMs). The development of biogeochemical components in ESMs has been advanced significantly over recent years. Results from the first generation of ESMs which incorporated an interactive carbon cycle are discussed, e.g., by Friedlingstein et al. (2006) and Denman et al. (2007). Results from the next generation of models in preparation for the 5th Coupled Model Intercomparison Experiment (CMIP5, Taylor et al. 2012) in support of the IPCC AR5 are currently evaluated and some analyses thereof are included in the current assessment.

ESMs provide insight into global connections and interactions between ocean basins, which might be important for the Canadian Arctic. Moreover they are able to provide an estimate of changes in response to rising atmospheric CO₂ and other greenhouse gas levels and climate warming. They allow us to put recent changes into perspective with past and projected climates, and to study influences on and feedbacks from energy flows, carbon cycling, and biological productivity. More specifically, they can be used to study how biogeochemical cycling will respond to transitions in temperature, vertical stratification, sea ice retreat, and acidification, a first step toward addressing consequences for socioeconomic activities (Deal et al. 2013). GCMs and ESMs do have drawbacks, however; they do not reliably simulate interannual and decadal variability, which might overlay and sometimes mask a longer term trend (e.g. Loder and van der Baaren 2013).

GCMs are also severely limited with respect to vertical and horizontal resolution. This is especially an issue in the Canadian Arctic, where shallow shelves and narrow passages are common features. Coarse-resolution GCMs usually artificially widen a strait to allow two-way flow or block passages which cannot be resolved. Hence, while they can provide projections of general long term trends, these models fail at properly representing small scale circulation systems, transport along and through narrow passages as well as coastal circulation and mixing processes in the ocean. This also limits model validation. Observations are often local snapshots (see Section 2) which are compared with ESM grid cells (representing areas of 50 to 200 km²). Hence, trends observed at a single land station do not necessarily represent the same trend as an areal average over an ocean basin and might thus be insufficient for model validation. Unfortunately, limited validation increases the uncertainty of the models.

Another measure of uncertainty can be obtained by using a multitude of models and calculate the multimodel mean and standard deviation. While the mean provides a best guess at the projected trend, the standard deviation gives some measure of uncertainty (the larger the standard deviation, the higher is the uncertainty). An overview of methods for skill and uncertainty estimates in GCMs and ESMs is given in Deal et al. (2013), and many of the specifics are presented in detail in the *Journal of Marine Systems*, Vol. 76, special issue.

One way to overcome the issue of low resolution, is regional downscaling, where higher resolution regional models are forced by GCM or ESM output at their lateral, upper/or lower boundaries (e.g., atmosphere regional models still require oceanic and sea ice boundary conditions from GCMs or ESMs, while regional ocean models require atmospheric forcing from the larger scale models). The main advantage of high resolution models is the ability to resolve advective processes and spatial details such as smaller-scale circulation, currents, orographic features, flow structures, and ocean eddies that contribute to mixing and transport. Regional downscaling from GCMs is recognized as an important tool in producing regional climate information for impact and adaptation studies. Relevant studies are at an early stage but have great potential for future research (Deal et al. 2013).

The assessment below includes analyses from several global and regional models which have been available to the authors, but also draws on available peer-reviewed publications, DFO technical reports and international assessment reports (e.g. from IPCC and AMAP).

3.1.2 Global

Earth System Models used in the CMIP5 and the IPCC AR5: ESMs are coupled atmosphere-ocean-land-biosphere models designed to run for time periods of centuries to thousands of years. They are forced by changes in atmospheric CO₂ and other greenhouse gases, aerosols, solar variability, volcanism, ozone, and land use change. The models are spun up with forcing levels fixed to preindustrial times. The spin-up time, determined by deep ocean overturning timescales, can be a few thousand years. After reaching a stable state, the models are run in historical mode, forced by known CO₂ concentrations or emissions levels from preindustrial to present (1850 - 2005). The models are then run under a variety of future scenarios.

Many simulations have been based on the scenarios outlined in the Special Report on Emission Scenarios (SRES, Nakicenovic et al. 2000). However, for the AR5, Representative Concentration Pathways (RCPs) have been created (Moss et al. 2010) in lieu of the SRES scenarios. The respective radiative forcing is shown in Figure 52 and the evolution of the atmospheric CO₂ for different RCPs is discussed in Arora et al. (2011). Rogelj et al. (2012) present a comparison of warming in projections with SRES and RCP scenarios to facilitate intercomparison of currently evaluated projections within the IPCC AR5 using RCP forcing with earlier literature (Figure 52b). The RCP8.5 scenario utilizes the highest total CO₂ emission scenario of the AR5 experiments; RCP4.5 is a “moderate mitigation” scenario. The RCP4.5 scenario stabilizes at 4.5 W/m² by 2050, while the RCP8.5 increases steadily to reach 8.5 W/m² by 2100. Recent green house gas emissions are tracking close to RCP8.5 and it appears to be the more likely scenario for the next 50 years unless substantial mitigation measures are introduced (Peters et al. 2012). In this assessment, six ESMs submitted to the IPCC AR5 are evaluated: CanESM2, GFDL-ESM2, HadGEM2-ES, IPSL-CM5A-LR, MPI-ESM-LR and MIROC-ESM (See Table 2 for model details). These models are run for a historical time period (eg.1950 - 2005) and for a future period (2006 - 2100) using the RCP8.5 and RCP4.5 scenarios. Data fields have been downloaded via the CMIP5 data portal (cmip-pcmdi.llnl.gov/cmip5/data_portal.html).

Table 2: List of AR5 - Earth System Models

Model	Institute and contact	Model information and reference
CanESM2 (Canadian Earth System Model, version 2.0))	Canadian Climate Center for Modeling and Analysis, Canada http://www.cccma.ec.gc.ca	atmos grid ~2.8° ocean grid ~1° x 1°, L40 Arora et al. 2011 Christian et al. 2010
GFDL-ESM2 (GFDL- Earth System Model)	NOAA Geophysical Fluid Dynamics Laboratory (GFDL), U.S.A. http://www.gfdl.noaa.gov	atmos grid 2° x 2.5° ocean grid ~ 1° x 1°, L50 Dunne et al. 2012
HadGEM2-ES (Hadley Global Environment Model, version 2)	Met Office Hadley Centre, U.K http://www.metoffice.gov.uk	atmos grid 1.875° x 1.25° at mid lats ocean grid 1° x 1°, L40 Booth et al. 2012
IPSL-CM5A-LR (IPSL's Low Resolution (LR) version of the Coupled ESM model 5A)	Institut Pierre Simon Laplace (IPSL), France http://icmc.ipsl.fr/	atmos grid 1.9° x 3.75° ocean grid 2°, L31 Marti et al. 2010
MPI-ESM-LR (MPI -Earth System Model – Low Resolution)	Max Planck Institute (MPI), Denmark http://www.mpimet.mpg.de	atmos grid ~1.9° ocean grid ~1.6°, L40 Brovkin et al. 2013
MIROC-ESM (Model for Interdisciplinary Research On Climate, MIROC)	Center for Climate System Research, Japan http://ccsr.aori.u-tokyo.ac.jp	atmos grid ~2.8° ocean grid ~1° x 1.4°, L44 Watanabe 2011

The global atmospheric variables analyzed for the Canadian Arctic are near-surface air temperature. The oceanic variables are sea surface temperature (T_s), sea surface salinity (S_s), sea ice concentration (SIC), March maximum mixed layer depth (Z_m , a measure of stratification), primary production (PP), particle flux at 100 m (EPC), surface nitrate (NO_3), as well as dissolved inorganic carbon (DIC), total alkalinity (TA), and sea water pH. All of the variables are available for each ESM, except HadGEM2-ES does not provide Z_m and MIROC-ESM does not provide Z_m , PP, EPC or NO_3 .

The marine ecosystem is represented either via single representations of nutrient (N), phytoplankton (P), zooplankton (Z), and detritus (D) groups (NPZD, for CanESM2 and MIROC-ESM); via enhanced representations including 2 - 3 limiting nutrients (MPI-ESM) and up to two phytoplankton groups (HadGEM2-ES); or via multiple representatives of all groups, adding up to > 20 tracers (GFDL-ESM2M, IPSL-CM5A).

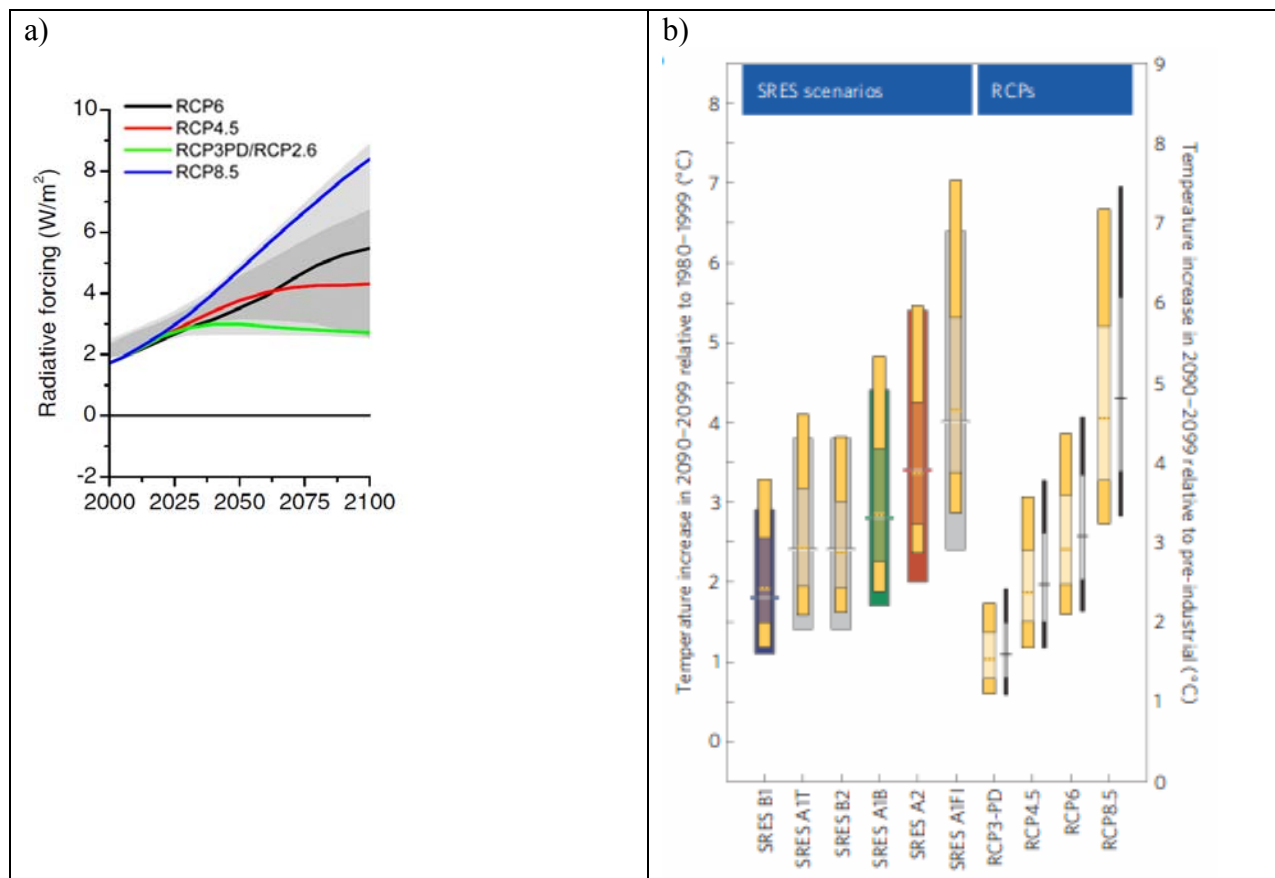


Figure 52: a) Representative Concentration Pathways as used for the IPCC AR5 (Moss et al. 2010). b) Comparison of projected warming in SRES and RCP scenarios (Roeglj et al. 2012).

The states of the ocean carbon system (saturation states for aragonite and calcite, Ω_A and Ω_C) were calculated offline from 3D fields of DIC, TA, T, and S in order to maintain consistency across models. All calculations were performed according to the Best Practices Guide of Dickson et al. (2007) using the equilibrium constants of Lueker et al. (2000). Saturation states were calculated using the expressions for mineral solubility of Mucci (1983) with the pressure correction of Millero (1979).

For most of the analysis, output from each of the six AR5-ESMs has been interpolated onto a standard $2^\circ \times 2^\circ$ (180×90) grid (Figure 53). The models' land masks differ from each other, especially in the Canadian Archipelago, which is not well resolved. In three cases (CanESM2, IPSL-CM5A-LR, and MIROC-ESM), the Canadian Archipelago (CAA) is nearly all land. The CAA throughflow is represented either via crude openings for Parry Channel and Nares Strait (GFDL-ESM2M, HadGEM2-ES), Nares Strait only (MPI-ESM-LR, MIROC-ESM, IPSL-CM5A-LR), or unresolved and approximated via diffusive mixing between Baffin Bay and the Beaufort Sea (CanESM2).

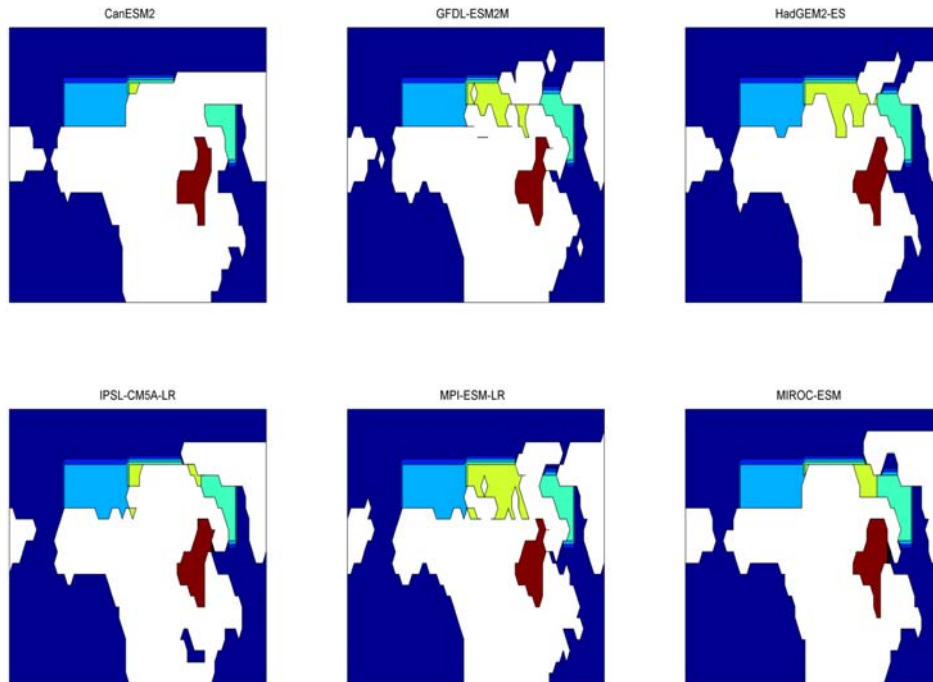


Figure 53: Locations of the ACCASP subregions on each of the AR5-ESM models. Note that the models have different land masks. Color index: Beaufort Sea - light-blue, Canadian Polar Shelf - green, Baffin Bay - cyan, Hudson Bay - red.

The model representation is shown in Figure 54 (left panel). For multimodel spatial analysis, grid points are set to ocean if one or more model is present; the associated landmark is shown in Figure 54 (right panel). Note that the landmark may change depending on the number of models included for a given variable, i.e. some variables are not available for all models.

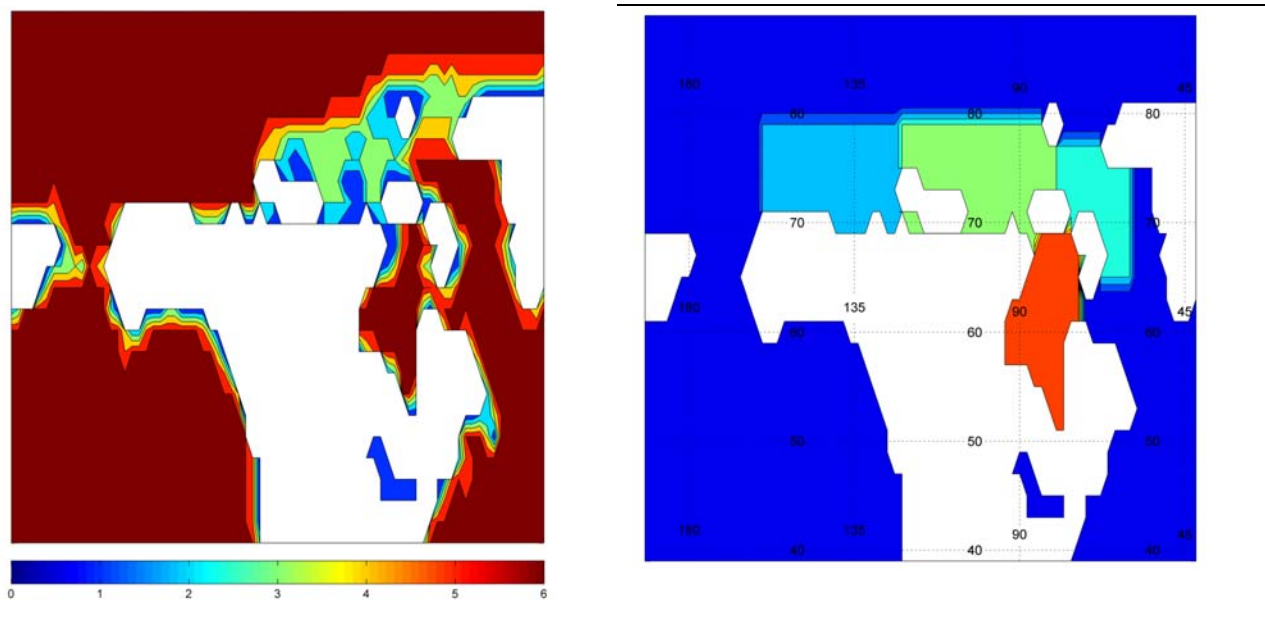


Figure 54: Number of models available per grid point (left panel); ACCASP subbasins with multimodel areas (right panel).

For the ACCASP Arctic evaluation, the Canadian Arctic is divided into four marine subbasins, as shown in Figure 1: Beaufort Sea (BS), Baffin Bay/Davis Strait (BB), Canadian Polar Shelf (CPS), and Hudson Bay (HB). The landmask and associated subbasins shown in Figure 54 (right panel) are used in the analysis for BS and CPS future projections of oceanic variables and have been chosen to match the subbasins defined in Figure 1 as close as possible. For some of the BB and HB analysis, models were analyzed on their original grid with subbasin coverage similar to what is shown (for details see Lavoie et al. 2013).

For the analysis, data are bidecadally averaged from 1966 to 2085, where the bidecades are: 1966 - 1985, 1986 - 2005, 2006 - 2025, 2026 - 2045, 2046 - 2065, and 2066 - 2085. The averaged data was used for both atmospheric and oceanic data analysis. Oceanic analysis for BB and HB also include monthly time series data with respective trend analysis (Lavoie et al. 2013).

3.1.3 Regional

The Canadian Regional Climate Model (CanRCM4): CanRCM4, run at the Canadian Centre for Climate Modelling and Analysis (CCCma), is an atmospheric downscaling model driven by CCCma's CanESM2 for historical and future time periods under the RCP4.5 and RCP8.5 forcing scenarios. Horizontal resolution is 0.44° (approx. 50 km) (Zadra et al. 2008; von Salzen et al. 2013; <http://www.cccma.ec.gc.ca/data/canrcm/CanRCM4>), the vertical resolution is the same as for CanESM2 (see Table 2) and ice and ocean boundary fields are from CanESM2, as well. CanRCM4 is a member of the Coordinated Regional Downscaling Experiment (CORDEX; <http://wcrp-cordex.ipsl.jussieu.fr>) and is run for the two CORDEX domains Arctic (ARC) and North America (NAM). While CORDEX is a multimodel exercise for regional downscaling models, like its predecessor, the North American Regional Climate Change Assessment Program (NARCCAP, <http://www.narccap.ucar.edu/>), CORDEX data have not been available in time for this assessment. Data used for this report have been obtained directly from CCCma.

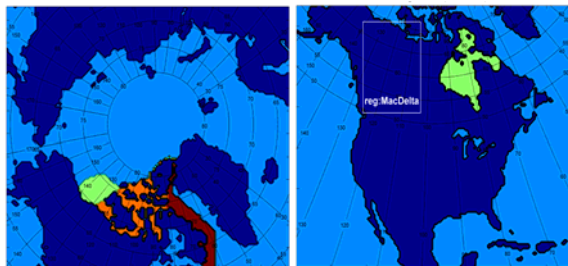


Figure 55: Location of the ACCASP subbasins on the ARC grid (left panel, green = Sea, orange = Canadian Polar Shelf, brown = Baffin Bay) and on the NAM grid north of 35°N (right panel, Mackenzie River Delta region, green = Hudson Bay).

NARCCAP data has been used for a large part of the projections analysis in the Pacific region (Christian and Foreman 2013), however the North American domain provides only limited cover of the Arctic and NARCCAP does not include an Arctic domain. Since CanRCM4 data was the only CORDEX data set available for analysis, results need to be taken with a grain of salt, since they only provide a one model view and errors or/and limitations from the forcing ESM transfer to a certain extent into the RCM.

A variety of CanRCM4 evaluation exercises are currently in progress and not yet available in publication. An example is a comparison of CanRCM4 output and observed data sets for daily maximum temperature T_{\max} , daily minimum temperature T_{\min} , and daily accumulated precipitation over eastern Canada (Hudson Bay area, 49 - 60°N, 260 - 298°E, Gachon et al. 2013, unpublished data). Two simulations have been performed based on two different driving atmospheric conditions (i.e. lateral boundary conditions): 1. NCEP/DOE (NCEP2, <http://www.esrl.noaa.gov/psd/data/gridded/data.ncep.reanalysis2.html>, 1979 - 2009) and 2. ERA-Interim (<http://www.ecmwf.int/research/era/do/get/era-interim>, 1989 - 2001). For validation the observed gridded data product ANUSPLIN has been used (National Land and Water Information service, www.agr.gc.ca/nwlis-snite, Hutchinson et al., 2009) providing daily T_{\max} , T_{\min} , and total precipitation on a 10-km grid. This product has been interpolated on a polar stereographic (PS) grid (resolution of 45 km at 60°N) to facilitate the CanRCM4 evaluation, as in Eum et al. (2012). For the analysis, raw data has been extracted over the study area (without water grid cells) for each CanRCM4 simulation and from the ANUSPLIN-PS grid (i.e. no interpolation). Then, daily time series for each grid point have been extracted, seasonal mean values computed, and box plots created for each model containing spatio-temporal information (e.g. CanRCM4, 13 years x 1576 grid points = 20,488 values over the common 1989 - 2001 period). In summary, CanRCM4 showed very good skill with respect to T_{\max} (warm bias less than 1°C in winter and no bias in summer) and some warm biases for T_{\min} (i.e. 2.5°C in winter and 1.6°C in summer). The T_{\min} biases are more noticeable than for T_{\max} and are higher for winter than for summer. The model shows quite similar skill (or biases) for the two different driving conditions (no distinguishable differences among the 2 runs). For total precipitation CanRCM4 shows very good skill in winter (no noticeable bias) and an overestimation in summer (i.e. 0.5 mm/day).

For the current assessment, trend analyses and spatial plots are prepared for the BS, CPS and BB on the ARC domain, and for the HB and Mackenzie River Delta on the NAM domain (Figure 55). Variables analyzed are air temperature (temperature at surface TAS), precipitation (P), and wind speed squared (WSS).

NAA-NEMO: The North American Arctic NEMO (NAA-NEMO) is a basin scale model of the Arctic and the North Atlantic (Figure 56, Hu and Myers 2013) based on the Nucleus for European Modelling (NEMOv3.1, Madec and the NEMO team (2008)) framework. It includes a coupled ocean (OPA) and sea ice model (LIM2; Lovain-la-Neuve sea ice model; Fichefet and Maqueda 1997) with modified elastic-viscous-plastic (EVP) ice rheology (Hunke and Dukowicz 1997). The horizontal resolution varies from ~11 to 15 km, and the model has 46 depth levels. The model is spun up with ocean temperature and salinity from the Polar Science Center Hydrographic Climatology (PHC, Steele et al. 2001), ocean surface forcing from Common Ocean-ice Reference Experiments version 2 (CORE2, Large and Yeager 2008, http://data1.gfdl.noaa.gov/nomads/forms/core/COREv2/code_v2.html), global model runoff (ORCA05 MGP; Barnier et al. 2006), and open boundary data from a global model simulation (Barnier et al. 2006). The model was spun up under these conditions for 18 years.

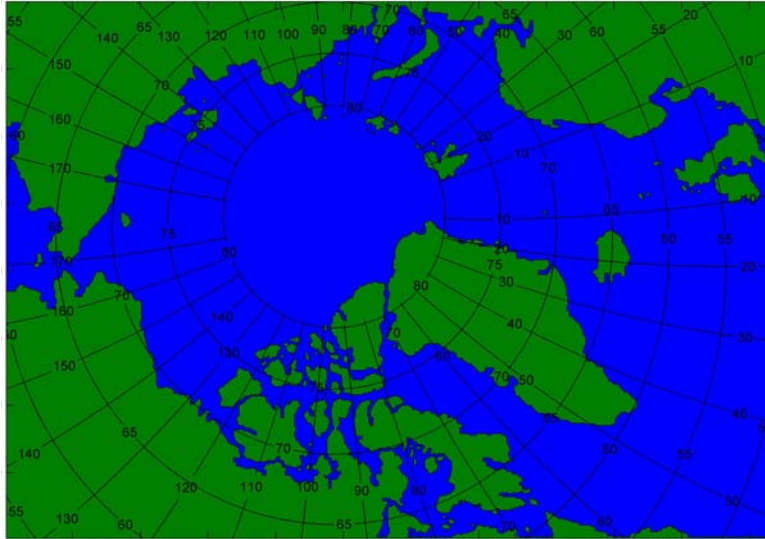


Figure 56: NAA-NEMO domain.

Two experiments were then carried out:

- 1970 - 1999 (forced with data from the HadCM3 model 20c3m run, Gordon et al. 2000)
- 2000 - 2100 (forced with data from the HadCM3 model under the SRES A1B scenario, IPCC 2000) and open boundaries data from the CCCma CGCM3.1 model (Flato and Boer 2001). Note that the SRES A1B scenario is more similar to the RCP4.5 than the RCP8.5 scenario.

The future forcing data are modified as described in Dumas et al. (2006). For air temperature and downward radiation, monthly output from HadCM3 has been added to the difference between the HadCM3 1970 - 1999 climatology and the CORE2 normal year climatology. For precipitation, snow and specific humidity, the CORE2 climatology is multiplied by a ratio of HadCM3 monthly time series data and the HadCM3 1970 - 1999 climatology. The basic idea of this pre-process is to simulate the responses of the ocean to the variations in HadCM3 atmospheric output. From these model results, regionally averaged time series have been derived and are presented for the BS, CPS and BB subbasins as shown in Figure 1. Spatial plots are provided for bidecadal means and differences between bidecades as described for the global models (3.1.1).

3.2 ATMOSPHERIC FORCING

3.2.1 Air temperature

Climate model projections have shown that lower-tropospheric warming in the Arctic is amplified compared to the projected warming in global mean temperature (e.g., Frierson 2006). However, substantial variation in the amplitude of polar amplification is simulated by different climate models (Hawkins and Sutton 2009). Räisänen et al. (2010) and Bracegirdle and Stephenson (2012) investigated multimodel ensembles from the 3rd Coupled Model Intercomparison Project (CMIP3, Meehl et al. 2007) and demonstrated that the intermodel spread in the projected change in surface air temperatures near the winter sea ice edge can be partially accounted for by differences in the means of the historical runs. They suggest that near the

ensemble mean sea ice edge; models that simulate colder present-day surface temperatures (associated with more sea ice) give more future warming, related to the transition from sea ice to open water state. Bracegirdle and Stephenson (2012) note that such a state dependence of the model response provides an emergent constraint (Collins et al. 2012) that can be used to reduce model-related uncertainty and give more precise projections. Bracegirdle and Stephenson (2013) point out that these constraints in multimodel ensembles (MMEs) may be spurious and can arise because of common errors in a particular MME or because of overly influential models. They assess the robustness of emergent constraints used for Arctic warming by comparing ensembles generated by CMIP3 and CMIP5 model experiments. They analyze Arctic wintertime surface air temperature change over the twenty-first century under the SRES A1B scenario in CMIP3 and the RCP4.5 scenario in CMIP5 and find the estimated emergent constraints to be reassuringly similar in CMIP3 and CMIP5 in most locations, and point out that differences could be due to sampling variation. Their analysis identifies one climate model in CMIP5 that has a notable influence over the Bering Sea and one in CMIP3 that has a notable influence more widely along the sea ice edge.

Loder and van der Baaren (2013) analyzed the AR5-ESMs with respect to their representation of historical observations with focus on Atlantic Canada and parts of the Canadian Arctic. They find the climatological means and annual cycles of surface air temperature to be approximately reproduced at most sites in most (but not all) of the models, but find that past interannual-to-decadal-scale variability is generally not reproduced. These results are not unexpected for coarse resolution global climate models.

Similar issues likely apply for other model variables (e.g. precipitation, wind). Keeping those limitations in mind, simulated past and future trends in air temperature from regional and global climate models (Section 3.1) are presented for the Arctic subbasins.

Beaufort Sea, Canadian Polar Shelf, Baffin Bay and Hudson Bay: Both the global and regional models project warmer near surface air temperatures (TAS) over all the regions. The AR5-ESM multimodel increase from 1986 – 2005 to 2046 – 2065 is shown in Figure 57. The change has large seasonal and spatial variability. In February, the Beaufort Sea (BS), Canadian Polar Shelf (CPS), and northern Baffin Bay (BB) warm by 5 - 10°C, while the Hudson Bay (HB) warms even more with an increase of 10 - 15°C. There is little change in May and August. In November, significant warming (10 - 15°C) is projected in the BS, CPS and northern BB, with little change to the south. A more detailed evaluation of the AR5-ESMs with focus on Atlantic Canada can be found in Loder and van der Baaren (2013).

The annual cycles of TAS are plotted at Resolute (74.7°N, 95°W), Alert (82.5°N, 62.3°W), Tuktoyaktuk (69.5°N, 133°W), Churchill (58.7°N, 94.1°W), and at sites in the BS (73°N, 140°W) and BB (74°N, 68°W). Resolute, Alert and Tuktoyaktuk are located within the CPS, and Churchill within the HB. At all sites, RCP8.5 projects more warming than RCP4.5 with a larger increase in winter than in summer for both RCPs (Figure 58). Each of the AR5-ESMs has a similar intensification in winter, but the projected winter increases in HadGEM2-ES are ~5 - 10°C higher than in other models (Figure 59). The annual mean sixty year change for the sites (RCP8.5) range from 6.2°C in the Beaufort Sea to 4.5°C at Churchill (data not shown).

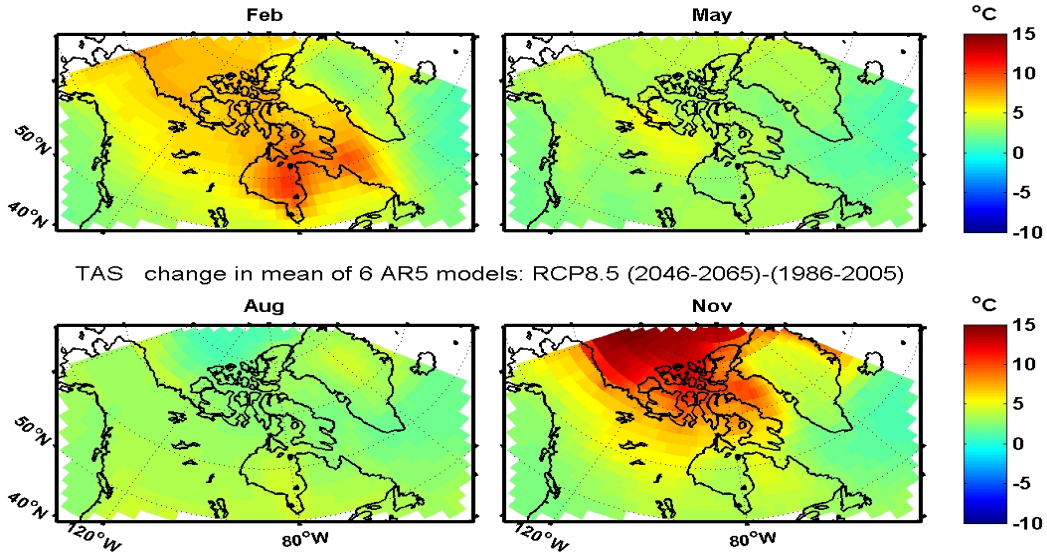


Figure 57: AR5-ESM multimodel mean sixty year change (difference between 1986 - 2005 and 2046 - 2065) of near surface air temperature for RCP8.5.

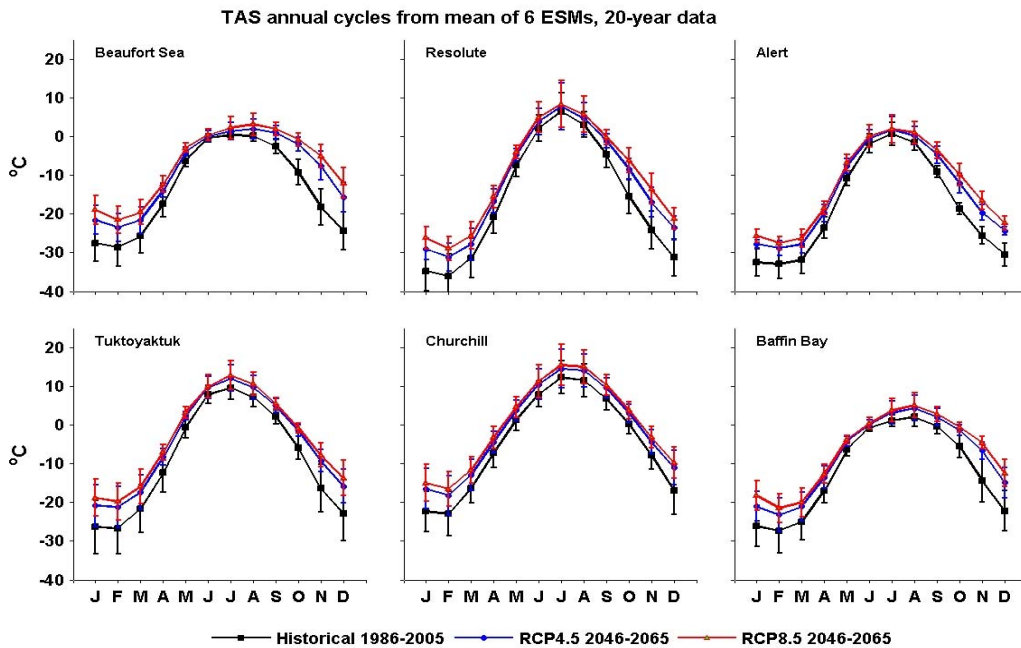


Figure 58: AR5-ESM multimodel mean annual cycles for 1986 - 2005, and 2046 - 2065 (RCP4.5 and 8.5).

In agreement with the global ESMs, the regional CanRCM4 projects similar increases in TAS for the Arctic ACCASP subbasins. The simulated sixty year change (2046 - 2065 minus 1986 - 2005) is 5.73°C, 5.18°C, 4.25°C, and 5.38°C for the BS, CPS, BB and HB subbasins respectively for scenario RCP8.5.

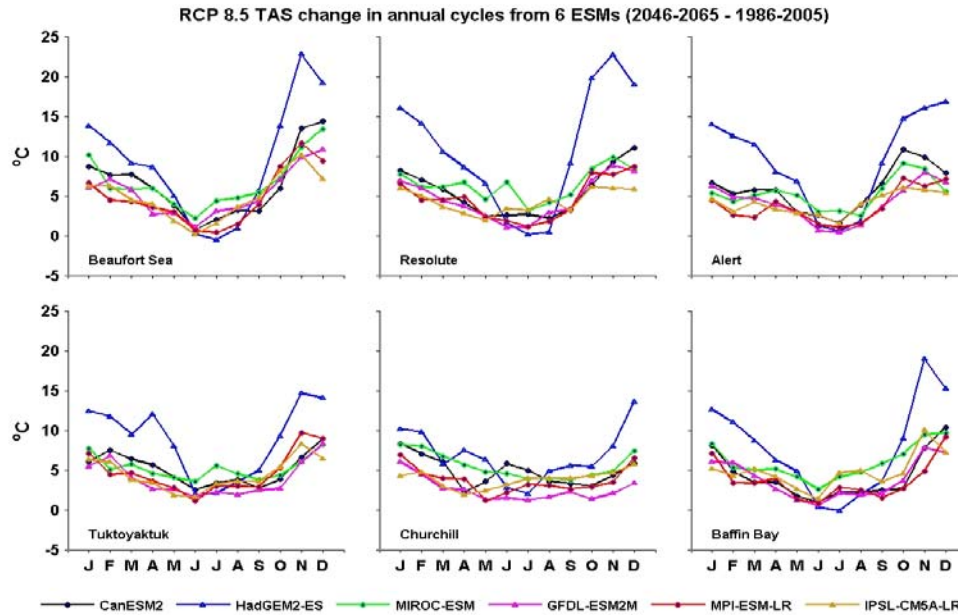


Figure 59: AR5-ESM individual model, sixty year change (difference between 1986 - 2005 and 2046 - 2065), in TAS annual cycles at specific site locations (see text).

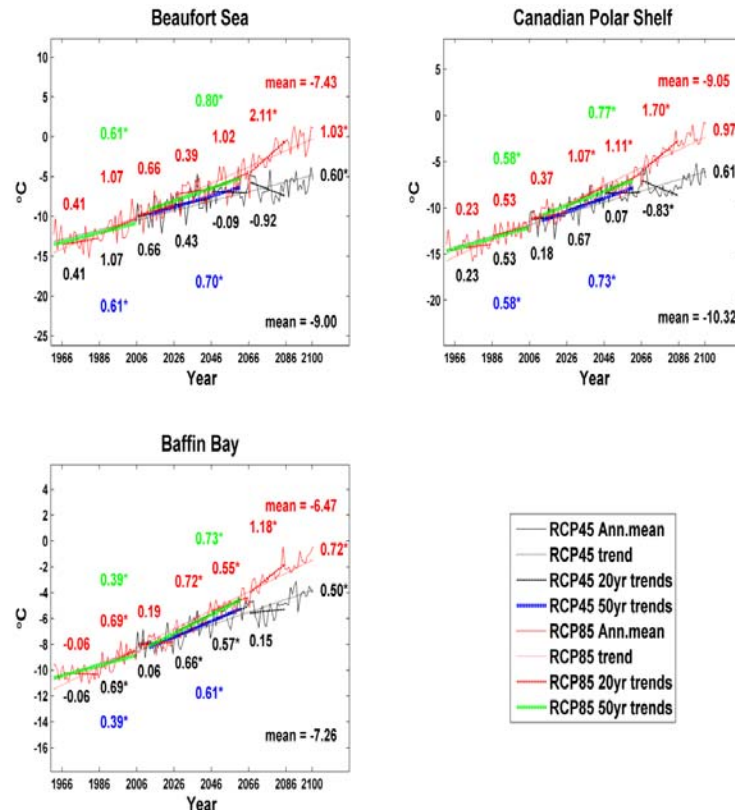


Figure 60: CanRCM4-ARC annual mean air temperature with bidecadal trends as well as a historical (1961 - 2005), a future fifty year (2012 - 2061), and a long term (1961 - 2100) trend for scenarios RCP4.5 and RCP8.5, averaged over the Arctic ACCASP subbasins. All trends are °C/decade. If marked with an asterisk, the trend is significant (on a 5% level).

Figure 60 shows time series of the annual mean air temperature with bidecadal trends as simulated with CanRCM4 for the historical and projection runs. Over the historical time period (1961 - 2005), CanRCM4 is warming. The air temperature trends for 1961 to 2005 in the BS, CPS and BB are 0.61, 0.58, and 0.38 °C/decade. These trends increase in the future for RCP8.5 and RCP4.5 forcing, and the future fifty year (2012 to 2061) trends are 0.80, 0.77, and 0.73 °C/decade (BS, CPS, and BB respectively) for RCP8.5. The persistent ice cover may explain why there is little difference between the scenarios in the CPS. The historical, future fifty year and long terms trends are all significant and positive. While bidecadal trends are provided and show some degree of variability, the reliability of decadal and multidecadal variability in these models is likely much lower than that of the underlying longer term trend.

Spatially, the historical (1986 - 2005) annual mean air temperatures in the BS and CPS range from -18°C to the east and -9°C towards the Canadian coast, while BB is warmer (-9 to -12°C, Figure 61). For RCP8.5 forcing, there is a 1 – 2°C increase in air temperature throughout the Canadian Arctic from 1966 - 1985 to 1986 - 2006, and again from 1986 - 2006 to 2006 - 2025 (with greater than 2°C of change north of the CPS). Over sixty years (2046 - 2065 minus 1986 - 2005) the air temperatures of the BS and CPS increase by 5 - 6°C, while BB, Greenland and the Canadian landmass warm by 3 – 5°C.

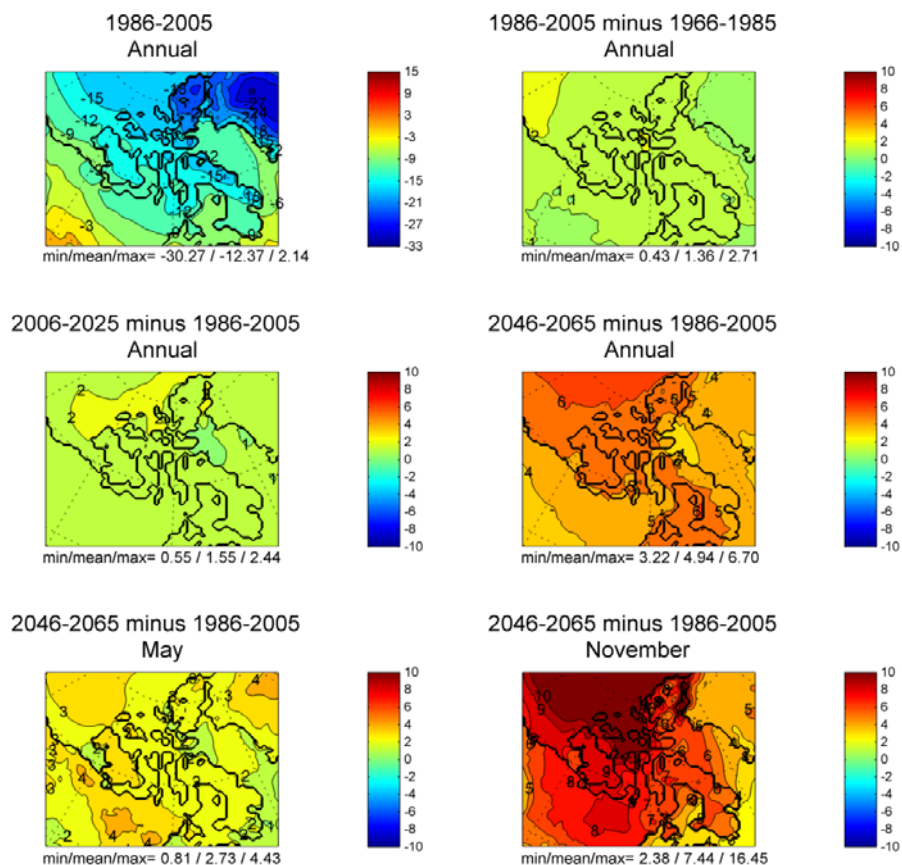


Figure 61: Annual mean and bidecadal changes of surface air temperature in the Canadian Arctic as modelled by CanRCM4 for RCP8.5.

Figure 61 also shows the seasonal difference in the increase in air temperature for CanRCM4, with more increase in the winter (i.e. November – February) which is also seen in the AR5-ESMs. For example, the change in November in the BS, CPS and BB is 6 - 14°C and less than 5°C in May.

Hudson Bay: CanRCM4 analysis for the Hudson Bay ACCASP region is done on the North American (NAM) grid (Figure 62). As seen in the BS, CPS and BB, the warming trend before 2005 in the HB is intensified under the RCP scenario forcing: the historical (1961 - 2005) trend is 0.48 °C/decade and the future fifty year (2012 - 2061) trend is 0.90 and 0.94 °C/decade for the RCP8.5 and RCP4.5 scenarios. Note that for this particular region, the RCP4.5 has a greater warming trend; although trends are strongly influenced by the start and end points. The long-term trends (1961 - 2100) show that RCP8.5 has a higher rate of warming overall (0.93 °C/decade vs 0.64 °C/decade for RCP4.5).

Spatially, the CanRCM4 historical (1986 - 2005) annual mean air temperatures in the HB range from -9 to 3°C (north to south) as part of the larger pattern over northern North America in which air temperatures are cooler in the north and increasingly warmer to the south. CanRCM4 air temperatures warm in broad bands over northern North America, with greater temperature increases in the north. The twenty year change (2006 - 2025 minus 1986 - 2005) is 1 - 2°C for the HB (and also for North America). Over sixty years, the HB warms by 5.0 - 6.0°C, with more warming to the northeast; the rest of northern North America changes by 3 – 6°C (Figure 63).

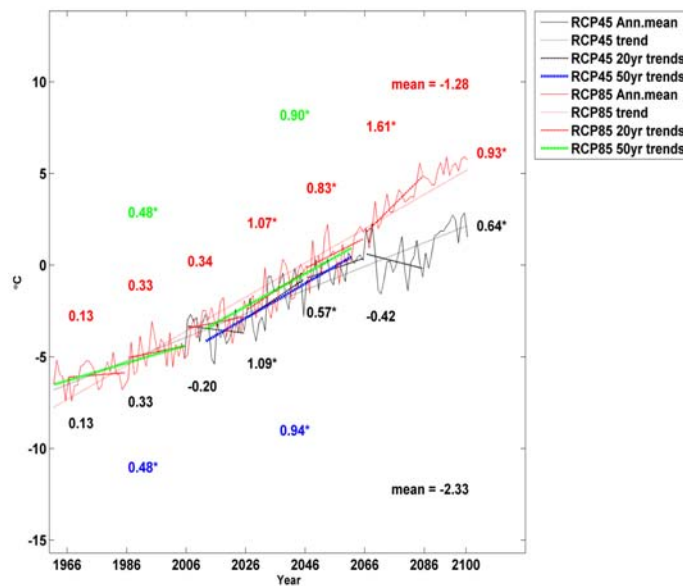


Figure 62: CanRCM-NAM annual mean air temperature with bidecadal trends as well as a historical (1961 - 2005), a future fifty year (2012 - 2061), and a long term (1961 - 2100) trend for scenarios RCP4.5 and RCP8.5, averaged over the ACCASP Hudson Bay subbasin. All trends are °C/decade. If marked with an asterisk, the trend is significant (on a 5% level).

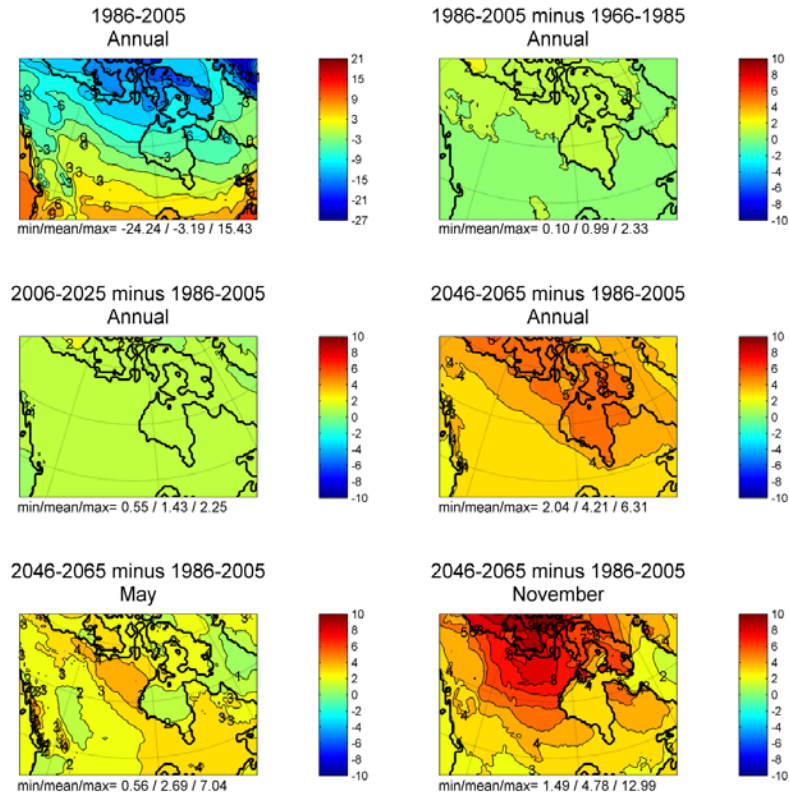


Figure 63: Annual mean and bidecadal changes of air temperature (TAS, °C) over North America, as modelled by CanRCM-NAM for RCP8.5.

Seasonally, the change in HB is greatest in winter (JFM) whereas the BS, CPS and BB change is greatest in winter and fall (OND). Consequently, the change in air temperature between May and November is less in the HB. This is also evident in the ESMs (Figure 57).

3.2.2 Precipitation

The IPCC-AR4 Summary for Policy makers (IPCC 2007) points out that there is now an improved understanding of projected patterns of precipitation, suggesting increases in the amount of precipitation to be very likely in high latitudes. Chassé et al. (2013) evaluate precipitation, evaporation and freshwater flux over Canada from the six AR5-ESMs. Their analysis shows increased precipitation, evaporation, precipitation minus evaporation (P - E) in the Arctic and Hudson Bay areas, with larger changes for RCP8.5 than for RCP4.5. For precipitation, the 2066 - 2085 bidecadal period relative to the 1986 - 2005 period shows an increase of 14.6% for the Hudson and 25.3% for the Arctic compared to 8.9% for the Atlantic and 15.4% for the Pacific. Similarly, the increase in evaporation for the same bidecadal period is 17.3% for the Hudson and 24.1% for the Arctic compared to 6.9% and 9.3% for the Atlantic, and the Pacific. These changes result in increased (P - E) of 10.9% for the Hudson and 26.2% for the Arctic. Chassé et al. (2013) compute the emergence times (ET) as the time (from the middle of the current period) at which the long term trend line emerges above the mean plus two standard deviations of the multimodel ensemble mean. ETs for both the precipitation and evaporation signals are calculated to 22 y for the Arctic with RCP8.5. Chassé et al. (2013) find significant differences in the future timing of the maximum runoff between models. The multimodel

ensemble mean gives an earlier occurrence of the freshwater pulse in the future with trends of around -10.0 and -14 days/century.

Beaufort Sea, Canadian Polar Shelf and Baffin Bay: Time series and trends of precipitation as simulated with CanRCM4 are shown in Figure 64. The historical trends (1961 - 2005) show small rates of increase with 0.01 mm/day/decade in the BS and CPS and no change for BB. Note that observations at individual land stations do show a higher positive trend (Section 2.1.2). While these land stations are not necessarily representative for the ocean average, it does remind us to regard the model results with some caution. The future fifty year trends (2012 - 2061) are somewhat larger: 0.03 – 0.04 mm/day/decade for the BS, CPS, and BB. These trends compare to long term mean precipitation values of 0.82 (BS), 0.90 (CPS), 1.11 (BB) for RCP8.5. The BS, CPS and BB subbasins all have positive bidecadal trends from 1966 - 2065 (RCP8.5). In most cases, the future fifty year trend for RCP8.5 is greater than RCP4.5, except for the BB subbasin. However, over the extended time period (1961 - 2100), the mean trend for RCP8.5 (0.034 mm/day/decade) is larger than for RCP4.5 (0.025 mm/day/decade) for the BB subbasin as well.

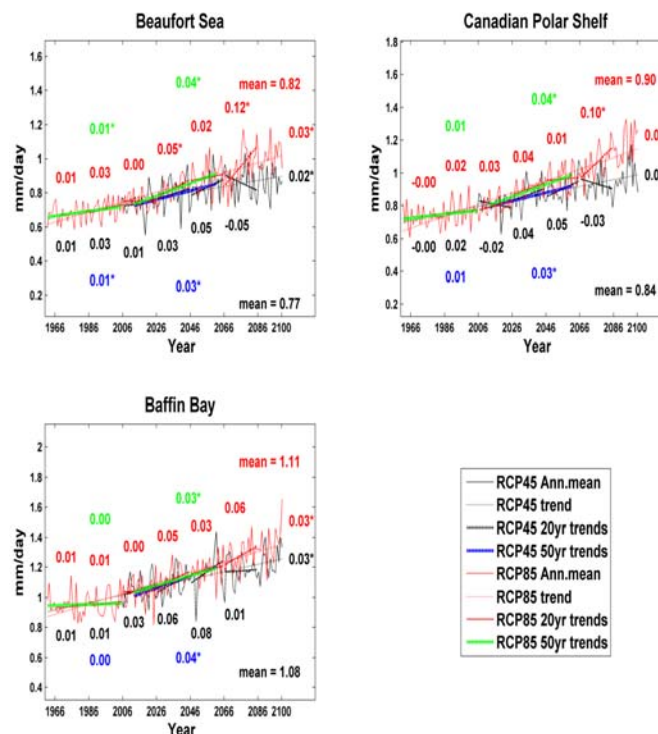


Figure 64: CanRCM4-ARC annual mean precipitation with bidecadal trends as well as a historical (1961 - 2005), a future fifty year (2012 - 2061), and a long term (1961 - 2100) trend for scenarios RCP4.5 and RCP8.5, averaged over the ACCASP subbasins. All trends are mm/day/decade. If marked with an asterisk, the trend is significant (on a 5% level).

The spatial pattern of annual mean 1986 - 2005 precipitation over the Canadian Arctic shows less precipitation over Greenland and the central Arctic and increasing amounts to the south (Figure 65). From 1966 - 1985 to 1986 - 2005, precipitation increases in most of the BS and CPS, as well as northern BB; precipitation decreases in the southern BB, and in a small portion of the western BS and CPS. Precipitation further increases by 2006 - 2025 for most regions. The sixty year change (2026 - 2045 minus 1986 - 2005) indicates an increase in precipitation

throughout the entire region, with a 0.1 - 0.2 mm/day increase in the BS, CPS and northern BB. It should be noted that while change seems low (0.1 mm/day/3.6 cm/y) with respect to added water, if falling as snow, the impact could be more relevant.

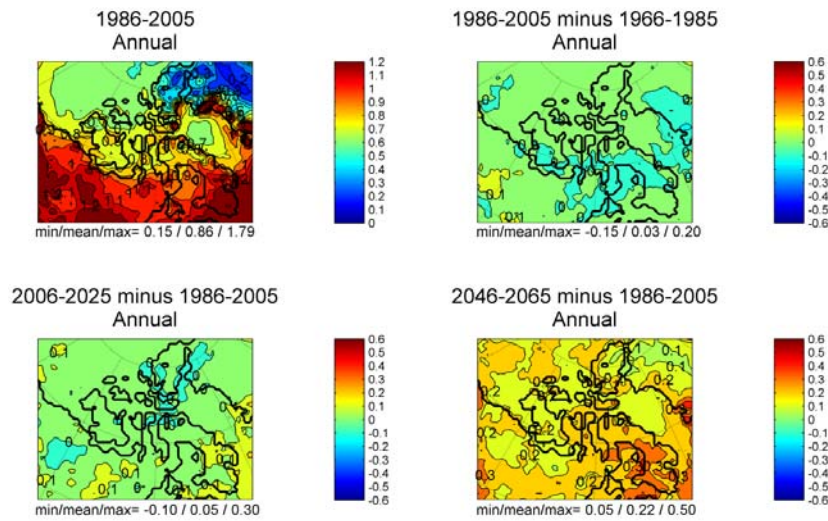


Figure 65: Annual mean and bidecadal changes of precipitation (mm/day) over the Canadian Arctic as modelled by CanRCM4-ARC for scenario RCP8.5.

Hudson Bay: The HB historical trend (1961 - 2005) for precipitation is 0.03 mm/day/decade, which increases to 0.05 - 0.06 mm/day/decade under RCP8.5 and RCP4.5 forcing (2012 - 2066). All of the bidecadal trends are positive for both scenarios. However, the trends under RCP8.5 are consistently 0.05 mm/day/decade or greater, whereas the RCP4.5 range from 0.00 to 0.06 mm/day/decade. The long-term trend (1961 - 2100) indicates that precipitation increases more under the RCP8.5 forcing than RCP4.5 (Figure 66).

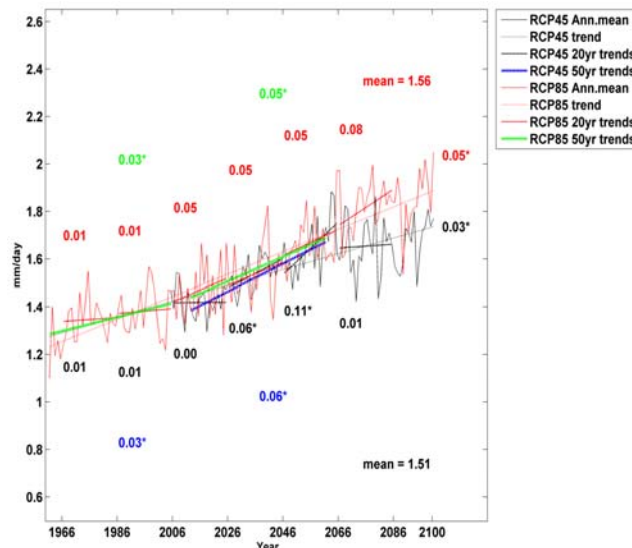


Figure 66: CanRCM4-NAM annual mean precipitation with bidecadal trends as well as a historical (1961 - 2005), a future fifty year (2012 - 2061), and a long term (1961 - 2100) trend for scenarios RCP4.5 and RCP8.5, averaged over the ACCASP Hudson Bay subbasins as shown in Figure 55. All trends are mm/day/decade. If marked with an asterisk, the trend is significant (on a 5% level).

The CanRCM4 historical (1986 - 2005) annual mean precipitation is greater in the southern HB (2.7 mm/day) than in the north (0.7 - 1.4 mm/day). The spatial pattern of change is a noisy pattern of increasing precipitation. Under RCP8.5 forcing, the twenty year change (2006 - 2025 minus 1986 - 2005) is 0 - 0.1 mm/day, where the sixty year change (2045 - 2065 minus 1986 - 2005) is 0.2 - 0.3 mm/day (Figure 67).

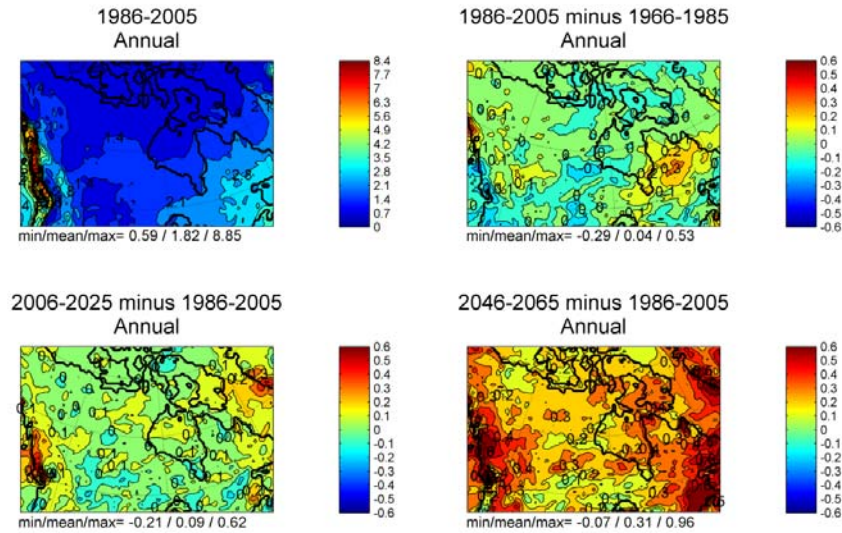


Figure 67: Annual mean and bidecadal changes of precipitation (mm/day) over North America as modelled by CanRCM4-NAM for scenario RCP8.5.

3.2.3 Circulation and wind

Beaufort Sea, Canadian Polar Shelf and Baffin Bay: The CanRCM4 windspeed squared (WSS) has very high temporal variability, resulting in almost zero long term trends. None of the trends are significant on a 5% level, except for the long term RCP8.5 trends (1961 - 2100) for two regions: the CPS WSS increases by 0.03 m²/s²/decade while the BB WSS decreases by 0.07 m²/s²/decade (not shown).

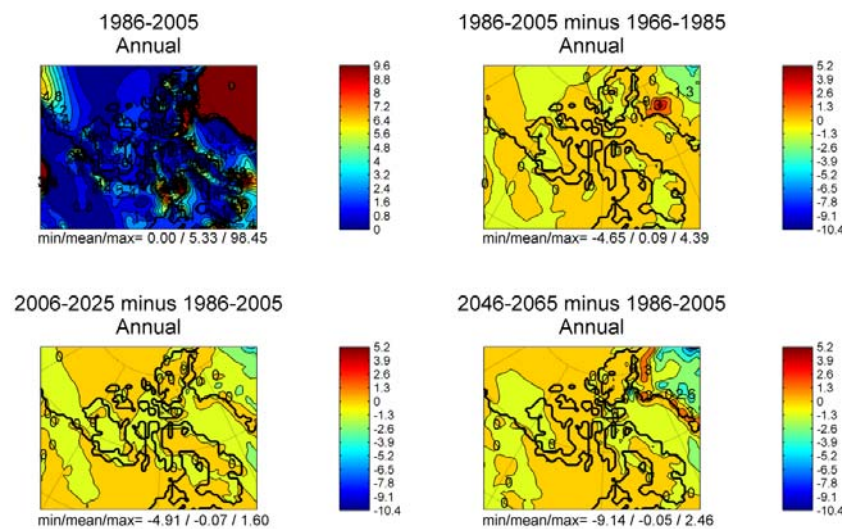


Figure 68: Annual mean and bidecadal changes of windspeed squared (m²/s²) in the Canadian Arctic as modelled by CanRCM4-ARC for scenario RCP8.5.

Spatially, the historical annual mean (1986 - 2005) of CanRCM4 WSS is very strong ($98 \text{ m}^2/\text{s}^2$) over Greenland and weaker over the Canadian Arctic. The WSS is about $5 \text{ m}^2/\text{s}^2$ over the eastern BS and $0 - 5 \text{ m}^2/\text{s}^2$ over the CPS and BB (with pockets of $10+ \text{ m}^2/\text{s}^2$). Over sixty years (2046 - 2065 minus 1986 - 2005), the WSS decreases over the eastern BS and the northern BB and increases over the CPS region (Figure 68).

Hudson Bay: The long term trends (1961 - 2100) of CanRCM4 windspeed squared (WSS) for both scenarios are significant (on a 5% level) and indicate an increase in WSS. The trends are 0.17 and $0.08 \text{ m}^2/\text{s}^2/\text{decade}$ for RCP8.5 and RCP4.5 respectively. None of the shorter trends are significant; the time series has high variability (Figure 69).

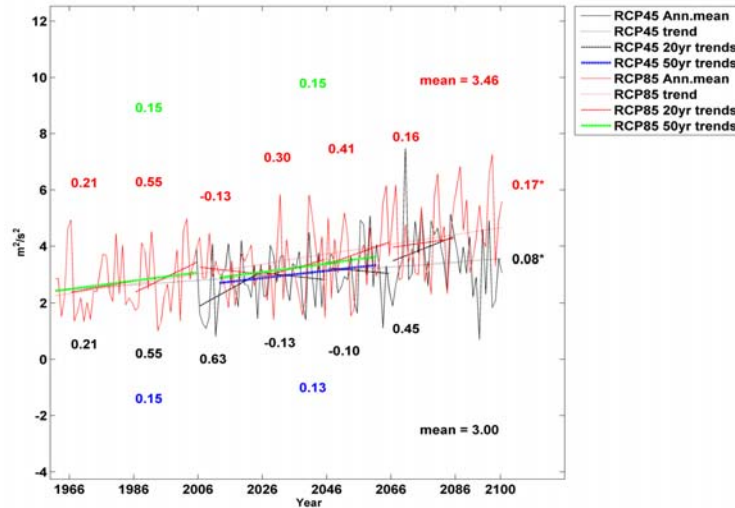


Figure 69: CanRCM-NAM annual mean windspeed squared (m^2/s^2) with bidecadal trends as well as a historical (1961 - 2005), a future fifty year (2012 - 2061), and a long term (1961 - 2100) trend for scenarios RCP4.5 and RCP8.5, averaged over the ACCASP Hudson Bay subbasin as shown in Figure 55. All trends are $^{\circ}\text{C}/\text{decade}$. If marked with an asterisk, the trend is significant (on a 5% level).

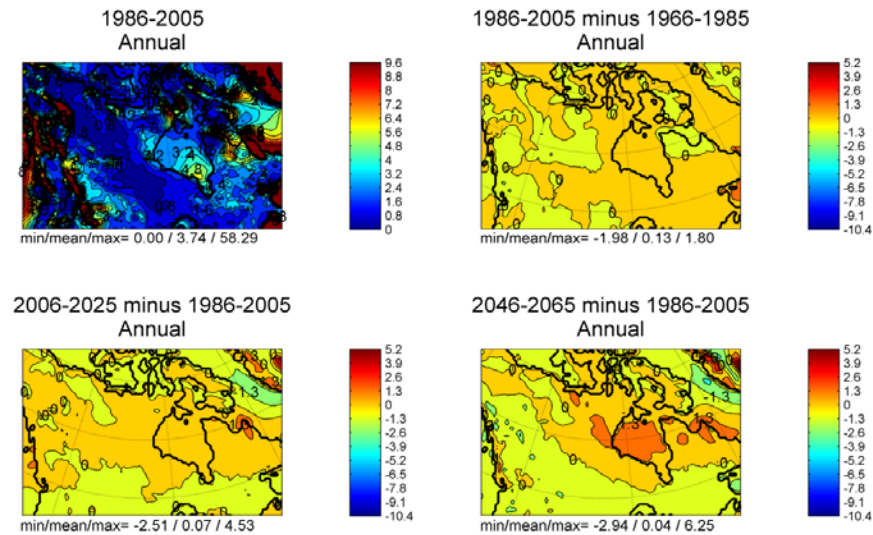


Figure 70: Annual mean and bidecadal changes of windspeed squared (WSS) (m^2/s^2) over North America as modelled by CanRCM for scenario RCP8.5.

Spatially, the historical annual mean (1986 - 2005) of WSS over the HB is greater in the south ($5.6 \text{ m}^2/\text{s}^2$) than in the north ($1.6 \text{ m}^2/\text{s}^2$). The change in WSS increases uniformly by $0 - 1.3 \text{ m}^2/\text{s}^2$ (twenty year change) and within the central HB by $1.3 - 2.6 \text{ m}^2/\text{s}^2$ (sixty year change) (Figure 70).

3.2.4 Wind, storm patterns and waves

Beaufort Sea: Guo et al. (unpublished data) study distributions, e.g. means and 10% highest values for winds, and waves for present climate, represented as 1970 - 1999, and future climate, represented as 2040 - 2069, and the impacts of climate change. Their simulations are made with the WAVEWATCH® (WW3) operational wave model on a basin-scale grid (resolution $2/3^\circ \times 1/6^\circ$), with a nested high-resolution ($1/6^\circ \times 1/24^\circ$) grid for the Beaufort Sea and waters near the Canadian Archipelago. Winds to drive the wave model are derived from CRCM (Canadian Regional Climate model), which is in turn forced by outputs from CCCma's CGCM3, following the SRES A1B scenario. The simulations focus on September when open water areas tend to be highest. The wave model is updated with estimated ice edges every 6 hours and the wave damping criteria damps waves to zero above 50% ice cover. An additional scenario assumes ice free conditions, representing estimated future conditions. Results suggest increases to the 10% mean strongest winds of about $+3 - 4 \text{ m/s}$, and about $2.5 - 3 \text{ m}$ in significant wave heights (Hs), particularly in the southern regions of the Beaufort and Chukchi Seas, near Bering Strait. Changes of Hs in waters off the Mackenzie Delta are estimated as not exceeding 0.5 m .

3.2.5 Climate Extremes

The Special Report on Extreme Events (SREX) of the IPCC (IPCC 2012) emphasizes the particular relevance of extreme climate events and their change to society and ecosystems due to their potentially severe impacts.

Sillmann et al. (2013b) analyzed projected changes in temperature and precipitation indices over land defined by the Expert Team of Climate Change Detection and Indices (ETCCDI) focusing on extreme events for CMIP3 and CMIP5 multimodel ensemble projections of the 21st century for both SRES and RCP scenarios. Results generally indicate an intensification of patterns of change already observed in temperature- and precipitation-based indices (e.g., Frich et al. 2002; Kiktev et al. 2003; Alexander et al. 2006; Min et al. 2010; Morak et al. 2011) with increasing radiative forcing. These patterns of change have also been found in model simulations of the historical climate (Sillmann et al. 2013a) and include a stronger warming and an increase in precipitation extremes in northern latitudes. In particular, changes in the seasonal minima of daily minimum temperatures are more pronounced in northern regions. Increases are stronger in winter than in summer. Based on the guidelines of the World Meteorological Organization (WMO) on the analysis of extremes in a changing climate (Klein Tank et al. 2009), projected changes in the indices are indicative of future climate change in extremes. Sillmann et al. (2013b) find their results with respect to temporal evolution and spatial patterns of changes to be in agreement with previous studies by Tebaldi et al. (2006) and Orłowsky and Seneviratne (2012), although somewhat different standardization procedures and definitions of indices were used in those studies. Sillmann et al. (2013b) find more inter model agreement for the projected changes in the temperature indices in all regions and less consistency among models for changes in the precipitation indices indicating large uncertainties for precipitation patterns. Sillmann et

al. (2013a) point out that while most models represent extremes reasonably well, including trends in the present climate, some indices are not well represented or difficult to evaluate with currently available observational datasets. They further indicate that future changes in temperature and precipitation extremes need to be assessed carefully in relation to changes in circulation patterns and other feedback mechanisms (e.g. snow, soil moisture, vegetation). The indices are based on daily minimum and maximum of near surface temperature (TN, TX) and daily precipitation amounts (PR) and the minimum of TN (TNn) and maximum of TX (TXx) represent the coldest or hottest day of a year, season, or month, respectively. (See ETCCDI website <http://etccdi.pacificclimate.org/> and references within Sillmann et al. (2013a), for more detailed information).

Temperature: Relative to the 1981 – 2000 reference period, Sillmann et al. (2013b) find a general increase in the annual TNn and TXx over land in the 21st century. They find the spatial patterns of change to be different in TNn and TXx with TNn increasing more strongly in Northern higher latitudes. The greatest changes in TNn, exceeding 12°C, are simulated in RCP8.5 in Northern higher latitudes and related to retreating snow cover. They find the regions covering the continental Canadian Arctic to experience the strongest median warming in TNn. In contrast to TNn, TXx is projected to warm more uniformly over land. The pattern of seasonal and regional changes in TNn and TXx is found to be similar for RCP4.5, albeit less pronounced compared with RCP8.5. In the Canadian Arctic land areas, TNn increases in winter by more than 2°C, even in the lowest forcing scenario. Frost days particularly decrease in western North America, strongest in RCP8.5 with reductions of 80 frost days and more by the end of the 21st century. Sillmann et al. (2013b) also analyze cold spell duration (CSDI) which is projected to decrease and warm spell duration (WSDI) which is projected to increase in all RCPs. Both WSDI and CSDI are found to be sensitive to the underlying climatological temperature variability of the respective region (see also Radinović and Ćurić 2012). The models project a consistent decrease in cold nights and cold days from the late 20th to the 21st century in all SRES and RCP scenarios. However, by the end of the 21st century, the responses for different scenarios diverge further apart. Warm nights and days, in the contrary, show a general increase toward the end of the 21st century. These projected changes are more pronounced in the summer season. Sillmann et al. (2013b) summarize that even under modest radiative forcing (RCP2.6), projected increases in the minimum of TN in winter exceed 3°C on seasonal and regional scales relative to the reference period 1981 – 2000, particularly in Northern high latitudes.

Precipitation: Sillmann et al. (2013b) show projected global land averaged precipitation indices to increase in the 21st century. Comparisons with observations for current and past time periods show that GCMs underestimate observed precipitation magnitudes, although CMIP5 models show an improvement compared to CMIP3 (Sillmann et al. 2013a). This model bias is partially attributed to the spatial scale mismatch between point estimates of precipitation in observations and grid-box-estimates in models suggesting that downscaling techniques (e.g., Bürger et al. 2012) should be considered for regional and local assessments of the projected changes. Sillmann et al. (2013b) evaluate the ratio of extreme precipitation expressed by very wet days to the total wet-day precipitation and find the greatest changes to be projected in high northern and southern latitudes under RCP8.5 and particularly extreme precipitation events to increase in Northern high latitudes. They also find a significant decrease in projected consecutive dry days at Northern high latitudes coinciding with large increases in the heavy

precipitation days index (R10mm) and the maximum 5 day precipitation index (RX5day). The models are shown to generally project a wetter climate in the future with increases in RX5day for all three RCPs (up to 20 – 30% in the Canadian Arctic), but less pronounced in summer than in winter. They also point out that extreme precipitation increases proportionally faster than total wet-day precipitation.

Attribution to human influence: Gillet et al. (2008) find that the observed changes in Arctic temperatures are not consistent with internal climate variability or natural climate drivers alone, and are directly attributable to human influence. Min et al. (2011) compare observed and multimodel simulated changes in extreme precipitation over the latter half of the twentieth century and show that human-induced increases in greenhouse gases have contributed to the observed intensification of heavy precipitation events found over approximately two-thirds of data-covered parts of Northern Hemisphere land areas. Coumou and Rahmsdorf (2012) argue that for some types of extremes (heatwaves, precipitation extremes), there is now strong evidence linking specific events or an increase in their numbers to the human influence on climate. For other types of extreme, such as storms, the available evidence is less conclusive, but based on observed trends and basic physical concepts it is nevertheless plausible to expect an increase.

Uncertainties: Multimodel ensemble simulations have been shown to outperform individual models and are also expected to provide more robust estimates of future changes and model related uncertainties (e.g., Gleckler et al. 2008; Sillmann et al. 2013a). The model spread and variations in response to the different SRES and RCP scenarios are indicative of uncertainties associated with natural internal variability of the climate system, structural, and parametric uncertainty as embodied by the range of climate models considered, and future forcing uncertainty (Sillmann et al. 2013b).

3.3 PHYSICAL OCEANOGRAPHY

The IPCC (2007) already states that there is now higher confidence in projected patterns of warming and other regional-scale features, including changes in wind patterns, precipitation and some aspects of extremes and of ice. With the projected warming being amplified in the Arctic (e.g. Frierson 2006, Meehl et al. 2007), amplified climate change effects can also be expected for Arctic Ocean properties. The most frequently discussed is the loss of sea ice, which as well as increased precipitation will affect the freshwater input into the Arctic Ocean, but also causes changes in radiative, momentum, and material transfers. These in turn will affect upper ocean water properties, circulation patterns, and waves.

This section will analyze model results with respect to projections of physical ocean variables keeping in mind the limitations of the models. Loder and van der Baaren (2013) in their AR5-ESM analysis of the North West Atlantic find lower agreement between the model and observed means and annual cycles of surface ocean temperatures and salinities than for air temperature, particularly for salinity. They find large-scale T_s and S_s structures of the NW Atlantic's subpolar and subtropical gyres are approximately reproduced in the models, but find significant differences in the location and structure of the boundary between the gyres as well as in the regional variability. They conclude that the comparison of the model and observed distributions and annual cycles of key variables indicates that there are substantial differences in the

representation of coupled ice-ocean variability, and in the detailed temporal and spatial patterns among the models and between models and observations. They also point out issues in the models' representation of detailed spatial and temporal patterns. They conclude that the discrepancies between the historical simulations and observations for a number of key variables in the Atlantic LAB indicate that the present generation of AOGCMs continues to have problems with resolving important features (e.g. sea ice, ocean gyres, Arctic outflows, annual cycles) of the coupled atmosphere-ice-ocean system in the Arctic and NW Atlantic.

3.3.1. Freshwater input

Beaufort Sea: Long and Perrie (2013) explore how fresh water content and sea surface height in the Beaufort Sea might be modified under warming-induced conditions due to climate change. They performed simulations from 1970 to 2069 with a coupled ice-ocean model (CIOM) implemented for the Arctic Ocean. The surface fields to drive CIOM were provided by the Canadian Regional Climate Model (CRCM), in turn driven by the third-generation Canadian global climate model (CGCM3) outputs following the SRES A1B scenario. The simulated sea ice concentration in the entire Arctic and the fresh water content in the Beaufort Sea are shown to have patterns consistent with those seen in observations and reanalysis data. In terms of the projected changes, the CIOM simulations suggest an 11% decrease per decade in ice volume, and the Arctic Ocean to become largely ice free in the summers by 2069. Moreover, due to increases in melting of sea ice and Ekman transport, there is an increasing trend in fresh water content (FWC) and sea surface height (SSH) in the Beaufort Sea. The projected increase is about 2.5 m for FWC and 6 cm for SSH from 1979 to 2069. The simulations also suggest that maximum increases in the FWC and SSH would occur near the center of the Beaufort Gyre, where FWC and SSH are the maximum.

Baffin Bay: Rignot et al. (2011) identified an acceleration in the rate of Greenland glacier discharge of 0.76 mSv/y between 1992 and 2010. The extrapolation of a mass loss acceleration rate based on only an 18 year record to predict glacial input 4 decades in the future is crude, but there is evidence to indicate that strong warming in southern Greenland over the last 2 decades and the associated acceleration in glacial melt rate is a response to general Northern Hemispheric warming associated with global warming rather than multidecadal natural variability (Hanna et al. 2008). Continued acceleration of mass loss might therefore be expected. Using the Greenland ice sheet mass loss acceleration rate of Rignot et al. (2011) and the Greenland drainage distribution defined by Bamber et al. (2012), an increase in Greenland meteoric water input into Baffin Bay from a present level of about 7.5 mSv to 26 mSv by 2050 is calculated. A similar acceleration in the mass loss rate of Canadian glaciers would add an additional 3 mSv. The increase in the freshwater input from the Greenland ice sheet and Canadian glaciers may be offset by reduced freshwater input through the CAA if the observed trend there (Section 2.2.5, Figure 35) proves to be more than decadal variability. Lenaerts et al. (2013) evaluate model projections until 2100 and show that even with a moderate climate warming scenario (RCP4.5) enhanced meltwater runoff from CAA glaciers is not sufficiently compensated by increased snowfall. Extrapolation of these results toward an AR5 multimodel ensemble results in sustained 21st century CAA glacier mass loss. The trend in increased meteoric input is a climate change-induced impact that can more confidently be expected to continue, albeit with large uncertainty in the magnitude of the increase. Based on the estimate of increased ice sheet input outlined above (22 mSv), and an assumption that this new freshwater will be transported within the

cyclonic coastal circulation pattern of Baffin Bay/Davis Strait, Hamilton and Wu (2013) calculate a freshening in the upper layer (top 150 m) of a broad (150 km wide) Baffin Island Current at Davis Strait of 0.4 ppt by 2050, assuming other freshwater inputs remain constant. There is high uncertainty in this estimate of the magnitude of the freshening, since future global warming-related changes in precipitation, albedo, cloud cover, and other factors on glacial mass loss are difficult to predict (Rignot et al. 2011). Nonetheless, there is a strong likelihood that freshwater input into Baffin Bay/Davis Strait from glacial mass loss will continue to increase as a result of anthropogenic climate change with potential consequences on upper ocean salinity and stratification in Baffin Bay, and freshwater export into the Labrador Sea via the Baffin Island Current.

Hudson Bay: Global climate model simulations consistently project increasing rates of pan-Arctic river discharge for the 21st century (e.g. Arnell 2005; Milly et al. 2005; Holland et al. 2007). Hudson Bay is no exception to the Arctic trend. ESMs predict an increase in river discharge by 7.5% (RCP4.5) and by 9.6% (RCP8.5) by 2065 (Chassé et al. 2013). Moreover, all the models show an earlier occurrence of the maximum runoff in the future at a rate of -12.6 day/century for RCP4.5 and -10.3 day/century for RCP8.5 (Chassé et al. 2013).

3.3.2 Water properties and Stratification

Beaufort Sea, Canadian Polar Shelf Temperature and Salinity: The AR5-ESMs simulate a warmer and fresher surface ocean for the Beaufort Sea (BS) and the Canadian Polar Shelf (CPS) under the RCP8.5 and RCP4.5 scenarios. Model sensitivity to the scenario forcing is regionally variable and is more evident in the CPS than the BS (Figure 71).

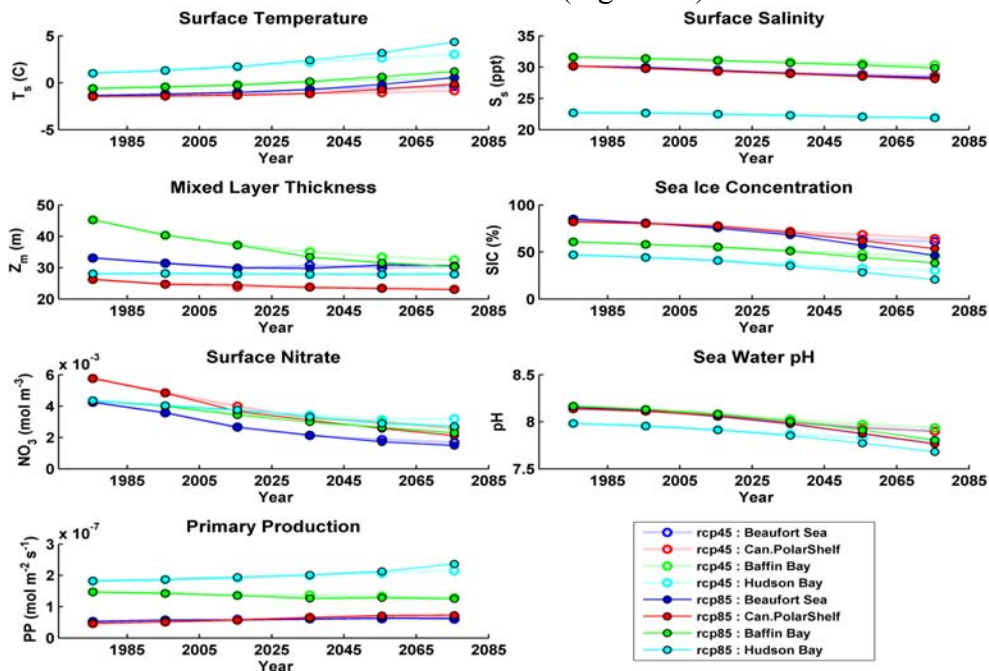
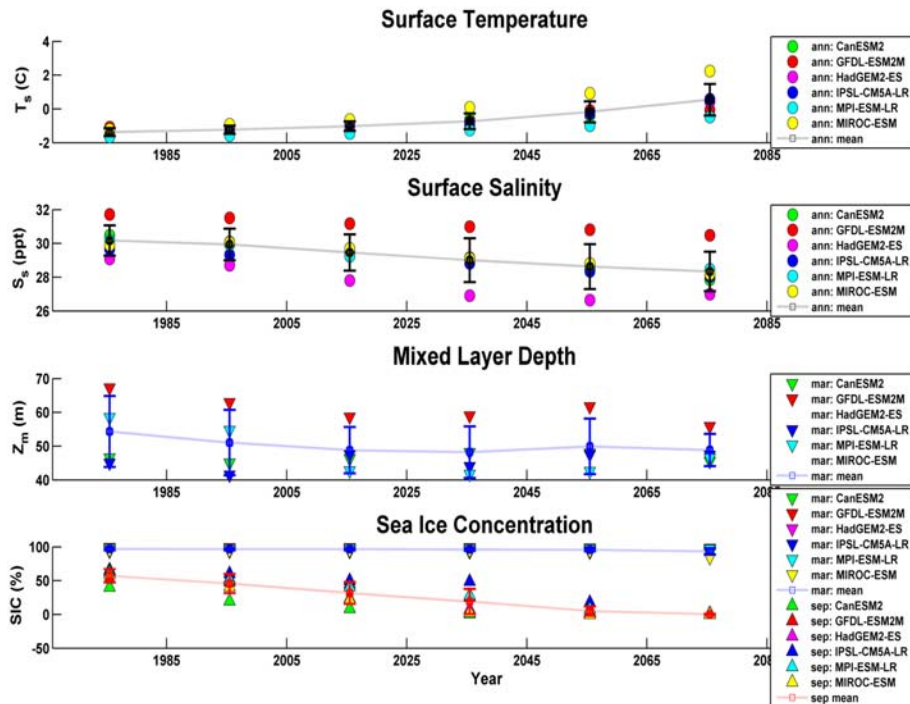


Figure 71: Bidecadally, annually and spatially averaged, AR5-ESM multimodel mean values for RCP4.5 (thin line) and RCP8.5 (thick line) for the Canadian Arctic subbasins: Beaufort Sea, Canadian Polar Shelf, Baffin Bay and Hudson Bay. Variables shown are: sea surface temperature (T_s) and salinity (S_s), maximum mixed layer depth (Z_m), sea ice concentration, (SIC) surface nitrate (NO_3), pH, and primary production (PP).

Beaufort Sea



Canadian Polar Shelf

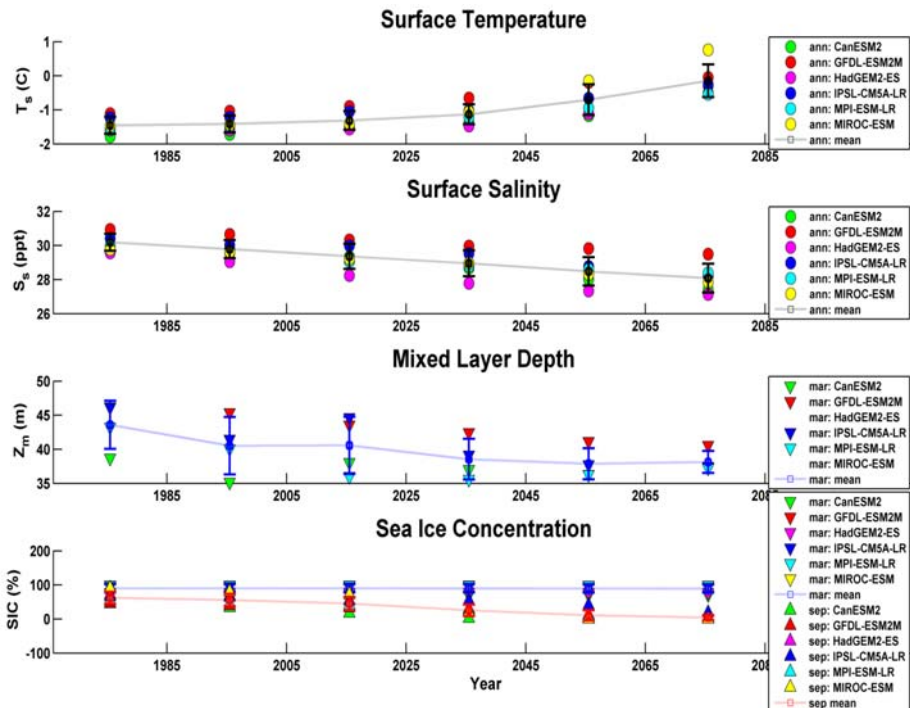


Figure 72: Bidecadally averaged, individual model results and multimodel means for RCP8.5: spatially averaged values for the Beaufort Sea (upper panel) and Canadian Polar Shelf (lower panel). Variables include: sea surface temperature (T_s) and salinity (S_s), maximum mixed layer depth (Z_m) and sea ice concentration (SIC). Averages are for annual means (ann, circles), March (mar, downward pointing triangles) or September (sep, upward pointing triangles). Solid lines are multimodel means, error bars are overlotted.

The projected sixty year change in sea surface temperature (T_s) and salinity (S_s) is calculated as the difference between the bidecadal means of 1986 - 2005 and 2046 - 2065. For the RCP8.5 scenario, the sixty year change in T_s for the BS and CPS is 1.05 and 0.70°C (0.21 and 0.14 °C/decade) respectively, which is an increase from the -1.23 and 1.41°C historical means (1985 - 2005). The standard deviation of the multimodel mean increases in time, indicating less agreement between the models in the future. For example, the T_s standard deviation increases from $\pm 0.24^\circ\text{C}$ (1966 - 1985) to $\pm 0.63^\circ\text{C}$ (2046 - 2065) in the BS and similarly in the CPS and for S_s from ± 0.94 ppt (1966 - 1985) to ± 1.33 ppt (2046 - 2065) in the BS. The projected future sixty year change for sea surface salinity (S_s) is -1.3 ppt (-0.26 ppt/decade) for both the BS and CPS, decreasing from a mean of 29.9 and 29.8 ppt (1986 - 2005). As in T_s , the model agreement in S_s decreases over time (see APPENDIX 1: Table 8).

Of the AR5-ESMs (RCP8.5), MIROC-ESM has the highest T_s and MPI-ESM-LR has the lowest T_s for all bidecades for the BS. The remaining models cluster around the multimodel mean. The CPS has similarly distributed inter-model differences, except GFDL-ESM2 has the highest T_s before 2045. For the BS and CPS, GFDL-ESM2 has consistently the highest S_s and HadGEM2-ES the lowest S_s (Figure 72). All models project ocean surface warming and freshening in the BS and CPS over the next sixty years.

Spatially, the BS warms in bands ranging from the biggest change ($\sim 1.6^\circ\text{C}$) along the coast out to 0.4°C at the northern edge of the subbasin over the next sixty years. The T_s change in the CPS is less ($0.4 - 0.8^\circ\text{C}$) and is more uniform than in BS (Figure 73). The models' standard deviation is highest along the BS coast and in the eastern CPS ($\pm 0.6 - 0.8^\circ\text{C}$). The CPS region is not well resolved by the models (see Section 3.1) and the inclusion of multimodel means based on only 1 or 2 models confounds the interpretation of the changes.

The spatial pattern of S_s in the BS also shows bands of change which continue into the CPS. In the BS, freshening occurs with -0.6 ppt change at the coast and -1.8 ppt to the north, while the CPS freshens from -0.4 to -1.0 ppt, except in the northwest of the CPS, where freshening is -1.6 ppt. The northern component of the simulated freshening in the BS and CPS is part of a larger pattern of freshening in the central Arctic. The center of the BS has the least model agreement (± 1.0 stdev).

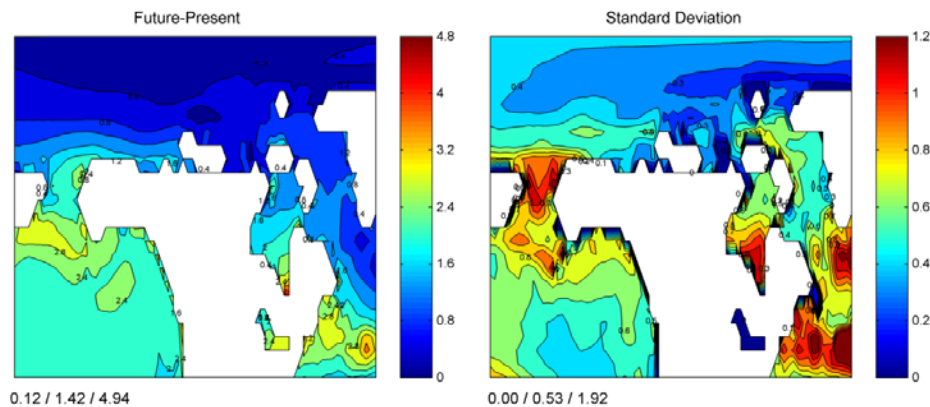


Figure 73a: Multimodel mean differences between the historical bidecadal mean (1986 – 2005) and the future (2046 - 2065) bidecadal mean (left) and standard deviation for all six AR5-ESMs and RCP8.5: Annual surface temperature ($^\circ\text{C}$).

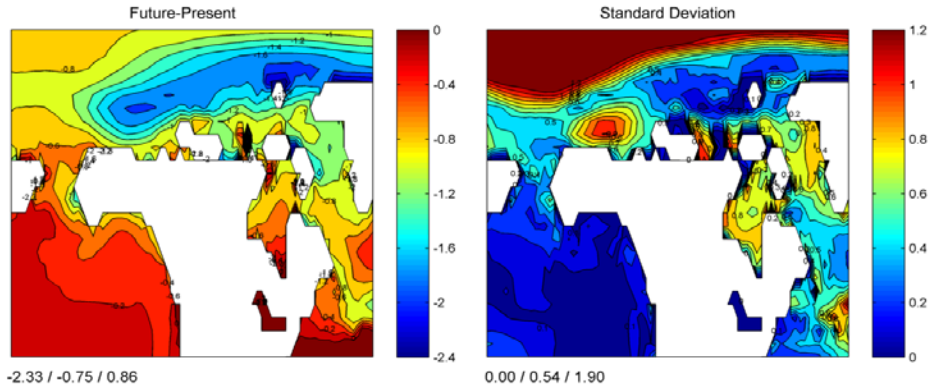


Figure 73b: As a) for annual surface salinity, S_s (ppt).

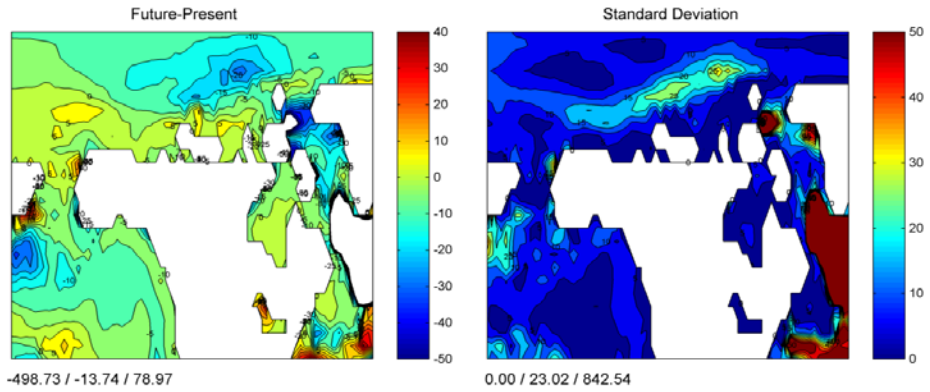


Figure 73c: As a) for March mixed layer depth, Z_m (m).

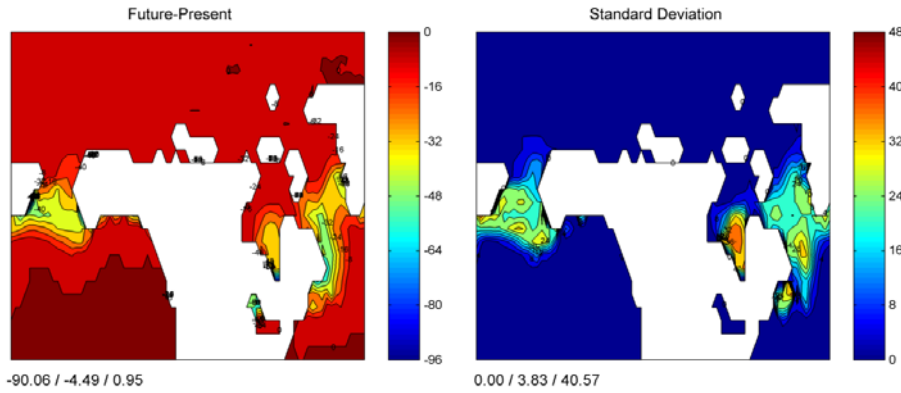


Figure 73d: As a) for March sea ice concentration, (SIC).

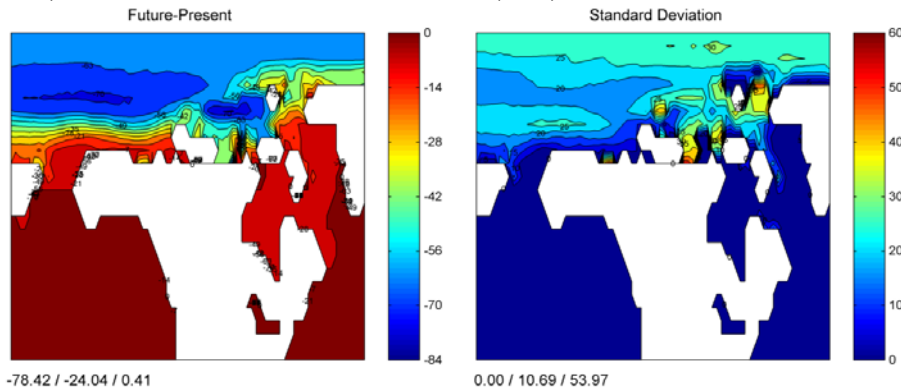


Figure 73e: As a) for September sea ice concentration, SIC.

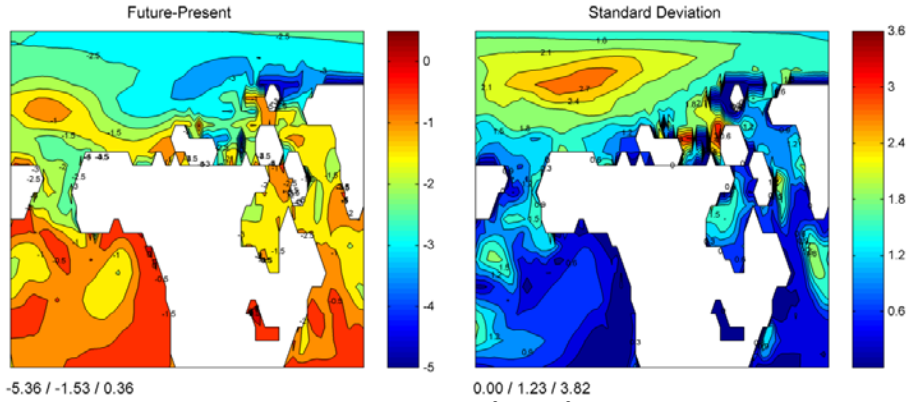


Figure 73f: As a) for annual surface nitrate ($\text{mol m}^{-3} \times 10^3$).

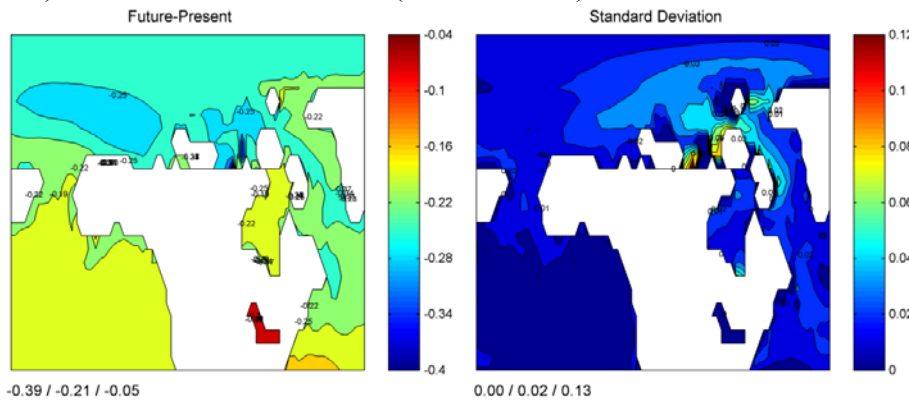


Figure 73g: As a) for annual pH.

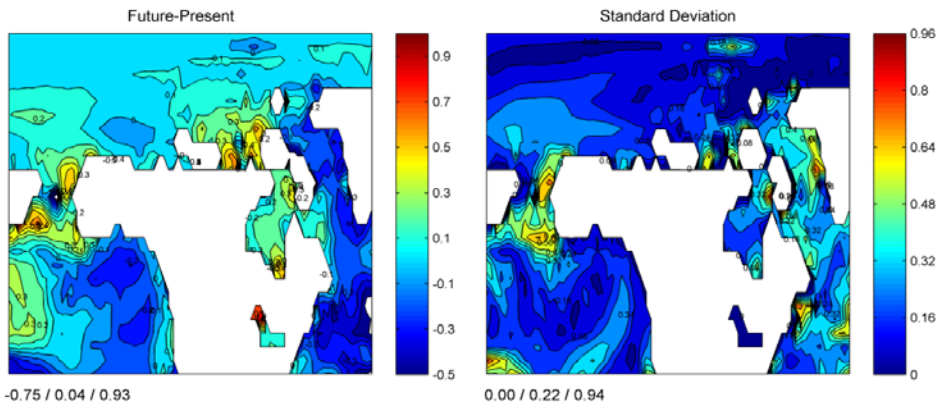


Figure 73h: As a) for annual PP.

Figure 73: AR5-ESM multimodel differences (left panel) and standard deviation (right panel) for T_s , S_s , Z_m , SIC, NO_3 , pH, PP under RCP8.5 scenario forcing for 2045 - 2065 minus 1986 - 2005.

Black lines and triangles in Figure 74 show profiles from the surface down to 350 m of observed T and S for the summer of 2005 in comparison with modelled bidecadally averaged annual mean profiles for 1986 - 2005 and 2066 - 2085 and multimodel mean averages for all bidecades at 75°N, 140°W in the Canada Basin (BS domain). The snapshot character of the observations severely limits the comparison (Observations are available for one month in one year, while vertical profiles of ESM results are only available as annual means). While the simulated profiles are generally in a similar range, the observed profiles show a layered near surface

structure in T which is not seen in the bidecadal model average. The observations show, below the surface water, a layer of advected Summer Pacific Water and below the deep halocline (100 – 200 m) Pacific Winter Water (PWW). Below the PWW layer is the Canada Basin intermediate layer which is influenced by Atlantic water.

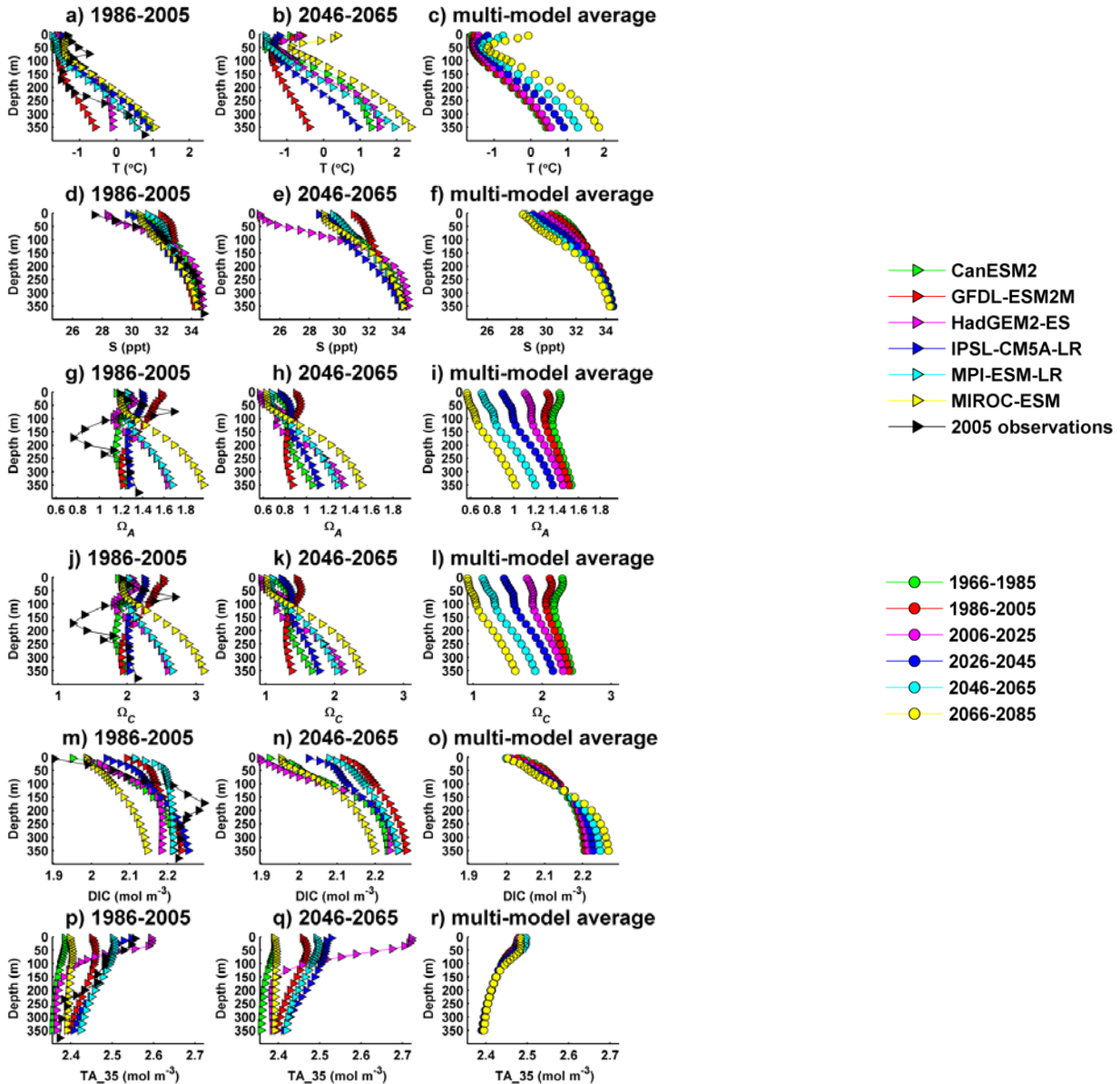


Figure 74: Simulated and observed ocean temperature (T), salinity (S), Ω_C , Ω_A , DIC, and TA₃₅ profiles from AR5-ESMs at 140°W, 75°N for 1986 - 2005 (left panel), simulated profiles for 2046 – 2065 for all models (middle panel), and multimodel mean change as indicated in the legend (right panel).

The AR5-ESMs simulate about 1°C warming over sixty years at the surface, minimal cooling at 50 m, and increasingly warmer temperatures down to 350 m (Figure 74, top panel), indicative of warmer Atlantic waters entering the Arctic. Salinity freshens most at the surface in response to ice melt. In both the historical (1986 - 2005) and future (2046 - 2065) bidecades, MIROC-ESM

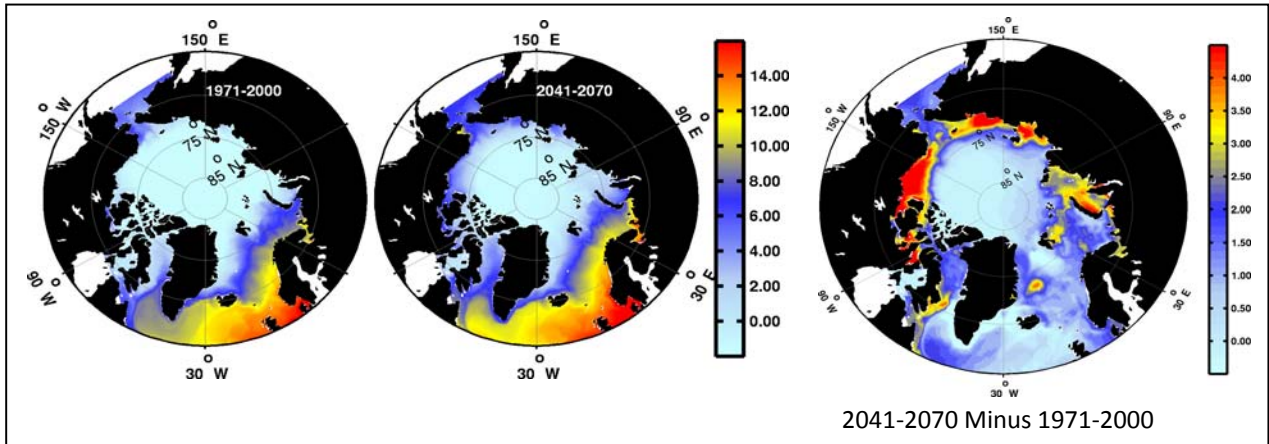
is the warmest throughout the water column and GFDL-ESM2 is the coolest (with the least amount of change). (Note: 1986 - 2005 mean CanESM2 temperature is overplotted by MIROC-ESM's temperature). IPSL-CM5A-LR shifts from nearly the warmest to the second coolest between the historical and future bidecades. HadGEM2-ES is the freshest at the surface and saltiest below 150 m. There is little change in the models distribution between bidecades. The simulated and observed salinity profiles are mostly in agreement. With the exception of the low salinity bias in HadGEM2-ES, the differences between the individual models' representation of the bidecadal means are to a large part retained in the projection runs, e.g. the prominent low salinity and high TA₃₅ signal in the surface ocean of the HadGem2-ES. The multimodel mean shows the continued warming more pronounced at the surface and in the Atlantic influenced intermediate waters and less warming in the Pacific influenced subsurface waters. Freshening is more pronounced in the near surface and Pacific waters, influenced by ice melt and enhanced stratification.

Table 3: NAA_NEMO change in T_s, S_s, SIC and SIT for BS, CPS and BB subbasins.

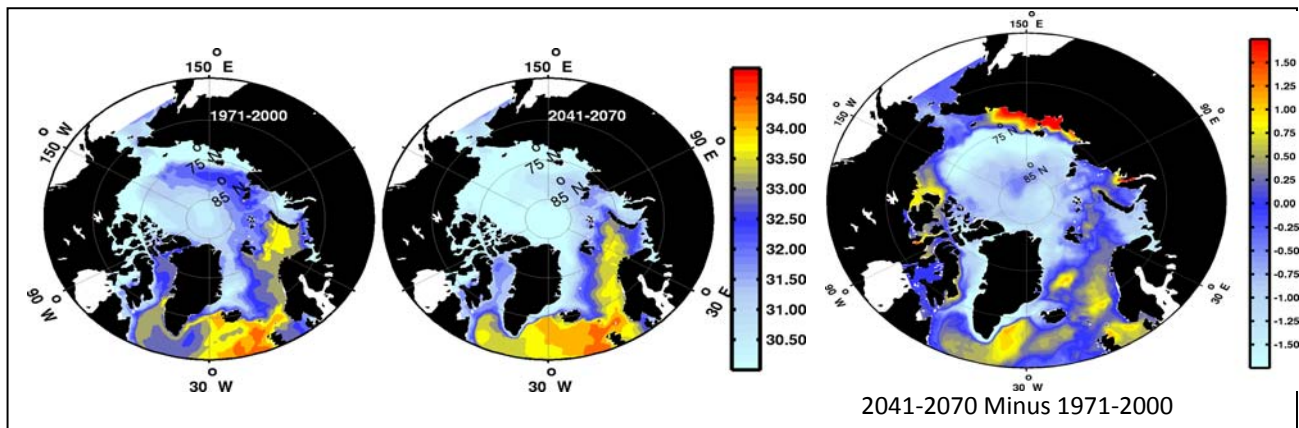
Region	T _s (C)				S _s (ppt)			
	1971-2100	1986-2005	2046-2065	diff	1971-2100	1986-2005	2046-2065	diff
Beaufort Sea	-0.47	-1.42	0.11	1.53	30.57	30.75	30.64	-0.11
CPS	-0.77	-1.23	0.45	1.68	30.72	30.91	30.78	-0.13
Baffin Bay	0.25	-0.24	0.80	1.04	32.17	32.49	31.98	-0.51

Region	SIC				SIT (m)			
	1971-2100	1986-2005	2046-2065	diff	1971-2100	1986-2005	2046-2065	diff
Beaufort Sea	0.62	0.80	0.51	-0.29	0.88	1.32	0.55	-0.77
CPS	0.69	0.76	0.64	-0.12	1.26	1.63	0.97	-0.66
Baffin Bay	0.52	0.61	0.39	-0.22	0.46	0.51	0.39	-0.12

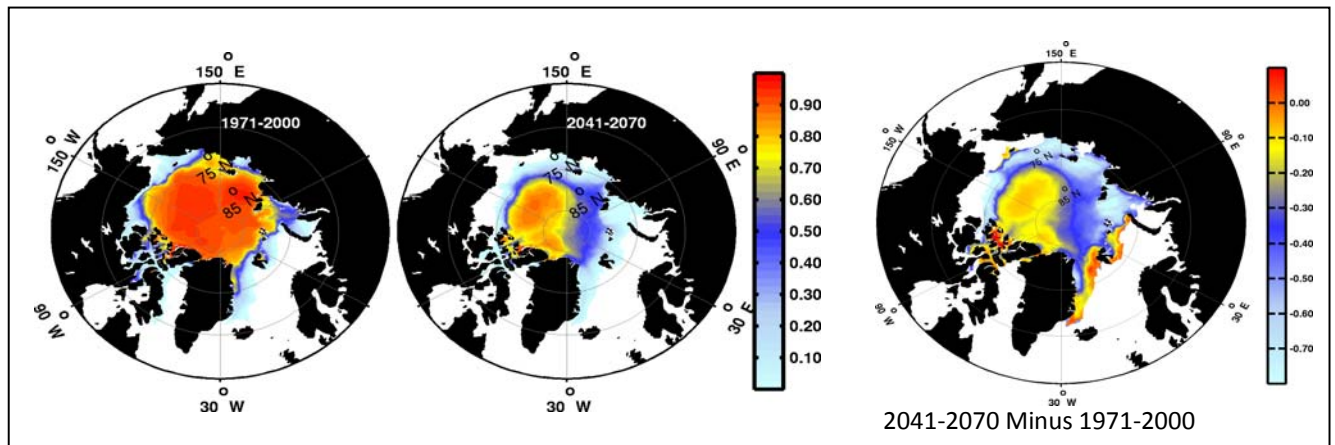
Projections with the higher resolution NAA-NEMO model, forced with global climate model output based on the SRES A1B scenario, show projected T_s and S_s for the BS and CPS similar to the AR5-ESM: T_s increases while S_s decreases. The sixty year change for the BS and CPS in T_s is 1.5°C and 1.7°C respectively, and in salinity is -0.11 and -0.13 ppt. (Table 3). The NAA-NEMO model simulates more warming in the BS and CPS and much less freshening than the AR5-ESM multimodel mean. For the 1986 - 2005 bidecade, the NAA-NEMO CPS is the coldest of the ACCASP subbasins and warms the most in sixty years. NAA-NEMO allows a more detailed view of the projected changes, specifically in the CPS. However, since it is based on a single model realization, the uncertainty is high.



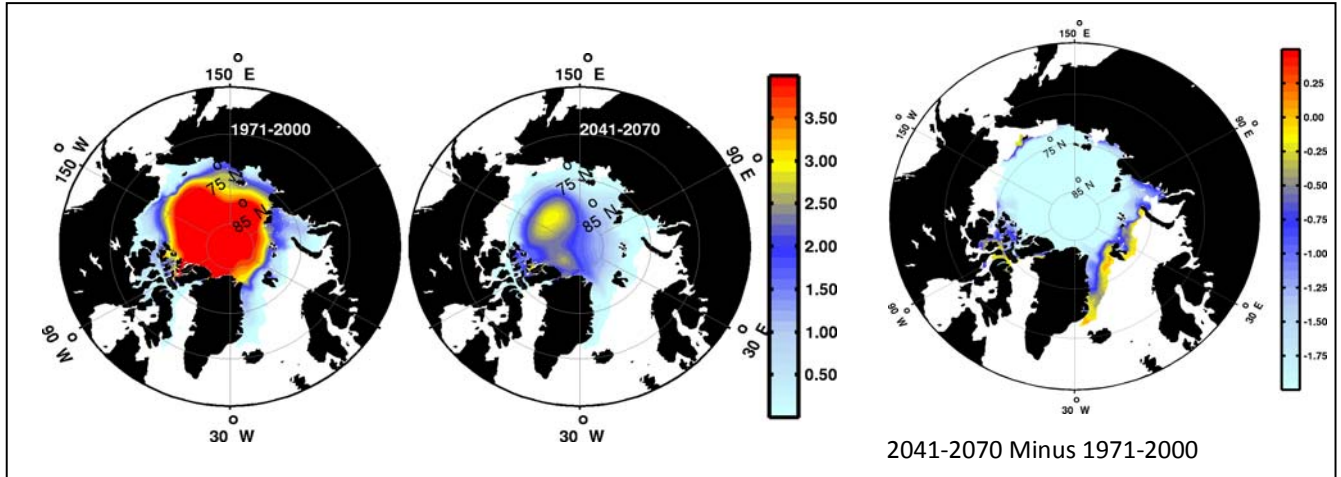
a) September T_s ($^{\circ}\text{C}$).



b) September S_s (ppt).



c) September SIC.

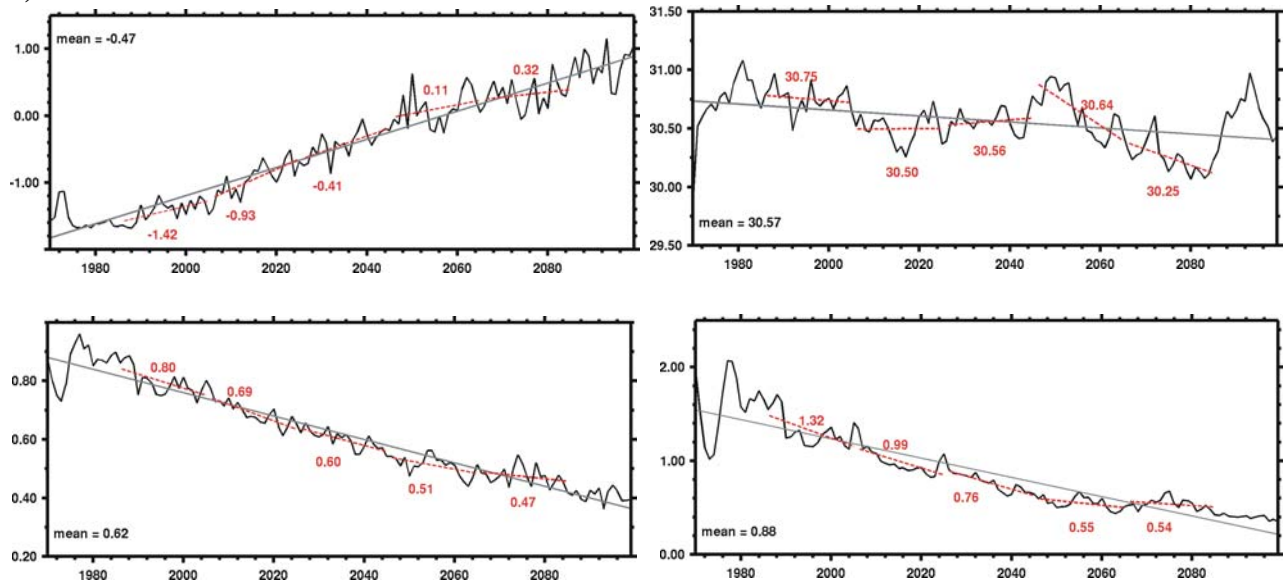


d) September SIT (m).

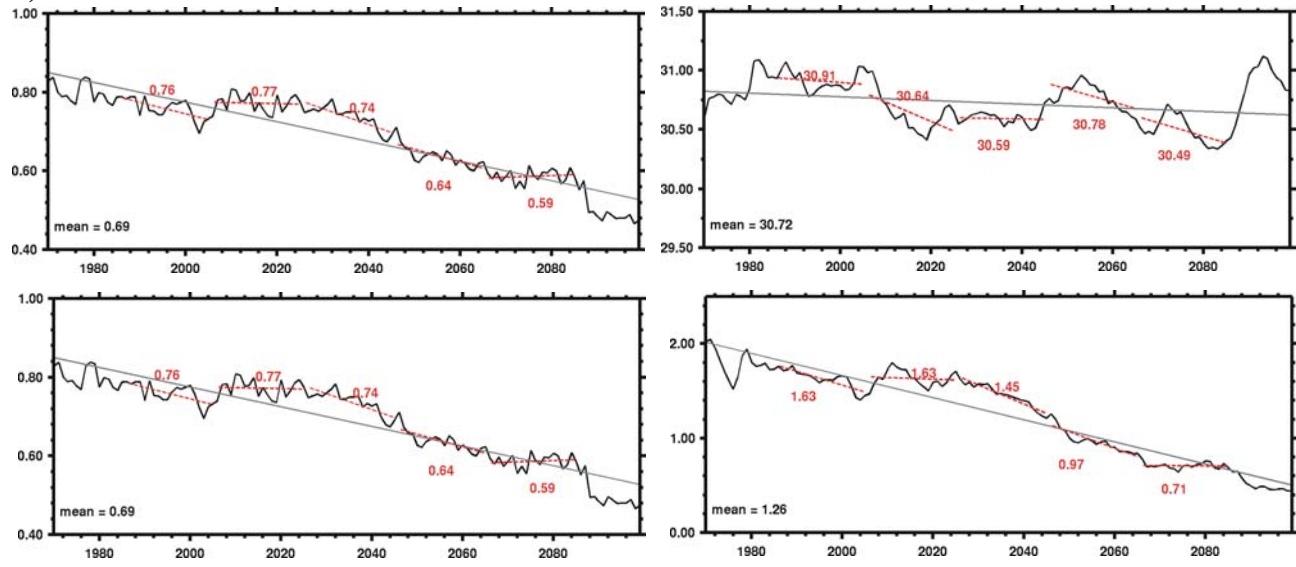
Figure 75: Simulations with the NAA-NEMO model for surface temperature T_s , salinity S_s , sea ice concentration SIC, and thickness SIT. Shown are the historical mean (1971 – 2000) and a projected mean (2041 – 2070) as well as the difference between both time periods on the right hand side.

Spatial plots of sea surface temperature (T_s) and sea surface salinity (S_s) for September (Figure 75a, b) illustrate modeled changes in the Arctic, between the historical period of 1971 - 2000 and future period of 2041 - 2070. The BS and the western CPS warm by 4.0°C , with little change in T_s over the eastern CPS. The western CPS and coastal BS is saltier (0.75 ppt) while the northern BS (central Arctic) and the eastern CPS is fresher (about -1.0 ppt). This spatial pattern with coastal warming, offshore freshening and little change in offshore temperature is simulated for both the NAA-NEMO BS and the AR5-ESM model mean. In comparison, the NAA-NEMO projects that the BB surface ocean warms by $\sim 2.0^\circ\text{C}$ in the north, $\sim 3.0^\circ\text{C}$ in the south, and freshens by ~ 1.0 ppt.

a) BS subbasin



b) CPS subbasin



c) BB subbasin

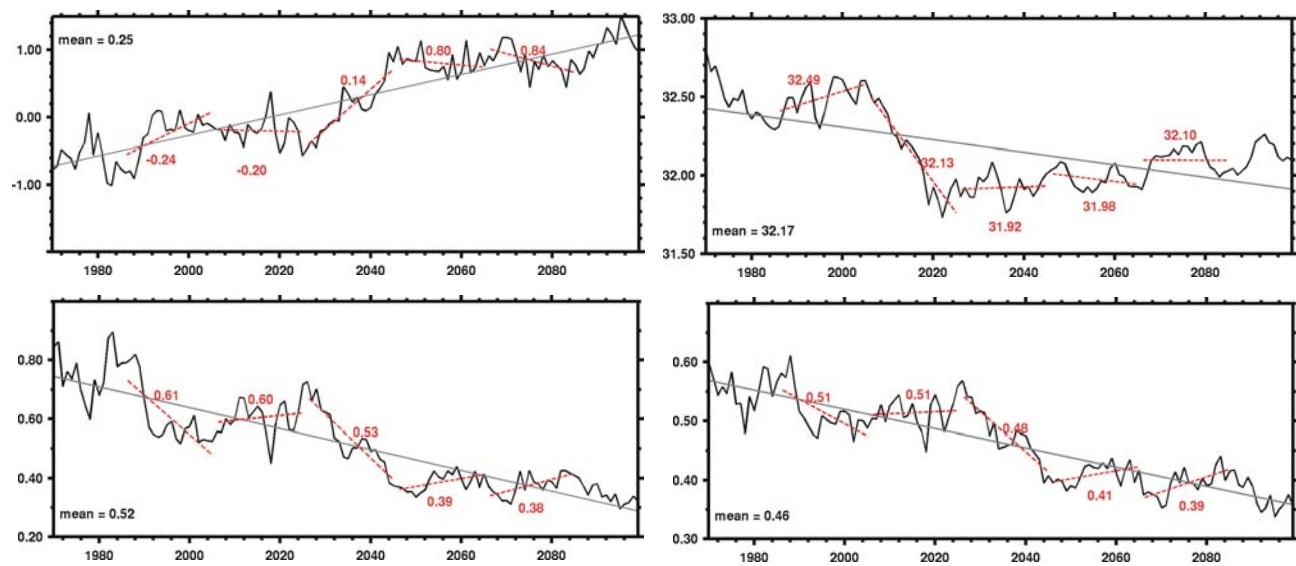


Figure 76: Time series of NAA-NEMO modeled variables averaged over the BS (a), CPS (b) and BB (c) subbasins. Each subfigure shows upper left and right panels: T_s and S_s . Lower left and right panels: SIC and SIT. Bidecadal means are included.

Spatial plots of sea surface temperature (T_s) and sea surface salinity (S_s) for September (Figure 75a, b) illustrate modeled changes in the Arctic, between the historical period of 1971 - 2000 and future period of 2041 - 2070. The BS and the western CPS warm by 4.0°C , with little change in T_s over the eastern CPS. The western CPS and coastal BS is saltier (0.75 ppt) while the northern BS (central Arctic) and the eastern CPS is fresher (about -1.0 ppt). This spatial pattern with coastal warming, offshore freshening and little change in offshore temperature is simulated for both the NAA-NEMO BS and the AR5-ESM model mean. In comparison, the NAA-NEMO projects that the BB surface ocean warms by $\sim 2.0^\circ\text{C}$ in the north, $\sim 3.0^\circ\text{C}$ in the south, and freshens by ~ 1.0 ppt.

For the CPS and BS, the NAA-NEMO changes in T_s over the long term and bidecadal periods are consistently positive, but S_s has bidecades of increase and decrease, with an overall freshening (Figure 76). It needs to be noted that confidence in the decadal scale variability of the model variables is very low.

Beaufort Sea and Canadian Polar Shelf Stratification: As a simplified measure of stratification, the monthly maximum ocean mixed layer depth (Z_m) for AR5-ESMs is evaluated. The Canada Basin has its maximum mixed layer depth in March, hence March Z_m is shown to point out the maximum mixing in the year and will be referred to as Z_m in the following. (Note that Z_m is not available for HadGEM2-ES and MIROC-ESM.) The models simulate a shallowing of the spatially averaged Z_m for the BS region between the 1966 - 1985 and 2006 - 2025 bidecades, with deepening by the 2066 - 2085 bidecade (Figure 73). In the CPS domain, Z_m gradually shallows from 1966 to 2086.

The future sixty year change in the maximum mixed layer depth in March (Z_m) is calculated as the difference between 1986 - 2005 and 2046 - 2065 (Appendix 1: Table 8). For the BS and CPS, the change in Z_m is -1 m and -3 m. For the BS and CPS, the multimodel mean standard deviation consistently decreases in time.

The respective individual model means for the RCP8.5 scenario are shown in Figure 72. For the BS, GFDL has the deepest Z_m , while the model with the shallowest Z_m switches from IPSL-CM5A-LR to MPI-ESM-LR after 2005. For the CPS, GFDL-ESM2 has the overall deepest Z_m , and CanESM2 has the shallowest Z_m until 2005 when MPI-ESM-LR's Z_m is shallower until the end of the run. The regional distribution of the sixty year change in March Z_m with model standard deviation for the RCP8.5 scenario is shown in Figure 73. It is shown that the shallowing of Z_m is not uniform across the Arctic, and Z_m in fact increases in several coastal areas (e.g. Beaufort Sea) and shelf seas (e.g. Chukchi Sea) (Steiner et al., unpublished data). The BS and CPS show deepening (0 - 5 m) nearer the coast and shallowing (10 - 15 m) offshore at the northern edge of the BS and CPS subbasins. The model standard deviation is highest in the area around the CPS northern shelf edge and close to the coast and in the Canadian Basin. This suggests increased uncertainty with respect to location of the front between increased and decreased mixing, likely linked to the model's representation of the atmospheric circulation pattern, the open water distribution, and the representation of shelves in the model.

The model distribution shifts between the historical and future (2005) time periods, indicating different model sensitivities to the scenario forcing with respect to surface layer mixing, which are likely linked to the model's projected timing of sea ice retreat.

Baffin Bay: The following two sections contain summarized results from Lavoie et al. (2013). They use a slightly different technique and regions for their analysis than what has been presented above. This provides additional information, however does not allow for a direct intercomparison. With respect to the historical conditions (1960 - 2005), the World Ocean Atlas (WOA09, http://www.nodc.noaa.gov/OC5/WOA09/pr_woa09.html) states that the annual average sea surface temperature (T_s) in the Baffin Bay varies between -1°C and 1.5°C with slightly higher temperature in the eastern area due to inflow from the Labrador Sea. Among the 5 AR5-ESMs, IPSL-CM5A-LR gives the better representation of these climatic conditions in

Baffin Bay. CanESM2 and GFDL-ESM2M T_s are a little cool while MPI-ESM-LR is too warm along the coast of Greenland. HadGEM2-ES is too cold over the entire region.

With the emission scenarios RCP4.5 and RCP8.5, the future projections (2012 - 2062) from all 5 AR5-ESMs project an increase of T_s in the Baffin Bay. The ESMs show an increase of $0.12 \pm 0.07^\circ\text{C}$ per decade for RCP4.5 and $0.21 \pm 0.09^\circ\text{C}$ per decade for RCP8.5. The T_s increase is spread rather uniformly, with the same amount of degrees gained almost everywhere within the bay.

For the BB, the NAA-NEMO simulates an overall warming and freshening. The sixty year T_s increase is 1.0°C ($0.21^\circ\text{C}/\text{decade}$) and the S_s decrease is -0.51 ppt (-0.1 ppt/decade). The change in T_s is similar to the AR5-ESMs' projection, but the change in S_s is only half of the AR5-ESMs (-1.10 ppt). Compared to the BS and CPS, the BB is the warmest subbasin. In 1986 - 2005 all the subbasins have mean temperatures below zero, but by 2045 - 2065, all are above zero. BB is saltier than the BS and CPS during 1986-2005 and it freshens the most by 2045-2065 (Table 3, Figure 75).

Average annual sea surface salinities given by WOA09 for the period of 1960 - 2005 are between 31 and 34 with saltier water in the southeast and fresher water in the southwest of the bay. CanESM2 and GFDL-ESM2M have a good representation of the average sea surface salinities in the bay but do not represent the east-west gradient in the south of the bay. On the other hand, MPI-ESM-LR and HadGEM2-ES have a good representation of the east-west salinity gradient but the salinity is too low on the east side of the bay.

Future projections in Baffin Bay show a decrease in S_s for all ESMs. The multimodel ensemble mean trends are -0.12 ± 0.12 and -0.19 ± 0.12 ppt per decade for RCP4.5 and RCP8.5 respectively. However, the regional pattern of the trends is not consistent from one ESM to another, suggesting increased uncertainty.

Baffin Bay is characterised by a strong pycnocline near the surface (10 - 30 m) in summer that deepens in winter (80 - 100 m, Melling et al. 2001). The simulated Z_m varies between 20 and 50 m (areal average). Because of the decreasing surface salinity and increasing surface temperature, Z_m decreases over the historical period (1960 - 2005). The multimodel ensemble mean trend of Z_m is -1.1 ± 0.8 m per decade. For the future, the ESMs project a negative trend of the mixed layer depth in Baffin Bay. The multimodel ensemble mean trends for Z_m (4 ESMs available) are -0.7 ± 0.6 and -1.0 ± 0.6 m per decade for RCP4.5 and RCP8.5 respectively.

Hudson Bay: The analysis by Lavoie et al. (2013) shows: in Hudson Bay, the annual average T_s given by the WOA09 is between $4 - 5^\circ\text{C}$ in the northwestern area to 0.5°C in the southwest. As for Baffin Bay, T_s is represented best in IPSL-CM5A-LR. CanESM2, GFDL-ESM2M and MPI-ESM-LR surface temperatures are in the observed range but are too cool in the center and in the North of the Bay, while T_s in HadGEM2-ES is too cold over the entire Bay. RCP4.5 and RCP8.5 projections (2012 - 2062) from all 5 AR5-ESMs show an increase of T_s in Hudson Bay. The multimodel ensemble mean T_s trend is $0.22 \pm 0.08^\circ\text{C}$ per decade for RCP4.5 and $0.31 \pm 0.07^\circ\text{C}$ per decade for RCP8.5 and shows low spatial variability.

WOA09 average annual sea surface salinities for the period of 1960 - 2005 are around 27 with fresher water in James Bay. CanESM2, IPSL-CM5A-LR and MPI-ESM-LR have a good representation of these climatic conditions while GFDL-ESM2M and HadGEM2-ES sea surface salinities are too low. Future projections (2012 - 2062) do not show significant trends of S_s . With the RCP4.5 emission scenario, three of the ESMs predict an increase in S_s (GFDL-ESM2M, MPI-ESM-LR and HadGEM2-ES) while two predict a decrease (CanESM2 and IPSL-CM5A-LR). With the RCP8.5 emission scenario, only IPSL-CM5A-LR predicts an increase of S_s . The multimodel ensemble mean trends are -0.10 ± 0.19 and -0.15 ± 0.18 ppt per decade for RCP4.5 and 8.5 respectively.

Historically (1960 - 2005), the Hudson Bay is characterised by an important vertical stratification. During summer, there is a strong pycnocline at 15 to 25 m that prevents vertical mixing between surface and deep waters. In the winter, salt rejection from sea ice formation tends to reduce stratification and mixing can reach 90 m in the central part of the bay (Ferland et al. 2011). With respect to model representation of stratification in Hudson Bay, GFDL-ESM2M seems to have a better representation of the mixed layer depth varying between 18 and 50 m on average (over the bay) and with greater mixed layer depths in the central part of the Hudson Bay. MPI and CanESM2 mixed layer depths are too shallow. There are no obvious trends over the historical period. The multimodel ensemble mean trend of Z_m is -3.8 ± 6.7 m per decade. There is no clear trend of Z_m in the future (2012 - 2062) in the Hudson Bay. CanESM2 simulates negative trends for Z_m (-0.15 and -0.42 m per decade for RCP45 and RCP85 respectively). GFDL-ESM2M and MPI-ESM-LR project positive trends (0.17 m per decade on average) and IPSL-CM5A-LR shows a very small trend for Z_m .

3.3.3 Sea Level Change

James et al. (2011) estimate the range of sea-level change expected in the next 90 years (2010 to 2100) for five communities in Nunavut (Kugluktuk and Cambridge Bay on the Canadian Polar Shelf, Whale Cove and Arviat in the Hudson Bay and Iqaluit in Davis Strait), derived from an assessment of published estimates of projected global sea-level change and an evaluation of vertical land motion. James et al. (2011) base their community projections on an assessment of the likely amount of global sea-level change spanning from 28 cm to 115 cm by the year 2100 (a range of 87 cm). They include spatial uniformities in the distribution of sea-level change from changing glaciers and ice caps. The net effect is that the range of projected sea-level change at each community is substantially less than the amount that would have been determined if meltwater redistribution had been assumed to be uniform. They find that some of the community sea-level projections are notable for significant sea-level fall due to land uplift, which is occurring due to glacial isostatic adjustment (e.g. Mazzotti et al. 2011). The rising land ameliorates the effects of global sea-level rise, especially for Arviat and Whale Cove, which are rising the fastest (Projected absolute sea level changes are between -70 and +25 cm for Arviat and -75 and +20 cm for Whale Cove). Respective ranges are -10 to +50 cm for Kugluktuk, -35 to +50 cm for Cambridge Bay and 0 to 70 cm for Iqaluit. These sea-level change projections include the effects of uncertainty in vertical land motion, which extends the range of projections significantly, although more than half of the range (uncertainty) in the community sea-level projections is due to the global sea-level projections. James et al. (2011) point out that an additional unquantified, but potentially large, source of error arises from the assumptions used in assessing the spatially variable meltwater redistribution. They conclude that significant progress

in reducing the current large range of sea-level projections could be realized by improving observations of vertical land motion and from carrying out an updated assessment of the spatially variable redistribution of meltwater from Arctic ice caps and the Greenland ice sheet.

3.3.4 Sea Ice Extent, Thickness and freeze/break-up

Climate models project a rapid retreat in sea ice cover since at least 1979 (e.g., Stroeve et al. 2005; Holland et al. 2006; Lemke et al. 2007; Stroeve et al. 2012a) as well as a shift from multi-year ice to thinner seasonal ice, suggesting a continuation of the trends already being observed (e.g., Maslanik et al. 2007; Giles et al. 2008; Kwok et al. 2009; Stroeve et al. 2012b). These changes are expected to have an important impact on the ocean circulation (Lemke et al. 2007). Models also suggest a loosening of the ice pack (Zhang et al. 2012) associated with the observed changes in ice conditions. Rampal et al. (2009) find an increase in sea ice mean speed and deformation rate suggesting an increase in the number of cracks and small leads, affecting the exchange of momentum, heat and gases. Stroeve et al. (2012) find that while CMIP5 models better capture the observed decline in Arctic sea ice than earlier models (Stroeve et al. 2005), the models exhibit a stronger seasonal cycle in both sea ice extent and volume and the inter-model scatter remains large, particularly in summer. It is also noted that the spatial pattern of ice thickness is not simulated well by the majority of models (Maslowski et al. 2012; Stroeve et al. 2012).

Beaufort Sea and Canadian Polar Shelf: The AR5-ESMs project a loss of annual sea ice concentration for all of the Canadian Arctic subbasins (BS, CPS, BB, and HB). Of the four subbasins, BS and CPS have the higher ice concentrations and lose ice cover at a faster rate (Table 4). The difference in forcing scenarios RCP4.5 and RCP8.5 is evident for SIC in all subbasins, where the change is amplified in the RCP8.5 case, especially after 2045 and in the BS (Figure 71).

The AR5-ESM multimodel mean for March (representative for the winter maximum) projects little change in ice cover for BS and CPS: the sixty year change (2046 - 2085 minus 1986 - 2005) is less than -0.9%. However, significant ice loss is simulated in September (representing the summer low). The sixty year change for BS and CPS is -40.6% and -44.6% respectively. The BS and CPS are about half ice covered (45.6 ± 14.0 and 55.5 ± 18 %, respectively) in September during the 1986 - 2005 bidecade, but by the 2046 - 2065 bidecade, the region is dominantly open water (SIC equals 4.9 ± 6.8 % and 10.9 ± 15 %, respectively). Notably, the standard deviation for the multimodel mean is high, indicating poor model agreement for all bidecades (APPENDIX 1: Table 8). However, most of the differences are related to the timing of ice loss, not the ice loss itself.

The distribution of individual model means for March shows that for the BS subbasin, GFDL-ESM2 simulates the most ice cover and CanESM2 simulates the least. All models have at least 90% ice cover for all bidecades, except MIROC-ESM which drops down to 84% during the 2066 - 2085 bidecade. For the CPS region, GFDL-ESM2 has the highest ice cover with most models retaining ice concentrations above 92%. HadGEM2-ES simulate about 77 - 78% and CanESM2 70%. For September, IPSL-CM5A-LR simulates the highest ice cover in the BS and CPS and CanESM2 simulates the lowest at least until 2045 when MIROC-ESM drops to zero ice cover in the CPS (Figure 72 and APPENDIX 1: Table 9).

Table 4: AR5-ESM multimodel mean sea ice concentration (SIC) for 1996 – 2005 and 2046 – 2065 and simulated differences (2046 – 2065 minus 1986 – 2005) for RCP8.5 and RCP4.5 emission scenarios.

Region	SIC (%)				
	RCP8.5			RCP4.5	
	1986-2005	2046-2065	diff	2046-2065	diff
Beaufort Sea	80.8	57.1	-23.8	63.7	-17.2
CPS	80.4	61.9	-18.5	68.4	-11.9
Baffin Bay	58.2	44.3	-13.8	47.9	-10.2
Hudson Bay	44.3	28.4	-15.9	32.8	-11.6

Spatial plots of the sixty year change in September SIC, and the associated model standard deviation for RCP8.5 are shown in Figure 73. The response to the scenario forcing is amplified under the RCP8.5, but the pattern of change is similar to the RCP4.5 case (not shown). The BS (and the Canada Basin) loses about 70% offshore and 7 - 21% near the coast during September. The CPS loss is similar to the coastal BS. Note that the standard deviation ranges from 10 to 30% in the BS and central CPS, with some points in the CPS with 40 - 60%. These values are greater than the change in ice concentration and are likely due to the differences in the projected timing of ice retreat among the models.

The high resolution regional model (NAA-NEMO) projects an ice thickness of 1.3 and 1.6 m for BS and CPS during 1986 - 2005, which decreases by 58% and 40% in sixty years (2045 - 2065 minus 1986 - 2005). Ice concentrations are similar in both subbasins during 1986 - 2005 (~62 - 69%) and 2046 - 2065 (~76 - 80%) with a greater sixty year loss in the BS (-29%) than the CPS (-12%) (Table 3). As the RCP4.5 forcing is more similar to the NAA-NEMO forcing than the RCP8.5, it is included here (Figure 77). The AR5-ESMs' ice cover is similar (for both bidecades represented, and subbasins), but has less loss in the BS (-24%) and loses more ice in the CPS (-18%) for RCP8.5. For RCP4.5, AR5-ESMs simulate much less loss in the BS (17%) and about the same in the CPS as the NAA-NEMO (12%) (Table 4). Some of the differences are likely due to the limited resolution of the CPS and throughflow passages. The NAA-NEMO simulates bidecades of decreasing ice interspersed with periods of (relatively) stable ice cover for the BS and CPS (Figure 76a, b), however, reliability of decadal variability is low and focus should be on the long term signal.

After seventy years (2041 - 2070 minus 1971 - 2000), NAA-NEMO projections for September show no ice left along the coast, about 70% decrease in the northern Beaufort Sea, and about 10% decrease in the central Arctic. Some gains occur in the CPS (Figure 75). In comparison, the AR5-ESMs retain ice along the coast during 2045 - 2065, with a sixty year (2045 - 2065 minus 1986 - 2005) loss of 7 - 21%, and a 70% loss in the northern BS (and the Canada Basin/central Arctic) for RCP8.5 (Figure 73). The sixty year change under RCP4.5 is similar to the RCP8.5 case along the coast, but has a loss of 56% in the northern BS and CPS (Figure 77).

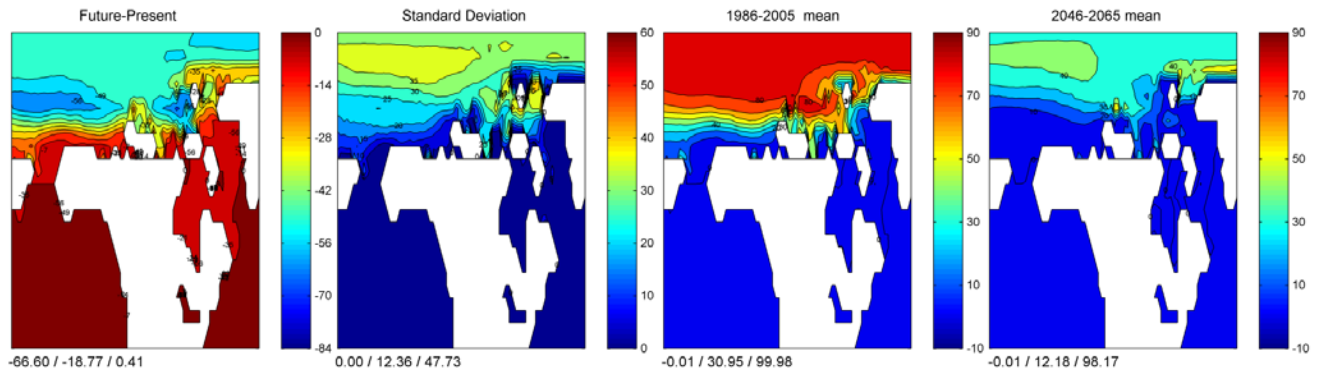


Figure 77: AR5-ESM multimodel averaged plots for September SIC under RCP4.5 scenario forcing. From left to right: difference (2045 - 2065 minus 1986 - 2005), standard deviation, 1986 - 2005 mean, 2045 - 2065 mean.

Hudson and Baffin Bays: Based on comparisons of historical runs with observations, among five AR5-ESMs analyzed (CanESM2, IPSL-CM5A-LR, GFDL-ESM2M, MPI-ESM-LR and HadGEM2-ES), HadGEM2-ES is the one that has the best representation of sea ice concentration in HB, while in BB, two models, GFDL-ESM2M and HadGEM2-ES, have a good representation of the historical SIC (Lavoie et al. 2013).

A diminution of SIT is predicted in all the AR5-ESMs and with both emission scenarios RCP4.5 and RCP8.5. In HB, the maximums SIT of the future climate conditions (2012 - 2062) are 160 cm, 175 cm and 200 cm for MPI-ESM-LR, HadGEM2-ES and IPSL-CM5A-LR respectively, with a corresponding decreasing trend of 12.5, 12 and 10 cm per decade (50 years). In BB, the maximums SIT of the future climate conditions are 150 cm, 175 cm and 250 cm for IPSL-CM5A-LR, MPI-ESM-LR and HadGEM2-ES respectively. The global diminutions are 10, 15, and 14 cm per decade for these ESMs. The HB and BB are almost completely covered by sea ice (SIC of 100 %) from January to April and no changes are projected for this period. However, sea ice is projected to form later in the fall, two weeks (IPSL-CM5A-LR and MPI-ESM-LR) to one month later (HadGEM2-ES). An earlier ice melt is also projected, two weeks (IPSL-CM5A-LR and MPI-ESM-LR) to three weeks earlier (HadGEM2-ES).

The AR5-ESM multimodel mean sixty year change in sea ice concentration (given as reductions in % concentration) for BB in September is -6.4%, much less than for the BS and CPS, and in March is -2.5%. During the 1986 - 2005 bidecade, BB is already seasonally ice free with about 90% ice concentration in March and 8.2% in September (APPENDIX 1: Table 8). In fact all of the ESMs retain very little ice for September in the BB region (Figure 72 and APPENDIX 1: Table 9).

The AR5-ESMs simulate less annual ice cover in the HB region than the other ACCASP subbasins (BS, CPS and BB), and is losing ice cover at a similar rate to the CPS region. The difference between the RCP8.5 and RCP4.5 is evident after 2045, where RCP8.5 projections lose ice faster (Figure 71). The March SIC decreases from ~90% during 1966 - 2025 to 79% by 2046-2065. The sixty year change is -11%. The region is partially ice covered in September, $29.2 \pm 7.1\%$ for 1986 - 2005, with a simulated loss of 26%, resulting in open water conditions within sixty years ($0.7\% \pm 9\%$). Again, model standard deviations are high, indicating

uncertainty, especially with respect to the timing of projected sea ice retreat (APPENDIX 1: Table 9).

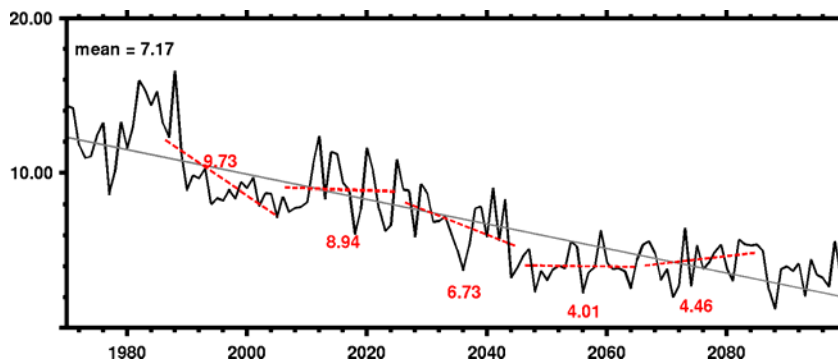


Figure 78: NAA-NEMO annual ice transport through Davis Strait (mSv).

Most of the ice cover lost in March occurs in southern Baffin Bay and Hudson Bay, where the ice cover decreases by 30 - 40%. The northern part of Hudson Bay retains its ice cover, as does most of the Arctic. The areas of ice loss in March coincide with regions of high model standard deviation (Figure 73). For the BB, the higher resolution NAA-NEMO ice thickness is 0.5 m during 1986 - 2005, about half of what is simulated in the BS and CPS. The BB shows a 24% decrease in ice thickness in sixty years (less than the BS and CPS). The NAA-NEMO ice concentrations of 61% for 1986 - 2005 and 39% for 2045 - 2065 are similar to the AR5-ESMs, but the NAA-NEMO projects ice concentrations to decrease by 22% in sixty years compared to 14% and 10% (RCP8.5 and RCP4.5) in the AR5-ESMs (Table 3, Table 4). The NAA-NEMO for BB shows bidecades of increasing or decreasing SIT and SIC, but a decrease overall (Figure 76c).

The NAA-NEMO also projects a net decrease of ice transported through Davis Strait from 1971 to 2100 (Figure 78).

3.4 CHEMICAL OCEANOGRAPHY

3.4.1 Carbon system and acidification

So far, model simulations of biogeochemical changes such as future Arctic ocean acidification are largely limited to global ESMs (e.g., Schneider et al. 2008; Steinacher et al. 2010) which have limited resolution as well as limited skill in the Arctic region mostly because the Arctic is characterized by few and seasonally-biased data and includes vast shelf areas requiring high vertical model resolution. Published results of ESM simulations generally simulate enhanced ocean acidification in polar regions (e.g. Orr et al. 2005; Steinacher et al. 2009; Denman et al. 2011; Joos et al. 2011; AMAP 2013; Steiner et al. 2013). Deal et al. (2013) present results for the Pacific Arctic (Bering and Chuckchi Seas) showing surface pH under RCP8.5 forcing to further decrease to about 7.9 by mid-century and below 7.7 by the end of the century, which corresponds with the results in Steinacher et al. (2009). Aragonite saturation state is projected to decrease by about 0.8 - 1.0 in most of the Pacific Arctic Region with somewhat smaller changes north and northeast of the Bering Strait, where surface waters have already become undersaturated in current times.

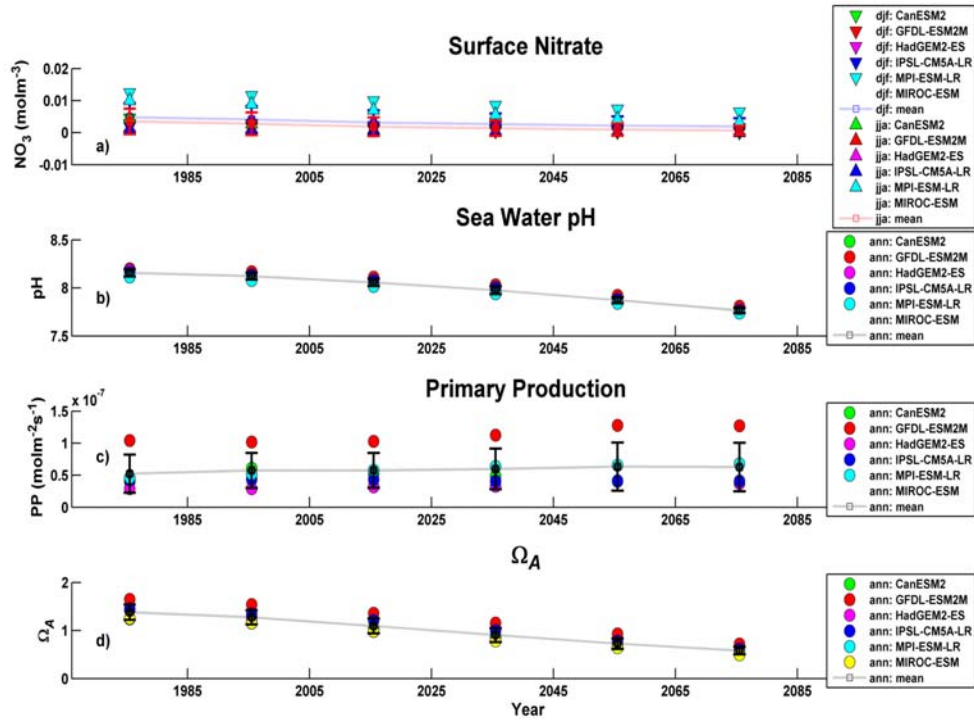
Simulated time series of the zonal mean saturation horizon (the layer where $\Omega = 1.0$) show a

continuous shoaling from preindustrial times to 2100 over most latitude bands. In the Arctic, in addition to a continuous shoaling of the deep saturation horizon, a shallow saturation horizon starts to form close to the surface. This is caused by the combination of increased CO₂ uptake and freshwater contributions at the surface which in the BS leads to surface and possibly subsurface undersaturation (AMAP 2013).

Retreating sea ice is one of the main components leading to increased acidification of the Arctic Ocean, both due to the addition of melt water and due to the increase in open water areas allowing for enhanced air-sea exchange. The latter leads to a more pronounced seasonality in atmosphere-ocean carbon fluxes with a later maximum in uptake in fall, and reduced uptake or even outgassing in summer (Steiner et al. 2013). The reduced uptake in summer is likely due to earlier ocean pCO₂ equilibration with enhanced flux during fall and winter, but also hints at a limited uptake capacity of Arctic surface waters as discussed in Cai et al. (2010). Steiner et al. (2013) also tested the implications of enhanced flux in ice covered areas in an earth system model application. They show the relative change due to the enhanced flux parameterization in the annual mean to be small if integrated over the whole Arctic region (below 2 - 3% for the area north of 68°N) but to be significantly higher for the predominantly ice covered central Arctic (up to 21% north of 80°N). They confirm accelerated ocean acidification with enhanced fluxes and conclude that the enhanced uptake could account for a one to two decade difference in the projected timing when surface aragonite undersaturation is reached in certain areas. A model study by Yamamoto et al. (2012) points out the importance of the sea ice reduction rate on acidification, suggesting that future reductions in pH and aragonite saturation states could be significantly faster than previously projected with increased pace in sea ice reduction. Another unknown is the potential release of methane, and its subsequent oxidation to CO₂. Biastoch et al. (2011) illustrated that the local pH values could be lowered by over 0.25 units assuming the release of 50% of the methane from hydrates over a period of 100 years (see AMAP 2013 for more details).

Beaufort Sea and Canadian Polar Shelf: Figure 79 shows simulated bidecadally and annually averaged pH time series for scenario RCP8.5 averaged over the BS and CPS regions. In the BS, GFDL-ESM2 has the highest pH while MPI-ESM-LR simulates the lowest. However, the spread between the models is small (< ~0.3). For the CPS region, the model spread is similar, but IPSL-CM5A-LR simulates the highest and MPI-ESM-LR consistently has the lowest pH. The AR5-ESMs show a continuous decrease in pH, with accelerated decrease after 2026 under the RCP8.5 forcing, and a more continuous decrease for RCP4.5 for the regional averages. The annual pH levels (and standard deviations) for the BS and CPS regions are very similar, dropping from 8.1 (1986 - 2005) to 7.9 (2046 - 2065) with a sixty year change of -0.25 and -0.24 respectively (Figure 71); (note that the BS pH line is overplotted by the CPS line). The regional view (Figure 73) shows that pH decreases everywhere in the North American domain, with the greatest loss in the BS and CPS (-0.25). The models have the largest standard deviations in the CPS, which is an area represented by few models. Differences in river input, model resolution and projected ice retreat might contribute to the larger spread.

a): BS subbasin



b) CPS subbasin

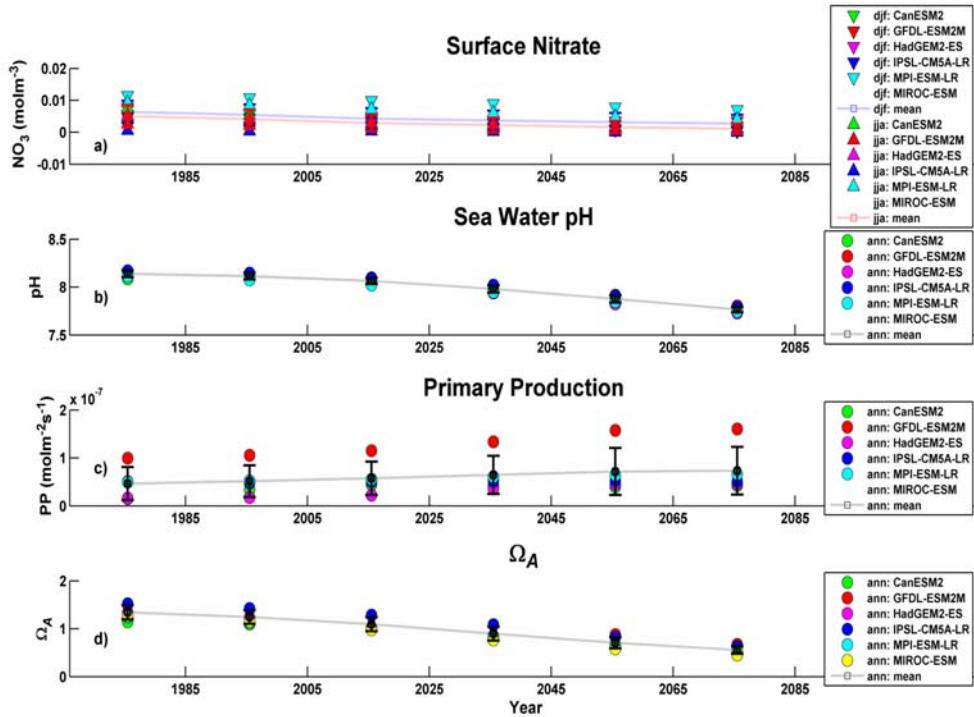


Figure 79: Bidecadally, annually averaged, individual mean and multimodel mean time series for scenario RCP8.5 for the BS (a) and CPS (b) regions for surface nitrate, sea water pH, and primary production and Ω_A .

Table 5: AR5-ESM individual model and multimodel means of surface saturation state (Ω) from 1966-2085 (bidecadal averages) for the BS and CPS regions.

Region	Variable	Timeperiod	Seas								DIFFtoHIST	
				Can	GFDL	Had	IPSL	MPI	MIROC	mean	stdev	(1986-2025)
Beaufort Sea	Ω_A	1966 1985	Ann	1.241	1.647	1.429	1.453	1.256	1.254	1.380	0.161	0.104
Beaufort Sea	Ω_A	1986 2005	Ann	1.180	1.540	1.273	1.346	1.155	1.159	1.276	0.150	0.000
Beaufort Sea	Ω_A	2006 2025	Ann	1.038	1.359	0.991	1.209	0.982	0.986	1.094	0.156	-0.181
Beaufort Sea	Ω_A	2026 2045	Ann	0.875	1.155	0.785	1.001	0.830	0.785	0.905	0.146	-0.370
Beaufort Sea	Ω_A	2046 2065	Ann	0.686	0.930	0.662	0.775	0.663	0.642	0.726	0.110	-0.549
Beaufort Sea	Ω_A	2066 2085	Ann	0.536	0.721	0.587	0.616	0.539	0.496	0.583	0.080	-0.693
Beaufort Sea	Ω_C	1966 1985	Ann	1.998	2.641	2.311	2.345	2.024	2.023	2.224	0.256	0.167
Beaufort Sea	Ω_C	1986 2005	Ann	1.902	2.471	2.061	2.175	1.862	1.868	2.057	0.238	0.000
Beaufort Sea	Ω_C	2006 2025	Ann	1.676	2.183	1.609	1.953	1.588	1.591	1.767	0.247	-0.290
Beaufort Sea	Ω_C	2026 2045	Ann	1.414	1.856	1.280	1.619	1.342	1.268	1.463	0.231	-0.593
Beaufort Sea	Ω_C	2046 2065	Ann	1.111	1.494	1.079	1.256	1.074	1.037	1.175	0.174	-0.882
Beaufort Sea	Ω_C	2066 2085	Ann	0.869	1.159	0.955	0.999	0.873	0.802	0.943	0.127	-1.114
CPS	Ω_A	1966 1985	Ann	1.147	1.510	1.345	1.524	1.252	1.275	1.342	0.150	0.097
CPS	Ω_A	1986 2005	Ann	1.099	1.414	1.242	1.424	1.131	1.158	1.245	0.143	0.000
CPS	Ω_A	2006 2025	Ann	1.023	1.287	1.022	1.279	0.986	0.979	1.096	0.146	-0.149
CPS	Ω_A	2026 2045	Ann	0.850	1.085	0.782	1.076	0.832	0.766	0.898	0.144	-0.346
CPS	Ω_A	2046 2065	Ann	0.671	0.878	0.611	0.825	0.675	0.583	0.707	0.118	-0.538
CPS	Ω_A	2066 2085	Ann	0.518	0.678	0.531	0.627	0.543	0.453	0.558	0.081	-0.686
CPS	Ω_C	1966 1985	Ann	1.848	2.426	2.171	2.454	2.018	2.057	2.162	0.239	0.154
CPS	Ω_C	1986 2005	Ann	1.774	2.274	2.009	2.296	1.826	1.869	2.008	0.228	0.000
CPS	Ω_C	2006 2025	Ann	1.653	2.071	1.658	2.061	1.593	1.582	1.770	0.232	-0.238
CPS	Ω_C	2026 2045	Ann	1.377	1.748	1.271	1.736	1.346	1.239	1.453	0.229	-0.555
CPS	Ω_C	2046 2065	Ann	1.089	1.415	0.995	1.335	1.093	0.944	1.145	0.189	-0.863
CPS	Ω_C	2066 2085	Ann	0.842	1.093	0.864	1.017	0.880	0.735	0.905	0.129	-1.103

The AR5-ESMs consistently simulate a reduction in the annual mean surface saturation state (Ω) of CaCO_3 . The regionally averaged model results are listed in Table 5. Changes over sixty years are about -0.5 in Ω_A and -0.8 for Ω_C (A and C indicate aragonite and calcite, respectively) both for the BS and CPS sub basins. The 1986 - 2005 saturation state for the BS and CPS regions is about 2.0 (Ω_C) and 1.2 (Ω_A), respectively. From 1966 - 2085, in the BS region, GFDL-ESM2 simulates the highest Ω_A while IPSL-CM5A-LR is highest in the CPS region. MIROC-ESM has the lowest for both regions (see also Figure 79). The Ω_C follows the pattern of Ω_A and is not shown here. Based on the multimodel mean, the surface BS and CPS regions become undersaturated (less than 1) by 2026 (Ω_A) and by 2066 (Ω_C) (Table 5).

An example for the vertical distribution of carbon variables is given in Figure 74. Black lines and triangles (Figure 74) show observed vertical profiles to 350 m for summer 2005 of DIC, TA and $\Omega_{A,C}$ in comparison with modelled bidecadally averaged annual mean profiles for 1986 -

2005 and 2066 - 2085 and multimodel mean averages for all bidecades at 75°N, 140°W in the Canada Basin. As discussed in Section 3.3, the snapshot character of the observations severely limits the comparison. The layered structure in the observed profiles which has been noted for the temperature profile is also observed for Ω , but again not simulated in the model average. The observations represent a shallow layer of undersaturated waters in the central Beaufort gyre where sea ice retreats in summer. Between about 20 and 100 m, waters are still supersaturated due to advection of Summer Pacific Water and photosynthesis at the subsurface Chl-*a* maximum. A band of undersaturated waters is found below the deep halocline (100 – 200 m). This subsurface undersaturated layer is maintained by advection of Pacific Winter Water (PWW), which is characterized by high nutrient concentrations and high pCO₂ due to remineralization of organic matter as the water flows over the shallow Chukchi shelf during winter. Below PWW is the Atlantic Water with high Ω , which flows into the intermediate layer of the Canada Basin. As for T and S, the large bias between the individual models' representation of the bidecadal means are to a large part retained in the projection runs, e.g. the low DIC/high Ω in the MIROC-ESM intermediate waters. The multimodel mean DIC profile (Figure 74o) shows a slow decrease for the Pacific water influenced upper layers as a consequence of dilution in Arctic near surface waters. In the Atlantic influenced intermediate layers, the multimodel mean trend follows the global increase of DIC in the ocean which is advected into the Arctic from the Atlantic. The multimodel mean change in alkalinity follows the salinity signal and, hence the normalized TA (Figure 74r) shows only little change. The acidification trend becomes most obvious in the multimodel mean Ω profiles (Figure 74i, l) which show a continuous reduction in saturation state. Surface waters are becoming undersaturated with respect to aragonite by 2026 – 2045, and full aragonite undersaturation for the 350 m profile is simulated by 2066 - 2085. Calcite undersaturation at the surface is simulated to be reached by 2066 - 2085 (Steiner et al. 2013, unpublished data).

Hudson and Baffin Bays: Surface pH in Hudson Bay varies between 7.9 and 8.1 (from measurements made in the 2000s, K. Azetsu-Scott, personal communication). These values are lower than those reported outside of Hudson Bay, e.g. 8.1 to 8.2 in Baffin Bay (Azetsu-Scott et al. 2010). Although pH values differ from one model to the other, all the AR5-ESMs simulate lower pH values in HB (Figure 80). In HB, three ESMs have a good representation of the pH at the surface: CanESM2, GFDL-ESM2M and IPSL-CM5A-LR. In Baffin Bay, all the ESMs have surface pH values within the observed range but MPI-ESM-LR has a better spatial representation, with higher value on the Greenland Shelf as observed by Azetsu-Scott et al. (2010). The historical surface pH trends are very similar from one model to the other with a pH decrease ranging between -0.05 and -0.08 over the 1960 - 2005 period.

In the Hudson and Baffin Bays, all the ESMs show similar negative trends for pH which are comparable in each layer (surface, 50 - 100 m, and 100 - 400 m). In HB, the multimodel mean trends for RCP4.5 and RCP8.5 are -0.022 ± 0.003 and -0.036 ± 0.003 units per decade at the surface, -0.022 ± 0.003 and -0.032 ± 0.007 units per decade in the 50 - 100 m layer, and -0.022 ± 0.004 and -0.033 ± 0.007 units per decade in the 100 – 400 m layer. In BB, the multimodel ensemble mean trends are slightly higher than in Hudson Bay, with -0.028 ± 0.004 and -0.043 ± 0.004 units per decade at the surface, -0.028 ± 0.005 and -0.038 ± 0.005 units per decade in the 50 - 100 m layer, and -0.028 ± 0.007 and 0.034 ± 0.007 units per decade in the 100 – 400 m layer. Future pH would thus decrease by an additional 0.06 to 0.22 units in the next 50 years.

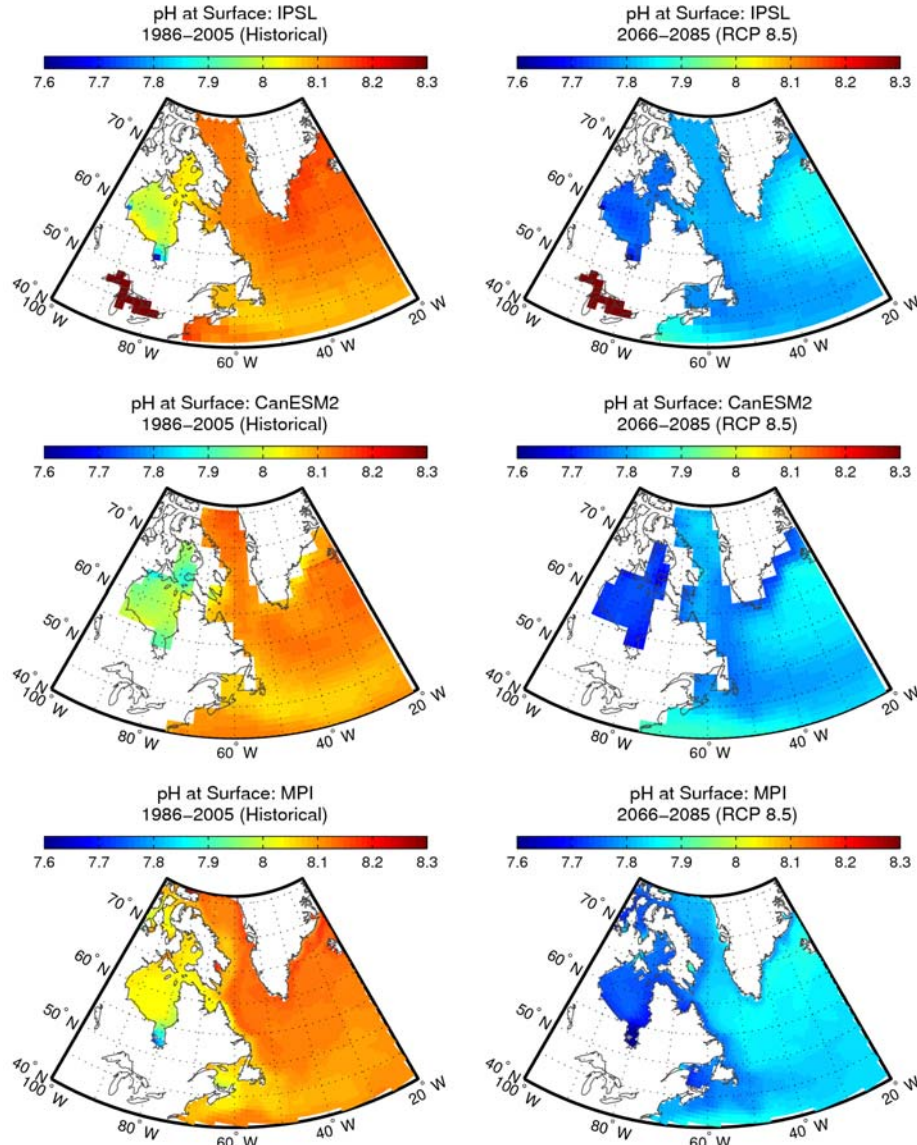


Figure 80: Mean simulated pH at the surface for the historical period (1986 - 2005) and future period (2066 - 2085) with the emission scenario RCP8.5 with three ESMs (IPSL-CM5A-LR, CanESM2, MPI-ESM-LR).

Surface DIC concentrations measured in 2004, 2005 and 2006 along a transect across the HB (MERICA transect, see Harvey et al. 2006) ranged between 1847 to 2029 $\mu\text{mol}/\text{kg}$ (or 1.8 and 1.98 mol m^{-3} , K. Azetsu-Scott, personal communication). GFDL-ESM2M and HadGEM2-ES DIC concentrations are too low, while the other ESMs (CanESM2, IPSL-CM5A-LR, and especially MPI-ESM-LR) have a better representation of the surface DIC (see Lavoie et al. 2013). In BB, DIC concentrations appear to be higher than in HB (2.10 mol/m^3 for 0 – 500 m layer, Azetsu-Scott et al. 2010). The ESMs reproduce this zonal difference (see Figure 81). As for HB, CanESM2 and MPI-ESM-LR have a good DIC concentration range in BB.

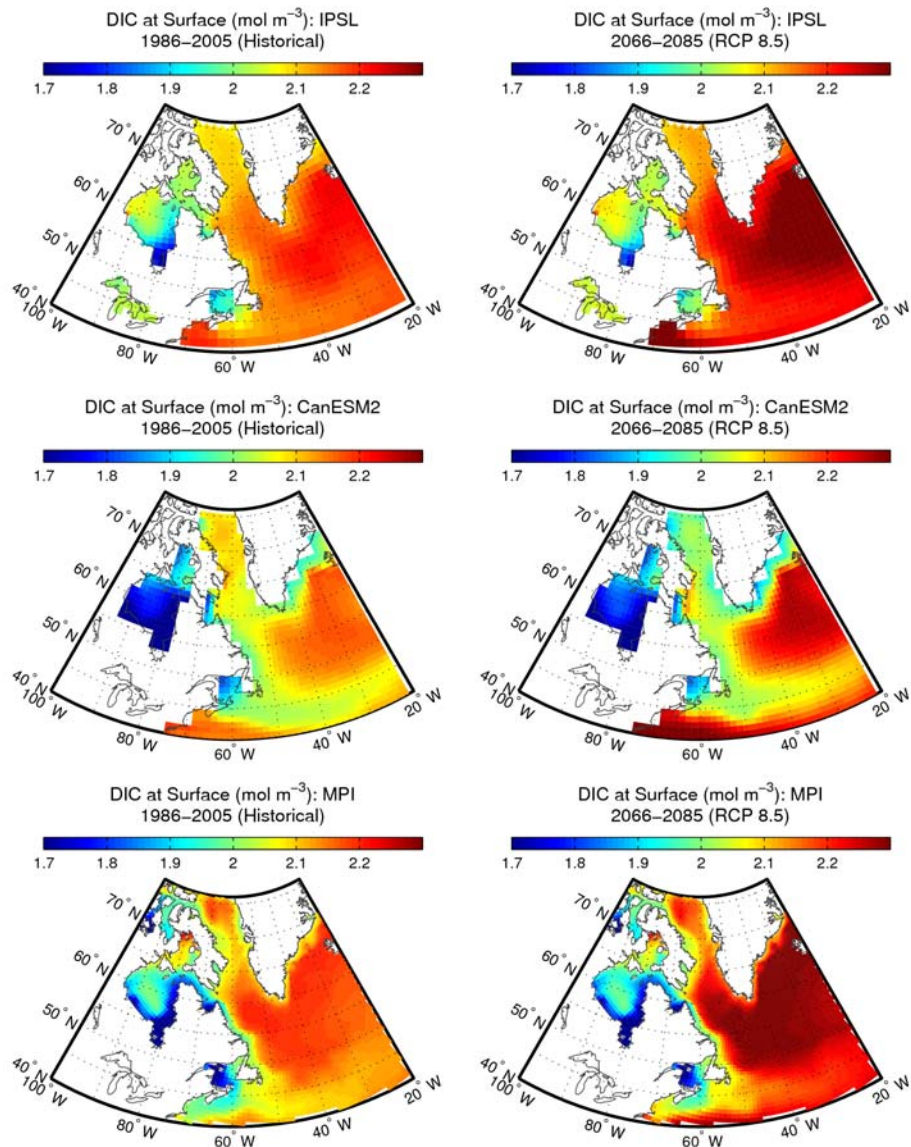


Figure 81: Mean simulated dissolved inorganic carbon (DIC) concentration (mol m^{-3}) at the surface for the historical period (1986 - 2005) and future period (2066 - 2085) for RCP8.5 with three ESMs (IPSL-CM5A-LR, CanESM2, MPI-ESM-LR).

In HB, the projected (DIC) concentration trends at the surface are weak and disparate, with three (two) positive trends and two (three) negative trends for RCP4.5 (RCP8.5). So we cannot conclude on any future trend (similarly for the deeper layers). The multimodel ensemble mean trends are presented in Table 6. In BB, the DIC concentration trends at the surface are divergent but all models show a positive trend in the 50 – 100 m (except CanESM2 for RCP8.5) and 100 - 400 m layers.

In the HB and BB subbasins, the calcite and aragonite saturation horizon has been analyzed for CanESM2. In HB, the saturation horizon depths obtained are too shallow (< 11 m for aragonite and < 40 m for calcite), while in BB the saturation horizon depths are closer to those measured

by Azetsu-Scott et al. (2010). In HB, the aragonite saturation depths (ASH) provided by CanESM2 for the period of 2012 to 2062 decrease at a rate of -69.5 cm and -116 cm per decade and reach the surface around 2065 and 2055 for RCP4.5 and RCP8.5 respectively. However, as mentioned above, the saturation depths are too shallow to start with. In BB, CanESM2 trends for ASH are -41 m and -60 m per decade for RCP4.5 and RCP8.5 respectively. Fifty years from now, mean ASH in Baffin Bay is projected to be less than 100 m with RCP4.5 and close to the surface with RCP8.5.

Table 6: Multimodel ensemble mean (3AR5-ESMs, IPSL-CM5A-LR, CanESM2, MPI-ESM-LR) of the projected (2012 - 2062) DIC concentration for Hudson and Baffin Bays.

Region	Scenario	DIC at Surface (mol/m ³)	DIC at 50-100m (mol/m ³)	DIC at 100-400m (mol/m ³)
Hudson Bay	RCP 4.5	-0.0023±0.011	-0.004±0.013	-0.0014±0.012
	RCP 8.5	-0.0026±0.011	-0.005±0.014	-0.0018±0.012
Baffin Bay	RCP 4.5	0.001±0.005	0.004±0.003	0.006±0.003
	RCP 8.5	6.3e-6±0.007	0.003±0.003	0.006±0.003

3.5 NUTRIENTS AND PRIMARY PRODUCTION

Steinacher et al. (2010) discuss discrepancies between results from empirical approaches and process-based ESMs and point out the importance of a realistic representation of nutrient cycling and distribution in order to project changes in primary production with some realism. In the Arctic, the loss of ice during spring could boost productivity > 3-fold above 1998 - 2002 levels, potentially altering marine ecosystem structure and the degree of pelagic-benthic coupling. Changes in carbon export could in turn modify benthic processes on the vast continental shelves (Arrigo et al. 2008). Vancopenolle et al. (2013), in a recent assessment of projected primary production, nutrient and sea ice concentrations in 11 CMIP5 ESMs, find that the mean model simulates Arctic-integrated primary production for 1998 - 2005 quite well, but the models neither agree on what limits primary production today, nor on the sign of future change. A balance of a decrease in available nutrients due to increased stratification and increased light availability due to a reduced sea ice cover operates in all models; however it depends on the model if the decrease in available nitrate is sufficient or not to overcome the benefits of the light increase. Vancopenolle et al. (2013) suggest that the main cause for the large inter-model spread is a poorly constrained observational data set of Arctic nitrate concentrations.

Beaufort Sea and Canadian Polar Shelf: The AR5-ESMs simulate a decrease in annual surface nitrate (NO₃) for the BS and CPS regions, with a larger decrease under the RCP8.5 forcing than the RCP4.5 (Figure 71). The CPS has higher NO₃ (~6 x 10³ mol m⁻³) levels than the BS region (~4 x 10³ mol m⁻³) during the 1966 - 1985 bidecade, however, the subbasins experience a similar rate of loss, dropping faster before 2025 than after.

The surface NO_3 from the AR5-ESMs shows a large seasonal cycle with nutrient drawdown in summer and replenishment in winter through mixing. The BS 1986 - 2005 winter and summer means are 4.1 ± 4.2 and $2.8 \pm 3.5 \times 10^3 \text{ mol m}^{-3}$ with a sixty year decrease of $1.9 \times 10^3 \text{ mol m}^{-3}$ in both seasons. The CPS has more surface NO_3 with smaller standard deviations, winter values of 5.4 mol m^{-3} , 4.0 mol m^{-3} for summer, and $2.3 - 2.5 \text{ mol m}^{-3}$ loss over sixty years. Although the seasonal variability is large, the sixty year change is similar for both seasons in both subbasins. For the BS and CPS, the standard deviations are large but decrease over time (APPENDIX 1: Table 8).

A spatial plot of the annual sixty year change in NO_3 (Figure 73) shows the most change in the central Arctic ($-3 \times 10^3 \text{ mol m}^{-3}$) with less loss near the BS coast (-1 to $-2 \times 10^3 \text{ mol m}^{-3}$) and a noisy pattern within the CPS with values ranging from -1 to $-2.5 \times 10^3 \text{ mol m}^{-3}$. The annual mean pattern is dominated by losses in March (the time of replenishment). Also, the NO_3 sixty year change shows a similar pattern to changes in SIC, with the greatest loss in the Arctic interior, where nitrate becomes depleted in summer due to primary production, and mixed layer shoaling reduces replenishment in winter.

For NO_3 in the BS region, MPI-ESM-LR shows the highest levels and the IPSL-CM5A-LR the lowest; the other models are closer to IPSL-CM5A-LR (Figure 79). The model intercomparison shows that if a model's NO_3 is high or low compared to other models, it is for both seasons; pointing out a systematic difference between the models (Vancoppenolle et al. 2013). The model NO_3 distribution is quite similar for CPS and BS.

The annual surface primary production (PP) as simulated by the AR5-ESMs is very similar for the BS and CPS and increases slightly with time. PP for the BS and CPS during 1986 - 2005 is 0.51 and $0.57 \text{ mol m}^{-2} \text{ s}^{-1}$, with a sixty year change (2045 - 2065 minus 1986 - 2005) of 0.06 and $0.20 \text{ mol m}^{-2} \text{ s}^{-1}$ respectively (Figure 71 and APPENDIX 1: Table 8). In a 1-D model study, Lavoie et al. (2010) simulate an increase in annual primary production of 6% between the period 1975 - 1992 and the period 2042 - 2059 resulting from an increase in the duration of the subsurface bloom.

The model distribution for the BS and CPS is also similar. The GFDL-ESM2 has a much larger PP than the other models. The HadGEM2-ES has the lowest PP, and the remaining models are clustered just above HadGEM-ES (Figure 79). Spatially, over sixty years, PP decreases (0 to $-0.1 \text{ mol m}^{-2} \text{ s}^{-1}$) in the center of the BS and increases in the surrounding area (0 to $0.1 \text{ mol m}^{-2} \text{ s}^{-1}$). The CPS shows an increase in PP, ranging from 0.1 to $0.6 \text{ mol m}^{-2} \text{ s}^{-1}$ (Figure 73).

Hudson Bay: Comparisons of model runs for historical time periods and observations point out that due to limited observations, it is difficult to determine the representativeness of the models; however, some of them display nitrate concentration that are definitely too high. In Hudson Bay, CanESM2 and HadGEM2-ES display nitrate concentrations that are too high both at the surface and at depth. In Baffin Bay, HadGEM2-ES concentrations at depth are too high, while GFDL-ESM2M and MPI-ESM-LR concentrations are too high at the surface. As for future projections (2012 - 2062) in Hudson Bay, all models show decreasing nitrate concentration at the surface and in the 50 -100 m for both emission scenarios (RCP4.5 and 8.5), except for IPSL-CM5A-LR that show an increasing trend in the 50 - 100 m layer for RCP4.5.

The multimodel ensemble mean trends are -0.19 ± 0.18 and -0.23 ± 0.18 mmol/m³ per decade at the surface for RCP4.5 and 8.5 respectively and 0.11 ± 0.15 and -0.24 ± 0.17 mmol/m³ per decade in the 50 - 100 m layer for RCP4.5 and RCP8.5 respectively. In Baffin Bay, the ESMs show divergent trends in nitrate concentration at the surface and in the 50 - 100 m layer and no conclusions on the trends can be reached. The multimodel ensemble mean trends at the surface are -0.09 ± 0.18 and -0.16 ± 0.15 mmol/m³ per decade for RCP4.5 and RCP8.5 respectively and $+0.11 \pm 0.34$ and -0.12 ± 0.50 mmol/m³ per decade in the 50 - 100 m layer for RCP4.5 and RCP8.5 respectively. In Hudson Bay, ESMs show no clear change in phytoplankton biomass at the surface over the next 50 years but project an increase in primary productivity (integrated over the water column) by 0.14 mol C m⁻² per decade for both scenarios.

3.6 MACKENZIE RIVER BASIN

3.6.1 Air temperature

Scenarios of climate change, based on experimental results from atmospheric GCMs, suggest that the Mackenzie Basin region could warm up by 4°C to 5°C between the 30 - year base-line period of 1951 - 1980 and the middle of the 21st century (MRBB 2004). The Center for Climate Research Studies, Japan, CCSR model (Emori et al. 1999) and the Canadian Global Climate Model CGCM (Boer et al. 2000) project an annual average warming of 4.2°C in 2025, 4.9°C in 2045, and 8.5°C in 2095 for the Mackenzie (Nijssen et al. 2001).

It is estimated that on average, the Mackenzie Valley could warm as much as 3.5 to 4°C by the 2050s (NRTEE 2010). Future climate model projections for the prairies areas indicate increases in temperature of about 6°C by the end of the 21st century. Results among different climate models vary. However, the use of an ensemble approach (multimodel means) is likely to reduce the uncertainty associated with any individual models and likely provides the best-projected climate change signal. The Canadian Climate Change Scenarios Network (CCCSN 2009) has produced a mean ensemble of the IPCC AR4 (IPCC 2007) modelling assessment for Canada based on the international dataset from twenty-four modelling centres based on mean change from 1961 to 1990. To project climate change in the year 2050 (2041 - 2070) in Canada, OURANOS (a partner of Environment Canada) has presented mean model results from their two latest versions of the Canadian Regional Climate Model (CRCM 4.2.0 and 4.2.3) (CCCSN 2009).

The CCCSN (2009) ensemble modelling approach projects that the mean annual air temperature in the Mackenzie River Basin will increase from 2°C in the upper Peace, Athabasca and Liard River basins to 4°C in the lower Mackenzie Basin and increase by 2.5 to 3.5°C in most parts of the basin areas by 2050 (Figure 82). This increase will be higher during the winter season ranging from 2.5°C (upper Athabasca) to 6°C in the Mackenzie Delta region (Figure 83). In spring, the increase in mean temperature is projected to be from 2.5°C to 3.5°C, in summer from 1.5°C (Mackenzie Delta) to 3°C (upper Athabasca, Figure 84), and in autumn from 2°C in the upper Liard, Peace and Athabasca basins to 5°C in the Mackenzie delta area. CRCM models (CCCSN 2009) project an annual mean temperature increase from 2.5°C in the upper Peace and Athabasca subbasins to 4.5°C in Mackenzie delta areas in 2050 (Figure 82). The CRCM winter season projection for the basin is 4°C in the upper Athabasca, up to 7°C in the Mackenzie delta with a general increase of 5 - 6°C in most of the Mackenzie River basin (Figure 83). Like the CCCSN models, CRCM projects a spring mean temperature increase from 1.5°C in the upper

Athabasca to 4°C in the Mackenzie delta. A temperature increase from 1.5°C in the Mackenzie delta to 3°C in the upper Athabasca is projected for summer (Figure 84) and from 2°C in the Peace, Athabasca and Slave subbasins to 4.5°C in the upper Mackenzie River basin for autumn.

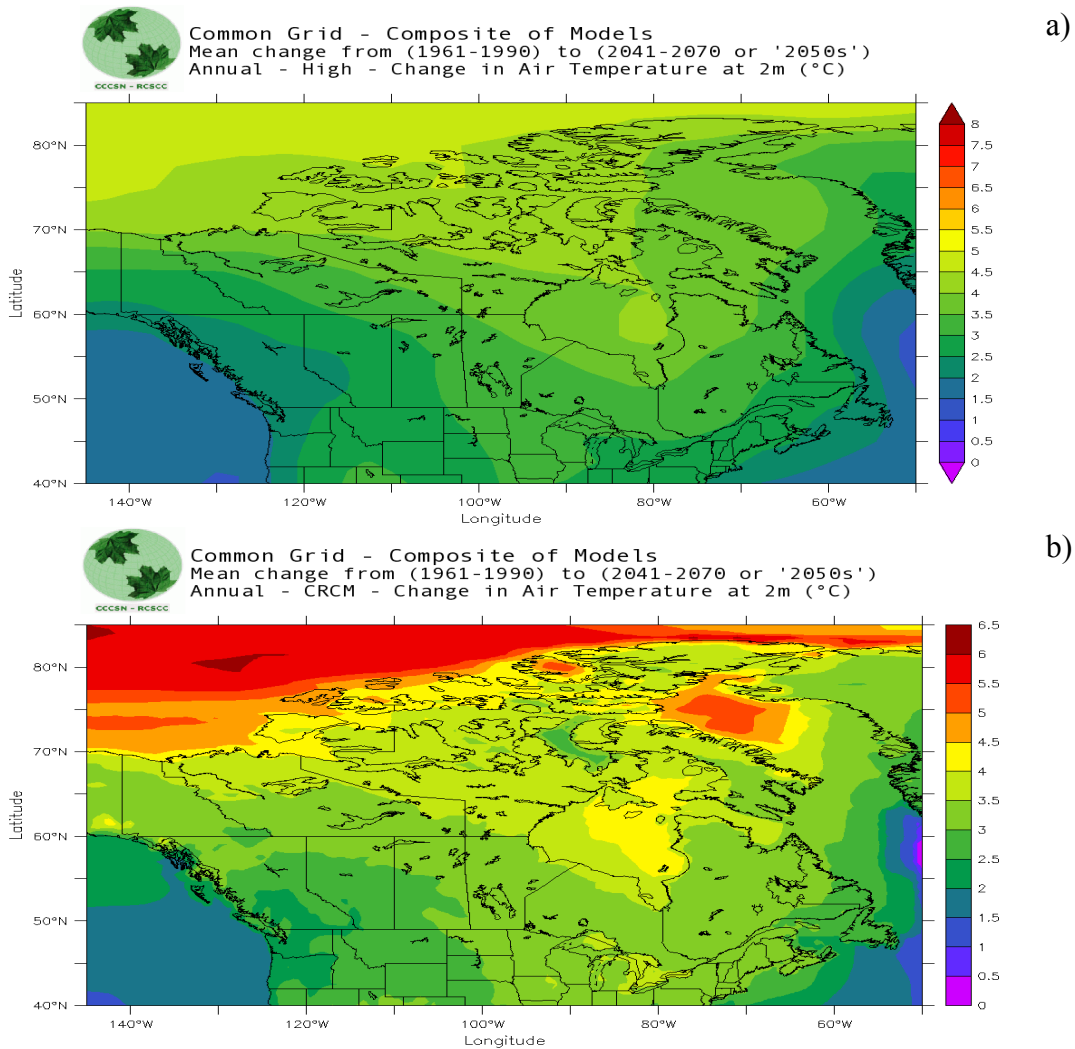


Figure 82: Projected change in annual mean air temperature from (1961 - 1990) to (2041 - 2070) (a) CCSN (2009) mean ensemble analysis from the IPCC AR4 (2007) modelling assessment for Canada contributed by 24 international modelling centres. (b) Mean model results from two recent versions of the OURANOS Canadian Regional Climate Model (CRCM).

The CCCma CanRCM4 Mackenzie River Basin (MRB) air temperatures on the NAM grid increase by 0.66 and 0.54 °C/decade (2012 - 2061) for the RCP8.5 and RCP4.5 scenarios respectively. For both scenarios, the fifty year trend (2012 - 2061) is greater than the historical trend (0.37 °C/decade for 1961 - 2005). The historical and fifty year trends are significant on the 5% level, but most of the bidecadal trends are not (Figure 85). The CanRCM-NAM sixty year change under RCP8.5 forcing for the MRB is 3.9°C (2046 - 2065 minus 1986 - 2005) with a trend of 0.66 °C/decade (Section 3.2.1).

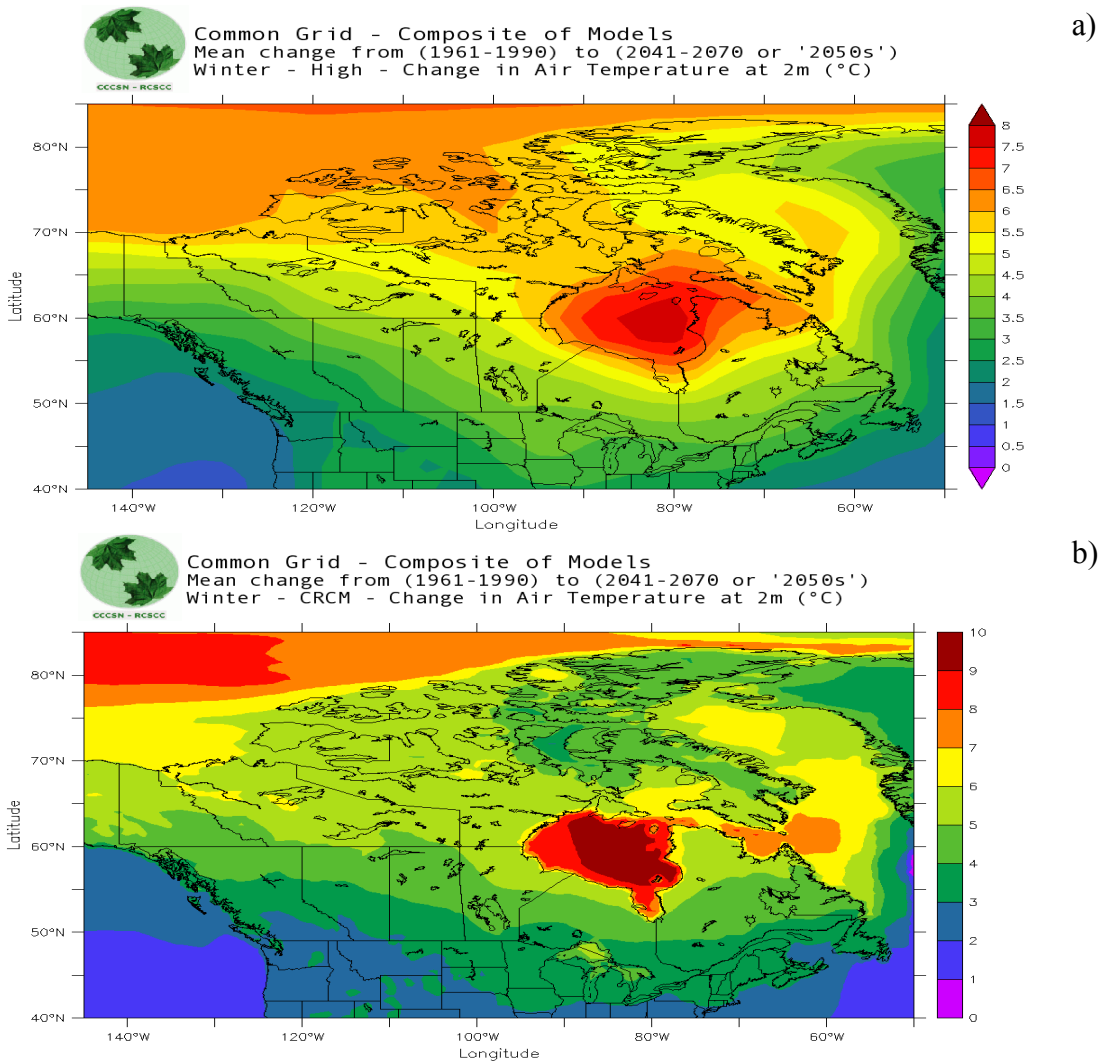


Figure 83: Projected change in mean winter air temperature from (1961 - 1990) to (2041 - 2070) (a) CCCSN (2009) mean ensemble analysis from the IPCC AR4 (2007) modelling assessment for Canada contributed by 24 international modelling centres. (b) Mean model results from two recent versions of the OURANOS Canadian Regional Climate Model (CRCM).

As described in section 3.2.1, the CanRCM4 historical (1986 - 2005) annual mean air temperatures over northern North America are cooler in the north and increasingly warmer to the south. The MRB air temperatures range from -6 to 6°C (north to south). The MRB twenty year change (2006 - 2025 minus 1986 - 2005) is 1 - 2°C and the sixty year change (2046 - 2065 minus 1986 - 2005) is 3°C in the south and 4 - 5°C in the north (Figure 63).

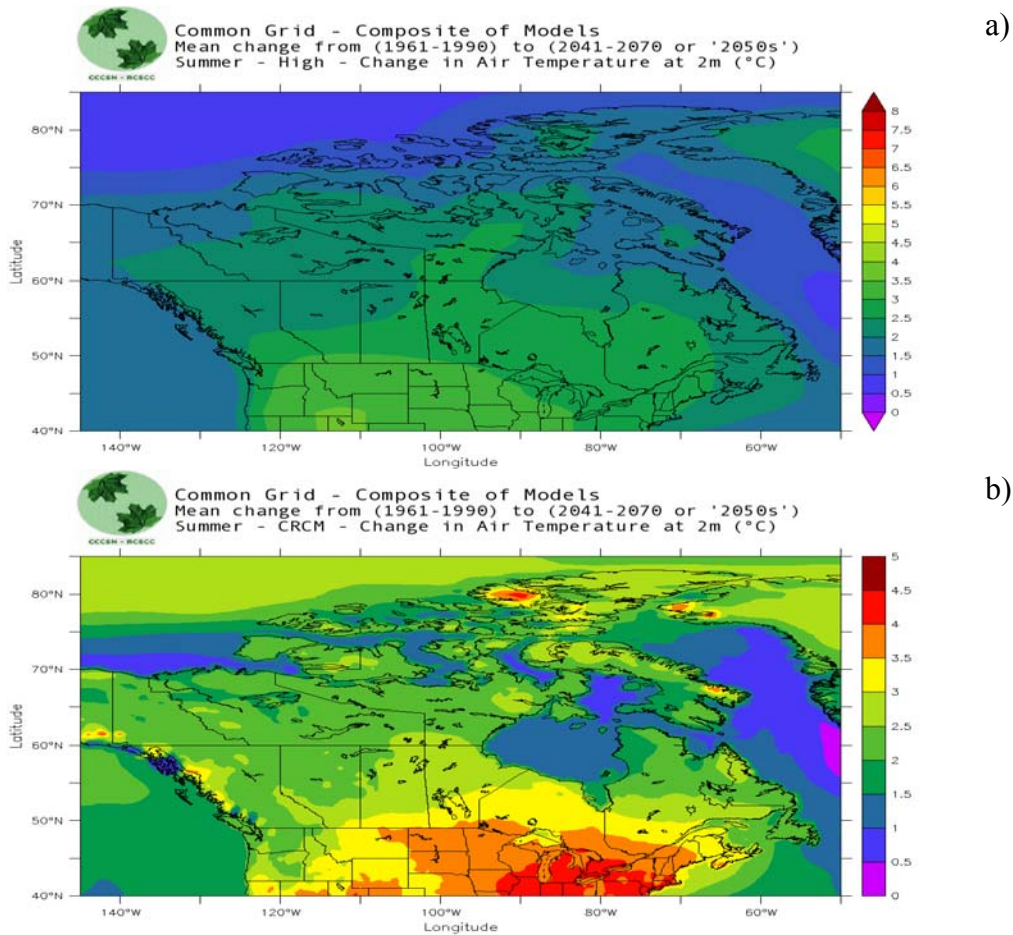


Figure 84: Projected change in mean summer air temperature from (1961 - 1990) to (2041 - 2070). (a) CCCSN (2009) mean ensemble analysis from the IPCC AR4 (2007) modelling assessment for Canada contributed by 24 international modelling centres. (b) Mean model results from two recent versions of the Canadian Regional Climate Model (CRCM).

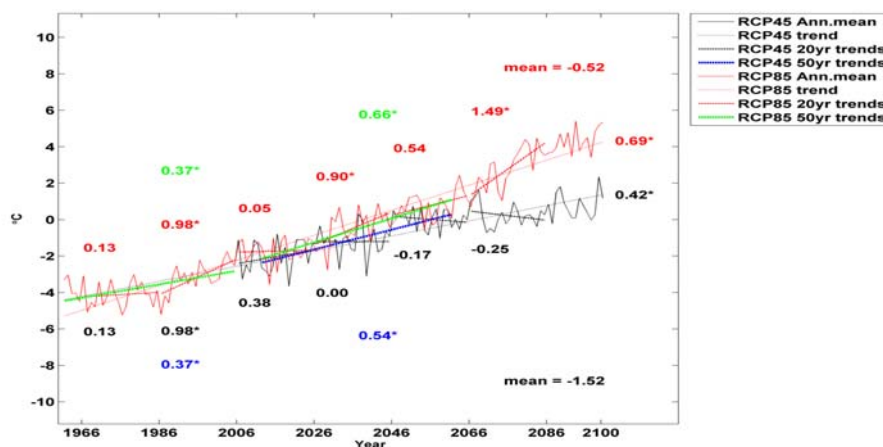


Figure 85: CanRCM-NAM annual mean air temperature with bidecadal trends as well as a historical (1961 - 2005), a future fifty year (2012 - 2061), and a long term (1961 - 2100) trend for scenarios RCP4.5 and RCP8.5, averaged over the Mackenzie River Basin as shown in Figure 55. All trends are °C/decade. If marked with an asterisk, the trend is significant (on a 5% level).

3.6.2 Precipitation

The 1986 - 2005 CanRCM4 annual mean spatial plot shows that most of the precipitation over northern North America occurs along the Canadian west coast; precipitation within the MRB ranges from ~3.5 mm/day in the southwest to 0.7 mm/day in the north. The spatial pattern of change is very noisy. The largest increase in precipitation occurs to the southwest of the MRB. Over sixty years (2045 - 2065 minus 1986 - 2005), the change in precipitation in the MRB ranges from 0 - 0.6 mm/day (Figure 67).

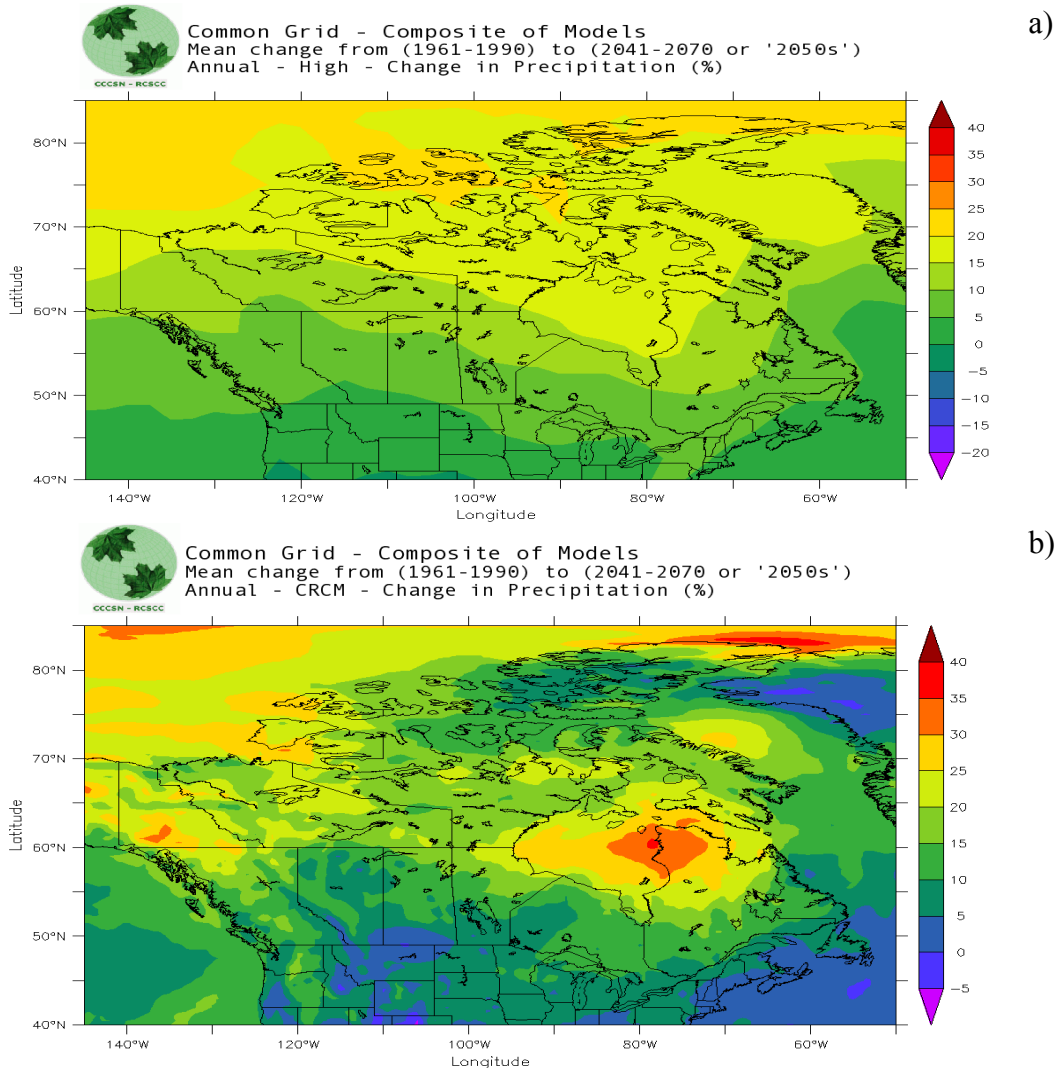


Figure 86: Projected percentage change in annual precipitation from (1961 - 1990) to (2041 - 2070). (a) CCCSN (2009) mean ensemble analysis from the IPCC AR4 (2007) modelling assessment for Canada contributed by 24 international modelling centres. (b) Mean model results from two recent versions of the Canadian Regional Climate Model (CRCM).

The CCCSN (2009) ensemble approach has projected an increase in annual precipitation from 10% in the upper Athabasca, Peace, Slave and Liard Rivers to 20% in the lower Mackenzie River by the middle of this century (Figure 86). In winter, the increase in precipitation is projected to be from 15% in the Peace, Athabasca, and Liard subbasins to 25% in the lower

Mackenzie River. Spring increase is projected to be 15% throughout the basin. During summer the precipitation is projected to be the same except of a 15% increase in the upper Mackenzie River basin (not shown). During autumn, precipitation is projected to increase from 10% in the upper Athabasca to 20% in the lower Mackenzie River basin. CRCM models project a 10 - 15% increase in annual precipitation in Mackenzie River basin with 25% increase in the Norman Wells area by the middle of this century (Figure 86). The same model projects a 20% increase in the upper Athabasca River to a 50% increase in the upper Mackenzie River Basin in winter. During spring, the projected increase is from 10% to 25% in different parts of the basin. CRCM has projected a 5% decrease in precipitation during summer in the Peace and the Athabasca River basins to a 35% increase in some parts of Mackenzie River basin in the Yukon and NWT parts of the basin. During autumn, an increase of 10 - 15% is projected in the Athabasca and Peace River and up to 35% in the Peel River basin. The Japan CCSR model and the Canadian CGCM model project changes in precipitation of 15.0% in 2025 to 27.6% in 2095 (Nijssen et al. 2001).

The historical trend (1961 - 2005) for the CanRCM4 MRB precipitation is 0.01 mm/day/decade. Trends increase to 0.06 and 0.02 mm/day/decade for RCP8.5 and RCP4.5 (2012 - 2061). All the bidecades have positive trends except for the bidecades from 2006 to 2066 in the RCP4.5 scenario, which are negative. Most of the trends are not significant to the 5% level (Figure 87).

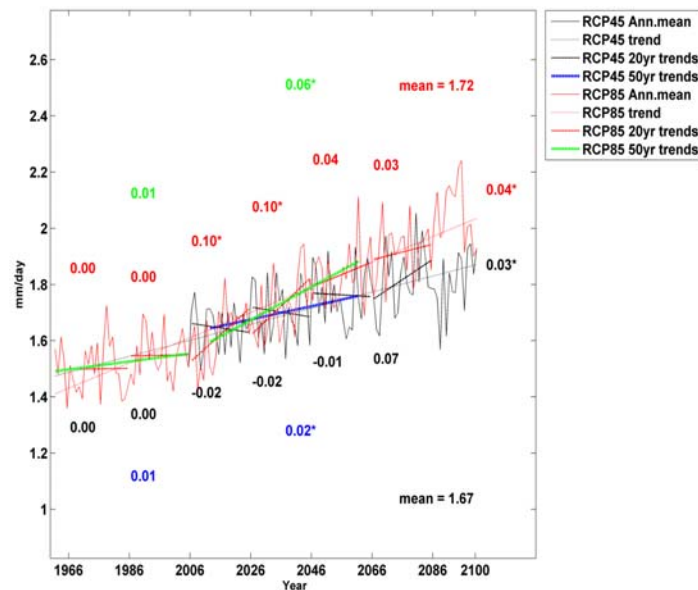


Figure 87: Same as Figure 85 but for annual mean precipitation (mm/day).

3.6.3 Wind

The CanRCM windspeed squared (WSS) has high variability over the MRB (Figure 88), resulting in weak trends and low confidence. For example, the long-term trend (1961 - 2100) under RCP8.5 forcing is $0.02 \text{ m}^2/\text{s}^2/\text{decade}^{-1}$ (and is significant on the 5% level) but the fifty year trend (2012 - 2061) is negative. The fifty year and bidecadal trends for 1966 - 2066 are not significant for either scenario.

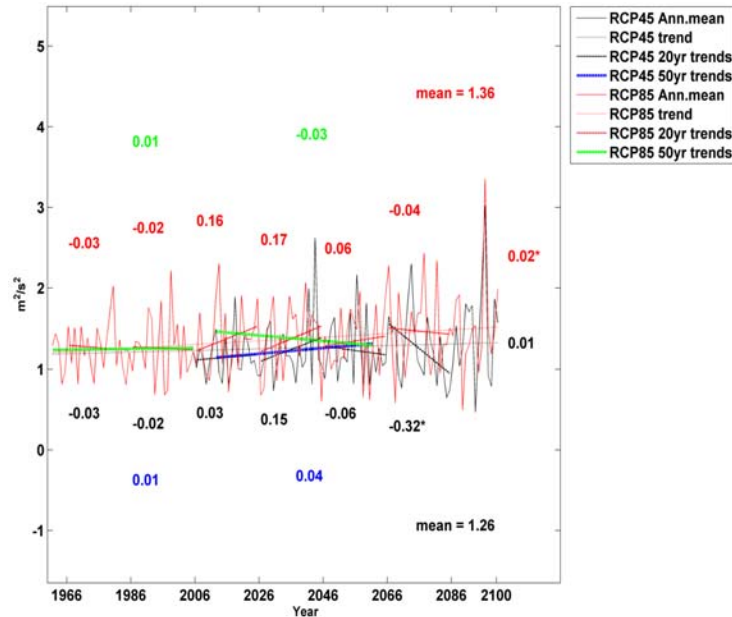


Figure 88: Same as Figure 85 but for annual mean windspeed squared (m^2/s^2).

The MRB shows a WSS of 0 - 1.6 m^2/s^2 throughout most of the region for 1985 - 2005 (CanRCM4), with areas of $\sim 15 - 25 \text{ m}^2/\text{s}^2$ to the west and south. The past twenty year (1986 - 2005 minus 1966 - 1985) and future twenty year (2006 - 2025 minus 1986 - 2005) change ranges from 1.3 to $-1.3 \text{ m}^2/\text{s}^2$. Over most of the MRB, the future sixty year (2045 - 2065 minus 1986 - 2005) change is 0 to $-1.3 \text{ m}^2/\text{s}^2$, with bands of increase (0 - $1.3 \text{ m}^2/\text{s}^2$) in the north and east of the MRB, and patches of greater decrease ($-2.6 \text{ m}^2/\text{s}^2$) in the southwest (Figure 70).

3.6.4 Hydrology

Manabe et al. (2004) predicted that as a result of climate warming, the annual flow of the Mackenzie River will increase by 21% by 2050 or even double that estimate if carbon dioxide continues to increase. Nohara et al. (2006) investigated the projections of river discharge for 24 major rivers in the world including the Mackenzie River during the twenty-first century, simulated by 19 coupled atmosphere-ocean GCMs. They show future flow in the Mackenzie River to be $14,271 \text{ m}^3 \text{ s}^{-1}$, compared to a simulated flow of $12,275 \text{ m}^3 \text{ s}^{-1}$ at present, hence, an increase of 16.3%. However, Rouse et al. (1997) predicted the Mackenzie River flow may be reduced and some climate models also suggest that a warmer climate in the Mackenzie River Basin will be accompanied by lower flows in the Mackenzie River (Kerr 1998; Spence 2002). The Mackenzie River system is unlikely to be significantly affected by changes in hydrologic processes operating within the Arctic and Sub-Arctic but rather depends on changes in water-balance processes operating well outside the Arctic. Compared to other Arctic high latitude rivers, the degree temperature increase is not that high for upper Mackenzie River Basin (Prowse et al. 2006b). Therefore, a comparable degree of headwater warming and hence snowmelt runoff is not projected for the Mackenzie Basin. Schindler and Smol (2006) also predicted that in the long term, the flow will decline because of declining snowpacks and glaciers in the headwaters of the Mackenzie River.

Climate change will significantly affect the timing and volume of flows in the Peace and Athabasca Rivers, as well as lake levels within the Peace Athabasca Delta. Prowse et al. (2006a) used a climate-based model of stream flow, verified with historical data to predict changes in water yield of several catchments in the Athabasca lowlands in the 21st century. The model projects significant decline in total April-October stream flow for the entire range of the catchment areas. With an average warming of 3°C projected for 2050, the average projected decline in stream flow is 8 - 26% for the various catchments areas. During the warmest dry years, this decline could be from 17 - 71%. With the evapotranspiration water losses, this could pose a large risk on the water supply in the Athabasca River.

The impact of projected atmospheric warming on the Liard River discharge is unclear. Changes include higher flow in winter because of wetter and warmer winters, lower spring freshets because of reduction in snow accumulations, and low summer flows indicating a warmer, drier summer climate. These changes can have potential consequences on ice jamming and floods. However, it is not clear if the recent decrease in stream flow on the Liard River is a long term climate fluctuation or an early signal of climate change (MRBB 2004). Thorne (2011) used SLURP, a hydrological model, to assess uncertainties in the Liard River discharge based on prescribed climate warming, resulting in 1 to 12 days earlier spring freshet, up to 22% decrease in summer runoff due to enhanced evaporation, and up to 48% increase in autumn flow. They find the magnitude of changes in river discharge to be highly uncertain, ranging from a 3% decrease to a 15% increase in annual runoff due to differences in GCM projections of basin-wide temperature and precipitation. Generally, in the Liard River, projections suggest the spring freshet to arrive earlier, autumn to spring discharge to increase, and summer flow to decrease, leading to an overall increase in annual discharge (Thorne 2011).

3.6.5 Lakes

Water temperatures in lakes are also expected to rise, with the greatest increase occurring in northern regions of Canada. Rao et al. (2012) studies the impact of climate warming on the Great Bear Lake using Canadian Regional Climate Model (CRCM) scenarios for the base climate (1970 – 2000) and future warmer climate (2041 – 2070). They project an increase in surface temperatures from 0.5°C to 1°C except in the northeast corner where a 2°C increase is projected. The results show that, as a result of warming, brief thermal stratification is possible in the deeper waters. The increase in water temperature caused by climate warming in the lake appears largely because of the positive increase in net long wave radiation and sensible heat flux (Rao et al. 2012). Based on increases in air temperature projected with the General Circulation Model Version 2 and climate-change scenarios CGCM2–IS92a, A2 and B2, Sharma et al. (2007) suggest that by 2100, lake water temperatures in the majority of Canada will increase by 5 – 10°C, and the northern regions of Canada could experience an increase of 10 – 18°C. Using general linear models to develop a Canada wide maximum lake surface-water temperature model they find more increase in the upper Mackenzie Basin region (Figure 89).

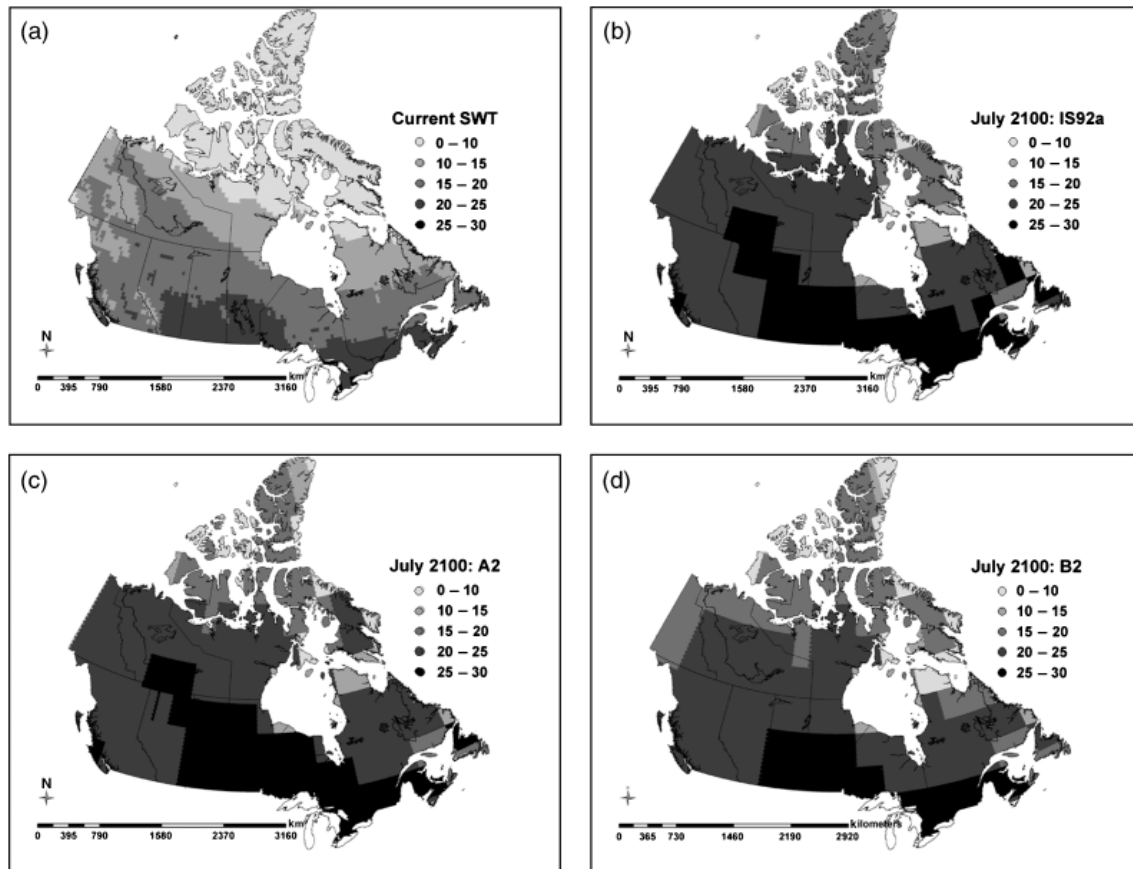


Figure 89: (a) Current lake surface-water temperatures in Canada based on multiple-regression Model 1. (b - d) Predicted future lake surface-water temperatures in Canada based on multiple-regression Model 2 and climate-change scenarios CGCM2-IS92a, A2 and B2 in July 2100 (Sharma et al. 2007).

A general decline in precipitation and an increase in air temperature, evaporation, and annual solar radiation will result in decreased flows and longer water renewal times for lakes. Lakes are suggested to become warmer with deeper epilimnions as thermoclines will be lowered (Schindler et al. 1996). With warmer water temperatures, the thermocline is expected to become more pronounced, the duration of stratification is projected to increase and the timing, extent and duration of winter mixing are expected to decrease (Lehman et al. 2000). With climate warming, dissolved oxygen may be a limiting factor to fish productivity and will significantly limit the availability of suitable habitat for some cold-water fishes, including lake trout (Lynch et al. 2010). Climate change and resultant change in hydrology will also influence the basin chemical exports to the lakes, thus influencing in-lake processes, lake chemistry and biological components (Environment Canada 2004).

3.6.6 Flooding and ice jams

Floods are a natural occurrence in the Mackenzie River basin and can be caused by ice jams or intense rainstorms. Ice jams are common along the Mackenzie River during spring break-up and can cause flooding by creating ice dams which can raise water as high as ten meters above normal river levels (MRBB 2004). A number of hydrologic shifts related to climate change will

affect seasonal flow patterns, ice-cover thickness and as a result the frequency and severity of extreme flood events. IPCC (2001) predicted probable changes in flood frequencies and increases in runoff due to increased precipitation in northern latitudes. Generally, the most severe spring floods are associated with a strong climatic gradient between the headwaters and the downstream reaches (Gray and Prowse 1993). Changes in the strength of this climatic gradient could change the severity of break-up and the associated flooding. In the regions that experience a more “thermal” or less dynamic ice break-up, the magnitude of the annual spring flood will very likely be reduced (Prowse et al. 2006b).

Earlier ice break-up and spring freshet on the river often occurs while the lake ice at the river mouth is still intact. This situation may result in ice jam flooding. Brock et al. (2010) used a palaeolimnological approach to reconstruct variations in the frequency of spring break-up flooding in the Slave River Delta based on multi-proxy analysis. They found that climate-driven change in the runoff regime of the upper Mackenzie River Basin is likely the principle driver of variability in flood frequency in the Slave River Delta.

Decreased winter precipitation reduces the early spring runoff from tributaries to the Peace River and reduces the likelihood of ice jam-induced floods in the lower Peace River near the Peace-Athabasca Delta. According to Timoney (2002), lack of recent flooding is almost entirely due to climate change. It is estimated that flow regulation by the dam has had a negligible effect on the occurrence of large ice jam-induced floods in the lower Peace River (Ashton 2003). A shortened ice season and thinner ice cover will also reduce ice-jam conditions and flooding during spring.

Wolfe et al. (2008) found close relationships between water balances and limnological conditions and suggested that past and future changes in hydrology are also likely to be coupled with alterations in water chemistry and, hence, the ecology of aquatic environments in the Peace Athabasca Delta.

3.6.7 Cryosphere

Future warming will result in a shortened ice season, thinner lake and river ice that will determine the severity of river-ice events, such as ice-jam flooding (increase or decrease) (Walsh et al. 2005). High-latitude lakes are more prone to be affected by climate change due to their strong absorption of solar radiation during the ice-free period.

3.6.8 Permafrost

Approximately half of the area underlain by permafrost in Canada contains permafrost warmer than -2°C that could ultimately disappear under projected climate warming (Smith and Burgess, 2004). Active-layer depth range is projected to increase from 0% to more than 50% during the next 50 years (Walsh et al. 2005). In the Mackenzie River Basin Valley, the depth to which the ground thaws in the summer could increase by 15 to 40% over the next century, in response to climate warming of 3 to 4°C (Furgal et al. 2008). With climate warming, the permafrost would become thinner in the continuous zone, and disappear altogether in some areas along the southern margin of the Mackenzie Valley such as the area of Fort Simpson in the NWT. In the continuous zone, the active layer would grow only slightly (Dyke et al. 1997).

3.6.9 Primary Production

Global warming is likely to have both direct and indirect effects on phytoplankton in terrestrial watersheds. Increased organic matter inputs as a result of watershed disturbance, warmer temperatures and longer growing season may result in enhance algal standing stocks and primary productivity (Smith et al. 2005; Smol et al. 2005). As a result of climate change, emergent aquatic plants are expected to expand their distribution northward and this will increase the overall primary production in small lakes and ponds in the Arctic, however the potential northern limit for emergent aquatic macrophytes is not fully known (Wrona et al. 2006). In the Mackenzie River Delta, some lakes are flooded annually. In these lakes, dissolved organic carbon (DOC) are recharged, however turbidity because of silt becomes a limiting factor for macrophyte growth and hence keeps productivity in check. However, if lakes are not flooded annually, the water becomes clearer after some time making way for macrophyte development (Squires and Lesack 2003). As a result, infrequently flooded lakes might become more productive in the Mackenzie Delta (Squires et al. 2002). Productivity in Arctic lakes could dramatically increase if these systems experience increases in temperature and nutrient concentrations as predicted by climate change models (Flanagan et al. 2003). With changing climate, more “zooplankton eaters” are expected to invade these lakes. These predators will release phytoplankton from grazer control causing increased algal biomass (Flanagan et al. 2003).

4: CONCLUSIONS AND RECOMMENDATIONS

In this assessment, past trends and future projections have been analysed with respect to environmental variables and key drivers of marine ecosystems. A summary of the main results, i.e. trends and projections of the identified main risk variables is provided in Table 7. The table outlines past climate trends (up to ~the last 50 years) as well as future projections (next 50 years) for the Arctic LAB. While the table provides a concise summary, it needs to be pointed out that the results presented there are a rather crude average of a hugely diverse region. A more detailed regional break down is provided in the sub region tables listed in Appendix 2, which have also been used for the Canadian Science and Advisory Secretariat risk analysis (CSAS 2013).

Table 7. Trends and projections summary table for the Arctic LAB (CSAS 2013).

Risk Factors (variables)	Trends (past conditions)	Projections (next 50 years)
Surface Air Temperature	Surface air temperature increase of 0.3 - 0.5°C per decade over Arctic land areas during the last 30 - 50 years. Records over marine basins are sparse.	Very likely increase in air temperature by 0 – 3°C in summer and 3 – 7°C in winter.
Precipitation	No clear observational record of precipitation trends across the Arctic LAB	Likely slight increases in precipitation, less in summer than in winter (15 - 50%).

Risk Factors (variables)	Trends (past conditions)	Projections (next 50 years)
Atmospheric Circulation (Wind)	Appreciable change in patterns of Arctic atmospheric circulation during the last 1 - 2 decades. Sea level pressure has increased in the eastern Canada Basin creating a stronger N-S pressure gradient and increased east wind across the southern Beaufort Sea.	Likely increase in storm strength and size with increased potential for storm surges (Beaufort Sea), coastal erosion and loss of coastline. Projections indicate only small changes in wind speed.
Waves	In the southern Beaufort Sea during the last decade: Northward retreat of the ice edge in summer and increased wind have fostered larger waves during autumn storms.	Likely small increase in summer in mean significant wave heights (SWH); increased storm waves and sediment mobilization.
Sea Ice	The Arctic-wide decrease in the extent of multi-year ice during the last 20 years has become evident in the Canadian Beaufort Sea, over the Canadian Polar Shelf and in Baffin Bay during the last decade. The expanse of ice-free water in late summer has increased correspondingly. The average age of remaining multi-year ice has decreased and its average thickness is less. First-year ice is forming later in the autumn in most areas and is dissipating earlier in summer. However, available data do not reveal any clear changes in the thickness of first-year ice throughout the Arctic LAB, either in the land-fast or pack-ice domains.	Very likely continued decrease in mean sea ice thickness (0.25 - 1.75 m). Further decline in multi-year ice area, possibly enabling an ice-free Arctic in late summer. Decrease in summer ice extent (10 - 80%), Longer open water season: earlier ice break-up and later freeze-up. Little change in winter ice conditions.
Ocean Surface Temperatures and Salinity	The temporal and spatial coverage of data are insufficient to delineate trends across the Arctic LAB. In the Beaufort Sea during the last decade, surface salinity has decreased in the Canada Basin and increased on the southern shelf. For Hudson Bay sea surface temperature trend is warming by 0.7 - 1.3°C over the 1985 - 2011	Very likely increased summertime sea-surface temperature (0 – 2°C) in ice-free areas. Some decrease in sea surface salinity (0 - 1.5 ppt) due to river inflow and sea ice melt. Little change in winter ocean conditions.

Risk Factors (variables)	Trends (past conditions)	Projections (next 50 years)
	period. For Baffin/Davis weak warming at surface, no trend at depth.	
Stratification (Mixed Layer Depth)	The temporal and spatial coverage of data are insufficient to delineate trends across the Arctic LAB.	Likely strengthening stratification with basin averaged maximum mixed layer depth decreasing by 1.5 m and 10 – 40 m locally in the central Beaufort Sea.
Large-Scale Circulation	The temporal and spatial coverage of data are insufficient to delineate trends across the Arctic LAB. In the Beaufort Sea during the last decade, the speed of westward surface drift has increased.	Likely intensification of large scale circulation, in response to strengthening of the Northern Annular Mode (NAM) Reduction in volume and freshwater transports through the Canadian Arctic Archipelago.
Sea Level	The temporal and spatial coverage of data are insufficient to delineate trends across the Arctic LAB.	Contributions to relative sea level from post-glacial rebound, compaction subsidence, ocean warming and melting of terrestrial ice sheets vary greatly across the Arctic LAB. The anticipated rise in global sea level via melting of the Greenland ice sheet may be masked over much of the Canadian Arctic by post-glacial rebound and lowered gravitational pull from Greenland.
Acidity (pH)	Near-surface ocean acidity has been observed to increase (i.e., pH decrease) during the last decade in the Beaufort Sea and over the Canadian Polar Shelf.	Very likely increased ocean acidity due to rising atmospheric CO ₂ . Decrease in pH (0.1 - 0.2) and decreased saturation states for aragonite and calcite forms of CaCO ₃ .
Nutrients	The temporal and spatial coverage of data are insufficient to delineate trends across the Arctic LAB.	Likely no major changes in open ocean basins. Changes in nutrient inventories in coastal and shelf areas.

Risk Factors (variables)	Trends (past conditions)	Projections (next 50 years)
Lakes	Earlier ice break-up and later freeze-up (0.7 to 1.0 days in each direction per year) for northern Arctic lakes.	Likely increase in lake temperatures and stratification, earlier ice break-up and later freeze-up. Increase in evaporation, longer water renewal times and decline in oxygen levels with potential hypoxic conditions at the bottom. Some increase in primary production with shifts in community structure.
Rivers/Stream Flow	The temporal and spatial coverage of data are insufficient to delineate trends across the Arctic LAB. Increased runoff for Hudson Bay since early 1990s.	Likely increase in winter and fall flows (up to 50%) and reduction in summer flows. Lower and earlier spring freshets, regionally variable, depending on headwaters. Increase in annual discharge from Greenland ice sheet, but magnitude uncertain. River ice break-up 15 - 35 days earlier and freeze-up 10 - 12 days later.
Permafrost	There has been widespread warming of terrestrial permafrost during the last two decades as well as a thickening of the permafrost active layer during the same period. Slow warming of sub-sea permafrost (Beaufort Sea) reflects the flooding of the shelf with rising sea level at the end of the last Ice Age.	Very likely continued permafrost degradation and increase in active layer depth.
Snow depth (land and lakes)	The temporal and spatial coverage of data are insufficient to delineate trends across the Arctic LAB.	Likely decrease in snow depth.

Potential changes during the next 10 years are not included in the table, but may in some cases be pro-rated versions of the 50-year projection. However, in most instances, natural intradecadal variability is expected to be at least as important during the next decade. A continuation of trends during the last decade is expected in the case of ocean acidity, surface air temperature, multi-year sea ice extent, first-year sea ice characteristics, storm waves and permafrost. In addition to these comparatively continuous changes, the report also points out that if greenhouse gas emissions continue to rise at the current pace or even accelerate large changes in extremes

are to be expected. Even under moderate radiative forcing (RCP2.6), which is very likely an underestimate, increases in the lowest daily minimum temperatures in winter exceeding 3°C are projected for northern high latitudes.

As discussed repeatedly in this report, the Arctic is a large and multifaceted geographic region. This causes a variety of issues associated with access affecting scientific sampling. Data sets frequently contain spatial, temporal and seasonal gaps in data. Often, spot measurements (single sampling stations) are used to represent larger areas which they might not be representative for. This affects horizontal and vertical as well as temporal interpolations. Another important note is the difference in the variability of atmospheric (100s of km) and oceanic (~10 km) scales, affecting the representativeness of station locations and model grid cells. Misrepresentations also arise in cases where terrestrial station data are the only data available to represent marine areas. The temporal scarcity of data in the Arctic is further reflected in the lack of long-term monitoring data sets for many regions. Most time series are too short, especially for ecosystem variables, and interannual and interdecadal variability might mask long term trends. However, studies show strong links between environmental variables and primary production as well as higher trophic level growth, breeding success and survival. This suggests changes in environmental variables will likely be reflected in ecosystem variables.

While it was agreed to use at least 10 years of data in order to detect a trend, it needs to be pointed out that trends are often not consistent over 1, 2, 3 or more decades. These limitations severely affect a) the ability to accurately interpret trends (e.g. lacking baseline data makes it difficult to identify causes of the detected trend) and b) the ability to develop and to validate models and hence reduce the confidence in model projections of climate change impacts.

Projections of climate change impacts on the marine ecosystem are further limited by the fact that high resolution Arctic climate models are lacking. Global Climate Models (GCMs) are generally too coarsely resolved to adequately represent the complex structure represented in the Arctic LAB, especially in the ocean. IPCC AR5 Earth System Models now contain biogeochemical fields, however show large intermodel biases. These models allow a glimpse of the general tendency and range of expected future change, but no reliable local details. This gap is exacerbated by our inability to differentiate natural variability (seasonal, annual, multidecadal) from climate change and anthropogenic stressors in the system on shorter time scales. In the future (i.e., on the 50 year timescale), anthropogenic changes may become dominant over those changes associated with natural variability.

Higher resolution regional climate models are currently limited to the atmosphere and provide only limited coverage of the Arctic. Available basin-scale models for the ocean still show large uncertainties with respect to ocean variables as well as sea ice projections. However, the loss of sea ice and changes in sea ice morphology represent significant features and drivers for change in the Arctic. Many of the impacts on the environment and infrastructure are linked to how sea ice will change in the future. Basin scale model projections for the Arctic Ocean are extremely sparse and nonexistent for biogeochemical variables. Such models provide more regional information, however, at this point uncertainties are large.

We conclude that while this assessment is based on our best knowledge, it is by no means

conclusive. We will not be able to retroactively expand our data base for the last 5 decades but we recommend improving monitoring in current and future times to allow the establishment of better baseline data sets against which future change can be measured. Also, much improvement can and still needs to be made with respect to regional and basin scale modelling, both for physical and for biogeochemical variables, in the atmosphere, sea ice and ocean environments. On the other hand, this also constitutes an opportunity, allowing to obtain a better view on potential future changes and the range of these changes in specific areas of the Canadian Arctic.

5: ACKNOWLEDGEMENTS

This assessment was carried out as part of the climate trends and projections activities in DFO's Aquatic Climate Change Adaptation Service Program (ACCASP), with the objective of providing input to ACCASP risk assessments for the Arctic Large Aquatic Basin (LAB). We thank everybody who was involved in pulling together the vast amount of observational data that has been compiled for the trend section of this report.

Many of the model fields used for the projection section were obtained directly or indirectly from the Climate Model Intercomparison Project Phase 5 (CMIP5) of the Program for Climate Model Diagnosis and Intercomparison (PCMDI; <http://www-pcmdi.llnl.gov/>). The organizations that contributed the model fields to CMIP5 are gratefully acknowledged for their immense and important work in the development and running of the models, and making the fields available. We thank Jim Christian of DFO-IO for making available the ESM fields on a common grid and providing the carbon chemistry fields. Regional model output from CanRCM4 fields has been obtained directly from the Canadian Centre for Climate Modelling and Analysis (CCCMA) and we thank the CCCMA regional modelling team for all the work they put into the model development and data preparation. We especially acknowledge Yanjun Jiao and John Scinocca for sharing the model fields and for their support in the CanRCM4 evaluation. We also thank Philippe Gachon for his contribution to the CanRCM4 validation. Finally we would greatly acknowledge Lizette Beauchemin for her technical assistance in getting this report in publication ready format.

6: REFERENCES

- Alexander, L.V., Zhang, X., Peterson, T.C., Caesar, J., Gleason, B., Klein Tank, A.M.G., Haylock, M., Collins, D., Trewin, B., Rahimzadeh, F., Tagipour, A., Ambenje, P., Rupa Kumar, K., Revadekar, J. and Griffiths, G. 2006. Global observed changes in daily climate extremes of temperature and precipitation. *J. Geophys. Res. Atmos.* 111: D05109. doi:10.1029/2005JD006290.
- AMAP Assessment. 2013. Arctic Ocean Acidification. Arctic Monitoring and Assessment Programme (AMAP), Oslo, Norway.
- Amundrud, T.L., Melling, H., Ingram, R.G. and Allen, S.E. 2006. The effect of structural porosity on the melting of ridge keels in pack ice. *J. Geophys. Res.* 111: C06004. doi:10.1029/2005JC002895.

- Ardyna, M., Gosselin, M., Michel, C., Poulin, M. and Tremblay, J.É. 2011. Environmental forcing of phytoplankton community structure and function in the Canadian High Arctic: contrasting oligotrophic and eutrophic regions. *Mar. Ecol. Prog. Ser.* 442: 37-57.
- Arnell, N.W. 2005. Implications of climate change for freshwater inflows to the Arctic Ocean. *J. Geophys. Res. – Atmos.* 110: D07105.
- Arora, V.K., Scinocca, J.F., Boer, G.J., Christian, J.R., Denman, K.L., Flato, G.M., Kharin, V.V., Lee, W.G. and Merryfield, W.J. 2011. Carbon emission limits required to satisfy future representative concentration pathways of greenhouse gases. *Geophys. Res. Lett.* 38. doi:10.1029/2010GL046270.
- Arrigo, K.R. and van Dijken, G.L. 2011. Secular trends in Arctic Ocean net primary production. *J. Geophys. Res.* 116: C09011.
- Arrigo, K.R., van Dijken, G. and Pabi, S. 2008. Impact of a shrinking Arctic ice cover on marine primary production. *Geophys. Res. Lett.* 35: L19603.
- Ashton, G.D. 2003. Ice jam flooding on the Peace River near the Peace-Athabasca Delta. Canadian Water Resources Association 56th Annual Conference, 11-13 June 2003. Vancouver, BC. pp. 315-323.
- Atkinson, D.E. 2005. Observed storminess patterns and trends in the circum-Arctic coastal regime. *Geo-Mar. Lett.* 25: 98–109. doi:10.1007/s00367-004-0191-0.
- Atkinson, D.E., Brown, R., Alt, B., Agnew, T., Bourgeois, J., Burgess, M., Duguay, C., Henry, G., Jeffers, S., Koerner, R., Lewkowicz, A.G., McCourt, S., Melling, H., Sharp, M., Smith, S., Walker, A., Wilson, K., Wolfe, S., Woo, M-k. and Young, K.L. 2006. Canadian cryospheric response to an anomalous warm summer: A synthesis of the climate change action fund project “the state of the arctic cryosphere during the extreme warm summer of 1998. *Atmos. Ocean.* 44: 347-375.
- Azetsu-Scott, K., Slauenwhite, D. and Starr, M. 2008. Freshwater and Carbon Dynamics in Hudson Bay: Results from Merica 2003-2006. ArcticNet Scientific Meeting 2008, Quebec City, Quebec.
- Azetsu-Scott, K., Clarke, A., Falkner, K.K., Hamilton, J., Jones, E.P., Lee, C., Petrie, B., Prinsenber, S., Starr, M. and Yeats, P. 2010. Calcium carbonate saturation states in the waters of the Canadian Arctic Archipelago and the Labrador Sea. *J. Geophys. Res.* 115: C11021. doi:10.1029/2009JC005917.
- Aziz, O.I.A. and Burn, D.H. 2006. Trends and variability in the hydrological regime of the Mackenzie River Basin. *J. Hydrology.* 319: 282-294.
- Bamber, J., van den Broeke, M., Ettema, J., Lenaerts, J. and Rignot, E. 2012. Recent large increases in freshwater fluxes from Greenland into the North Atlantic. *Geophys. Res. Lett.* 39: L19501. doi:10.1029/2012GL052552.

- Barber, D.G. and Massom, R.A. 2007. The Role of Sea Ice in Arctic and Antarctic Polynyas. Elsevier Oceanography Series. 74: 1-54.
- Barnier, B., Madec, G., Penduff, T., Molines, J-M., Treguier, A-M., Le Sommer, J., Beckmann, A., Boning, C., Dengg, J., Derval, C., Durand, E., Gulev, S., Remy, E., Talandier, C., Theerren, S., Maltrud, M., McClean, J. and de Cuevas, B. 2006. Impact of partial steps and momentum advection schemes in a global ocean circulation model at eddy-permitting resolution. *Ocean Dynamics*. 56(5-6): 543-567. [doi:10.1007/s10236-006-0082-1](https://doi.org/10.1007/s10236-006-0082-1).
- Bates, N. and Mathis, J. 2009. The Arctic ocean marine carbon cycle: Evaluation of air-sea CO₂ exchanges, ocean acidification impacts and potential feedbacks. *Biogeosciences*. 6: 2433–2459.
- Bates, N.R., Cai, W.J. and Mathis, J.T. 2011. The ocean carbon cycle in the western Arctic Ocean: Distributions and air-sea fluxes of carbon dioxide. *Oceanogr*. 24: 186-201.
- Biaostoch, A., Treude, T., Rüpke, L.H., Riebesell, U., Roth, C., Burwicz, E.B., Park, W., Latif, M., Böning, C.W., Madec, G. and Wallmann, K. 2011. Rising Arctic Ocean temperatures cause gas hydrate destabilization and ocean acidification. *Geophys. Res. Lett.* 38: L08602. [doi:10.1029/2011GL047222](https://doi.org/10.1029/2011GL047222).
- Bill, L., Crozier, J. and Surrendi, D. 1996. A report of wisdom synthesized from the traditional knowledge component studies. Northern River Basins Study Synthesis Report 12. 366 p.
- Boer, G.J., Flato, G. and Ramsden, D. 2000. A Transient Climate Change Simulation with Greenhouse Gas and Aerosol Forcing: Projected Climate to the Twenty-First Century. *Climate Dyn*. 16: 427-450.
- Booth, B.B., Dunstone, N.J., Halloran, P.R., Andrews, T. and Bellouin, N. 2012. Aerosols implicated as a prime driver of twentieth-century North Atlantic climate variability. *Nature*. 484(7393): 228-32. [doi:10.1038/nature10946](https://doi.org/10.1038/nature10946).
- Bouchard, C. and Fortier, L. 2011. Circum-arctic comparison of the hatching season of polar cod *Boreogadus saida*: A test of the freshwater winter refuge hypothesis. *Prog. Oceanogr*. 90: 105-116.
- Bracegirdle, T.J. and Stephenson, D.B. 2012: Higher precision estimates of regional polar warming by ensemble regression of climate model projections. *Climate Dyn*. 39: 2805–2821. [doi:10.1007/s00382-012-1330-3](https://doi.org/10.1007/s00382-012-1330-3).
- Bracegirdle, T.J. and Stephenson, D.B. 2013. On the Robustness of Emergent Constraints Used in Multimodel Climate Change Projections of Arctic Warming. *J. Climate*. 26: 669-678. [doi:10.1175/JCLI-D-12-00537.1](https://doi.org/10.1175/JCLI-D-12-00537.1)
- Brock, B.E., Martin, M.E., Mongeon, C.L., Sokal, M.A., Wesche, S.D., Armitage, D., Wolfe, B.B., Hall, R.I. and Edwards, T.W.D. 2010. Flood Frequency Variability during the Past 80 Years in the Slave River Delta, NWT, as determined from Multi-Proxy Paleolimnological Analysis. *Canadian Water Resources Journal*. 35: 281-300.

- Brovkin, V., Boysen, L., Raddatz, T., Gayler, V., Loew, A. and Claussen, M. 2013. Evaluation of vegetation cover and land-surface albedo in MPI-ESM CMIP5 simulations. *J. Adv. Model Earth Syst.* 5(1): 48-57. doi:10.1029/2012MS000169.
- Brown, R.D. and Côté, P. 1992. Inter-annual variability of land-fast ice thickness in the Canadian High Arctic, 1950-89. *Arctic.* 45: 273-284.
- Brown, R.D. and Braaten, R.O. 1998. Spatial and temporal variability of Canadian monthly snow depths, 1946-1995. *Atmos. Ocean.* 36(1): 37-54.
- Brown, R.D., Demuth, M.N., Goodison, B.E., Marsh, P., Prowse, T.D., Smith, S.L. and Woo, M.K. 2004. Climate variability and change cryosphere. *In Threats to Water Availability in Canada.* Environment Canada, Meteorological Service of Canada, National Water Research Institute, NWRI Scientific Assessment Report Series No. 3: 107-116.
- Bürger, G., Murdock, T.Q., Werner, A.T., Sobie, S.R. and Cannon, A.J. 2012. Downscaling extremes—An intercomparison of multiple statistical methods for present climate. *J. Climate.* 25: 4366-4388. doi:10.1175/JCLI-D-11-00408.1.
- Burn, C.R. and Kokelj, S.V. 2009. The environment and permafrost of the Mackenzie Delta area. *Permafrost and Periglacial Processes.* 20: 83-105.
- Burn, D.H., AbdulAziz, O.I. and Pietroniro, A. 2004a. A Comparison of Trends in Hydrological Variables for Two Watersheds in the Mackenzie River Basin. *Canadian Water Resources Journal.* 29: 283-298.
- Burn, D.H., Cunderlik, J.M. and Pietroniro, A. 2004b. Hydrological trends and variability in the Liard River basin. *Hydrolog. Sci. J.* 49(1): 53-67.
- Cai, W.-J., Chen, L., Chen, B., Gao, Z., Lee, S.H., Chen, J., Pierrot, D., Sullivan, K., Wang, Y., Hu, X., Huang, W.J., Zhang, Y., Xu, S., Murata, A., Grebmeier, J.M., Jones, E.P. and Zhang, H. 2010. Decrease in the CO₂ uptake capacity in an ice-free Arctic ocean basin. *Science.* 329: 5991. doi:10.1126/science.1189338.
- Canadian Ice Service (CIS). 2002. *Sea Ice Climatic Atlas-Northern Canadian Waters 1971-2000.* Ottawa, Ont. 995 p.
- Carmack, E. and McLaughlin, F. 2011. Towards recognition of physical and geochemical change in Subarctic and Arctic Seas. *Prog. Oceanogr.* 90: 90-104.
- Cavalieri, D.J. and Parkinson, C.L. 2012. Arctic sea ice variability and trends, 1979-2010. *The Cryosphere.* 6: 881-889. doi:10.5194/tc-6-881-2012.
- Chassé, J., Lambert, N. and Lavoie, D. 2013. Precipitation and Freshwater Flux over Canada from six Global Climate Models. *Can. Tech. Rep. Hydrog. Ocean. Sci.* In press.

- Chierici, M. and Fransson, A. 2009. Calcium carbonate saturation in the surface water of the Arctic Ocean: Undersaturation in freshwater influenced shelves. *Biogeosciences*. 6: 2421-2432.
- Christian, J.R. and Foreman, M.G.G. 2013. Climate trends and projections for the Pacific Large Aquatic Basin. *Can. Tech. Rep. Fish. Aquat. Sci.* 3032: xi + 113 p.
- Christian, J., Arora, V., Boer, G., Curry, C., Zahariev, K., Denman, K., Flato, G., Lee, W., Merryfield, W., Roulet, N. and Scinocca, J. 2010. The global carbon cycle in the Canadian Earth System Model (CanESM1): Preindustrial control simulation, *Journal of Geophysical Research*. 115. doi:10.1029/2008JG000920.
- Crane, R.G. 1978. Seasonal variations of sea ice extent in the Davis Strait-Labrador Sea area and relationships with synoptic-scale atmospheric circulation. *Arctic*. 31: 434–447.
- CCCSN (Canadian Climate Change Scenarios Network). 2009. Ensemble Scenarios for Canada. 2009. Edited by Comer, N. Canadian Climate Change Scenarios Network (CCCSN.CA). Adaptation and Impacts Research Division, Environment Canada.
- Cohen, S.J. 1997. What if and so what in northwest Canada: Could climate change make a difference to the future of the Mackenzie Basin? *Arctic*. 50: 293-307.
- Collins, M., Chandler, R.E., Cox, P.M., Huthnance, J.M., Rougier, J. and Stephenson, D.B. 2012. Quantifying future climate change. *Nat. Climate Change*. 2: 403–409. doi:10.1038/nclimate1414.
- Coumou, D. and Rahmstorf, S. 2012. A decade of weather extremes. *Nature Climate Change*. 2: 491–496. doi:10.1038/nclimate1452.
- Craymer, M, Henton, J. and Piraszewski, M. 2006. Sea level change and vertical crustal motion in the Canadian Arctic using GPS and tide gauges: Challenges and preliminary results. *Eos Transactions. AGU*. 87(52). Fall Meeting Supplement G23B-1288.
- Culp, J.M., Cash, K.J. and Wrona, F.J. 2000. Cumulative effects assessment for the Northern River Basins Study. *J. Aquat. Ecosys. Stress Recov.* 8: 87-94.
- Culp, J.M., Prowse, T.D. and Luiker, E.A. 2005. Mackenzie River Basin. *In Rivers of North America*. Edited by Benke A.C. and Cushing C.E. Elsevier Academic Press, Burlington, MA. pp. 805-837.
- Cuny, J., Rhines, P.B. and Kwok, R. 2005. Davis Strait volume, freshwater and heat fluxes. *Deep Sea Res.* 52: 519–542.
- Curry, B., Lee, C.M. and Petrie, B. 2011. Volume, freshwater, and heat fluxes through Davis Strait, 2004-2005. *J. Phys. Oceanogr.* 41: 429-436.
- Cushing, C.E., Cummins, K.E. and Minshall, G.W. (eds.). 2006. River and stream ecosystems of the world. University of California Press, Berkeley, CA. 817 p.

- Darnis, G., Robert, D., Pomerleau, C., Link, H., Archambault, P., Nelson, R.J., Geoffroy, M., Tremblay, J.E., Lovejoy, C., Ferguson, S.H., Hunt, B.P.V. and Fortier, L. 2012. Current state and trends in Canadian Arctic marine ecosystems: II. Heterotrophic food web, pelagic-benthic coupling and biodiversity. *Clim Change*. 115: 179–205. doi:10.1007/s10584-012-0483-8.
- Deal, C. J., Steiner, N., Christian, J., Kinney, J.C., Denman, K., Elliott, S., Gibson, G., Jin, M., Lavoie, D., Lee, S., Lee, W., Maslowski, W., Wang, J. and Watanabe, E. 2013. Progress and challenges in biogeochemical modeling of the Pacific Arctic region. *In The Pacific Arctic Region: Ecosystem Status and Trends in a Rapidly Changing Environment*. Edited by Grebmeier J. and Maslowski, W. Springer, New York. In press.
- Denman, K.L., Brasseur, G., Chidthaisong, A., Ciais, P., Cox, P., Dickinson, R.E., Haugustaine, D., Heinze, C., Holland, E., Jacob, D., Lohmann, U., Ramachandran, S., daSilvaDias, P.L., Wofsy, S.C. and Zhang, X. 2007. Couplings between changes in the climate system and biogeochemistry. *In Climate Change 2007: The Physical Science Basis. Contribution of Working Group I to the Fourth Assessment Report of the Intergovernmental Panel on Climate Change*. Edited by Solomon, S., Qin, D., Manning, M., Chen, Z., Marquis, M., Averyt, K.B., Tignor, M. and Miller, H.L. Cambridge University Press, Cambridge, United Kingdom and New York, NY, USA. pp. 499-587.
- Denman, K., Christian, J.R., Steiner, N., Pörtner, H-O. and Nojiri, Y. 2011. Potential impacts of future ocean acidification on marine ecosystems and fisheries: current knowledge and recommendations for future research. *ICES Journal of Marine Science*. 68: 1019–1029. doi:10.1093/icesjms/fsr074.
- Déry, S.J. and Wood, E.F. 2004. Teleconnection between the Arctic Oscillation and Hudson Bay river discharge. *Geophys. Res. Lett.* 31: L18205.
- Déry, S.J., Stieglitz, M., McKenna, E.C. and Wood, E.F. 2005. Characteristics and trends of river discharge into Hudson, James, and Ungava Bays, 1964-2000. *J. Climate*. 18: 2540-2557.
- Déry, S.J., Hernandez-Henriquez, M.A, Burford, J.E. and Wood, E.F. 2009. Observational evidence of an intensifying hydrological cycle in northern Canada. *Geophys. Res. Lett.* 36.
- Déry, S.J., Mlynowski, T.J., Hernández-Henríquez, M.A. and Straneo, F. 2011. Interannual variability and interdecadal trends in Hudson Bay streamflow. *J. Marine Syst.* 88: 341-351.
- Deser, C., Walsh, J.E. and Timlin, M.S. 2000. Arctic sea ice variability in the context of recent wintertime atmospheric circulation trends. *J. Climate*. 13: 617–633.
- DFO. 2013. Risk-based assessment of climate change impacts and risks on the biological systems and infrastructure within Fisheries and Oceans Canada's mandate - Arctic Large Aquatic Basin. DFO Can. Sci. Advis. Sec. Sci. Resp. 2012/042.
- Dickson, A., Sabine, C. and Christian, J. 2007. Guide to best practices for ocean CO₂ measurements. PICES Special Publication 3. 191 p.

- Diemand, D. 2001. Icebergs. *In* Encyclopedia of Ocean Sciences. Edited by Steele, J.H., Thorpe, S.A. and Turekian, K.K. 2nd Edition Academic Press. 3399 p.
- Drinkwater, K.F. 2004. Atmospheric and sea ice conditions in the Northwest Atlantic during the decade, 1991-2000. *Journal of Northwestern Atlantic Fisheries Science*. 34: 1-11.
- Dumas, J.A., Flato, G.M. and Brown, R.D. 2006. Future projections of landfast ice thickness and duration in the Canadian Arctic. *J. Climate*. 19(20): 5175-5189.
- Dunbar, M.J. and Moore, D.M. 1980. Marine life and its environment in the Canadian Eastern Arctic: A biogeographic study. Marine Science Centre Manuscript No. 33. McGill University, Montreal.
- Dunne, J.P., John, J., Adcroft, A., Gries, S., Hallberg, R., Shevliakova, E., Stoufer, R., Cooke, W., Dunne, K., Harrison, M., Krasting, J., Malyshev, S., Milly, P., Phillipps, P., Sentman, L., Samuels, B., Spelman, M.J., Winton, M., Wittenberg, A. and Zadeh, N. 2012. GFDL's ESM2 global coupled climate-carbon earth system models. Part I: Physical formulation and baseline simulation characteristics. *Journal of Climate*. 25: 6646-6665.
- Dyke, L.D., Aylsworth, J.M., Burgess, M.M., Nixon, F.M. and Wright, F. 1997. Permafrost in the Mackenzie Basin, its influence on land-altering processes, and its relationship to climate change. *Mackenzie Basin Impact Study: Final report*. pp.112-117.
- EC (Environment Canada). 2004. Threats to Water Availability. Canada. National Water Research Institute, Burlington, Ontario. NWRI Scientific Assessment Report Series No. 3 and ACSD Science Assessment Series No. 1. 128 p.
- EDI. 2006. Peel River Watershed Fisheries Information Summary Report, Preliminary Assessment. Edi Environmental Dynamics Inc. Whitehorse, YT EDI Project #: 06-YC-0011.
- Else, B.G.T., Papakyriakou, T.N., Granskog, M.A. and Yackel, J.J. 2008a. Observations of sea surface fCO₂ distributions and estimated air-sea CO₂ fluxes in the Hudson Bay region (Canada) during the open water season. *J. Geophys. Res.-Oceans*. 113: C08026.
- Else, B.G.T., Yackel, J.J. and Papakyriakou, T.N. 2008b. Application of satellite remote sensing techniques for estimating air-sea CO₂ fluxes in Hudson Bay, Canada during the ice-free season. *Remote Sens Environ*. 112: 3550-3562.
- Emori, S., Nozawa, T., Abe-Ouchi, A., Numaguti, A., Kimoto, M. and Nakajima, T. 1999. Coupled Ocean-Atmosphere Model Experiments of Future Climate Change with an Explicit Representation of Sulfate Aerosol Scattering. *Journal of Meteorological Society, Japan* 77: 1299-1307.
- Environment Canada Climate Trends and Variations dataset AHCCD (Adjusted and Homogenized Canadian Climate Data. <http://ec.gc.ca/dccha-ahccd/default.asp?lang=En&n=B1F8423A-1>).

- Estrada, R., Harvey, M., Gosselin, M., Starr, M., Galbraith, P.S. and Straneo, F. 2012. Late-summer zooplankton community structure, abundance, and distribution in the Hudson Bay system (Canada) and their relationships with environmental conditions, 2003–2006. *Prog. Oceanogr.* 101(1): 121–145.
- Eum, H.-I., Gachon, P., Laprise, R. and T. Ouarda, T. 2012: Evaluation of regional climate model simulations versus gridded observed and regional reanalysis products using a combined weighting scheme. *Climate Dynamics.* 38(7-8): 1433-1457. doi:10.1007/s00382-011-1149.
- Ferguson, S., Berteaux, D., Gaston, A., Higdon, J., Lecomte, N., Lunn, N., Mallory, M., Reist, J., Russell, D., Yoccoz, N. and Zhu, X. 2012. *Climatic Change.* 115: 235–258. doi:10.1007/s10584-012-0476-7.
- Ferland, J., Gosselin, M. and Starr, M. 2011. Environmental control of summer primary production in the Hudson Bay system: The role of stratification. *J. Marine Syst.* 88: 385-400.
- Fichefet, T. and Maqueda Morales, M.A. 1997. Sensitivity of a global sea ice model to the treatment of ice thermodynamics and dynamics. *J. Geophys. Res.* 102(C6): 12609-12646. doi:10.1029/97JC00480.
- Fissel, D.B. and Melling, H. 1990. Inter-annual Variability of Oceanographic Conditions in the Southeastern Beaufort Sea. *Can. Contr. Rep. Hydrogr. Oc. Sc.* 35. 102 p.
- Flanagan, K.M., McCauley, E., Wrona, F. and Prowse T. 2003. Climate change: the potential for latitudinal effects on algal biomass in aquatic ecosystems. *Can. J. Fish. Aquat. Sci.* 60: 635-639.
- Flato, G.M. and Boer, G.J. 2001. Warming asymmetry in climate change simulations. *Geophys. Res. Lett.* 28: 195-198. <http://dx.doi.org/10.1029/2000GL012121> (accessed 20 May 2013).
- Foster, T.T. 1972. Haline convection in polynyas and leads. *J. Phys. Oceanogr.* 2: 462-469.
- Francis, O.P., Panteleev, G.G. and Atkinson, D.E. 2011. Ocean wave conditions in the Chukchi Sea from satellite and in situ observations *Geophys. Res. Lett.* 38: L24610. doi:10.1029/2011GL049839.
- Friedlingstein, P., Cox, P., Betts, R., Bopp, L., von Bloh, W., Brovkin, V., Cadule, P., Doney, S., Eby, M., Fung, I., Bala, G., John, J., Jones, C., Joos, F., Kato, T., Kawamiya, M., Knorr, W., Lindsay, K., Matthews, H.D., Raddatz, T., Rayner, P., Reick, C., Roeckner, E., Schnitzler, K.-G., Schnur, R., Strassmann, K., Weaver, A.J., Yoshikawa, C. and Zeng, N. 2006. Climate carbon cycle feedback analysis: Results from the C4MIP Model Intercomparison. *Journal of Climate.* 19(14): 3337-3353.
- Frierson, D.M.W. 2006: Robust increases in midlatitude static stability in simulations of global warming. *Geophys. Res. Lett.* 33: L24816. doi:10.1029/2006GL027504.

- Frich, P., Alexander, L.V., Della-Marta, P., Gleason, B., Haylock, M., Klein Tank, A.M.G. and Peterson, T. 2002. Observed coherent changes in climatic extremes during the second half of the twentieth century. *Clim. Res.* 19: 193–212. doi:10.3354/cr019193.
- Furgal, R., Prowse, T.D., Bonsal, B., Chouinard, R., Dickson, C., Edwards, T., Jackson, F., Melling, H., Milburn, D., Nickels, S., Nuttal, M., Ogden, A., Peters, D., Reist, J.D., Smith, S., Westlake, M. and Wrona, F. 2008. Northern Canada. *In* Impacts to adaptation: Canada in a changing climate 2007. Edited by Lemmen, D.S., Warren, F.J., Lacroix, J. and Bush, E. Government of Canada, Ottawa, ON. Chapter 3. pp. 57-118.
- Gagnon, A.S. and Gough, W.A. 2005. Trends in the dates of ice freeze-up and break-up over Hudson Bay, Canada. *Arctic.* 58: 370-382.
- Galbraith, P.S. and Larouche, P. 2011. Sea-surface temperature in Hudson Bay and Hudson Strait in relation to air temperature and ice cover break-up, 1985-2009. *J. Marine Syst.* 87: 66-78.
- Gattuso, J.-P. and Hansson, L. (eds.). 2011. Ocean acidification. Oxford University Press, New York. 352 p.
- Gearheard, S., Matumeak, W., Angutikjuaq, I., Maslanik, J., Huntington, H.P., Leavitt, J., Kagak, D.M., Tigullaraq, G. and Barry, R.G. 2006. “It’s not that simple”: a collaborative comparison of sea ice environments, their uses, observed changes, and adaptations in Barrow, Alaska, USA, and Clyde River, Nunavut, Canada. *Ambio.* 35: 203–211.
- Gibson, J.J., Prowse, T.D. and Peters, D.L. 2006. Partitioning impacts of climate and regulation on water level variability in Great Slave Lake. *J. Hydrology.* 329: 196-206.
- Giles, K., Laxon, S. and Ridout, A. 2008. Circumpolar thinning of Arctic sea ice following the 2007 record ice extent minimum. *Geophys. Res. Lett.* 35(22): L22502. doi:10.1029/2008GL035710.
- Gill, A.E. 1982. *Atmos. Ocean Dynamics.* Academic Press Inc. London, UK. 662 p.
- Gillett, N.P., Stone, D.A., Stott, P.A., Nozawa, T., Karpechko, A.Y., Hegerl, G.C., Wehner, M.F., and Jones, P.D. 2008. Attribution of polar warming to human influence. *Nature Geoscience.* 1: 750–754. doi:10.1038/ngeo338.
- Gleckler, P.J., Taylor, K.E. and Doutriaux, C. 2008. Performance metrics for climate models. *J. Geophys. Res.* 113: D06104. doi:10.1029/2007JD008972.
- González-Dávila, M., Santana-Casiano, M. and González-Dávila, E. 2007. Interannual variability of the upper ocean carbon cycle in the northeast Atlantic Ocean. *Geophys. Res. Lett.* 34: L07608. doi:10.1029/2006GL028145.
- Goodison, B.E., Brown, R.D. and Crane, R.G. 1999. Cryospheric Systems. *In*: EOS Science Plan, Chapter 6, National Aeronautics and Space Administration. pp. 261-307.

- Gordon, C., Cooper, C., Senior, C.A, Banks, H., Gregory, J.M., Johns, T.C., Mitchell, J.F.B. and Wood, R. 2000. The simulation of SST, sea ice extents and ocean heat transports in a version of the Hadley Centre coupled model without flux adjustments. *Climate Dyn.* 16: 47-168.
- Gough, W.A. and Wolfe, E. 2001. Climate change scenarios for Hudson Bay, Canada, from general circulation models. *Arctic.* 54: 142-148.
- Granskog, M.A., Macdonald, R.W., Mundy, C.J. and Barber, D.G. 2007. Distribution, characteristics and potential impacts of chromophoric dissolved organic matter (CDOM) in Hudson Strait and Hudson Bay, Canada. *Cont. Shelf Res.* 27: 2032-2050.
- Granskog, M.A., Macdonald, R.W., Kuzyk, Z.Z.A., Senneville, S., Mundy, C.J., Barber, D.G., Stern, G.A. and Saucier, F. 2009. Coastal conduit in southwestern Hudson Bay (Canada) in summer: Rapid transit of freshwater and significant loss of colored dissolved organic matter. *J. Geophys. Res.-Oceans.* 114: C08012.
- Granskog, M.A., Kuzyk, Z.Z.A., Azetsu-Scott, K. and Macdonald, R.W. 2011. Distributions of runoff, sea ice melt and brine using $\delta^{18}\text{O}$ and salinity data - A new view on freshwater cycling in Hudson Bay. *J. Marine Syst.* 88: 362-374.
- Gray, D.M. and Prowse, T.D. 1993. Snow and floating ice. *In Handbook of Hydrology.* Edited by Maidment, D.R. McGraw-Hill, New York, NY. pp. 7.1-7.58.
- Greenan, B., Harrison, G., Yashayaev, I., Azetsu-Scott, K., Head, E., Li, W. and Loder, J. 2010. Physical, Chemical, and Biological Conditions in the Labrador Sea in 2009. *AZMP Bulletin.* 9: 11-19. (Accessed June 28, 2013).
- Hamilton, J.M. and Wu, Y. 2013. Synopsis and trends in the physical environment of Baffin Bay and Davis Strait. *Can. Tech. Rep. Hydrogr. Ocean Sci.* 282: vi + 39 p.
- Hanna, E., Huybrechts, P., Steffen, K., Cappelen, J., Huff, R., Shuman, C., Irvine-Fynn, T., Wise, S. and Griffiths, M. 2008. Increased runoff from melt from the Greenland ice sheet: A response to global warming. *J. Climate.* 21: 331–341.
- Harvey, M., Therriault, J.C. and Simard, N. 1997. Late-summer distribution of phytoplankton in relation to water mass characteristics in Hudson Bay and Hudson Strait (Canada). *Can. J. Fish. Aquat. Sci.* 54: 1937-1952.
- Harvey, M., Starr, M., Therriault, J.-C., Saucier, F.J. and Gosselin, M. 2006. MERICA-Nord Program: Monitoring and research in the Hudson Bay Complex. *AZMP Bulletin PMZA.* 5: 27-32.
- Harwood, L.A. 2009. Status of anadromous Arctic charr (*Salvelinus alpinus*) of the Hornaday River, Northwest Territories, as assessed through harvest-based sampling of the subsistence fishery, August-September 1990-2007. *Can. Manuscr. Rep. Fish. Aquat. Sci.* 2890: viii + 33 p.

- Harwood, L.A., Smith, T.G. and Melling, H. 2000. Variation in reproduction and body condition of the ringed seal (*Phoca hispida*) in western Prince Albert Sound (NT Canada) as assessed through a harvest-based sampling program. *Arctic*. 53(4): 422-431.
- Harwood, L.A., Smith, T.G., Melling, H., Alikamik, J. and Kingsley, M.C.S. 2012. Ringed seals and sea ice in Canada's Western Arctic: harvest-based monitoring 1992-2011. *Arctic*. 65: 377-390.
- Harwood, L.A., Sandstrom, S.J., Pabst, M.H. and Melling, H. 2013. Kuujjua River Arctic char: Monitoring stock trends using catches from an under-ice subsistence fishery, Victoria Island, Northwest Territories Canada 1991-2009. *Arctic*. In press.
- Hawkins, E. and Sutton, R. 2009. The potential to narrow uncertainty in regional climate predictions. *Bull. Amer. Meteor. Soc.* 90: 1095–1107.
- Herron, T., Craymer, M., Leyzack, A. and Robinson, C. 2008. Monitoring changes in mean sea level across the Arctic with tide gauges and GPS receivers. *Proc. Can. Hydrogr. Conf. & Nat. Survey Conf. 2008. Poster P4-3.*
http://hydrography.ca/assets/files/2008conference/session_4/P4-3_Herron_et_al.pdf
(accessed 20 May, 2013).
- Henry, M. 2011. Sea ice trends in Canada. *Statistics Canada Environstats Bulletin*. 5(4). Catalogue no. 16-002-X.
- Hill, V. and Cota, G. 2005. Spatial patterns of primary production on the shelf, slope and basin of the Western Arctic in 2002. *Deep-Sea Res.* 52: 3344-3354.
- Hochheim, K.P. and Barber, D.G. 2010. Atmospheric forcing of sea ice in Hudson Bay during the fall period, 1980-2005. *J. Geophys. Res.-Oceans*. 115: C05009.
- Hochheim, K.P., Lukovich, J.V. and Barber, D.G. 2011. Atmospheric forcing of sea ice in Hudson Bay during the spring period, 1980-2005. *J. Marine Syst.* 88: 476-487.
- Holland, M., Bitz, C. and Tremblay, B. 2006. Future abrupt reductions in the summer Arctic sea ice. *Geophys. Res. Lett.* 33(23): L23503. doi:10.1029/2006GL028024.
- Holland, M.M., Finnis, J., Barrett, A.P. and Serreze, M.C. 2007. Projected changes in arctic ocean freshwater budgets. *J. Geophys. Res.-Biogeosciences*. 112: G04s55.
- Howell, S.E.L., Brown, L.C., Kang, K. and Duguay, C. R. 2009. Variability in ice phenology on Great Bear Lake and Great Slave Lake, Northwest Territories, Canada, from SeaWinds/QuikSCAT: 2000-2006. *Remote Sens. Environ.* 113: 816-834.
- Xianmin, H. and Myers, P.G. 2013. A Lagrangian View of Pacific Water Inflow Pathways in the Arctic Ocean during Model Spin-Up. *Ocean Modelling*. In press.

- Hutchinson, M, Mckenney, D.W., Lawrence, K. and Pedlar, J.H. 2009: Development and testing of Canada-wide interpolated spatial models of daily minimum–maximum temperature and precipitation for 1961–2003. *J. Appl. Meteorol. Climatol.* 48: 725–741.
- Hudak, D.R. and Young, J.M.C. 2002. Storm climatology of the southern Beaufort Sea. *Atmos-Oceans.* 40: 145-158.
- Hudson, E. 1997. The climate of the Peace, Athabasca and Slave River basins. Report no. 124. Northern River Basins Study, Edmonton, Alberta.
- Hunke, E.C. and Dukowicz, J.K. 1997. An elastic-viscous-plastic model for sea ice dynamics. *J. Phys. Oceanogr.* 27(9): 1849-1867.
[http://dx.doi.org/10.1175/1520-0485\(1997\)027<1849:AEVPMF>2.0.CO;2](http://dx.doi.org/10.1175/1520-0485(1997)027<1849:AEVPMF>2.0.CO;2) (accessed 20 May, 2013).
- IPCC (Intergovernmental Panel on Climate Change). 2000. Special report on emissions scenarios. Edited by Nakicenovic, N. and Swart, R. Cambridge University Press, Cambridge, UK. 570 p.
- IPCC (Intergovernmental Panel on Climate Change) 2001. Climate change 2001: the scientific basis. *In* Contribution of Working Group I to the Third Assessment Report of the Intergovernmental Panel on Climate Change. Edited by Houghton, J.T., Ding, Y., Griggs, D.J., Noguer, M., van der Linden, P.J., Dai, X., Maskell, K. and Johnson. C.A. Cambridge University Press, Cambridge, UK. 881 p.
- IPCC. 2007. Summary for Policymakers. *In*: Climate Change 2007: The Physical Science Basis. Contribution of Working Group I to the Fourth Assessment Report of the Intergovernmental Panel on Climate Change. Edited by Solomon, S., Qin, D., Manning, M., Chen, Z., Marquis, M., Averyt, K.B., Tignor, M. and Miller, H.L. Cambridge University Press, Cambridge, United Kingdom and New York, NY, USA
- IPCC. 2012. Managing the Risks of Extreme Events and Disasters to Advance Climate Change Adaptation. A Special Report of Working Groups I and II of the Intergovernmental Panel on Climate Change. Cambridge University Press, Cambridge, UK, and New York, NY, USA. 582 p.
- James, T.S., Simon, K.M., Forbes, D.L., Dyke, A.S. and Mate, D.J. 2011. Sea-level projections for Five Pilot Communities of the Nunavut Climate Change Partnership. Geological Survey of Canada Open File 6715. 23 p.
- Jensen, H.M., Pedersen, L., Burmeister, A. and Hansen, B.W. 1999. Pelagic primary production during summer along 65 to 72 degrees N off West Greenland. *Polar Biology.* 21: 269-278.
- Jones, E.P., Dryssen, D. and Coote, A.R. 1984. Nutrient regeneration in deep Baffin Bay with consequences for measurements of the conservative tracer NO and fossil fuel CO₂ in the oceans. *Can. J. Fish. Aquat. Sci.* 41: 30–35.

- Jones, E.P., Swift, J.H., Anderson, L.G., Civitarese, G., Falkner, K.K., Kattner, G., Lipizer, M., McLaughlin, F. and Olafsson, J. 2003. Tracing Pacific water in the North Atlantic Ocean. *J. Geophys. Res.* 108: 3116.
- Joos, F., Frölicher, T.L.M., Steinacher, M. and Plattner, G.-K. 2011. Impact of climate change mitigation on ocean acidification projections. *In Ocean Acidification*. Edited by Gattuso, J.-P. and Hansson, L. Oxford University Press, New York, USA. pp. 272-290.
- Kang, K.K., Duguay, C.R. and Howell, S.E.L. 2012. Estimating ice phenology on large northern lakes from AMSR-E: algorithm development and application to Great Bear Lake and Great Slave Lake, Canada. *The Cryosphere*. 6: 235-254.
- Kerr, J. 1998. Future Water Levels and Flows for Great Slave and Great Bear Lakes, Mackenzie River and Mackenzie Delta. *In Mackenzie Basin Impact Study (MBIS)*. Edited by Cohen, S. Environment Canada, No. En 50-118/7997-IE: 73-97.
- Kiktev, D., Sexton, D.M.H., Alexander, L. and Folland, C.K. 2003. Comparison of modeled and observed trends in indices of daily climate extremes. *J. Climate*. 16: 3560–3571. doi:10.1175/1520-0442(2003).
- Klein Tank, A.M.G., Zwiers, F.W. and Zhang, X. 2009. Guidelines on analysis of extremes in a changing climate in support of informed decisions for adaptation, Climate data and monitoring. WCDMP-No. 72, WMO-TD No. 1500. 56 p.
- Kopp, R.E., Mitrovica, J.X., Griffies, S.M., Yin, J., Hay, C.C. and Stouffer, R.J. 2010. The impact of Greenland melt on local sea levels: A partially coupled analysis of dynamic and static equilibrium effects in idealized water-hosing experiments. *Clim Ch.* 103: 619–625. doi:10.1007/s10584-010-9935-1.
- Kouwen, N. 1996. WATFLOOD/ WATROUTE: Hydrological model routing & flow forecasting system. Surveys and Information Branch, Ecosystem Science and Evaluation Directorate, Environment Canada. Ottawa: 217 p.
- Kozo, T.L. 1983. Initial Model Results for Arctic Mixed Layer Circulation under a Refreezing Lead. *J. Geophys. Res.* 88: 2926-2934.
- Kuzyk, Z.A., Macdonald, R.W., Granskog, M.A., Scharien, R.K., Galley, R.J., Michel, C., Barber, D. and Stern, G. 2008a. Sea ice, hydrological, and biological processes in the Churchill River estuary region, Hudson Bay. *Estuarine Coastal and Shelf Science*. 77: 369-384.
- Kuzyk, Z.Z.A., Goni, M.A., Stern, G.A. and Macdonald, R.W. 2008b. Sources, pathways and sinks of particulate organic matter in Hudson Bay: Evidence from lignin distributions. *Marine Chemistry*. 112: 215-229.
- Kuzyk, Z.Z.A., Macdonald, R.W., Johannessen, S.C., Gobeil, C. and Stern, G.A. 2009. Towards a sediment and organic carbon budget for Hudson Bay. *Marine Geology*. 264: 190-208.

- Kwok, R. and Rothrock, D.A. 2009. Decline in Arctic sea ice thickness from submarine and ICES at records, 1958-2008. *Geophys. Res. Lett.* 36: L15501. doi:10.1029/2009GL039035.
- Kwok, R., Cunningham, G.F. and Pang, S.S. 2004. Fram Strait sea ice outflow. *J. Geophys. Res.* 109: C01009. doi:10.1029/2003JC001785.
- Kwok, R., Cunningham, G., Wensnahan, M., Rigor, I. and Zwally, H. 2009. Thinning and volume loss of the Arctic ocean sea ice cover: 2003-2008. *J. Geophys. Res. Oceans.* 114: C07005. doi:10.1029/2009JC005312.
- Ladouceur, S. 2007. Évaluation des changements hydrographiques de la Baie d'Hudson et du Bassin de Foxe au cours des derniers siècles à partir de traceurs palynologiques et micropaléontologiques. Thesis (MSc) Université du Québec à Montréal, Montreal, PQ. 78 p.
- Laidre, K.L., Heide-Jørgensen, M.P., Ermold, W. and Steele, M. 2010. Narwhals document continued warming of Baffin Bay. *J. Geophys. Res.* 115: C10049.
- Lalande, C. and Fortier, L. 2011. Downward particulate organic carbon export and jellyfish blooms in southeastern Hudson Bay. *J. Marine Syst.* 88: 446-450.
- Lammers, R.B., Shiklomanov, A.I., Vörösmarty, C.J., Fekete, B.M. and Peterson, B.J. 2001. Assessment of contemporary Arctic river runoff based on observational discharge records. *J. Geophys. Res.* 106(D4): 3321-3334.
- LaPierre, T., Geoph, P., Arnott, A., Hawkins, C., Simpson, K. and Davis, D. 2011. Environmental Impact Assessment for Marine 2D Seismic Reflection Survey Baffin Bay and Davis Strait offshore Eastern Canada. Report No. HOPH417(B), RPS Energy, Halifax, Nova Scotia.
- Lapoussière, A., Michel, C., Gosselin, M. and Poulin, M. 2009. Spatial variability in organic material sinking export in the Hudson Bay system, Canada, during fall. *Cont. Shelf Res.* 29: 1276-1288.
- Large, W.G. and Yeager, S.G. 2009. CORE2: The global climatology of an interannually varying air-sea flux data set. *Climate Dyn.* 33(2): 341-364.
- Latifovic, R. and Pouliot, D. 2007. Analysis of climate change impacts on lake ice phenology in Canada using the historical satellite data record. *Remote Sens. Environ.* 106: 492-507.
- Lavoie, D., Denman, K.L. and Macdonald, R.W. 2010. Effects of future climate change on primary productivity and export fluxes in the Beaufort Sea. *J. Geophys. Res.* 115: C04018. doi:10.1029/2009JC005493
- Lavoie, D., Lambert, N. and van der Breen, A. 2013. Projections of future physical and biogeochemical conditions in Hudson and Baffin Bays from CMIP5 Global Climate Models. *Can. Tech. Rep. Fish. Aquat. Sci.* In press.

- Lehman, J.T., Brooks, A.S. and Zastrow, J.C. 2000. Water Ecology. *In* Great Lakes Regional Assessment Report. Preparing for a Changing Climate: The Potential Consequences of Climate Variability and Change in the Great Lakes Region. Edited by Sousounis, P.J. and Bisanzm, J. University of Michigan Atmospheric, Oceanic and Space Sciences Department, Mann Arbor, MI. pp. 43–50.
- Lemke, P., Ren, J., Alley, R., Allison, I., Carrasco, J., Flato, G., Fujii, Y., Kaser, G., Mote, P., Thomas, R., Zhang, T., Box, J., Bromwich, D., Brown, R., Cogley, G., Comiso, J., Dyurgerov, M., Frauenfeld, O.W., Fricker, H., Greuell, W., Gudmundsson, H., Haas, C., Haeberli, W., Hagen, J.O., Harris, C., Hinzman, L., Hock, R., Hoelzle, M., Isaksen, K., Jansson, P., Jenkins, A., Joughin, I., Kottmeier, C., Kwok, R., Laxon, S., MacAyeal, D., McDonald, K.C., Melling, H., Payne, A., Prowse, T., Raup, B., Raymond, C., Rignot, E., Rigor, I., Robinson, D., Rothrock, D., Shiyin, L., Smith, S., Walsh, J., Worby, A., Yamada, T. and Zhao, L. 2007. Observations: Changes in Snow, Ice and Frozen Ground. *In*: Climate Change 2007: The Physical Science Basis. Contribution to of Working Group 1 to the Fourth Assessment Report of the Intergovernmental Panel on Climate Change. Edited by Solomon, S., Qin, D., Manning, M., Chen, Z., Marquis, M., Averyt, K.B., Tignor, M. and Miller, H.L. Cambridge University Press, Cambridge, United Kingdom and New York, NY, USA. pp. 337-383.
- Lenaerts, J.T.M, van Angelen, J.H., van den Broeke, M.R., Gardner, A.S., Wouters, B. and van Meijgaard, E. 2013. Irreversible mass loss of Canadian Arctic Archipelago glaciers. *Geophys. Res. Lett.* 40. doi:10.1002/grl.50214.
- LGL. 1983. Biological Environment of Eastern Lancaster Sound and Western Baffin Bay: Components and Important Processes. Environmental Studies No. 30. Northern Affairs Program, Indian and Northern Affairs, Ottawa. 288 p.
- Li, W.K.W., McLaughlin, F.A., Lovejoy, C. and Carmack, E.C. 2009. Smallest algae thrive as the Arctic Ocean freshens. *Science*. 326: 539. doi:10.1126/science.1179798.
- Loder, J.W. and van der Baaren, A. 2013. Climate change projections for the Northwest Atlantic from six CMIP5 Earth System Models. *Can. Tech. Rep. Hydrogr. Ocean. Sci.* In press.
- Long, Z. and Perrie, W. 2013. Impacts of climate change on fresh water content and sea surface height in the Beaufort Sea. *Ocean Modelling*. In press.
- Long, Z., Perrie, W., Tang, C.L., Dunlap, E. and Wang, J. 2012. Simulated interannual variations of fresh water content and sea surface height in the Beaufort Sea. *J. Climate*. 17 p. doi:10.1175/2011JCLI4121.1.
- Louie, P.Y.T., Hogg, W.D., MacKay, M.D., Zhang, X. and Hopkinson, R.F. 2002. The water balance climatology of the Mackenzie Basin with reference to the 1994/95 water year. *Atmos. Ocean*. 40: 159-180.
- Lueker, T., Dickson, A., Keeling, C.D. 2000. Ocean pCO₂ calculated from dissolved inorganic carbon, alkalinity, and equations for K₁ and K₂: validation based on laboratory measurements of CO₂ in gas and seawater at equilibrium. *Mar. Chem.* 70: 105-119.

- Lynch, A.J., Taylor, W.W and Smith, K.D. 2010. The influence of changing climate on the ecology and management of selected Laurentian Great Lakes fisheries. *J Fish Biol.* 77: 1764–1782.
- Macdonald, R.W. and Yanling, Y. 2006. The Mackenzie Estuary of the Arctic Ocean. *Estuaries*. 5H: 91-120.
- Madec, G. and the NEMO team. 2008. NEMO ocean engine. Note du Pole de modélisation, Institut Pierre-Simon Laplace (IPSL), France. No 27 ISSN No 1288-1619.
- Magnuson, J.J., Robertson, D.M., Wynne, R.H., Benson, B.J., Livingstone, D.M., Arai, T., Assel, R.A., Barry, R.D., Card, V., Kuusisto, E., Granin, N.G., Prowse, T.D., Stewart, K.M. and Vuglinski, V.S. 2000. Ice cover phenologies of lakes and rivers in the Northern Hemisphere and climate warming. *Science*. 289(5485): 1743-1746.
- Manabe, S., Milly, P.C.D. and Wetherald, R. 2004. Simulated long-term changes in river discharge and soil moisture due to global warming. *Hydrol. Sci. J.* 49: 625 642.
- Manson, G.K. and Solomon, S.M. 2007. Past and future forcing of Beaufort Sea coastal change. *Atmos-Ocean*. 45: 107–122. doi:10.3137/ao.450204.
- Markus, T., Stroeve, J.C. and Miller, J. 2009. Recent changes in Arctic sea ice melt onset, freeze-up, and melt season length. *J. Geophys. Res.* 114: C12024. doi:10.1029/2009JC005436.
- Marti, O., Braconnot, P., Dufresne, J.-L., Bellier, J., Benshila, R., Bony, S., Brockmann, P., Cadule, P., Caubel, A., Codron, F., de Noblet, N., Denvil, S., Fairhead, L., Fichet, T., Foujols, M.-A., Friedlingstein, P., Goosse, H., Grandpeix, J.-Y., Guilyardi, E., Hourdin, F., Idelkadi, A., Kageyama, M., Krinner, G., Lévy, C., Madec, G., Mignot, J., Musat, I., Swingedouw, D. and Talandier, C. 2010. Key features of the IPSL ocean atmosphere model and its sensitivity to atmospheric resolution, *Climate Dynamics*. 34: 1–26. doi:10.1007/s00382-009-0640-6.
- Martin, J., Tremblay, J.É., Gagnon, J., Tremblay, G., Lapoussière, A., Jose, C., Poulin, M., Gosselin, M., Gratton, Y. and Michel, C. 2010. Prevalence, structure and properties of subsurface chlorophyll maxima in Canadian Arctic waters. *Mar. Ecol. Prog. Ser.* 412: 69-84.
- Maslanik, J., Fowler, C., Stroeve, J., Drobot, S., Zwally, H., Yi, D. and Emery, W. 2007. A younger, thinner ice cover: increased potential for rapid, extensive ice loss. *Geophys. Res. Lett.* 34: (L24501). doi:10.1029/2007GL032043.
- Maslowski, W., Kinney, J.C., Higgins, M. and Roberts, A. 2012. The future of Arctic sea ice, *Annu. Rev. Earth Planet. Sci.* 40: 625–654. doi:10.1146/annurev-earth-042711-105345.
- Maxwell, J.B. 1986. A climate overview of the Canadian inland seas. *In Canadian inland seas*. Edited by Martini, I.P. Elsevier Oceanography Series 44. Elsevier Science Publishers, Amsterdam. pp. 79-99.

- Maxwell, B. 1997. Responding to global climate change in Canada's Arctic. The Canada Country Study: Climate Impacts and Adaptation, Vol. 2. Environment Canada, Ottawa. 82 p.
- Mazzotti, S., Lambert, A., Henton, J., James, T.S. and Courtier, N. 2011. Absolute gravity calibration of GPS velocities and glacial isostatic adjustment in mid-continent North America. *Geophys. Res. Lett.* 38: L24311. doi:10.1029/2011GL049846.
- McCabe, G.J., Clark, M.P. and Serreze, M.C. 2001. Trends in northern hemisphere surface cyclone frequency and intensity. *J. Clim.* 14: 763-2768. doi:10.1175/1520-0442.
- McClelland, J.W., Dery, S.J., Peterson, B.J., Holmes, R.M. and Wood, E.F. 2006. A pan-arctic evaluation of changes in river discharge during the latter half of the 20th century. *Geophys. Res. Lett.* 33: L06715.
- McLaughlin, F.A., Carmack, E.C., Macdonald, R.W. and Bishop, J.K.B. 1996. Physical and geochemical properties across the Atlantic/Pacific water mass front in the southern Canadian Basin. *J. Geophys. Res.* 101: 1183-1197.
- McLaughlin, F.A., Carmack, E.C., Proshutinsky, A., Krishfiled, R.A., Guay, C., Yamamoto-Kawai, M., Jackson, J.M. and Williams, B. 2011. The rapid response of the Canada Basin to climate forcing: From bellwether to alarm bells. *Oceanogr.* 24: 146-159.
- Meehl, G.A., Covey, C., Delworth, T., Latif, M., McAvaney, B., Mitchell, J.F.B., Stouffer, R.J. and Taylor, K.E. 2007. The WCRP CMIP3 multimodel dataset: A new era in climate change research. *Bull. Amer. Meteor. Soc.* 88: 1383-1394.
- Meier, W.M., Stroeve, J. and Gearheard, S. 2006. Bridging perspectives from remote sensing and Inuit communities on changing sea ice cover in the Baffin Bay region. *Annals of Glaciology.* 44: 433-438.
- Mekis, E. and Vincent, L. 2011. An overview of the second generation adjusted daily precipitation dataset for trend analysis in Canada. *Atmos. Ocean.* 49: 163-177.
- Melling, H. 2002. Sea ice of the northern Canadian Arctic Archipelago. *J. Geophys. Res.* 107: 3181. doi:10.1029/2001JC001102.
- Melling, H., Gratton, Y. and Ingram, G. 2001. Ocean circulation within the North Water polynya of Baffin Bay. *Atmos. Ocean.* 39(3): 301-325.
- Melling, H., Riedel, D.A. and Gedalof, Z. 2005. Trends in the draft and extent of seasonal pack ice, Canadian Beaufort Sea. *Geophys. Res. Lett.* 32: L24501. doi:10.1029/2005GL024483.
- Melling, H., Francois, R., Myers, P.G., Perrie, W., Rochon, A. and Taylor, R.L. 2012. The Arctic Ocean - A Canadian Perspective. *Climatic Change.* 115: 89-114. doi:10.1007/s10584-012-0576-4.

- Michel, C., Ingram, R.G. and Harris, L.R. 2006. Variability in oceanographic and ecological processes in the Canadian Arctic Archipelago. *Prog Oceanogr.* 71: 379-401. doi:10.1016/j.pocean.2006.09.006.
- Millero, F.J. 1979. Thermodynamics of the carbon dioxide system in the oceans. *Geochim. Cosmochim. Acta.* 59: 661-677.
- Milly, P.C.D., Dunne, K.A. and Vecchia, A.V. 2005. Global pattern of trends in streamflow and water availability in a changing climate. *Nature.* 438: 347-350.
- Min, S.-K., Zhang, X., Zwiers, F.W. and Hegerl, G.C. 2011. Human contribution to more-intense precipitation extremes. *Nature.* 470: 378–381. doi:10.1038/nature09763.
- Monk, W.A., Peters, D.L. and Baird, D.J. 2012. Assessment of ecologically relevant hydrological variables influencing a cold-region river and its delta: the Athabasca River and the Peace-Athabasca Delta, Northwestern Canada. *Hydrol. Proc.* 26: 1827-1839.
- Morak, S., Hegerl, G.C. and Kenyon, J. 2011. Detectable regional changes in the number of warm nights. *Geophys. Res. Lett.* 38: L17703. doi:10.1029/2011GL048531.
- Moss, R.H., Edmonds, J.A., Hibbard, K.A., Manning, M.R., Rose, S.K., van Vuuren, D.P., Carter, T.R., Emori, S., Kainuma, M., Kram, T., Meehl, G.A., Mitchell, J.F., Nakicenovic, N., Riahi, K., Smith, S.J., Stouffer, R.J., Thomson, A.M., Weyant, J.P. and Wilbanks, T.J. 2010. The next generation of scenarios for climate change research and assessment. *Nature.* 463. doi:10.1038/nature08823.
- Motard-Côté, J., Levasseur, M., Scarratt, M.G., Michaud, S., Gratton, Y., Rivkin, R.B., Keats, K., Gosselin, M., Tremblay, J.É., Kiene, R.P. and Lovejoy, C. 2012. Distribution and metabolism of dimethylsulfoniopropionate (DMSP) and phylogenetic affiliation of DMSP-assimilating bacteria in northern Baffin Bay/Lancaster Sound. *J. Geophys. Res.* 117: C00G11.
- MRBB (Mackenzie River Basin Board). 2004. Mackenzie River Basin State of the Aquatic Ecosystem Report 2003. Mackenzie River Basin Board Secretariat, Fort Smith, NWT. 213 p.
- Moore, G.W.K. 2012. Decadal variability and a recent amplification of the summer Beaufort Sea high. *Geophys. Res. Lett.* 39: L10807. doi:10.1029/2012GL051570.
- Mucci, A., 1983. The solubility of calcite and aragonite in seawater at various salinities, temperatures, and one atmosphere total pressure. *Am. J. Sci.* 283: 780-799.
- Myers, P.G., Chris, D. and Ribergaard, M.H. 2009. Structure and variability of the West Greenland Current in summer derived from 6 repeat standard sections. *Prog. Oceanogr.* 80: 93-112.

- Nakicenovic, N., Alcamo, J., Davis, G., de Vries, B., Fenhann, J., Gaffin, S., Gregory, K., Grübler, A., Jung, T.Y., Kram, T., La Rovere, E.L., Michaelis, L., Mori, S., Morita, T., Pepper, W., Pitcher, H., Price, L., Riahi, K., Roehrl, A., Rogner, H.-H., Sankovski, A., Schlesinger, M., Shukla, P., Smith, S., Swart, R., van Rooijen, S., Victor, N. and Dadi, Z. 2000. IPCC Special Report on Emissions Scenarios. Cambridge University Press, Cambridge, United Kingdom and New York, NY, USA. 599 p.
- Nijssen, B., O'Donnell, G.M., Hamlet, A.F. and Lettenmaier, D.P. 2001. Hydrologic sensitivity of global rivers to climate change. *Climatic Change*. 50: 143-175.
- Nohara, D., Kitoh A., Hosaka, M. and Oki, T. 2006: Impact of Climate Change on River Discharge Projected by Multimodel Ensemble. *J. Hydrometeorol.* 7: 1076–1089.
- NRTEE (National Round Table on the Environment and the Economy). 2010. Degrees of Change: Climate Warming and the Stakes for Canada. National Round Table on the Environment and the Economy, Ottawa, Ont.
- Olafsson, J. and Olafsdottir, S.R. 2009. Rate of Iceland Sea acidification from time series measurements. *Biogeosciences*. 6: 2660-2668.
- Orlowsky, B. and Seneviratne, S.I. 2012. Global changes in extreme events: Regional and seasonal dimension. *Clim. Chang.* 110: 669–696. doi:10.1007/s10584-011-0122-9.
- Orr, J.C., Fabry, V.J., Aumont, O., Bopp, L., Doney, S.C., Feely, R.A., Gnanadesikan, A., Gruber, N., Ishida, A., Joos, F., Key, R.M., Lindsay, K., Maier-Reimer, E., Matear, R., Monfray, P., Mouchet, A., Najjar, R.G., Plattner, G.-K., Rodgers, K.B., Sabine, C.L., Sarmiento, J.L., Schlitzer, R., Slater, R.D., Totterdell, I.J., Weirig, M.-F., Yamanaka, Y. and Yool, A. 2005. Anthropogenic ocean acidification over the twenty-first century and its impact on calcifying organisms. *Nature*. 437: 681–686. doi:10.1038/nature04095.
- Overland, J.E. and Wang, M. 2005. The Arctic climate paradox: The recent decrease of the Arctic Oscillation. *Geophys. Res. Lett.* 32: L06701. doi:10.1029/2004GL021752.
- Overland, J., Wang, M. and Salo, S. 2008. The recent Arctic warm period. *Tellus*. 60: 589-597.
- Overland, J.E., Francis, J.A., Hanna, E. and Wang, M. 2012. The recent shift in early summer Arctic atmospheric circulation. *Geophys. Res. Lett.* 39: L19804. doi:10.1029/2012GL053268.
- Parkinson, C.L. and Cavalieri, D.J. 2008. Arctic sea ice variability and trends, 1979-2006. *J. Geophys. Res.* 113: C07003. doi:10.1029/2007JC004558.
- Perovich D.K., Richter-Menge, J.A., Jones, K.F., Light, B., Elder, B.C., Polashenski, C., Laroche, D., Markus, T. and Lindsay, R.L. 2011. Arctic sea ice melt in 2008 and the role of solar heating. *Ann Glaciol.* 52: 1-5.

- Peters, G.P., Andrew, R.M., Boden, T., Canadell, J.G., Ciais, P., Le Quéré, C., Marland, G., Raupach, M.R. and Wilson, C. 2013. The challenge to keep global warming below 2°C. *Nature Climate Change*. 3: 4-6. doi:10.1038/nclimate1783.
- Peterson, I.K. and Pettipas, R. 2013. Trends in air temperature and sea ice in the Atlantic Large Aquatic Basin and adjoining areas. *Can. Tech. Rep. Hydrogr. Ocean Sci.* In press.
- Peterson, B.J., Holmes, R.M., McClelland, J.W., Vorosmarty, C.J., Lammers, R.B., Shiklomanov, A.I., Shiklomanov, I.A. and Rahmstorf, S. 2002. Increasing river discharge to the Arctic Ocean. *Science*. 298: 2171-2173.
- Peterson, B.J., McClelland, J., Curry, R., Holmes, R.M., Walsh, J.E. and Aagaard, K. 2006. Trajectory shifts in the Arctic and subarctic freshwater cycle. *Science*. 313: 1061-1066.
- Peterson, I., Hamilton, J., Prinsenberg, S. and Pettipas, R. 2012. Wind forcing of volume transport through Lancaster Sound. *J. Geophys. Res.* 117: C11018. doi:10.1029/2012JC008140.
- Prinsenberg, S.J. 1980. Man-made changes in the fresh-water input rates of Hudson and James Bays. *Can. J. Fish. Aquat. Sci.* 37: 1101-1110.
- Prinsenberg, S.J. 1986. Chapter 9. Salinity and Temperature Distributions of Hudson Bay and James Bay. *In Elsevier Oceanography Series*. Volume 44. Edited by Martini, I.P. Elsevier. pp. 163-186.
- Prinsenberg, S.J. 1988. Ice-cover and ice-ridge contributions to the fresh-water contents of Hudson Bay and Foxe Basin. *Arctic*. 41: 6-11.
- Proshutinsky, A. and Johnson, M.A. 1997. Two circulation regimes of the wind-driven Arctic Ocean. *J. Geophys. Res.* 102: 12493-12514.
- Proshutinsky, A., Krishfield, R., Timmermans, M.L., Toole, J., Carmack, E.C., McLaughlin, F.A., Williams, W.J., Zimmermann, S., Itoh, M. and Shimada, K. 2009. Beaufort Gyre freshwater reservoir: State and variability from observations. *J. Geophys. Res.* 114: C00A10. doi:10.1029/2008JC005104.
- Prowse, T. and Conly, M. 1996. General Hydrology and Effects of Flow Regulation on the Peace and Slave Rivers. Northern River Basins Study Synthesis Report No. 1.
- Prowse, T.D., Conly, F., Church, M. and English, M.C. 2002. A review of hydro-ecological results of the “Northern River Basins Study”, Canada: Part 1. Peace and Slave Rivers. *River Research and Applications*. 18: 429-446.
- Prowse, T.D., Beltaos, S., Gardner, J.T., Gibson, J.J., Granger, R.J., Leconte, R., Peters, D.L., Pietroniro, A., Romolo, L.A. and Toth, B. 2006a. Climate change, flow regulation and land-use effects on the hydrology of the Peace-Athabasca-Slave system; findings from the Northern River Ecosystem Initiative. *Environmental Monitoring and Assessment*. 113: 167-197.

- Prowse, T.D., Wrona, F.J., Reist, J.D., Gibson, J.J., Hobbie, J.E., Lévesque, L.M.J. and Vincent, W.F. 2006b. Climate Change Effects on Hydroecology of Arctic Freshwater Ecosystems. *Ambio*. 35: 347-358.
- Radinović, D. and Ćurić, M. 2012. Criteria for heat and cold wave duration indexes. *Theor. Appl. Climatol.* 107: 505–510. doi:10.1007/s00704-011-0495-8.
- Räisänen, J., Ruokolainen, L. and Ylhäisi, J. 2010. Weighting of model results for improving best estimates of climate change. *Clim Dyn.* 35: 407–422. doi:10.1007/s00382-009-0659-8
- Rampal, P., Weiss, J. and Marsan, D. 2009. Positive trend in the mean speed and deformation rate of Arctic sea ice, 1979-2007. *J. Geophys. Res. Oceans.* 114 (C5). doi:10.1029/2008JC005066.
- Rao, Y.R., Huang, A., Schertzer, W.M. and Rouse, W.R. 2012. Modelling of Physical Processes and Assessment of Climate Change Impacts in Great Bear Lake. *Atmos. Ocean.* 50: 317-333. doi:10.1080/07055900.2012.668492.
- Rayner, N.A., Parker, D.E., Horton, E.B., Folland, C.K., Alexander, L.V., Rowell, D.P., Kent, E.C. and Kaplan, A. 2003. Global analyzes of sea surface temperature, sea ice, and night marine air temperature since the late nineteenth century. *J. Geophys. Res.* 108(D14): 4407. doi:10.1029/2002JD002670
- Ribergaard, M.H., Olsen, S.M. and Mortensen, J. 2008. Oceanographic Investigations off West Greenland 2007. NAFO Scientific Council Documents. 07/003.
- Rignot, E., Velicogna, I., van der Broeke, M., Monaghan, A. and Lenerts, J. 2011. Acceleration of the contribution of the Greenland and Antarctic ice sheets to sea level rise. *Geophys. Res. Lett.* 38: L05503. doi:10.1029/2011 GL046583.
- Rigor, I.G. and Wallace, J.M. 2004. Variations in the age of Arctic sea ice and summer sea ice extent. *Geophys. Res. Lett.* 31: L09401. doi:10.1029/2004GL019492.
- Rigor, I.G., Wallace, J.M. and Colony, R.L. 2002. Response of sea ice to the Arctic Oscillation. *J. Clim.* 15: 2648-2663.
- Ringuette, M., Fortier, L., Fortier, M., Runge, J.A., Bélanger, S., Larouche, P., Weslawski, J.M. and Kwasniewski, S. 2002. Advanced recruitment and accelerated population development in Arctic calanoid copepods of the North Water. *Deep Sea Res. II.* 49: 5081-5099.
- Rogelj, J., Meinshausen, M. and Knutti, R. 2012. Global warming under old and new scenarios using IPCC climate sensitivity range estimates. *Nature Climate Change.* 2: 248-253.
- Rosenberg, D.M. and Barton, D.R. 1986. The Mackenzie River system. *In* The ecology of river systems. Edited by Davies, B.R. and Walker, K. F. W. Junk Publishers, The Netherlands. pp. 425-433.

- Rouse, W., Douglas, M., Hecky, R., Kling, G., Lesack, L., Marsh, P., McDonald, M., Nicholson, B., Roulet, N. and Smol, J.P. 1997. Effects of climate change on fresh waters of Region 2: Arctic and sub-Arctic North America. *Hydrol. Proc.* 11: 873-902.
- Rouse, W.R., Oswald, C.M., Binyamin, J., Blanken, P.D., Schertzer, W.M. and Spence, C. 2003. Interannual and seasonal variability of the surface energy balance and temperature of central Great Slave Lake. *J. Hydrometeorol.* 4: 720-730.
- Saucier, F.J., Senneville, S., Prinsenberg, S., Roy, F., Smith, G., Gachon, P., Caya, D. and Laprise, R. 2004. Modelling the sea ice-ocean seasonal cycle in Hudson Bay, Foxe Basin and Hudson Strait, Canada. *Climate Dyn.* 23: 303-326.
- Schneider, B., Bopp, L., Gehlen, M., Segschneider, J., Frölicher, T.L., Cadule, P., Friedlingstein, P., Doney, S.C., Behrenfeld, M.J. and Joos, F. 2008. Climate-induced interannual variability of marine primary and export production in three global coupled climate carbon cycle models. *Biogeoscience.* 5: 597–614.
- Schindler, D.W. and Donahue, W.F. 2006. An impending water crisis in Canada's western prairie provinces. *Proceedings of the National Academy of Sciences.* 103: 7210-7216.
- Schindler, D.W. and Smol, J.P. 2006. Cumulative effects of climate warming and other human activities on freshwaters of Arctic and Subarctic North America. *Ambio.* 35: 160-168.
- Schindler, D., Bayley, S., Parker, B., Beaty, K., Cruikshank, D., Fee, E., Schindler, E. and Stainton, M. 1996. The effects of climatic warming on the properties of boreal lakes and streams at the Experimental Lakes Area, Northwestern Ontario. *Limnol. Oceanogr.* 41: 1004-1017.
- Serreze, M.C. and Barrett, A.P. 2011. Characteristics of the Beaufort Sea High. *J. Clim.* 24: 159-182. doi:10.1175/2010JCLI3636.
- Sharma, S., Jackson, D.A., Minns, C.K. and Shuter, B.J. 2007. Will northern fish populations be in hot water because of climate change? *Global Change Biology.* 13: 2052-2064.
- Sillmann, J., Kharin, V.V., Zhang, X., Zwiers, F.W. and Bronaugh, D. 2013a. Climate extremes indices in the CMIP5 multimodel ensemble: Part 1. Model evaluation in the present climate. *J. Geophys. Res. Atmos.* 118: 1–18. doi:10.1002/jgrd.50203.
- Sillmann, J., Kharin, V.V., Zhang, X., Zwiers, F.W. and Bronaugh, D. 2013b. Climate extremes indices in the CMIP5 multimodel ensemble: Part 2. Future Climate Projections. *J. Geophys. Res. Atmos.* 118: 1–21. doi:10.1002/jgrd.50188.
- Simmonds, I., Burke, C. and Keay, K. 2008. Arctic climate change as manifest in cyclone behavior. *J. Clim.* 21: 5777-5796. doi:10.1175/2008JCLI2366.
- Smith, M.W. and Burgess, M.M. 2004. Sensitivity of permafrost to climate warming in Canada. *Geological Survey of Canada Bulletin* 579. 24 p.

- Smith, L.C., Sheng, Y., Forster, R.R., Steffen, K., Frey, K.E. and Alsdorf, D.E. 2003. Melting of small Arctic ice caps observed from ERS scatterometer time series. *Geophys. Res. Lett.* 30(20): 2034. doi:10.1029/2003GL017641.
- Smith, L.C., Sheng, Y., MacDonald, G.M. and Hinzman, L.D. 2005. Disappearing arctic lakes. *Science.* 308: 1429.
- Smol, J.P., Wolfe, A.P., Birks, H.J.B., Douglas, M.S.V., Jones, V.J., Korholai, A., Pienitz, R., Rühland, K., Sorvari, S., Antoniades, D., Brooks, S.J., Fallu, M., Hughes, M., Keatley, B.E., Laing, T.E., Michelutti, N., Nazarova, L., Nyman, M., Paterson, A.M., Perren, B., Quinlan, R., Rautio, M., Saulnier-Talbot, É., Siitonen, S., Solovieva, N. and Weckström, J. 2005. Climate-driven regime shifts in the biological communities of Arctic lakes. *Proceedings of the National Academy of Sciences.* 102: 4397-4402.
- Spence, C. 2002. Streamflow Variability (1965 to 1998) in Five Northwest Territories and Nunavut Rivers. *Canadian Water Resources Journal.* 27: 135-154.
- Squires, M.M. and Lesack, L.F.W. 2003. The relation between sediment nutrient content and macrophyte biomass and community structure along a water transparency gradient among lakes of the Mackenzie Delta. *Can. J. Fish. Aquat. Sci.* 60: 333-343.
- Squires, M.M., Lesack, L.F.W. and Huebert, D. 2002. The influence of water transparency on the distribution and abundance of macrophytes among lakes of the Mackenzie Delta, western Canadian Arctic. *Freshwater Biology.* 47: 2123-2135.
- Stein, M. 2004. Climatic overview of NAFO Subarea 1, 1991–2000. *J. Northw. Atl. Fish. Sci.* 34: 29-41.
- Stein, M. 2005. Atlantic Subpolar Gyre Warming – Impacts on Greenland Offshore Waters? Northwest Atlantic Fisheries Organization Serial No. N5072 NAFO SCR Doc. 05/1.
- Steinacher, M., Joos, F., Frölicher, T., Plattner, G.-K. and Doney, S. 2009. Imminent ocean acidification of the Arctic projected with the NCAR global coupled carbon-cycle climate model. *Biogeosciences.* 6(4): 515–533.
- Steinacher, M., Joos, F., Frölicher, T., Bopp, L., Cadule, P., Cocco, V., Doney, S., Gehlen, M., Lindsay, K., Moore, J., Schneider, B. and Segschneider, J. 2010. Projected 21st century decrease in marine productivity: a multi-model analysis. *Biogeosciences.* 7: 979{1005}.
- Steiner, N.S., Lee, W.G. and Christian, J.R. 2013. Enhanced gas fluxes in small sea ice leads and cracks - effects on CO₂ exchange and ocean acidification. *J. Geophys. Res. Oceans.* 118: 1195–1205. doi:[10.1002/jgrc.20100](https://doi.org/10.1002/jgrc.20100).
- Steele, M., Morley, R. and Ermold, W. 2001. PHC: A global ocean hydrography with a high-quality Arctic Ocean. *J. Climate.* 14: 2079-2087.
- Stewart, D.B. and Lockhart, W.L. 2005. An Overview of the Hudson Bay Marine Ecosystem. *Can Tech Rep Fish Aquat Sci* 2586. Canada Department of Fisheries and Oceans. 487 p.

- Stewart, D.B. and Barber, D.G. 2010. The Ocean-Sea Ice-Atmosphere System of the Hudson Bay Complex. *In: A Little Less Arctic: Top predators in the world's largest northern inland sea, Hudson Bay.* Edited by Ferguson, S.H., Loseto, L.L. and Mallory, M.L. Springer Netherlands. pp. 1-38.
- Stewart, R.E., Crawford, R.W., Leighton, H.G., Marsh, P., Strong, G.S., Moore, G.W.K., Ritchie, H., Rouse, W.R., Soulis, E.D. and Kochtubajda, B. 1998. The Mackenzie GEWEX study: the water and energy cycles of a major North American river system. *Bull. Amer. Meteor. Soc.* 79: 2665-2683.
- Stewart, R.E., Bussi eres, N., Cao, Z., Cho, H. R., Hudak, D.R., Kochtubajda, B., Leighton, H.G., Louie, P.Y.T., MacKay, M.D., Marsh, P., Strong, G.S., Szeto, K.K. and Burford, J.E. 2002. Hydrometeorological Features of the Mackenzie Basin Climate System during the 1994/95 Water year: A Period of Record Low Discharge. *Atmos. Ocean.* 40: 257-278.
- St-Laurent, P., Straneo, F., Dumais, J-F. and Barber, D.G. 2011. What is the fate of the river waters of Hudson Bay? *J. Marine Syst.* 88: 352-361.
- Straneo, F. and Saucier, F. 2008. The outflow from Hudson Strait and its contribution to the Labrador Current. *Deep Sea Res. I.* 55: 926-946.
- Stroeve, J., Serreze, M., Fetterer, F., Arbetter, T., Meier, W., Maslanik, J. and Knowles, K. 2005. Tracking the Arctic's shrinking ice cover: Another extreme september minimum in 2004. *Geophys. Res. Lett.* 32 (4): L04501. doi:10.1029/2004GL021810.
- Stroeve, J.C., Kattsov, V., Barrett, A., Serreze, M., Pavlova, T., Holland, M. and Meier, W.N. 2012a. Trends in Arctic sea ice extent from CMIP5, CMIP3 and observations. *Geophys. Res. Lett.* 39: L16502. doi:10.1029/2012GL052676.
- Stroeve, J.C., Serreze, M.C., Holland, M.M., Kay, J.E., Malanik, J. and Barrett, A.P. 2012b. The Arctic's rapidly shrinking sea ice cover: a research synthesis. *Climatic Change.* 110: 1005-1027.
- Taylor, K.E., Stouffer, R.J. and Meehl, G.A. 2012. An overview of CMIP5 and the experiment design. *Bull. Amer. Meteor. Soc.* 93: 485-498. doi:10.1175/BAMS-D-11-00094.1
- Tang, C.L., Ross, C.K., Yao, T., Petrie, B., Detracey, B.D. and Dunlap, E. 2004. The circulation, water masses and sea ice of Baffin Bay. *Prog. Oceanogr.* 63: 183-228.
- Tarasov, L. and Peltier, W.R. 2004. A geophysically constrained large ensemble analysis of the deglacial history of the North American ice-sheet complex. *Quat Sci Rev.* 23: 359-388. doi:10.1016/j.quascirev.2003.08.004.
- Tebaldi, C., Hayhoe, K., Arblaster, J. and Meehl, G. 2006. Going to extremes. An intercomparison of model-simulated historical and future changes in extreme events. *Clim. Chang.* 79: 185-211. doi:10.1007/s10584-006-9051-4.

- Thompson, D.W.J. and Wallace, J.M. 1998. The Arctic oscillation signature in the wintertime geopotential height and temperature fields. *Geophys. Res. Lett.* 25: 1297-1300. doi:10.1029/98GL00950.
- Thorne, R. 2011. Uncertainty in the impacts of projected climate change on the hydrology of a subarctic environment: Liard River Basin. *Hydrol. Earth Syst. Sci.* 15: 1483-1492.
- Timoney, K. 2002. A dying delta? A case study of a wetland paradigm. *Wetlands.* 22: 282-300.
- Tivy, A., Howell, S.E.L., Alt, B., McCourt, S., Chagnon, R., Crocker, G., Carrieres, T. and Yackel, J.J. 2011a. Trends and variability in summer sea ice cover in the Canadian Arctic based on the Canadian Ice Service Digital Archive, 1960–2008 and 1968–2008. *J. Geophys. Res.* 116: C03007. doi:10.1029/2009JC005855.
- Tivy, A., Howell, S.E.L., Alt, B., McCourt, S., Chagnon, R., Crocker, G., Carrieres, T. and Yackel, J.J. 2011b. Correction to “Trends and variability in summer sea ice cover in the Canadian Arctic based on the Canadian Ice Service Digital Archive, 1960–2008 and 1968–2008. *J. Geophys. Res.* 116: C06027. doi:10.1029/2011JC007248.
- Tong, J., Déry, S.J., Jackson, P.L. and Derksen, C. 2010. Snow distribution from SSM/I and its relationships to the hydroclimatology of the Mackenzie River Basin, Canada. *Advances in Water Resources.* 33: 667-677.
- Tremblay, J.E., Robert, D., Varela, D.E., Lovejoy, C., Darnis, G., Nelson R.J. and Sastri, A.R. 2012. Current state and trends in Canadian Arctic marine ecosystems: I. Primary production. *Climatic Change.* 115: 161–178. doi:10.1007/s10584-012-0496-3.
- Trefry, J.H., Rember, R.D. and Trocine, R.P. 2005. Sources, concentrations and dispersion pathways for suspended sediment in the coastal Beaufort Sea-Executive summary. OCS Study MMS 2005-051, U.S. Department of the Interior Minerals Management Service. pp. 28-31.
- Tucker, W.B., Weatherly, J.W., Eppler, D.T., Farmer, L.D. and Bentley, D.L. 2001. Evidence for rapid thinning of sea ice in the western Arctic Ocean at the end of the 1980s. *Geophys. Res. Lett.* 28: 2851-2854.
- Vancoppenolle, M., Bopp, L., Madec, G., Dunne, J.P., Ilyina, T., Halloran, P.R. and Steiner, N. 2013. Future Arctic Ocean Primary Productivity from CMIP5 Simulations: Uncertain Outcome but Consistent Mechanisms. *Global Biogeochemical Cycles.* In press.
- Våge, K., Pickart, R.S., Thierry, V., Reverdin, G., Lee, C.M., Petrie, B., Agnew, T., Wong, A. and Ribergaard, M.H. 2009. Surprising return of deep convection to the subpolar North Atlantic Ocean in winter. *Nature Geoscience.* 2: 67-72. doi:10.1038/NCEO382. <http://www.nature.com/ngeo/journal/v2/n1/abs/ngeo382.html> (accessed 9 February, 2012).
- Van Gerwen-Toyne, M., Walker-Larsen, J. and Tallman, R.F. 2008. Monitoring spawning populations of migratory inconnu and coregonids in the Peel River, NWT: the Peel River fish study 1998-2002. *Can. Manuscr. Rep. Fish. Aquat. Sci.* 2851: 56p.

- Vincent, L.A., Zhang, X., Bonsal, B.R. and Hogg, W.D. 2002. Homogenization of daily temperatures over Canada. *J. Climate*. 15: 1322-1334.
- von Salzen, K., Scinocca, J.F., McFarlane, N.A., Li, J., Cole, N.S., Plummer, D., Reader, M.C., Ma, X., Lazare, M. and Solheim, L. 2013. The Canadian Fourth Generation Atmospheric Global Climate Model (CanAM4). Part I: Physical processes (2013): *Atmos. Ocean*. 51. doi:10.1080/07055900.2012.755610.
- Wadhams, P., McLaren, A.S. and Weintraub, R. 1985. Ice thickness in Davis Strait in February from submarine sonar profiles. *J. Geophys. Res.* 90: 1069-1077.
- Waleron, M., Waleron, K., Vincent, W.F. and Wilmotte, A. 2007. Allochthonous inputs of riverine picocyanobacteria to coastal waters in the Arctic Ocean. *FEMS Microbiology Ecology*. 59: 356-365.
- Walsh, J.E. 1978. A data set on Northern Hemisphere sea ice extent, 1953 – 76. *Glaciol. Data Rep. GD-2. Arctic Sea Ice, Part 1. World Data Center for Glaciology, Boulder, Colo.* pp. 49–51. <http://nsidc.org/>.
- Walsh, J.E., Chapman, W.L. and Shy, T.L. 1996. Recent decrease of sea level pressure in the central Arctic. *J. Clim.* 9: 480-486.
- Walsh, J.E., Anisimov, O., Hagen, J.O.M., Jakobsson, T., Oerlemans, J., Prowse, T.D., Romanovsky, V., Savelieva, N., Serreze, M., Shiklomanov, A., Shiklomanov, I., Solomon, S., Arendt, A., Atkinson, D., Demuth, M.N., Dowdeswell, J., Dyurgerov, M., Glazovsky, A., Koerner, R.M., Meier, M., Rech, N., Sigurdsson, O., Steffen, K. and Truffer, M. 2005. Cryosphere and hydrology. *In: Arctic Climate Impact Assessment*. Cambridge University Press, Cambridge, United Kingdom. pp. 183-242.
- Wan, H., Wang, X.L. and Swail, V.R. 2010. Homogenization and trend analysis of Canadian near-surface wind speeds. *J. Clim.* 23: 1209-1225. doi:10.1175/2009JCLI3200.1.
- Wang, J., Mysak, L.A. and Ingram, R.G. 1994. Interannual variability of sea ice cover in Hudson Bay, Baffin Bay and the Labrador Sea. *Atmos-Ocean*. 32: 421-447.
- Wang J., Zhang, J., Watanabe, E., Ikeda, M., Mizobata, K., Walsh, J.E., Bai, X. and Wu, B. 2009. Is the Dipole Anomaly a major driver to record lows in Arctic summer sea ice extent? *Geophys. Res. Lett.* 36: L05706. doi:10.1029/2008GL036706.
- Watanabe, S., Hajima, T., Sudo, K., Nagashima, T., Takemura, T., Okajima, H., Nozawa, T., Kawase, H., Abe, M., Yokohata, T., Ise, T., Sato, H., Kato, E., Takata, K., Emori, S. and Kawamiya, M. 2011. Miroc-esm 2010: model description and basic results of cmip5-20c3m experiments. *Geoscientific Model Development*. 4 (4): 845872. doi:10.5194/gmd-4-845-2011.
- Watson, E. and Luckman, B.H. 2004 Tree-ring-based mass-balance estimates for the past 300 years at Peyto Glacier, Alberta, Canada. *Quaternary Research*. 62: 9-18.

- WKSS (West Kitikmeot Slave Study). 2001. West Kitikmeot Slave Study Final Report. West Kitikmeot Slave Study Society, Yellowknife.
- Wolfe, B.B., Hall, R.I., Edwards, T.W.D., Vardy, S.R., Falcone, M.D., Sjunneskog, C., Sylvestre, F., McGowan, S., Leavitt, P.R. and van Driel, P. 2008. Hydroecological responses of the Athabasca Delta, Canada, to changes in river flow and climate during the 20th century. *Ecology*. 1: 131-148.
- Woo, M.K. and Thorne, R. 2003. Stream flow in the Mackenzie Basin, Canada. *Arctic*. 56: 328-340.
- Wood, K.R., Overland, J.E., Jónsson, T. and Smoliak, B.V. 2010. Air temperature variations on the Atlantic-Arctic boundary since 1802. *Geophys. Res. Lett.* 37: L17708. doi:10.1029/2010GL044176.
- Wrona, F.J., Prowse, T.D., Reist, J.D., Hobbie, J.E., Lévesque, L.M.J. and Vincent, W.F. 2006. Climate Change Effects on Aquatic Biota, Ecosystem Structure and Function. *Ambio*. 35: 359-369.
- Wu, Y., Hannah, C.G., Petrie, B., Pettipas, R., Peterson, I., Prinsenberg, S., Lee, C. and Moritz, D. 2013. Ocean current and sea ice statistics for Davis Strait. *Can. Tech. Rep. Hydrogr. Ocean Sci.* In press.
- Xu, F., Perrie, W. and Solomon, S. 2013. Shallow water dissipation processes for wind-waves off the Mackenzie Delta. *Atmos. Ocean*. In press.
- Yamamoto-Kawai, M., McLaughlin, F.A., Carmack, E.C., Nishino, S. and Shimada, K. 2009. Aragonite under-saturation in the Arctic Ocean: Effects of ocean acidification and sea ice melt. *Science*. 236: 1098–1100.
- Yamamoto-Kawai, M., McLaughlin, F.A. and Carmack, E.C. 2011. Effects of ocean acidification, warming and melting of sea ice on aragonite saturation of the Canada Basin surface water. *Geophys. Res. Lett.* 38: L03601. doi:10.1029/2010GL045501.
- Yamamoto, A., Kawamiya, M., Ishida, A., Yamanaka, Y. and Watanabe, S. 2012. Impact of rapid sea ice reduction in the Arctic Ocean on the rate of ocean acidification. *Biogeosciences*. 9(6): 2365-2375.
- Yip, Q.K.Y., Burn, D.H., Seglenieks, F., Pietroniro, A. and Soulis, E.D. 2012. Climate Impacts on Hydrological Variables in the Mackenzie River Basin. *Canadian Water Resources Journal*. 37(3): 209-230. doi:10.4296/cwrj2011-899.
- Zadra, A., Caya, D.D., Côté, J., Dugas, B., Jones, C., Laprise, R., Winger, K. and Caron, L.-P. 2008: The next Canadian Regional Climate Model. *Physics in Canada*. Special Issue on Fast Computing. 64: 75-83.
- Zhang, X., Vincent, L.A., Hogg, W.D. and Niitsoo, A. 2000. Temperature and precipitation trends in Canada during the 20th century. *Atmos. Ocean*. 38: 395-429.

- Zhang, X., Walsh, J.E., Zhang, J., Bhatt, U.S. and Ikeda, M. 2004. Climatology and Interannual Variability of Arctic Cyclone Activity: 1948–2002. *J. Climate*. 17: 2300–2317.
- Zhang, X., Brown, R., Vincent, L., Skinner, W., Feng, Y. and Mekis, E. 2011. Canadian climate trends, 1950-2007. *Canadian Biodiversity: Ecosystem Status and Trends 2010, Technical Thematic Report No. 5*. Canadian Councils of Resource Ministers. Ottawa, ON. iv + 21 p. <http://www.biodivcanada.ca/default.asp?lang=En&n=137E1147-0>
- Zhang, J., Lindsay, R., Schweiger, A. and Rigor, I. 2012. Recent changes in the dynamic properties of declining Arctic sea ice: A model study. *Geophys. Res. Lett.* 39: L20503. doi:10.1029/2012GL053545.
- Zweng, M.M. and Münchow, A. 2006. Warming and freshening of Baffin Bay, 1916–2003. *J. Geophys. Res.* 111: C07016. doi:10.1029/2005JC003093.

7: APPENDICES

7.1 APPENDIX 1

7.1.1 AR5-ESM Multi-Model Means and Standard Deviations

Table 8. AR5-ESM multimodel means and standard deviations for the BS, CPS, BB, HB subbasins for T_s , S_s , Z_m , SIC, NO_3 , pH, PP, and $CaCO_3$ at 100 m for bidecades 1986 - 2005, 1966 - 1985, 2005 - 2025 and 2045 - 2065. Also included are the differences between the most recent past (1986 - 2005) and the past (1966 - 1985) and the recent past and the future (20 years and 60 years).

Region	Variable	Seas	Hist	Stdev	Past	Stdev	Future20	Stdev	Future60	Stdev	Past	Future20	Future60	
												-Hist	-Hist	-Hist
Beaufort Sea	Surface Temperature	Ann	-1.2300	0.243	-1.370	0.238	-1.023	0.282	-0.177	0.627	-0.140	0.206	1.053	
Beaufort Sea	Surface Salinity	Ann	29.939	0.935	30.171	0.896	29.459	1.079	28.626	1.327	0.233	-0.480	-1.312	
Beaufort Sea	Mixed Layer Depth	Mar	51.026	9.683	54.359	10.509	48.793	6.857	49.917	8.212	3.332	-2.233	-1.109	
Beaufort Sea	Sea Ice Concentration	Mar	96.548	1.901	96.848	2.002	96.529	1.933	95.647	2.073	0.300	-0.018	-0.900	
Beaufort Sea	Sea Ice Concentration	Sep	45.583	14.049	57.284	9.601	31.715	16.097	4.945	6.828	11.701	-13.867	-40.638	
Beaufort Sea	Surface nitrate	DJF	4.117	4.165	4.775	4.409	3.132	3.824	2.179	2.905	0.658	-0.985	-1.938	
Beaufort Sea	Surface nitrate	JJA	2.782	3.519	3.480	3.962	1.825	2.925	0.929	1.850	0.699	-0.957	-1.852	
Beaufort Sea	Sea Water pH	Ann	8.123	0.035	8.156	0.037	8.057	0.038	7.872	0.032	0.033	-0.066	-0.250	
Beaufort Sea	Primary Production	Ann	0.574	0.274	0.524	0.297	0.574	0.271	0.634	0.375	-0.050	0.000	0.060	
CPS	Surface Temperature	Ann	-1.412	0.251	-1.455	0.248	-1.313	0.275	-0.702	0.449	-0.042	0.100	0.710	
CPS	Surface Salinity	Ann	29.788	0.532	30.187	0.502	29.361	0.736	28.477	0.833	0.399	-0.426	-1.311	
CPS	Mixed Layer Depth	Mar	40.516	4.214	43.582	3.536	40.569	4.196	37.870	2.287	3.067	0.054	-2.646	
CPS	Sea Ice Concentration	Mar	90.011	11.855	90.069	12.099	89.913	11.918	89.363	11.906	0.059	-0.097	-0.647	
CPS	Sea Ice Concentration	Sep	55.507	18.188	62.125	17.395	45.322	19.016	10.872	14.974	6.618	-10.185	-44.635	
CPS	Surface nitrate	DJF	5.426	3.270	6.363	3.481	4.224	3.284	3.153	2.854	0.937	-1.202	-2.274	
CPS	Surface nitrate	JJA	4.098	3.025	5.018	3.535	2.863	2.614	1.602	1.902	0.920	-1.235	-2.496	
CPS	Sea Water pH	Ann	8.114	0.034	8.139	0.036	8.064	0.032	7.876	0.038	0.025	-0.050	-0.238	
CPS	Primary Production	Ann	0.514	0.332	0.463	0.345	0.575	0.346	0.717	0.489	-0.051	0.061	0.202	
Baffin Bay	Surface Temperature	Ann	-0.440	0.402	-0.614	0.361	-0.245	0.492	0.649	0.913	-0.173	0.196	1.090	
Baffin Bay	Surface Salinity	Ann	31.393	1.119	31.608	1.216	31.061	1.238	30.311	1.303	0.215	-0.332	-1.082	
Baffin Bay	Mixed Layer Depth	Mar	73.814	11.514	84.379	12.495	64.595	4.513	50.936	9.693	10.564	-9.219	-22.878	
Baffin Bay	Sea Ice Concentration	Mar	90.112	7.593	90.131	7.466	89.997	7.532	87.678	7.051	0.019	-0.114	-2.434	
Baffin Bay	Sea Ice Concentration	Sep	8.246	11.066	11.489	14.806	5.763	8.304	1.877	4.535	3.243	-2.483	-6.369	
Baffin Bay	Surface nitrate	DJF	5.303	3.623	5.748	3.619	4.652	3.833	3.767	3.606	0.444	-0.652	-1.536	
Baffin Bay	Surface nitrate	JJA	1.580	1.296	1.762	1.524	1.191	1.146	0.688	0.810	0.182	-0.389	-0.891	
Baffin Bay	Sea Water pH	Ann	8.133	0.016	8.165	0.016	8.083	0.016	7.913	0.030	0.033	-0.050	-0.220	
Baffin Bay	Primary Production	Ann	1.425	0.846	1.470	0.926	1.359	0.851	1.286	0.923	0.045	-0.066	-0.139	
Hudson Bay	Surface Temperature	Ann	1.315	1.059	1.021	0.977	1.725	1.074	3.188	1.685	-0.294	0.410	1.873	
Hudson Bay	Surface Salinity	Ann	22.656	5.069	22.693	5.056	22.513	5.053	22.054	5.176	0.036	-0.143	-0.602	
Hudson Bay	Mixed Layer Depth	Mar	39.967	10.070	39.366	8.643	38.851	8.477	39.202	7.835	-0.601	-1.116	-0.765	
Hudson Bay	Sea Ice Concentration	Mar	90.172	8.305	90.456	8.308	89.715	8.023	78.867	14.152	0.284	-0.457	-11.305	
Hudson Bay	Sea Ice Concentration	Sep	0.292	0.712	0.390	0.941	0.131	0.320	0.007	0.017	0.098	-0.161	-0.285	
Hudson Bay	Surface nitrate	DJF	5.412	3.173	5.717	3.435	5.182	2.955	4.360	2.372	0.305	-0.230	-1.052	
Hudson Bay	Surface nitrate	JJA	1.908	2.108	2.317	2.536	1.549	1.657	0.677	0.724	0.409	-0.359	-1.230	
Hudson Bay	Sea Water pH	Ann	7.955	0.066	7.984	0.071	7.913	0.061	7.773	0.067	0.029	-0.042	-0.182	
Hudson Bay	Primary Production	Ann	1.867	0.629	1.822	0.566	1.942	0.699	2.128	0.862	-0.045	0.075	0.262	

Hist=1986-2005 Past=1966-1985, Future20=2006-2025, Future60=2046-2065
Model data are from AR5_ESM/ACCASP20/
Primary Production = intpp and intp = intpp * 1e7 so readable in table. Original units = mol m-2 s-1
Surface Nitrate = no3 and no3 = no3 * 1e3 so readable in table. Original units = mol m-3
Values of -99 indicate missing data
Run for scenario rcp85

Table 9. AR5-ESM March (above) and September (below) SIC individual and multimodel means for RCP8.5 (green=model with least ice cover, red= model with most ice cover).

			CanESM2	GFDL	Had	IPSL	MPI	MIROC	mean	stdev	
Beaufort Sea	1966	1985	Mar	93.823	99.184	96.643	98.048	98.092	95.296	96.848	2.002
Beaufort Sea	1986	2005	Mar	93.742	99.075	96.630	97.237	97.567	95.034	96.548	1.901
Beaufort Sea	2006	2025	Mar	93.643	99.043	96.453	97.156	97.787	95.095	96.529	1.933
Beaufort Sea	2026	2045	Mar	92.774	98.821	96.302	97.205	97.342	94.855	96.217	2.133
Beaufort Sea	2046	2065	Mar	92.512	98.271	95.856	95.755	97.276	94.214	95.647	2.073
Beaufort Sea	2066	2085	Mar	90.819	98.055	95.160	94.733	96.944	84.309	93.337	5.067
CPS	1966	1985	Mar	71.450	99.423	78.197	97.592	98.827	94.925	90.069	12.099
CPS	1986	2005	Mar	71.963	99.370	78.185	97.285	98.751	94.508	90.011	11.855
CPS	2006	2025	Mar	71.711	99.344	78.167	97.334	98.819	94.106	89.913	11.918
CPS	2026	2045	Mar	70.810	99.230	78.139	97.342	98.156	93.717	89.565	12.060
CPS	2046	2065	Mar	71.028	99.083	77.984	96.458	98.559	93.067	89.363	11.906
CPS	2066	2085	Mar	71.101	98.992	77.677	95.701	98.188	92.900	89.093	11.772
Baffin Bay	1966	1985	Mar	75.436	93.170	89.346	94.962	93.369	94.501	90.131	7.466
Baffin Bay	1986	2005	Mar	75.180	94.128	89.183	94.958	93.194	94.027	90.112	7.593
Baffin Bay	2006	2025	Mar	75.107	94.119	89.290	94.357	93.300	93.812	89.997	7.532
Baffin Bay	2026	2045	Mar	75.046	94.193	89.365	93.805	93.075	90.850	89.389	7.267
Baffin Bay	2046	2065	Mar	74.227	91.899	88.837	92.361	92.597	86.147	87.678	7.051
Baffin Bay	2066	2085	Mar	73.468	90.672	87.867	91.471	90.837	77.937	85.375	7.725
Hudson Bay	1966	1985	Mar	76.162	98.199	84.934	94.713	95.282	93.445	90.456	8.308
Hudson Bay	1986	2005	Mar	75.784	97.779	84.842	94.098	95.423	93.105	90.172	8.305
Hudson Bay	2006	2025	Mar	75.576	96.406	84.779	94.182	94.541	92.808	89.715	8.023
Hudson Bay	2026	2045	Mar	73.127	95.184	84.340	93.034	94.383	75.295	85.894	9.870
Hudson Bay	2046	2065	Mar	66.716	79.103	83.971	92.139	93.394	57.880	78.867	14.152
Hudson Bay	2066	2085	Mar	34.441	70.592	77.220	89.754	89.500	31.236	65.457	26.329
			CanESM2	GFDL	Had	IPSL	MPI	MIROC	mean	stdev	
Beaufort Sea	1966	1985	Sep	40.248	52.305	65.614	64.083	62.537	58.919	57.284	9.601
Beaufort Sea	1986	2005	Sep	19.820	48.287	52.649	60.252	51.235	41.254	45.583	14.049
Beaufort Sea	2006	2025	Sep	8.652	44.980	23.463	50.177	40.964	22.057	31.715	16.097
Beaufort Sea	2026	2045	Sep	0.976	25.593	7.737	48.705	28.216	2.987	19.036	18.541
Beaufort Sea	2046	2065	Sep	0.149	2.646	1.558	17.654	7.662	0.000	4.945	6.828
Beaufort Sea	2066	2085	Sep	0.000	1.230	0.044	1.030	0.046	0.000	0.392	0.576
CPS	1966	1985	Sep	45.393	46.604	71.607	65.596	53.016	90.536	62.125	17.395
CPS	1986	2005	Sep	33.708	39.881	68.721	64.153	46.495	80.084	55.507	18.188
CPS	2006	2025	Sep	17.345	33.163	54.942	53.685	41.075	71.722	45.322	19.016
CPS	2026	2045	Sep	2.579	20.332	29.623	54.141	25.968	19.721	25.394	16.870
CPS	2046	2065	Sep	1.836	3.424	12.080	40.108	7.783	0.000	10.872	14.974
CPS	2066	2085	Sep	0.000	2.390	4.111	18.357	0.364	0.000	4.204	7.123
Baffin Bay	1966	1985	Sep	0.000	0.924	27.136	4.041	3.312	33.520	11.489	14.806
Baffin Bay	1986	2005	Sep	0.000	1.244	22.464	1.801	1.408	22.557	8.246	11.066
Baffin Bay	2006	2025	Sep	0.000	0.857	18.206	0.073	0.915	14.525	5.763	8.304
Baffin Bay	2026	2045	Sep	0.000	0.801	13.469	0.039	0.717	2.777	2.967	5.243
Baffin Bay	2046	2065	Sep	0.000	0.040	11.134	0.030	0.058	0.000	1.877	4.535
Baffin Bay	2066	2085	Sep	0.000	0.026	6.596	0.005	0.014	0.000	1.107	2.689
Hudson Bay	1966	1985	Sep	0.000	0.003	2.310	0.026	0.000	0.000	0.390	0.941
Hudson Bay	1986	2005	Sep	0.000	0.006	1.745	0.000	0.000	0.000	0.292	0.712
Hudson Bay	2006	2025	Sep	0.000	0.000	0.784	0.000	0.000	0.000	0.131	0.320
Hudson Bay	2026	2045	Sep	0.000	0.000	0.184	0.000	0.000	0.000	0.031	0.075
Hudson Bay	2046	2065	Sep	0.000	0.000	0.041	0.000	0.000	0.000	0.007	0.017
Hudson Bay	2066	2085	Sep	0.000	0.000	0.000	0.000	0.000	0.000	0.000	0.000

7.2 APPENDIX 2

7.2.1 Summary of Climate Change Trends and Projection for the Arctic Large Aquatic Basin - Beaufort Sea and Canadian Polar Shelf

Summary of Climate Change Trends and Projections							
Part 1: 50 Year (Projections estimated as changes from 1971-2000 to 2041-2070 for AR4 scenarios and 1986-2005 to 1946-2065 for AR5 scenarios)							
Changes are presented as total change over the whole time period unless specified otherwise (e.g. changes per decade noted as change/dec)							
		Beaufort Sea			Canadian Polar Shelf		
Risk Factors (Variables)	Summary Statement	Past Trend (Half-century to Century scale, or longest available if less)	Projected Change (uncertain, sign, order of magnitude, range)	Likelihood (or Probability) of Change, and/or Confidence (or Uncertainty)	Past Trend (Half-century to Century scale, or longest available if less)	Projected Change (uncertain, sign, order of magnitude, range)	Likelihood (or Probability) of Change, and/or Confidence (or Uncertainty)
Air Temperature	Likely increase in temperature, 0-3 degrees in summer, 3-7 degrees in winter	Station data (Barrow) +0.008K/y, 1.8C over 50 y from data on land	Increase: AR5-CanRCM +3.5C, AR4-CRCM+(4-7)C winter +(0-3)C summer AR4-GCM3-CRCM +2.5C	likely/medium	1.5C over 50 y from data on land	Increase: AR5-CanRCM +3.5 C AR4-NARCCAP +3.5C winter, +1.5C summer, AR4-CRCM +(3-6)C winter, +(0-3)C Summer; AR4-CGCM-CRCM + 2C	likely/medium
Precipitation	likely a slight increase	No data over the ocean	slight increase: AR5-CanRCM +0.15	Moderately likely/medium	Insufficient geographic scope; serious time-variable observational bias	slight increase: AR5-CanRCM +0.15	likely/medium
P-E			slight increase AR5-CanRCM +0.12,	Moderately likely/medium	see above	AR5-CanRCM +0.2	likely/medium
Atmos Circulation / Winds	No discernible trend in storm count, but increased strength and size. Models project a moderately likely increase in storm strength and size	Winds about +0.005m/s/y: Change in cyclone intensities in summer and autumn ~ +2 hPa per century. No discernible trend in annual storm count since 1970. Trend to increased storm strength & size	AR5-CanRCM no significant changes, AR4-CGCM-CRCM: more cyclonic, SLP decrease - ~1hPa	Moderately likely/medium	No analysis found	AR5-CanRCM no significant changes; AR4-CGCM-CRCM, not significant	likely/medium
Sea Ice thickness	very likely decrease (0.25-1.75m), regionally variable		Decrease: AR4-NAA-NEMO -(0.75-1.75)m	very likely/high	(multi-year): Insufficient data; Ice thickness (first year ice): No change	Decrease: AR4-NAA-NEMO -(0.25-1.25)m(W)	regionally variable likely
Sea Ice Concentration	Trend towards decrease in summertime ice presence, small over the shelf (caused mainly by earlier clearing), large over the basin (caused by loss of multi-year ice). Projections for a very likely decrease in summer ice extent (10-	Sea ice extent decline - 0.73x10 ⁶ km ² per decade. Ice coverage (No 50-y records): Over 40 y, decrease in summertime ice presence, small over the shelf (caused mainly by earlier clearing), large over the basin (caused by loss of multi-year ice). No change in winter (Nov through Apr)	Decrease: AR5-ESMs -0.0% (Mar) -33% (Sep), AR4-NAA-NEMO -(2-5)% (Mar), -(10-80)%(Sep) ; AR4-CGCM-CRCM decrease -50%	regionally variable - likely/medium	Ice coverage: No 50-y records	Decrease: AR5-ESMs -0.6% (Mar) -37% (Sep), AR4-NAA-NEMO - 0-5% (Mar) -(0-80)% (Sep)	regionally variable - (Mar)/likely (Sep) very likely/high

	80% regionally) variable, longer open water season. No change in winter.						
Streamflow		See Mackenzie Basin entries			Insufficient geographic/temporal scope		
Temperature - SST	Likely increase in sea surface temperature, 0.5K in winter, 0-2 K in summer.	Insufficient geographic/temporal scope	Increase: AR5-ESMs +0.7C, AR4-NAA-NEMO +0.5(W) 0-2 (S)	likely	Insufficient geographic/temporal scope	Increase: AR5-ESMs +0.36K, AR4-NAA-NEMO +0.5(W) 1-2(S)	likely
Salinity - SSS	Likely decrease in sea surface salinity by 0-1.5 ppt.	Insufficient geographic/temporal scope	Decrease: AR5-ESMs -1.1ppt, AR4-NAA-NEMO -(0-1.5) ppt	likely	Insufficient geographic/temporal scope	Decrease: AR5-ESMs -1.1ppt, AR4-NAA-NEMO -(0-1.5) ppt	likely
Stratification - MLD	Likely strengthening stratification with maximum MLDs decreasing by 1.5m	Insufficient geographic/temporal scope	Strengthening, MLD declines AR5-ESMs -1.5m	likely	Insufficient geographic/temporal scope	Strengthening, MLD declines: AR5-ESMs -1.3m	likely
Large-Scale Circulation	Intensification of BG circulation	Insufficient geographic/temporal scope	AR4-CGCM-CRCM, Beaufort Gyre intensification	moderately likely	Insufficient geographic/temporal scope		
Coastal Circulation		Insufficient geographic/temporal scope			Insufficient geographic/temporal scope		
Waves		Insufficient geographic/temporal scope			Insufficient geographic/temporal scope		
Sea Level		Insufficient geographic/temporal scope	AR4-CGCM-CRCM +6cm in SSH in 50 y	moderately likely	Insufficient geographic/temporal scope	AR4-CGCM-CRCM, not significant	moderately likely
Acidity (pH)	Observations show reduced pH but insufficient coverage for trend analysis. Models project a very likely decrease in pH by 0.18 and decreasing CaCO ₃ saturation states.	Insufficient geographic/temporal scope	PH decreases: AR5-ESMs -0.19, CaCO ₃ saturation state decreases	very likely	Decrease in general, but insufficient geographic/temporal scope	PH decreases: AR5-ESMs -0.18, CaCO ₃ saturation state decreases	likely
Nutrients		Insufficient geographic/temporal scope	ESMs do not project a significant change		Insufficient geographic/temporal scope	ESMs do not project a significant change	likely
Dissolved Oxygen		Insufficient geographic/temporal scope	not analyzed		Insufficient geographic/temporal scope	not analyzed	
Primary Production	Models project a slight increase in PP	Insufficient geographic/temporal scope	slight increase: AR5-ESMs +0.04 mol C m ²	likely/medium representation of foodwebs in GCMs only in an early stage	Insufficient geographic/temporal scope	slight increase: AR5-ESMs +0.16 mol C m ²	likely/medium representation of foodwebs in GCMs only in an early stage

Note: Unless specified, numbers represent annual mean changes. In ice covered regions these changes are usually dominated by changes during the ice free season (e.g. temperature primary production). Hence the change during the ice free season might be significantly higher

Note: Trend estimates need to be based on at least 10 years of data. Shorter time series cannot be included. E.g. The recent Beaufort State of the Ocean report only covers the last 5 years.

Note: Spot measurements at 1 oceanic station are not representative enough for the whole region

Likelihood of the Projected Change based on expert judgment; e.g. Very likely >80%, Likely 60-80%, Moderate 41-60%, Unlikely 21-40%, Very unlikely <20%

7.2.2 Summary of Climate Change Trends and Projection for the Arctic Large Aquatic Basin - Baffin Bay and Davis Strait

Summary of Climate Change Trends and Projections for Baffin Bay and Davis Strait				
Acronyms & Abbreviations: W=Winter, Sp=Spring, S=Summer, F=Fall; ss=statistically-significant@95%, ns=not-statistically-significant; AR4(5) = IPCC 4(5)th Assessment Report; HM = Hu & Myers; AOGCM = Atmosphere-Ocean General Circulation Model; CRCM = Canadian Regional Climate Model; NAO = North Atlantic Oscillation; CAA = Canadian Arctic Archipelago;				
Likelihood Scale: Very Likely >80%, Likely 61-80%, Moderately Likely 41-60%, Unlikely 20-40%, Very Unlikely <20%;				
Confidence (in information): VH = Very High, H = High, M = Medium, L = Low, VL = Very Low				
Part 1: 50-Year (Projections based on change estimates over 50-70 yrs; e.g. 1971-2000 to 2041-2070, or 1986-2005 to 2046-2065)				
Risk Factors (Variables)	Summary Statement	Past Trend (Half-century to century scale, or longest available if less)	Projected Change over 50-70 yrs (sign, and order or range of magnitude)	Likelihood (or Probability) of Change, and/or Confidence in Information
<u>Air Temperature</u> (°C): C=°C; C/dec = °C/decade	Likely increase by 1-5°C in winter and 1-3°C in summer. (M)	<u>Century:</u> weak (ns) annual warming at Greenland stns; ss (0.2-0.3°C/dec) in W only. <u>Half-century:</u> No ss trends at Greenland sites; ns warming of 0.1-0.5 at Baffin Island sites, except ss increase (0.3-0.6°C/dec) at 3 of 4 in F.	<u>Ranges in °C:</u> AR4 Models: W~0.5-6, S~0.5-2; AR5 Models: W~1.5-7, S=1-3.5; CanRCM annual ~4°C. Overall: W=0.5-7, S=0.5-3.5. Best estimate ~1-3(S), 1-5(W). Large differences among models.	Very Likely warming >0.5°C in all seasons, Likely >1, Moderate >2(S) & >3(W), Unlikely >3(S) & >5(W), Very Unlikely >3.5(S) & >6(W). <u>Confidence:</u> Very High for direction of change; Medium to Low for magnitudes.
<u>Precipitation:</u> %/dec=%/decade	Likely increase by >15%. (M)	1950-2007: Spatial variability in sign of (mostly ns) seasonal changes in precipitation rate at Baffin Island (BI) sites. Increase at Alert. Increase in number of days with precipitation at BI sites.	AR4 CRCMs (AMNO): Annual increase by ~20%; Larger in W & F (than Sp & S) in CGCM but not in ECHAM. CanRCM: Increase in annual rate by ~0.2mm/day (~20%). AR5 Models: Annual ~0.0-1.0 mm/day (0 to 50%)	Increase Likely, but magnitude and seasonality uncertain.
<u>Evaporation</u>		No info.	CanRCM: Increase in annual Evap rate by ~0.1 mm/day (~20%)	Increase Likely, but magnitude and seasonality uncertain.
<u>Streamflow & Run-off</u>	Very Likely large increase in annual discharge from Greenland ice sheet, but magnitude uncertain. (H) Timing of peak flows uncertain. (VL)	Not known	Significant and accelerating increased run-off of glacial ice melt from Greenland expected, but magnitude uncertain. Possibility that freshwater input will become half of CAA input	Large increase in freshwater input Very Likely.
<u>Sea Level Pressure & Atmospheric Circulation</u>	Likely intensification of Northern Annular Mode (NAM). (H) Moderately Likely more positive North Atlantic Oscillation (NAO). (M)	<u>NAO trends</u> 1895-2011: -0.14 per dec (ss) 1961-2011: +1.2 per dec (ns) 1981-2011: -2.4 per dec (ns)	Likely poleward shift of Jet Stream and Likely intensification of Northern Annular Mode (NAM). Moderately Likely more positive North Atlantic Oscillation (NAO)	
<u>Winds & Storms</u>	Regional model indicates small increase in number of fall storms. (M) Models indicate only small changes in mean wind speeds, but recent trends suggest possible increase. (M)	1955-2011: Increases in mean wind speed of 0.3 (0.6) m/s/decade at Alert (Clyde). <u>Last 2 decades:</u> Winds increased by 0.4%.	CanRCM: ns change in wind speed squared. CRCM: Changes in mean wind speed (m/s): W~1.1, S~0.6. Increase in number of storms by 5-10%. <u>Past ss trend</u> suggests continued increase in wind speed.	Confidence: Medium Substantial uncertainty remains.
<u>Sea Ice Area (SIA), Concentration (SIC), Extent (SIE) & Thickness (SIT)</u>	Very Likely reductions in area, thickness, concentration (SIC) and duration , especially in DS (H). Likely reductions in SIC by >30% in late spring and late fall.	1968-2010: -10(-14)% /decade for Baffin Bay in Jun-Oct (Davis Strait in Jun-Nov) from initial SIA, both ss (decreases by 42(59%) from initial) 1983-2012: Larger decreases	AR5 Models: Decrease by a few % in March (but mean SIC still >90%), and from 10% to a few % in Sept. HM: SIC decreases by 10-50% in late Sp and late F.. SIT decreases by 0.1-0.4m.	Very Likely decrease in all seasons, but magnitudes uncertain. <u>Confidence:</u> High for direction of change; Low for magnitudes. Poorly resolved in AOGCMs.
<u>Icebergs</u>	Changes uncertain - possible increased occurrence associated with melting of Greenland ice sheet.	NW Greenland dynamic ice loss events since 1985 (in 1985-1993 and 2005-2010) may have been triggered by ocean warming in Baffin Bay	Changes uncertain - possible increased occurrence associated with melting of Greenland ice sheet.	<u>Confidence:</u> Low.
<u>Ocean Temperature:</u> Surface or Near-	Likely small (<1°C) increases in winter and larger (1-2°C) increases in other seasons where	<u>Century:</u> indication of weak warming in SST datasets. <u>Half-century:</u> indication of weak warming in SST	<u>Ranges in °C:</u> AR4 Models: Small (<1°C) increase (larger in S than W) but	Likely (Very Likely) increase in W (S). Likely <(>)1°C in W(S).

surface	no sea ice (M). Uncertainty due to inadequate resolution in AOGCMs and most ocean models.	datasets but no trend in 0-50m data. Strong influences of decadal variability.	differences among models. HM: Warming by 1-3°C in Jun-Nov in BB, & by ~3 in S and 1-2 in Sp & F in DS. AR5 Models: Little increase in W and increase by ~2°C in S. Region poorly resolved in AOGCMs. Best Estimates: W~0-1, ~1-2°C in other seasons	Confidence: High for direction of change; Low for magnitudes. Poorly resolved in AOGCMs.
Ocean Temperature: Bottom (shelf) or Deep (off-shelf)	Continued slow warming Likely. (M)	Half-century: overall warming (~0.3°C/dec, marginal ss) in BB (200-1000m) based on summer/fall data, but significant decadal variability	Continued warming, based on trend	Likely
Salinity - Surface	Likely decrease in annual mean in 0.5-1.0 range , with smaller changes in summer. (M) Uncertainties due to coarse model resolution.	Weak freshening (ns) in 0-50m layer since 1950.	AR5 models indicate decrease by ~0.8. HM: decrease by 0.9, largest in W. Poor resolution in AOGCMs. Potential larger decrease due to Greenland ice sheet melt.	Decrease Very Likely. Magnitude >0.5 Likely. Confidence: Very High for sign, but Medium for magnitudes.
Salinity - Deep/Bottom	Likely decrease but magnitudes uncertain. (M)	Weak (ns) increase in salinity of 0.02 /dec in 200-1000m layer since 1950.	Likely decrease in annual mean in 0.5-1.0 range on shelf, with smaller changes in summer and off-shelf..	Confidence: High for sign, Medium for magnitude.
Stratification & Mixed Layer Depth	Very Likely increase in seasonal near-surface stratification. (H) Very Likely decrease in surface mixed layer depths (H) , by ~10m (M). Very Likely earlier onset of stratification & later end of stratification. (H).	No info	Very Likely increase in seasonal near-surface stratification. (H) Very Likely decrease in surface mixed layer depths (H). AR5 models: Decrease in mixed layer depth of 2-9 m over southern Baffin Bay (south of 75N). Very Likely earlier onset of stratification & later end of stratification. (H) Potential additional complexity and uncertainty in BB with multiple freshwater inflows.	
Large-Scale Circulation	Very Likely increase in glacial FW input (H). Moderately Likely reduction in volume and FW transports through CAA (M) Magnitudes uncertain.	Little information on long-term trends.	Increasing FW input from Greenland melt expected to become 30% of FW input into the North Atlantic by 2050. HM: reduced volume and FW inflow from Arctic, with decadal variability.	Very Likely increase in glacial FW input, but L-M confidence in magnitudes. L-M confidence in magnitude of change in Arctic Ocean inputs.
Coastal/Shelf Circulation	Likely increase in buoyancy-driven circulation from increasing Greenland glacial melt (M).	No info	Likely increasing in volume and FW transport in West Greenland and Baffin Island Currents.	Medium Confidence
Waves	Likely small decrease in summer in mean Significant Wave Heights (SWH). (M) Likely increases in SWH in areas with reduced ice cover. (M)	Last 4 decades. ns decreases (~10%) in seasonal extremes of SWH in W & F	Increased wave activity with diminishing ice cover in Sp & F. Decreases of mean and strongest SWH by 10% in S	Medium Confidence
Coastal Mean Sea Level (MSL)	Likely spatial variability in direction of change from combination of local land movements & regional ocean dynamics. (H) Magnitudes uncertain.	1970-2009: Increase of steric height by 0.5 cm/dec. Land motion not included.	Changes in the range of -10 to 20 cm from AR4 ocean model, updated Ice sheet model and Glacial Isostatic Adjustment model. Spatial variability.	Low to Medium Confidence
Extreme Sea Level	Moderately Likely increase in extreme high levels in some areas (L)	No info	Moderately Likely increase in extreme high levels in some areas due to land subsidence, MSL rise, reduced ice cover and/or possible intensification of strongest storms. (L)	
Acidity	Likely decrease in pH by ~0.1. (M) Likely large shallowing (approaching surface) of aragonite saturation depth over shelves. (M)	No historical time series but expect pH to be decreasing faster than global and Lab Sea rates. Aragonite saturation depth on shelf/slope (central BB) only about 200m (700m).	AR5 models: pH decrease of ~0.1 over the next 50 years. Expect substantial rise in aragonite saturation depths, possibly approaching surface on shelf/slope. Amplified by glacial meltwater and Arctic outflow.	Very Likely (Likely) for sign (approximate magnitude) of pH change. Likely for saturation depth approaching surface. Medium Confidence
Nutrients	Potential for reduced supply to surface due to increased stratification and for other changes due to changes in inflows (L).	No info	AR5 Models: Multi-model means indicate decrease at surface and increase in 100-400m layer, but large differences among models	Changes uncertain. Low Confidence.
Dissolved Oxygen	Very Likely reductions in concentration and saturation levels (M).	No info	AR5 Models: Decreases of ~0.005 mol m ⁻³ for the surface, and~ 0.01 mol m ⁻³ for 100-400m layer, but significant differences among models.	Decreases Very Likely but magnitudes uncertain. Medium Confidence.

7.2.3 Summary of Climate Change Trends and Projection for the Arctic Large Aquatic Basin - Hudson Bay

Summary of Climate Change Trends and Projections for Hudson Bay				
GCM=Global Climate Models AR5=IPCC 5th Assessment Report dec=decade				
Likelihood Scale: Very Likely >80%, Likely 61-80%, Moderately Likely 41-60%, Unlikely 20-40%, Very Unlikely <21%;				
Part 1: 50-Year (based on change estimates over 50-70 yrs; e.g. 1971-2000 to 2041-2070, or 1986-2005 to 1946-2065)				
Risk Factors (Variables)	Summary Statement	Past Trend from observations and AR5 Global Climate Models for 1960-2005 (period specified if different)	Projected change Future trends simulated by AR5 Global Climate Models (GCMs) from draft reports by Lavoie et al. (2013) and Chassé et al. (2013) GCM=Global Climate Models AR5=IPCC 5th Assessment Report	Likelihood (or Probability) of Change, and/or Confidence (or Uncertainty)
Air Temperature	Likely increase	Warming by 0.1 to 0.3 °C/decade or 2.2 °C/century. Warming more pronounced in fall. Warming trend greater than the pan-Arctic change by up to 0.2°C/dec.		Very likely warming Confidence: High Agreement between climatologies and NCEP (Nat. Centers for Environmental Prediction - USA)
Precipitation /Evaporation	Likely increase in precipitation and evaporation	Insufficient data	AR5 models: increase in precipitation by 6-15% and increase in evaporation by 7-17%	Likely increase; Confidence: Medium No published observations. Models predict acceleration of water cycle
Atmos Circulation / Winds		Insufficient data		
Sea Ice	Very likely decline in extent, earlier ice break-up, later freeze-up	SI Extent decline by -19.5%/dec. Date of ice break-up earlier by -3.7 d/dec SI Concentration decrease by -8% to -27%/decade, most pronounced in fall SI Thickness decrease by -19 cm to -40 cm AR5 models: decrease in sea ice extent		Very likely Increase in length of ice-free season Confidence: High Agreement between models and observations from Canadian Ice Service and satellite data
River discharge		No long-term trend in annual streamflow but decadal variations	AR5 models: low/insignificant increase by 5-11%	Moderate Observed variability in river discharge part of decadal trend or climate change? Confidence: High
Sea Surface Temperature	Very likely warming of surface waters	Warming of 0.7-1.3 °C (1985-2011) or 2.7 °C/century.	AR5 models: warming of 1.0-1.5 °C	Very likely Warming of surface waters Confidence: High GCMs models show increases in agreement with satellite observations
Salinity	possible freshening of the surface	Increase in bottom waters (1920-1992)	AR5 models: freshening of 0.5-0.75 ppt at surface	Uncertain Confidence: Low No published observations. Models predict a freshening of surface waters, magnitude uncertain
Stratification/MLD		Insufficient data	AR5 models: Low/insignificant trends	Uncertain Confidence: Low No published observations. Models diverge on direction of trend
pH	very likely decrease in pH	Insufficient data	AR5 models: pH decrease of 0.11-0.18	Very Likely decrease in pH magnitude uncertain Confidence: Medium Models show significant decreases
Nutrients	likely decrease in nutrients at surface	Surface NO ₃ decrease -0.81 mmol m ⁻³ /dec deep NO ₃ increase 1.7 mmol m ⁻³ /dec deep PO ₄ increase 0.26 mmol m ⁻³ /dec deep silicate increase 7.2 mmol m ⁻³ /dec AR5 models: decrease of NO ₃ at surface and at 50-100 m	AR5 models: decreasing nitrate concentration at surface -0.5-1.2 mmol m ⁻³	Likely Decrease at surface, magnitude uncertain Likely Increase at depth Confidence: Medium
Dissolved Oxygen		Insufficient data	AR5 models: Increase at the surface but divergent trends in the 50-100 m layer.	Uncertain; Confidence: medium All models show decreases No observations available
DIC		Insufficient data	AR5 models: divergent trends	Uncertain; Confidence: Low No agreement among

				models and no observations
Chlorophyll a		Shift in algal community composition from diatoms to dinoflagellates between late 1980s and 2000s	AR5 models: low divergent trends	Uncertain; Confidence: Low Possible shift in phytoplankton community composition
Primary production	likely increase in PP, magnitude uncertain	Increase in PP and in sedimentation orgC of marine origin (1900 -1992) Decrease in PP between late 1980s and 2000s	AR5 models: increasing trend in vertically integrated production of 0.7mol C m⁻²	Likely increase, magnitude of change uncertain
Note: Unless specified, numbers represent annual mean changes. In ice covered regions these changes are usually dominated by changes during the ice free season (e.g. temperature primary production). Hence the change during the ice free season might be significantly higher				

7.2.4 Summary of Climate Change Trends and Projection for the Arctic Large Aquatic Basin - Mackenzie River Basin

Summary of Climate Change Trends and Projections - Mackenzie River Basin				
Part 1: 50-Year (Projections estimated as changes from 1971-2000 to 2041-2070 for AR4 scenarios and 1986-2005 to 1946-2065 for AR5 scenarios)				
Changes are presented as total change over the whole time period unless specified otherwise (e.g. changes per decade noted as change/dec)				
Risk Factors (Variables)	Summary Statement	Past Trend (Half-century to Century scale, or longest available if less)	Projected Change (uncertain, sign, order of magnitude, range)	Likelihood (or Probability) of Change, and/or Confidence (or Uncertainty)
Air Temperature	Likely increase in air temperature 2.5-7K in winter and 1.5-3 in summer	Increase 1.5-2C regionally variable	Increase: AR4-GCMsup to 5C, AR4-CCCSN 2.5-6C (winter) 1.5-3 (summer), AR4 CRCM 4-7 C (winter) 1.5-3 summer. Regionally variable lower in Athabasca and Peace subbasins, higher in Mackenzie delta area	likely
Precipitation	Likely increase in precipitation, regionally variable 15-50%, less in summer than in winter.	Mostly increase with some regional variations including decrease, more spring rain and less spring snow	Increase: AR4-GCMsup to 20%, AR4-CCCSN 15-25% (winter) 15% (summer), AR4-CRCM 20-50% (winter) -5-35 % (summer) regionally variable less in Athabasca and Peace subbasins, more in Mackenzie delta area	likely/medium
Evaporation		Increase	Increase in lake evaporation	
Atmos Circulation / Winds			AR4-CanRCM not significant.	
Permafrost	Permafrost: Likely increase in active layer depth	Permafrost temperature increase 0.3-0.8 C between 20-30m (1980-2002)	Increase in Active Layer Depth 0-50% over 50 years. Thaw depth could increase 15-40%	likely/moderate confidence
Snow cover	Likely decrease in snow depth	Decrease	Decrease in snow depth and snow cover duration	moderate confidence
Lake Ice			Delay infreeze-up, earlier break up	likely
Lake Temperature	Likely increase in lake temperatures	Increase	Increase: AR4-GCM 5-10, higher in the north	likely
Lake Stratification	Likely increased stratification in lakes		Increased stratification, brief thermal stratification in deeper waters	likely
Erosion		Increase		
River flow	Likely increase in winter and fall flows (up to 50%) and reduction in summer flows. Likely lower and earlier spring freshets, regionally variable, depending	Decrease in summer, increase in winter, spring freshet earlier. Climate change influence hard to detect due to strong decadal variability and damming	Projections mostly show increase in winter and fall flows (up to 50%) and reduction in summer flows. Lower and earlier spring freshets. Some inconsistencies, strong dependence on headwaters and representation of declining snow packs and glaciers in models	moderate confidence

	on headwaters			
Lake Levels		no trend or decrease		
Dissolved Oxygen (Lakes)	Likely decline in oxygen levels in lakes with potential hypoxic conditions at the bottom		Decline , potential hypoxia at lake bottoms	
Primary Production (Lakes)	Likely increase in primary production with shifts in community structure		Increase, shifts in community structure	likely
Note: Unless specified, numbers represent annual mean changes. In ice covered regions these changes are usually dominated by changes during the ice free season (e.g. temperature primary production). Hence the change during the ice free season might be significantly higher				